AMERICAN UNIVERSITY OF BEIRUT

STOCHASTIC MODELING OF SALTWATER INTRUSION IN HIGHLY HETEROGENEOUS COASTAL AQUIFERS

by
AMIR SAFI

A thesis
submitted in partial fulfillment of the requirements
for the degree of Doctor of Philosophy
to the Department of Civil and Environmental Engineering
of the Faculty of Engineering and Architecture
at the American University of Beirut
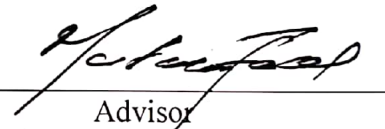
Beirut, Lebanon
March 2019

AMERICAN UNIVERSITY OF BEIRUT

STOCHASTIC MODELING OF SALTWATER INTRUSION IN

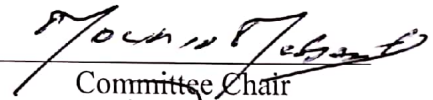# HIGHLY HETEROGENEOUS COASTAL AQUIFERS
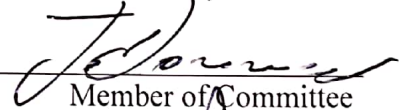
by
AMIR SAFI

Approved by:

_____
Dr. Mutasem El-Fadel, Professor   Advisor
Civil and Environmental Engineering, AUB

_____
Dr. Mounir Mabsout, Professor   Committee Chair
Civil and Environmental Engineering, AUB

_____
Dr. Joanna Doummar, Assistant Professor   Member of Committee
Geology, AUB
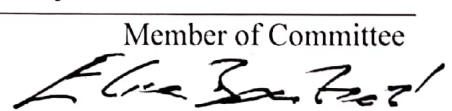
_____
Dr. Ibrahim Alameddine, Assistant Professor   Member of Committee
Civil and Environmental Engineering, AUB

_____
Dr. Steen Christensen, Associate Professor   Member of Committee
Geosciences, Aarhus University (External)

_____
Dr. Elie Bou-Zeid, Professor   Member of Committee
Civil and Environmental Engineering, Princeton University (External)

_____
Dr. Majdi Abou Najm, Assistant Professor   Member of Committee
Land, Air and Water Resources, University of California Davis (External)

Date of dissertation defense: March 14, 2019

AMERICAN UNIVERSITY OF BEIRUT

THESIS, DISSERTATION, PROJECT RELEASE FORM

Student Name: _Safi_ _Amir_ _Mohammadreza_
                      Last   First   Middle

◯ Master's Thesis   ◯ Master's Project   ◯ Doctoral Dissertation

☒ I authorize the American University of Beirut to: (a) reproduce hard or electronic copies of my thesis, dissertation, or project; (b) include such copies in the archives and digital repositories of the University; and (c) make freely available such copies to third parties for research or educational purposes.

☐ I authorize the American University of Beirut, to: (a) reproduce hard or electronic copies of it; (b) include such copies in the archives and digital repositories of the University; and (c) make freely available such copies to third parties for research or educational purposes

after : **One ---- year from the date of submission of my thesis, dissertation, or project.**
        Two ---- years from the date of submission of my thesis, dissertation, or project.
        Three ---- years from the date of submission of my thesis, dissertation, or project.

[signature]   May 15, 2019

Signature   Date

ACKNOWLEDGEMENTS

AN ABSTRACT OF THE DISSERTATION OF

Amir Safi   for   Doctor of Philosophy
                            Major: Environmental and Water Resources Engineering

Title: Stochastic modeling of saltwater intrusion in highly heterogeneous coastal aquifers

This research presents a novel method for a reliable quantification of uncertainties with the prediction of saltwater intrusion (SWI) in poorly field-characterized heterogeneous coastal aquifers. The method uses crude prior information about hydrogeological input parameters, and simultaneously incorporates parameter uncertainty and imprecision in prior information to infer the required statistics for a Monte Carlo (MC) simulation into the uncertainty analysis. Compared with other methods, it is a computationally effective method for uncertainty analysis in highly heterogeneous coastal aquifers. In this method, the Sequential Gaussian Simulation (SGS) is used to create random parameter fields while fuzzy set theory accounts for the imprecision pertaining to prior information. Prediction uncertainties are evaluated by generating a large number of calibration-constrained models using the Null Space Monte Carlo (NSMC) method.

This research presents another novel method that is used to design additional hydrogeological field-investigations towards reducing the prediction uncertainties in a SWI system. The method provides flexibility concerning model dimensionality, allows for any desired task-oriented formulation, targets any measurement type, accounts for various sources of uncertainty while also ensuring that it is cost-effective. It expands on the existing linear data-worth analysis method through the incorporation of Bayesian model averaging (BMA) and genetic algorithms (GA) when conducting a three-dimensional location search for sampling new data in non-linear systems. Both methods can use any model independent tools for parameter estimation and any variable-density simulation codes.

The efficiencies of these methods in quantifying and reducing prediction uncertainties were demonstrated using the SEAWAT model and data from an actual heterogeneous coastal aquifer with limited hydrogeological field-data. Located along the Eastern Mediterranean (Beirut), the pilot aquifer consists of karstified limestone of Cretaceous age overlain by Upper Tertiary and Quaternary unconsolidated deposits. The SEAWAT model was used to predict the displacement of the 3D salt/freshwater interface caused by 50 years of groundwater abstraction as well as the volume of freshwater remaining in the aquifer after such abstraction. The simulations results were further used to enhance the understanding of the response of coastal aquifer systems to local and global stresses as well as the role of adaptation strategies in alleviating SWI.

The prediction uncertainty was quantified in response to the uncertainty with heterogeneity in the hydraulic conductivity. The estimated uncertainty of the model prediction was more

realistic for the proposed method than for the traditional methodologies. The outcome revealed that a source of freshwater with the volume of 1.3 to 1.5 km3 exists in the deep parts of the Beirut aquifer. The design method identified the optimal locations of 1 to 5 observation wells for sampling future head/salinity data in order to reduce uncertainties with the model prediction. The optimal number of observation wells was found to be depended mostly on the ratio between the start-up cost of the monitoring project and the cost of drilling the first observation well, while the implementation cost of additional observational wells was secondary but also important. The outcome of model simulations suggested that anthropogenic activities have more noticeable impacts on SWI compared with climate change. Interestingly, coupling anthropogenic activities and climate change had a synergistic effect that aggravated the intrusion beyond the sum of the individual impacts. The effectiveness of adaption strategies in alleviating SWI was found to hinge on proper planning in terms of timing, duration, capacity and context.

Keywords: Saltwater intrusion, heterogeneous coastal aquifers, anthropogenic interventions, global climate change, NSMC, SGS, Fuzzy, BMA, GA

CONTENTS

ILLUSTRATIONS

TABLES

LIST OF ABBREVIATIONS

CODESA-3D	Coupled variable Density and Saturation 3-Dimensional model
CSS	Composite Scaled Sensitivities
DSS	Dimensionless Scaled Sensitivity
DW	Data Worth
FEFLOW	Finite Element subsurface FLOW and transport simulation system
FEMFAT	Finite Element Method Fatigue
FEMWATER	Finite Element Model for Groundwater
GMS	Groundwater Modeling System
GUI	Graphical User Interfaces
HANI	Horizontal Anisotropy
HK	Horizontal Hydraulic Conductivity
LSI	Land-Surface Inundation
MCMC	Markov Chain Monte Carlo
MOCDENSE3D	3-D Method-Of-Characteristics Variable Density ground-water flow and transport model
MODFLOW	Modular 3-D finite-difference groundwater flow
MoEW	Ministry of Energy and Water
NSMC	Null-Space Monte Carlo
OD	Optimal Design
PSS	prediction Scaled Sensitivity
SGS	Sequential Gaussian Simulation
SLR	Sea-level Rise
SOR	Successive Over-Relaxation
SUTRA	Saturated-unsaturated variable-density groundwater flow with solute or energy transport
SVD	Singular Value Decomposition
SWI	Saltwater intrusion
USGS	United State Geological Survey
VANI	Vertical Anisotropy

I would like to dedicate this research to my beloved wife and our beautiful daughter.

CHAPTER 1

INTRODUCTION

1.1   Background

Groundwater constitutes a main source of drinking water in many coastal urban areas in arid or semi-arid regions. Aquifer over-pumping, land-use change, and climatic changes can cause the intrusion of seawater into groundwater, generally known as saltwater intrusion (SWI) (Sophiya & Syed, 2013). Large hydraulic conductivities (e.g. fracture zones) along the coast may intensify SWI (Werner et. al., 2013) which is invariably becoming an increasing threat to urban coastal communities worldwide by contaminating groundwater and impairing its productive and consumptive value (Selmi, 2013; Park et al., 2012). As such, decision makers are increasingly under pressure to plan and protect the economic, social, and environmental security of coastal communities as large populations rely on these reservoirs (Sanford & Pope, 2010). Adopting a well-founded management strategy to protect groundwater quality in coastal aquifers requires an understanding of the relative impacts of drivers forcing the SWI (Safi et al., 2018). While the impacts of climate change and local pressures have been repeatedly assessed in urbanized coastal aquifers, their synergistic impacts remain ambiguous (Werner et al., 2013). In this context, mathematical models can be used to evaluate the impacts of drivers and their synergistic impacts (Cobaner et al., 2012) and serve as policy planning tools to examine the sustainability of groundwater exploitation in coastal aquifers. However, model predictions are invariably associated with uncertainties due to limited field-data to ascertain these predictions thus limiting their value in providing sustainable management of water resources (Werner et al., 2013).

It is important to determine the uncertainty with model predictions when they are used for decision support (Keating et. al., 2010). Several Monte Carlo-like methods have been reported during the past two decades to quantify the uncertainty associated with model predictions of a hydrogeological system (Harvey & Gorelick, 1995; Beven & Binley, 1992; Tavakoli et al., 2013; Kitanidis, 1996; Yeh et al., 1996; Woodbury & Ulrych, 2000; Carrera et al., 2005; Tonkin and Doherty, 2009). They can be used to generate a range of model predictions obtained by using different parameter sets (multiple realizations) that are conditioned by calibration dataset (Keating et al. 2010). However, these methods are either excessively time consuming to apply for SWI modeling in highly parameterized systems due to long model runtime, and mathematical complexities of inverse methods (e.g. Markov Chain Monte Carlo) or require a detailed prior probability distribution (e.g. lognormal distribution) to generated multiple calibration-constraints realizations (e.g. NSMC). In cases where the expert knowledge or the available calibration dataset provide limited information about parameters that inform model predictions, the prediction uncertainty can be underestimated using these methods. This is particularly the case for all SWI systems if the salt/fresh water interface is located in the deeper parts of an aquifer with limited information about its deep hydrogeology. If the prediction uncertainty is underestimated, it may lead to results that can mislead decision makers, and thus cause undesirable management decisions (Uusitalo et al., 2015).

Prediction uncertainties can be reduced by collecting additional field-data to be used as a calibration dataset through model inversion (Dausman et al., 2010). In practice, the locations and type of additional data are often determined based on expert opinion with no guarantee that sampling locations can contribute to optimal reduction in uncertainties (Vilhemsen and Ferre, 2017). Given the high cost of data collection, it is imperative to design a sound monitoring network that could constrain prediction uncertainties. Several methods

have been proposed during the past two decades to guide the design of monitoring networks (Tiedeman et al. 2003; Herrera et al. 2000; Rizzo et al. 2000; Reed et al. 2000; Cieniawski et al. 1995; Wagner 1995; Andricevic and Foufoula-Georgiou 1991; Loaiciga 1989; Rouhani and Hall 1988; Wohling et al. 2016; Dausman et al. 2010). Existing methods however fail to simultaneously provide the flexibility concerning model dimensionality, allow for a desired task-oriented formulation targeting any observation type, and account for various sources of uncertainty (e.g. geologic structure, heterogeneity, boundary condition, and source/sink) while keeping the cost of data collection at a minimum.

This research aims to fill a gap in the field of SWI modeling and uncertainty analysis by developing new methods and tools to quantify prediction uncertainties in deep heterogeneous systems that lack field-data, and design allocation of future field-data towards reducing prediction uncertainties in such systems. The methods are applied to a karstic coastal aquifer located along the Eastern Mediterranean (Beirut, Lebanon) for evaluating their performances. The results are used to better understand the processes that govern SWI in urban coastal aquifers. The urbanized coastal aquifer of Beirut has been increasingly reported to be vulnerable to intensive SWI due to over-exploitation of groundwater, urbanization, climate change, and large hydraulic conductivities (i.e. faulted zones) along the coast (Rachid el al., 2017, 2015; Safi et al., 2018). Although SWI in the upper parts of the aquifer have been assessed through field investigations, studies addressing SWI in the deeper parts of the aquifer as well as simulating SWI in the entire aquifer through mathematical modeling are lacking. For this reason, the Beirut aquifer system is not well protected and is poorly managed. Nevertheless, due to lack of input data about the aquifer's hydrogeology, large uncertainties are expected in any modeling effort. Model prediction uncertainties should be quantified and ideally reduced by collecting more data if the model is used for decision support.

1.2   Research Objectives

The proposed research targets the following objectives:

(1) Develop a method to quantify uncertainties associated with model predictions of SWI in a heterogeneous coastal aquifer for which deep hydrogeological characteristics are not known;

(2) Set-up and calibrate a 3D variable-density groundwater flow and solute transport model for simulating SWI in the Beirut coastal aquifer; address data challenges in modeling of SWI; evaluate the role of model inversion in estimating hydraulic conductivities; and analyze the impact of uncertainty with estimated hydraulic conductivities on the prediction of SWI in this aquifer;

(3) Evaluate the efficiency of the method to quantify prediction uncertainties by simulating SWI variables in the deep parts of the Beirut coastal aquifer for which hydrogeological data is almost non-existent:

(4) Develop a method to guide collection of future hydrogeological field-data that can contribute to reducing prediction uncertainties in non-linear 3D groundwater systems;

(5) Evaluate the performance of the method by identifying the best locations for sampling new (yet to be collected) head and salinity data from the deep parts of the Beirut coastal aquifer to reduce uncertainties in predicting SWI;

(6) Examine the dynamics of SWI under anthropogenic interventions and global climate change, and their synergistic impacts; and evaluate the effectiveness of local adaptation planning in alleviating SWI in urbanized coastal aquifers;

(7) Analyze the impacts of uncertainty with input data about aquifer discharge (water consumption rate and population growth rate) on the seasonal and annul predictions of SWI in the Beirut aquifer; and assess the effectiveness of local adaptation planning (in line

with the national plans) to provide informed policy and decision making for sustainable groundwater management in the Beirut aquifer.

1.3   Research innovation

While research on stochastic modeling of groundwater flow and solute transport has been recurrently carried out for heterogeneous aquifers, studies addressing SWI in highly heterogeneous coastal aquifer systems with poor hydrogeological characterization in their deep parts are lacking. The proposed research is innovative because it is the first to develop a method that quantifies the uncertainty with prediction of SWI in such situations. The developed method can be applied to any heterogeneous aquifer systems with deficit in any type of hydrogeological data (e.g. hydraulic conductivity, porosity, groundwater abstraction rate …). In addition, while several studies have been proposed for optimal design of monitoring networks towards reducing uncertainties in model predictions, limited to none identifies the 3D allocation of additional field-data while considering uncertainty with a conceptual model. The proposed research is equally innovative because it is the first to develop a method that optimizes the number and allocation of additional field measurements with different depths at a single and multiple spatial location by constraining cost to remain at a minimum and considering model non-linearity. Application of the developed methods in the field of groundwater modeling can be worldwide. They can be applied to any 3D hydrogeological system that lacks an adequate amount of field-data required as modeling input.

The proposed research is also innovative in the use of three-dimensionality for comprehensively appraising the displacement of the salt/fresh water interface and mass encroachment of salinity by linking the impacts of anthropogenic interventions, global

climate change and heterogeneity, and their synergistic impacts on the spread of SWI in a highly heterogeneous coastal aquifer. The outcome of the research is the first detailed assessment of the impacts of SWI drivers to the propagation of intrusion in the Beirut coastal aquifer. Concurrently, this study is the first to evaluate the effectiveness of local adaptation planning (in line with national plans) to provide informed policy and decision making for sustainable aquifer management in the Beirut aquifer. As a main outcome, this dissertation attempts to comprise the first comprehensive 3D multi-objective variable-density groundwater flow and solute transport model for the Beirut coastal aquifer. While the propagation of SWI has been reported as increasing in the upper part of the Beirut aquifer, limited to no work focused on the spread of SWI in the entire aquifer as well as the prediction of the volume of freshwater stored in the deep parts of this aquifer. This is an area worthy of further investigations because the limited remaining freshwater resources in the upper aquifer is likely to encourage authorities to start tapping the deeper parts of the system in the near future. Hence, this research is innovative in its prediction outcome about the future of the Beirut coastal aquifer.

1.4   Dissertation structure

This dissertation is presented in seven chapters. Figure 1-1 illustrated coupling the objectives to the chapters.

Chapter 1 is a general introduction on modeling of SWI in heterogeneous coastal aquifers, the main research objectives, innovations, and Dissertation structure.

Chapter 2 comprises a literature review on SWI in heterogeneous coastal aquifers, and a review of the challenges and gaps in the mathematical modeling of SWI.

Chapter 3 presents a method for a reliable quantification of uncertainty with predictions of SWI in a heterogeneous coastal aquifer system for which the deep

hydrogeological characteristics are not known. The efficiency of the proposed method in quantifying the prediction uncertainty is demonstrated using a SEAWAT model and data from the Beirut coastal aquifer. A 3D variable-density flow and solute transport model (SEAWAT) was set-up for the Beirut aquifer. The proposed method was used to quantify uncertainties with predicting two variables in the deep parts of the Beirut aquifer that lacks hydrogeological field-data: (1) the displacement of the salt/fresh water interface caused by 50 years of groundwater abstraction (from 1969 to 2019), and (2) the volume of freshwater remaining in the aquifer after groundwater abstraction (in 2019). The results were compared to uncertainty estimates obtained through the former uncertainty analysis method.

Chapter 4 develops a design methodology to optimize multiple locations of new (yet to be collected) observation wells that can contribute to reducing uncertainties in predicting multiple variables in a nonlinear groundwater model. The method optimizes simultaneous measurements with different depths at a single and multiple observation locations (i.e. three dimensions) at a minimum cost. The performance of the method was demonstrated by reducing uncertainties with predicting the two variables simulated in Chapter 2. The target of the optimization was to identify the best locations for placing 1, 2…, 5 new observation wells with head and salinity measurements at different depths.

Chapter 5 analyzes the dynamic of SWI in response to anthropogenic activities and global climate change as well as their synergy by predicting SWI in the Beirut aquifer for the near future from 2012 to 2032. The analysis considered scenarios of groundwater abstraction rates (water consumption and population growth rates) and climate change (sea level rise and temperature) based on reported rates/values for the Beirut aquifer. In line with national plans, adaptation strategies were evaluated to inform decision makers about their effectiveness in alleviating SWI in the Beirut aquifer.

Chapter 6 summarizes the Dissertation and concludes with corresponding challenges to address in future work.

Chapter 7 lists bibliographic citations for the whole Dissertation.

Chapter	Content
Chapter 1	- General introduction on modeling of SWI in high heterogeneous coastal aquifers - Research objectives, research innovations, and dissertation structure
Chapter 2	- Literature review on SWI in high heterogeneous coastal aquifers - Review of the challenges and gaps in the mathematical modeling of SWI
Chapter 3	**Objective 1:** Develop a method to quantify uncertainties associated with model predictions of SWI in a heterogeneous coastal aquifer for which deep hydrogeological characteristics are not known.
	Objective 2: Set-up and calibrate a 3D variable-density groundwater flow and solute transport model for simulating SWI in the Beirut coastal aquifer; address data challenges in modeling of SWI; evaluate the role of model inversion in estimating hydraulic conductivities; and analyze the impact of uncertainty with estimated hydraulic conductivities on the prediction of SWI in this aquifer.
	Objective 3: Evaluate the efficiency of the method to quantify prediction uncertainties by simulating SWI variables in the deep parts of the Beirut coastal aquifer for which hydrogeological data is almost non-existent.
Chapter 4	**Objective 4:** Develop a method to guide collection of future hydrogeological field-data that can contribute to reducing prediction uncertainties in non-linear 3D groundwater systems.
	Objective 5: Evaluate the performance of the method by identifying the best locations for sampling new (yet to be collected) head and salinity data from the deep parts of the Beirut coastal aquifer to reduce uncertainties in predicting SWI.
Chapter 5	**Objective 6:** Examine the dynamics of SWI under anthropogenic interventions and global climate change, and their synergistic impacts; and evaluate the effectiveness of local adaptation planning in alleviating SWI in urbanized coastal aquifers.
	Objective 7: Analyze the impacts of uncertainty with input data about aquifer discharge (water consumption rate and population growth rate) on the seasonal and annul predictions of SWI in the Beirut aquifer; and assess the effectiveness of local adaptation planning (in line with the national plans) to provide informed policy and decision making for sustainable groundwater management in the Beirut aquifer.
Chapter 6	Summary of thesis
Chapter 7	Bibliography

Figure 1-1 Dissertation structure and coupling of research objectives to chapters

CHAPTER 2

MODELING SALTWATER INTRUSION IN COASTAL AQUIFERS: A CRITICAL REVIEW AND FRAMEWORK FOR UNCERTAINTY ANALYSIS

Abstract

Saltwater intrusion (SWI) is recognized as an increasing threat to coastal communities worldwide by contaminating groundwater and impairing its consumptive value. The extent of intrusion is primarily driven by anthropogenic activities, human induced climate change and their synergy. Mathematical models have been developed to understand the drivers and responses of SWI in order to properly manage water resources in coastal aquifers. During the past century, considerable modeling efforts have been reported on many of the hydrological and hydro-chemical characteristics of SWI. Despite much progress, challenges persist to understand the dynamics of SWI in response to its drivers due to the uncertainty associated with model predictions of SWI models. This review presents the state of the knowledge on the mechanisms, types and drivers of SWI, its mathematical modeling with emphasis on sources of uncertainty in predicting SWI including previously applied methods to address such uncertainties. We define the main limitations, controlling factors, computational demands, and required prior information of existing techniques to quantify and reduce uncertainties. We conclude in outlining research gaps and future needs with a framework to fill in existing gaps.

Keywords**:** Saltwater intrusion, prediction uncertainty

2.1 Introduction

Coastal aquifers provide freshwater resources for more than one third of the world's population living in coastal regions (Li et al. 2013). Groundwater constitutes a main source of drinking water in many coastal urban areas particularly in arid or semi-arid regions (Yakirevich et al. 1998; Hosseinifard and Aminiyan 2015). The use of coastal groundwater for drinking, agriculture or industry increases the susceptibility of coastal aquifers to the landward encroachment of saltwater into the aquifer, generally known as saltwater intrusion (SWI) (Freeze and Cherry 1979; Bear et al. 1999). With increasing groundwater extraction and climate change impacts, SWI has become a growing threat to urban coastal communities worldwide by contaminating groundwater and impairing its productive and consumptive value (Park et al., 2012). As such, decision makers are increasingly under pressure to plan and protect the economic, social, and environmental welfare of coastal communities relying on these reservoirs (Sanford and Pope 2010).

The spread of SWI is promoted by many factors that can be divided into two categories: 1) those that drive the intrusion such as natural processes (climate change, sea level rise (SLR), increased temperatures and evapotranspiration, and reduced precipitation) and anthropogenic activities (groundwater over-pumping, decreased aquifer recharge, pollution, leakage, sewers induced by urban development) (Kumar et al. 2007; IPCC 2014; Singh 2014); and 2) those that intensify the intrusion such as large hydraulic conductivities (e.g. fracture zones) and irregular fissures along the coast, and conduits (Werner et. al., 2013). The combination of these factors and their synergy with different mechanisms (i.e. lateral and vertical) and various types of SWI (i.e. passive, active, and passive-active) can produce a complex hydrodynamic system. This complexity makes it difficult for water resources managers and decision makers to understand the future of SWI in order to plan a

management strategy to secure the quantity and quality of groundwater in coastal aquifers (Tribbia and Moser 2008; Comte et al. 2016).

Considerable efforts have been dedicated to assess the dynamics of SWI in response to its drivers and influencing factors involving field monitoring and mathematical modeling that can account for temporal and spatial variations in hydrological (source/sink) and hydrogeological (geologic structure, boundary conditions, head and salinity distribution, position of salt/fresh water interface) input parameters through analytical or numerical solutions (Sophiya and Syed 2013; Cobaner et al. 2012; El Shinnawy and Abayazid 2011; Rasmussen et al. 2013). In these studies, model predictions of SWI are invariably associated with uncertainties due to limited field-data about input parameters that are vital for accurate predictions, thus limiting their value in the context of sustainable water resources management (Werner et al. 2013). It is crucial to reduce these uncertainties when they are used for supporting decision-makers (Vilhemsen and Ferre 2017). While much efforts targeted the development, review and application of various techniques to quantify and reduce prediction uncertainties in groundwater models, limited work was reported about uncertainties in SWI predictions (Herckenrath et al. 2011). Thus, coastal management decisions have often been made without considering the failure risk associated with a given strategy due to model predictions uncertainties (Lecca and Cau 2004).

While several reviews of SWI drivers and analysis of their impacts using mathematical modeling have been reported in the literature (e.g. Werner et al. 2013; Ketabchi et al. 2016; White and Kaplan 2017), none targeted knowledge gaps in the uncertainty analysis of SWI models. Prediction uncertainty analysis is particularly important in simulating SWI in coastal aquifer systems because some elements in the conceptual model (e.g. heterogeneity in hydraulic conductivity of deep layers) that highly affect SWI predictions can seldom be identified from available data or expert knowledge (Sanz and Voss

2006; Werner and Simmons 2009). This study presents the state of knowledge in SWI

mechanisms, type, influencing factors along with the progress in related mathematical

modeling. In particular, we emphasize the gaps in prediction uncertainty analysis in SWI

modeling. We divide the sources of SWI prediction uncertainty into two categories relating to

model structural errors and parameter uncertainties including methods to quantify and reduce

such errors/uncertainties. Finally, we examine methods of uncertainty analysis and suggest

future needs.

2.2   SWI dynamics and drivers

Sustainable management of freshwater along coastal aquifers is imperative to protect

the economic, social, and environmental security of coastal communities as large populations

rely on these reservoirs. Enforcing a well-founded management strategy requires an

understanding of the dynamic of SWI in response to the factors influencing the intrusion.

2.2.1   Dynamics of SWI

In coastal aquifers, a salt/fresh water interface is formed between saltwater and

freshwater by maintaining the hydrostatic pressure between the two fluids near the coast

(Bear et al. 1999) (Figure 2-1a). Prolonged decrease in groundwater levels lowers the

hydrostatic pressure, which increases the landward encroachment of saltwater into the aquifer

(Freeze and Cherry 1979). SWI occurs to some extent in most coastal aquifers owing to a

change in the hydraulic pressure between saltwater and freshwater (Anderson et al. 2005).

The mechanism of intrusion is usually through the lateral encroachment of saltwater from

coastal waters (Figure 2-1a) (e.g. Carneiro et al. 2010; Ferguson and Gleeson 2012) and/or

vertical upward movement of saltwater (so-called upconing) near pumping wells from deeper

salty zones (Paniconi et al. 2001; Michael et al. 2010; Gaaloul et al. 2012; Kura et al. 2014)

(Figure 2-1b). As for the latter, over pumping fresh groundwater lowers the water table at the

pumping well and forces the interface to rise and reach a new equilibrium between saltwater

and freshwater (Bear et al. 1999).
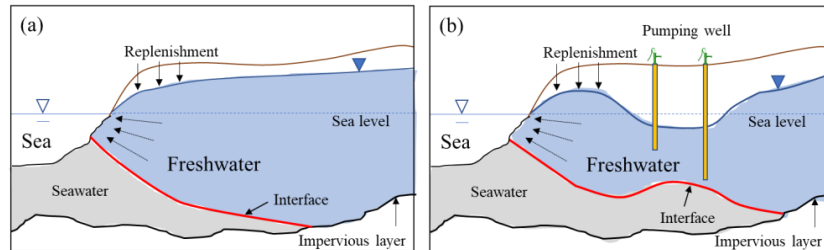
Figure 2-1 Salt/fresh water interface in coastal aquifers: (a) under natural condition; (b) with vertical movement of saltwater (upconing) in the vicinity of a pumping well

Previous studies have classified the occurrence of SWI into passive and active

depending on the direction of migration/movement of saltwater and freshwater near the coast

(Werner et al., 2012). In passive SWI, groundwater level is higher than sea-level (Figure

2-2a), and thus the direction of freshwater flow is seaward, whereas saltwater moves

landward beneath the freshwater zone (Morgan et al., 2012). The hydraulic gradient with a

slope towards the sea results in discharging the submarine groundwater into the sea

(Mahesha, 1995). During passive SWI, the interface moves slowly, and in some cases, it may

take hundreds of years for the interface to move a significant distance landward (Howard and

Israfilov 2012). In active SWI, the groundwater table is lower than the sea-level near the

coast, and thus the direction of freshwater flow is similar to that of saltwater along the coast

(Morgan et al., 2012) (Figure 2-2b). The submarine groundwater is not discharged to the sea,

and hence a more aggressive intrusion occurs (Fetter 2001; Badaruddin et al. 2017).

Compared with passive SWI, the interface moves more rapidly during active SWI till it

reaches to the cone of dispersion at the center of pumping (Howard and Israfilov 2012). More

recently, Werner (2017) further recognized a third type of SWI (referred to as passive-active)

that can occur in coastal aquifers receiving distributed recharge (Figure 2-2c). The third type

of SWI is a combination of active SWI occurring on the landward side of the interface (e.g. near the toe) and passive SWI occurring closer to the shoreline.
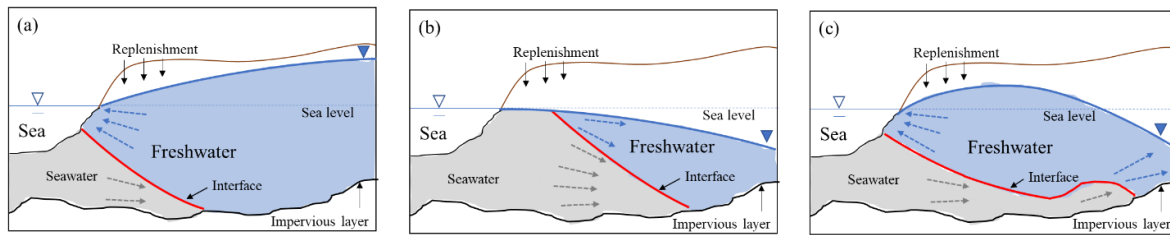
Figure 2-2 Types of SWI Occurrence in coastal aquifers: (a) passive; (b) active; and (c) passive-active

While the passive type of SWI has been widely recognized and investigated using hypothetical and real case studies (Abd-Elhamid and Javadi 2011; Post et al. 2018), similar studies addressing active and passive-active SWI are limited (Yakirevich et al. 1998; Ozler 2001; Fetter 2001; Werner and Gallagher 2006; Kura et al. 2014; Morgan and Werner 2015; Klassen and Allen. 2017).

2.2.2 Drivers of SWI

SWI is a naturally occurring process that can be affected by human activity. White and Kaplan (2017) classified the drivers forcing SWI into natural, anthropogenic, and synergistic. Natural drivers of SWI include storm surges (Danard et al., 2003; Stoltman et al., 2007; Debernard et al., 2002; Romanowski, 2010; Klassen and Allen 2017), hurricanes (Steyer et al. 2007; Williams 2010), climatic change (Sherif and Singh 1999; Carneiro et al. 2010; Oude Essink et al. 2010), drought (Drexler et al. 2001; Angelini et al. 2016), sea-level rise (SLR) (Chesnaux 2015; Luoma and Okkonen 2014; Michael et al. 2013; Stigter et al. 2014), tidal oscillations (Neubauer et al. 2013; Sutter et al. 2015; Pierfelice et al. 2017; Yuan and Zhu 2015), and subsidence (Morton et al. 2002). They can act over a long (millennial) timescale (e.g. geologic uplift and subsidence) or a short time scale (e.g. drought, climate oscillation, hurricanes, tsunami) (White and Kaplan 2017). They are also different in spatial

scales. For example, hurricane, tsunami and drought have regional effects on SWI while climate oscillation and SLR influence the intrusion globally.

Climate change in particular is reportedly expected to drive SWI at time and location with increased temperatures and reduced precipitation (IPCC 2014) (Figure 2-3). Rising temperatures increase evaporation rates in lakes, rivers and storm waters, and particularly in shallow subsurface waters, which further leads to less aquifer recharge (Sanford and Pope, 2010; Cobaner et al., 2012). In recent years, melting glaciers induced by global warming coupled with increased seawater temperature led to SLR that is also expected to further increase potential SWI (Ketabchi et al. 2016; Loaiciga *et al.* 2012; Chang *et al.* 2011; Werner *et al.* 2013; Carretero *et al.* 2013). A few studies assessed the impact of land-surface inundation (LSI) due to the landward movement of the interface (Ferguson and Gleeson 2012; Carneiro et al. 2010; Oude Essink et al. 2010; Yechieli et al. 2010; Loaiciga et al. 2012; Laattoe et al. 2013; Morgan et al. 2013; Sefelnasr and Sherif 2014; Luoma and Okkonen 2014; Chesnaux 2015). Reportedly, LSI can induce an order of magnitude more intense SWI compared with the vertical SLR (Ataie-Ashtiani et al. 2013).
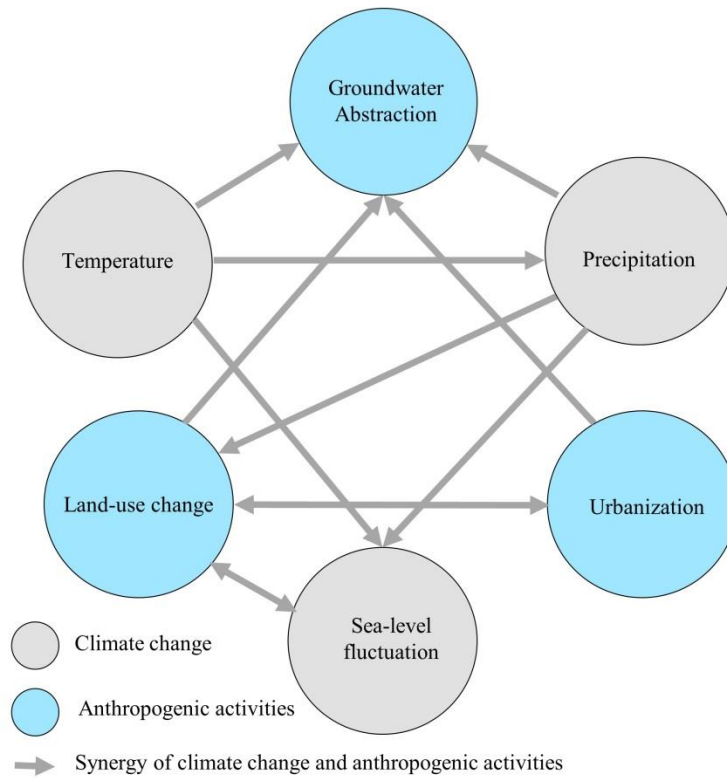
Figure 2-3 Main drivers forcing SWI in coastal aquifers and their interactions

Similarly, several studies examined the influence of tidal oscillations on SWI (Robinson et al. 2006; Kuan et al. 2012). Ataie-Ashtiani et al. (1999) and Chen and Hsu (2004) indicated that tides produce rapid intrusion near the shore and force the intrusion further inland. In contrast, Werner and Lockington (2006) argued that tides produce a dispersed mixing zone near the shore but do not extend the intrusion landward. On the other hand, the findings of Kuan et al. (2012) highlighted the significant impact of tidal oscillation on both vertical and landward movement of the interface. The inconclusive findings highlight the potential for future investigations on the impacts of tides on the mechanism of intrusion.

Anthropogenic drivers of SWI or the alteration in the local environment by human activity mainly occur through aquifer over-exploitation (Zhang et al. 1999; Sherif and Singh 1999; Aliewi et al. 2001; Vandenbohede and Lebbe 2003; Kura et al. 2014; Safi et al. 2018), land-use change (Dogan and Fares 2008) and urban development (Chang et al. 2016; Akbarpour and Niksokhan 2018), which in turn reduce fresh water resources stored in coastal

16

aquifers (Nicholls and Cazenave 2010; Beck and Bernauer 2011; Goudie 2013; Deng et al. 2017). Compared with all other drivers, the extent of SWI is driven primarily by groundwater over-exploitation and land-use change caused by mismanagement or lack of regulatory enforcement (Singh 2014; Werner et al. 2013; Sophiya & Syed, 2013). Urban development in particular increases impervious surfaces, which reduces aquifer recharge and lowers freshwater balance (Ragan et al. 2000; Ranjan et al. 2006; Uddameri et al. 2013; Alameddine et al. 2018; Jeppesen et al. 2011). As such, increased water demand associated with population growth and decreased aquifer recharge induced by urban development along coastal areas, promotes SWI most significantly (Werner et al., 2013; Singh, 2014). Examples of SWI due to anthropogenic activities are numerous globally (Asia (China (Shi and Jiao 2014; Cheng and Chen 2001; Wang and Chiao 2001; Wu et al. 2008); India (Datta et al. 2009; Bobba 2002; Singaraja et al. 2015); Bangladesh (Mahmuduzzaman et al. 2014), Indonesia (Nur et al. 2001); Oman (Walther et al. 2012); UAE (Hussain et al., 2016); Iran (Mahmoodzadeh et al., 2014); Lebanon (Safi et al. 2018; Masciopinto 2013); Turkey (Demirel 2004); Africa (Egypt (Gemeil et al. 2011); Libya (Alfarrah et al. 2017); Tanzania (Mtoni et al. 2013); Tunisia (Paniconi et al., 2001); Morroco (Sedki and Ouazar 2011); Djibouti, Kenya and Somalia on the east coast, Mozambique in the south and Nigeria in the west (Steyl and Dennis, 2010)), Australia (Morgan and Werner 2015; Werner 2010; Ivkovic et al., in 2012), Europe (Italy (Cherubini and Pastore 2011; Trotta et al. 2015); Greece (Kazakis et al. 2016), Netherlands (Oude Essink, 2001), Spain (Martínez Fernández and Selma 2004)), and America (Barlow and Reichard, 2009; Sanford and Pope 2010)).

Much of the reported literature on SWI focuses on the impacts of anthropogenic activities (over-pumping of groundwater and urbanization) and climate change (reduced precipitation, surface runoff, recharge, and sea-level fluctuations) on the intrusion (Werner et al. 2013). Anthropogenic activities and natural stressors can also act interactively to create a

more intense SWI (Safi et al. 2018a) (Figure 2-3). Increased temperature associated with climate change or drought can increase the demands for groundwater (Alameddine et al. 2018). Anthropogenic activities may alter the timing and magnitude of climatic cycles (SLR) and extreme events (hurricane) (White and Kaplan 2017). While the interaction between anthropogenic activities and natural stressors can aggravate the intrusion (El Shinnawy & Aba Yazid, 2011; Melloul & Collin, 2006; Conrads et al. 2010; Dausman & Langevin, 2005; Niang et al. 2010; Oude Essink, 2001; Ranjan et al. 2006), the magnitude of their impacts remains challenging to quantify (Safi et al. 2018a).

While the spread of SWI is driven by anthropogenic activities and climate change, geology can control the physical trends of SWI (Werner et al. 2013), large hydraulic conductivities along the coast may expedite SWI (Bear et al., 1999). In fractured media, irregular fissures enable saltwater to enter the freshwater using existing flow pathways, which further exacerbate the landward/upward movement of seawater (Pinault et al., 2004). Although few studies have characterized the role of geologic structure in controlling the interface displacement in heterogeneous coastal aquifers (Kerrou and Renard. 2009), the impacts of large hydraulic conductivities (e.g. faults and fracture zones) and heterogeneity in Karstic aquifers on the position of the interface in response to transient stresses remain challenging to quantify (Werner et al. 2013), mainly due to difficulties in charctrizing heterogeneity as well as lack of enough information about the origin and hydraulic properties of fractures/conduits.

2.3   Predicting SWI

Understanding the extent of the salt/fresh water interface in response to SWI drivers has important water management implications because a small change in the position of interface can increase the amount of salinity in groundwater significantly and impair its

consumption value (Aberca and Clement 2009). Making an accurate prediction of the interface is however a significant challenge. Mathematical modeling of the flow and solute transport in the subsurface environment have been often suggested as a tool to provide substantial information about the mechanism and extent of intrusion (Sophiya & Syed, 2013; Cobaner et al., 2012; El Shinnawy & Abayazid, 2011). Past efforts have resulted in the development of a large number of analytical and numerical solutions to solve the governing flow and transport equations and predict the location and movement of the salt/fresh water interface. Depending on the representation of the salt/fresh water interface, these models are categorized into sharp-interface and variable-density models (Kooi and Groen 2001). The sharp-interface models are based on the assumption that the width of the saltwater-freshwater mixing zone is much smaller than the thickness of the aquifer (Figure 2-4a). Therefore, freshwater and saltwater are assumed as two immiscible fluids (but without the capillary pressure that exists between the two fluids), which are separated by a sharp interface (Bear et al. 1999). The variable-density models consider the saltwater-freshwater interface as a wide transition zone due to strong saltwater hydrodynamic dispersion, which is a more physically representative approach for the simulation of SWI (Huyakorn *et al.,* 1987) (Figure 2-4b).
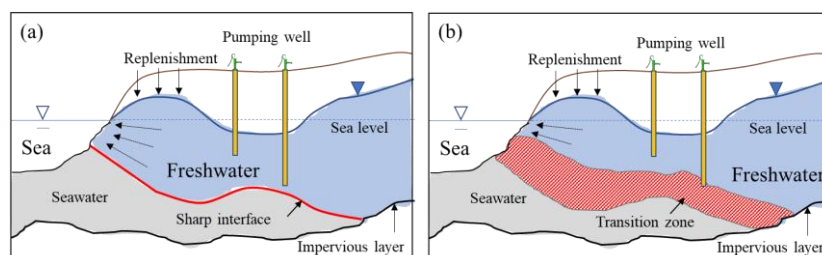
Figure 2-4 Salt/fresh water interface in coastal aquifers: (a) Sharp interface; (b) Transition zone

2.3.1 *Analytical solutions*

The application of sharp-interface models for simulating SWI initiated by the Ghyben and Herzberg formula and followed by analytical solutions that were mainly based

on simple synthetic cases (Mehdizadeh et al., 2015). Although the solution of the interface is simplified significantly using analytical models (Werner et al. 2013), analytical solutions are especially useful for simulating SWI in large-scale problems due to lack of their dependency on detailed data (Shi et al. 2011). While such solutions are practical for the case where the transition mixing zone is relatively thin (Bear 1979), the steady-state estimation of the sharp-interface and transient prediction of the interface at its early times are valid only when the migration of the salinity is mainly dominated by advection while dispersion can be ignored (Sakr 1999). Shi et al. (2011) validated the steady-state solution of the sharp-interface models in homogeneous coastal aquifers and Llopis-Albert and Pulido-Velazquez (2014) found that the applicability of the sharp-interface approach strongly depends on the placement of the pumping wells and the hydrodynamic coefficients. The approximation of the toe position is valid when the values of the layer thickness and longitudinal dispersion coefficients are high and/or the values of surface recharge, transmissivity and distance of pumping wells to the shoreline are low. Similarly, Mehdizadeh et al. (2015) found that the sharp-interface model is valid in a SWI system where the interface is close to the pumping wells. In summary, the use of analytical solutions for variable-density flow limits a real-world SWI system to a simplified version through various assumptions (e.g. homogeneity and simple geometries). Such limitation increased the demand for numerical solutions/codes as tools to get more insights into the real-world systems (Anderson et al. 2015).

2.3.2   Numerical solutions

Past efforts resulted in a number of numerical solutions to solve the variable density groundwater flow and solute transport equations for complex systems (Pinder and Cooper 1970; Shamir and Dagan 1971). The physical and computational concepts of the most frequently used variable-density codes are outlined in Table 2-1 along with their

corresponding applications in real and hypothetical case studies. Most codes couple the density-driven flow and advection–dispersion equations for simulating SWI and all codes are computationally demanding. The differences between the codes are mainly centered at code dimensionality, saturated/unsaturated solution of flow, steady-state solution of SWI, and numerical solution (e.g. Finite Differences, Finite Elements) of the flow and solute transport equations.

Numerical solutions of variable density flow have been employed by numerous studies to predict different forecasts of interest. For example, Post et al. (2018) used the SEAWAT code to determine the sustainable yield of freshwater resources on an Island. The same code was used to explore the implications of storm-induced barriers to alleviate SWI in a coastal aquifer by Elsayed and Oumeraci (2018). Change et al. (2018) applied a SEAWAT 2D model to predict SWI and the displacement of the interface due to groundwater over-pumping. Xiao et al. (2018) used SUTRA to evaluate the impact of SLR on SWI. Kanzari et al. (2018) applied HYDRUS-1D to simulate salinity migration in a coastal aquifer. Szymkiewicz et al. (2018) combined HYDRUS and SWI2 packages for modeling recharge in SWI systems.

Table 2-1 Physical characteristics of commonly used computer codes for simulating variable density flow and solute transport

Code	Physical characteristics				Reference	Application	
	Flow	Transport & reaction	mension	Di		Real case studies	Hypothetical cases
MOCDENSE3D	St, SF, TF	AD, TT	3D	2D,	Oude Essink, 1998	Oude Essink *2001;* Oude Essink et al. 2010; Giambastiani et al. 2007	
FEMFAT	SU, SF, TF	AD, Ad, CR, ST, TT	3D	2D,	Yeh et al. 1996		Cheng et al. (1998); Tsai and Kou (1998); Zhang et al. (2001); Volker et al. (2002); Asada et al. (2005)
CODESA-3D	SU, SF, TF	AD, Ad, ST, TT	3D	2D,	Gambolati et al., 1999	Paniconi et al. 2001; Cau et al. 2002; Qahman et al. 2005; Lecca and Cau (2009)	
FAST-C	St, SF	AD, Ad, ST, TT	3D	2D,	Holzbecher, 1998		Kaleris (2006); Holzbecher (2001, 2005a, 2015b)
SEAWAT	St, ST, TF	AD, Ad, CR, ST, TT	3D	2D,	Guo & Langevin, 2002	Lathashri and Maheshab (2015); Cherubini and Pastore (2011); Vandenbohede and Lebbe (2011); El-Bihery (2009); Lin et al. (2009); Abdullah et al. (2010); Safi et al. (2018)	Bakker et al. (2004); Langevin et al. (2010); Webb and Howard (2011); Mao et al. (2006a, 2006b); Kourakos and Mantoglou (2009); Dausman et al. (2010)
FEMWATER	SU, SF, TF	AD, Ad, ST, TT	3D	2D,	Lin et. al., 1996	Datta et al. (2009), Carneiro et al. (2010), Insigne and Kim (2010); Tularam and Singh (2009)	Kim et al. 2012
FEFLOW	SU, SF, TF	AD, Ad, CR, ST, TT	3D	2D,	Diersch 1996	Gossel et al. (2010); Yechieli et al. (2010); Soupios (2015)	Watson et al. (2010);
SUTRA	SU, SF, TF	AD, Ad, CR, ST, TT	3D	2D,	Voss 1984	Narayan et al. (2007); Kumar (2001); Nishikawa et al. (2009);	Sanz and Voss (2006); Pool and Carrera (2010)

St: Saturated, SU: Saturated/Unsaturated, SF: Steady state flow, TF: Transient flow, AD: Advection-dispersion equation,
Ad: Adsorption, CR: Chemical reaction, ST: Steady state transport, TT: Transient transport

2.4   Uncertainty in predicting SWI

Effective management of groundwater resources in coastal aquifers often requires a reasonably well-characterized variable-density model to accurately evaluate and predict the dynamics of SWI in response to changes made through a management strategy (Werner et al. 2013). Accurate and reliable model predictions are hence essential for sound groundwater management practices. A basic framework generally used consists of constructing a groundwater model for water resources management purposes. Vilhemsen and Ferre (2017) stripped down this framework into four steps: collection of existing data to derive an initial baseline model, collection of additional data (e.g., through boreholes or geophysical logs) to build required structural information about the subsurface environment, spatial and temporal refinement of the numerical model, and finally applying the modeling results in a decision/management framework. The complexities with conceptualizing groundwater systems, and common limitations in collecting hydrogeological data, can prohibit attaining the first two steps indicating that uncertainty is an inherent characteristic of a groundwater model (Bakalowicz 2005).

Sources of prediction uncertainty in groundwater modeling are manifold including model input parameters, boundary and initial conditions, representations of physical processes, numerical solution, and observation error/noise (Gourley and Vieux 2006). JiChun and XianKui (2013) classified the modeling uncertainties into the uncertainty of model input parameters, conceptual model uncertainty, and the uncertainty derived from observation error/noise. The sources of uncertainty associated with SWI modeling have rarely been reviewed. In what follows, we classified the main sources of uncertainty with a

23

SWI model into uncertainty in the conceptualization of physical processes (referred to as structural error), and uncertainty of input parameters due to lack of data. Figure 2-5 depicts this classification with corresponding potential solutions.
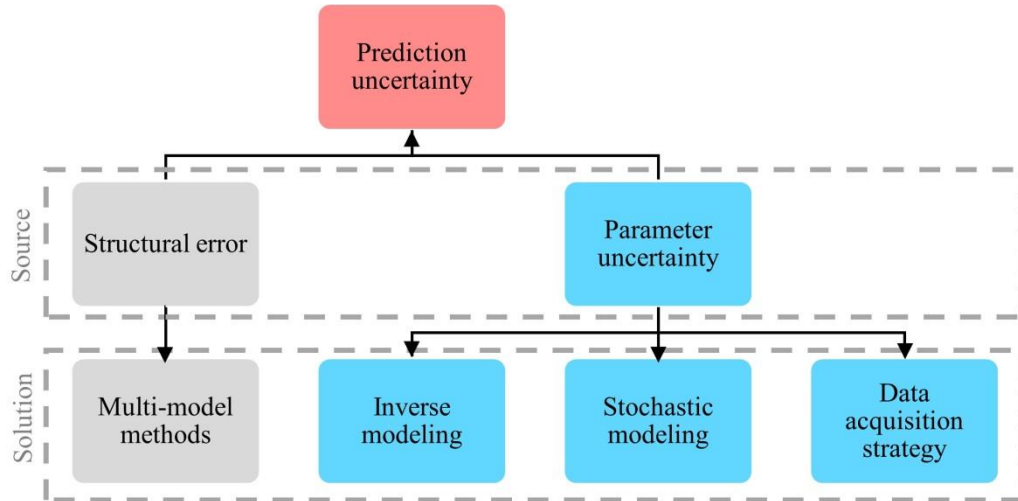
Figure 2-5 Main sources of prediction uncertainty in a SWI model along with methods to quantify/reduce prediction uncertainty

2.4.1 *Structural error*

Ignoring conceptual uncertainty or structural errors can lead to overconfidence in the predictive performance of a groundwater model (Rojas et al., 2008). Structural error is not random and hence cannot be quantified (Anderson et al., 2015). Its magnitude depends on the degree of model simplification (Beven, 2005) and/or incorrect conceptualization of the real-world system e.g. boundary and initial conditions, stratigraphy and geology, model borders, spatial and temporal refinement of the model, and aquifer geometry (Xu et al., 2017). One concern is that structural errors can increase the total error variance of a model prediction that depends on parameters omitted from the conceptual model due to simplification (Cushman & Tartakovsky, 2016). Another concern is that structural errors

24

can force the adjustment of input parameters to compensate for structural errors during

model calibration, further resulting in biased model predictions (Xu et al., 2017).

Structural errors associated with a SWI model have not received enough attention.

Limited studies examined a few types of errors that are mainly associated with boundary

and initial conditions, aquifer geometry, and geologic simplifications with recent interest in

exploring the impact of inland boundary conditions on SWI due to SLR (Werner &

Simmons, 2009; Carretero et al., 2013; Morgan et al., 2015). Rasmussen et al. (2013)

demonstrated that the assessment of climate change impacts on SWI is highly sensitive to

the boundary conditions of a model. Under the influence of SLR, the seaside boundary of a

SWI domain has been frequently defined as a head-controlled boundary condition (Sherif

& Singh, 1999; Feseker, 2007; Watson et al., 2010; Chang et al., 2011; Michael et al.,

2013; Luoma & Okkonen, 2014; Chesnaux, 2015; Stigter et al., 2014; Sefelnasr & Sherif,

2014; Lu & Werner, 2013; Webb & Howard, 2011; Oude Essink et al., 2010; Giambastiani

et al., 2007), a flow-controlled boundary condition (Chesnaux, 2015; Luoma & Okkonen,

2014; Michael et al., 2013; Morgan et al., 2013; Koussis et al., 2012; Werner et al., 2012;

Chang & Clement, 2012; Chang et al., 2011; Yechieli et al., 2010; Watson et al., 2010;

Feseker, 2007) or a general head boundary condition (Giambastiani et al., 2007; Lu &

Werner, 2013; Green & MacQuarrie, 2014). Werner and Simmons (2009) and Werner et al.

(2012) showed that the extent of SWI is in the order of tens of meters for flux-controlled

boundary conditions, and up to several kilometers for head-controlled boundary conditions.

Sun et al. (2017) evaluated the impacts of three inland (head-controlled, flux-controlled and

general head) boundary conditions on modeling SWI due to SLR in coastal aquifers. They

concluded that the characterization of the hydraulic response of fresh groundwater to the

sea-level fluctuation is more realistic by applying the general head boundary condition than the other types.

The initial position of the mixing zone can also highly affect the predicted state of SWI in transient models, hence it should be well-characterized at the beginning of the simulation period (Werner et al., 2013). Common strategies for collecting information about the position of the mixing zone is to drill wells near the coast and monitor salinity concentration or to use geophysical investigation through Electrical resistivity tomography (ERT) or Electromagnetic (EM) methods (Beaujean et al., 2014). In cases where the initial position of the mixing zone is not known, a steady-state simulation is typically used to adjust the salinity distribution with the hydraulic head to estimate the initial saltwater wedge profile that would exist in the system prior to stressors (Safi, Rachid, et al., 2018). In this approach, the solute transport model is run under transient conditions with a steady-state hydraulic head until a steady-state concentration distribution is achieved (Guo & Langevin, 2002). The starting salinity distribution for the solute transport model is usually set to an entirely saline or freshwater aquifer (Werner et al., 2013). It is expected that the initial position of the mixing zone can be approximated using this approach. In general, the initial salinity concentration prior to stressors can alter the density of water and subsequently the flow velocity during the transient simulation in a SWI model. Limited to no work targeted the prediction uncertainty arising from the approximated mixing zone at the beginning of the simulation in a SWI system.

Perhaps, the main structural error is related to geologic simplification and inadequate characterization of aquifer geometry. Chitsazan et al., (2015) showed that the improper definition of stratigraphy structures can lead to large uncertainties with model

predictions of SWI. Additional parameters representing sea side slope, bed slope toward the land and the sea are required for accurately introducing aquifer geometry in the conceptual model of SWI (Abd-Elhamid et al., 2016). Equivalent hydraulic conductivity has been repeatedly reported to be the most important input geologic parameter in SWI modeling because it controls the position of the toe of interface (Kerrou & Renard, 2010). In recent years, much efforts were devoted to evaluating the impact of geologic simplification on SWI predictions in complex (heterogeneous) subsurface environments with a first attempt by Dagan and Zeitoun (1998) who showed that neglecting the layered heterogeneity in SWI modeling can increase the uncertainty associated with estimating the interface toe. Similarly, Lu et al (2009) found that neglecting layered heterogeneity leads to overestimation of the toe penetration length. In contrast, heterogeneity was reported to have a negligible impact on the upward movement of flow within the interface but produces a significant concentration plume (Rahman et al., 2005). Interestingly, the impacts of heterogeneity on SWI can differ significantly in 2D and 3D simulations, confirming the major influence of the third dimension of heterogeneity on the prediction of intrusion (Kerrou & Renard, 2010). Thus, neglecting heterogeneity and three-dimensionality can result in large uncertainties in model predictions (Werner et al., 2013).

Depending on the complexity of a geologic structure, a conceptual model may require additional parameters to explain the real-world system. For example, in a highly heterogeneous Karstic system, a conceptual model requires additional parameters representing conduit/fracture networks, fault orientation and friction factor for accurately simulating SWI (Bakalowicz, 2005). Fleury et al. (2007) recognized conduits and fractures as the primary elements of a Karst conceptual model influencing SWI. Parameters

27

representing conduit diameter, friction factor, matrix hydraulic conductivity, and effective medium porosity should be included in a SWI model for Karst (Xu & Hu, 2017). In addition, orientation of fractures affects the shape of the salt/fresh water interface (Dokou & Karatzes, 2012). Spechler (2001) explained the upward movement of saline water in northeastern Florida due to the geologic structural irregularities such as fractures, collapse features, and faults, and suggested that Karst should be characterized properly for SWI simulations.

Structural errors in Karst models typically arise from the lack of a robust method to characterize Karst hydrogeology (i.e. conduits and fractures). Methods used for characterizing the latter in the context of dual continuum (DC) (discrete pipe network coupled to a matrix continuum with turbulent flow) and discrete fracture (DF) (conduit/fractured flow; applied with porous medium) have reportedly been demonstrated successfully (Berkowitz et al., 1988). In the same context, Xu and Hu (2017) developed a hybrid discrete-continuum numerical model that couples a discrete pipe network (DC) with Darcian flow in porous medium. Dokou and Karatzes (2012) characterized the main fractures/faults of a karst system using discrete fractures (DF). Scanlon et al. (2003) however conditioned the applicability of the DC and DF methods for characterizing Karst to various factors such as the modeling objective, the karstification degree, the model scale, and most importantly the availability of geologic field data (e.g. conduits and fractures properties, and heterogeneity in hydraulic conductivity). Bakalowicz (2005) argued that it is difficult to use the DC and DF methods to characterize Karst in many aquifer systems because of the limitations in detailed data about conduits/fractures.

Other studies examined the structural error associated with the use of the equivalent porous medium (EPM) approach (that requires less field-data) in parameterizing Karst and simulating SWI. For example, Ghasemizadeh et al., (2015) used the EPM method to simulate groundwater flow and solute transport in a Karstic aquifer located in Puerto Rico. They demonstrated that the structural error encountered in the EPM is limited in the model prediction of SWI in an intermediate scale Karstic system. Khadra and Stuyfzand (2018) compared the predicted results of SWI obtained from the EPM with the DC. They found that both approaches predicted similar results although the DC reproduced some local irregularities for chloride concentration. In cases where the local distribution of salinity is of interest, the structural error associated with using EPM should be accounted for in a prediction uncertainty analysis. When applying the EPM, the geology of Karst is represented by a geologic system with a high degree of heterogeneity in hydraulic conductivity. Therefore, conduits/fractures are modeled as high conductivity zones with no turbulence. The frequency distribution of the hydraulic conductivity is assumed to follow a log-normal distribution that can be positively or negatively skewed depending on the presence of major conduits with very high hydraulic conductivity (Halihan et al., 2000).

2.4.1.1 <u>Multi-model methods</u>

In recent years, several studies used multi-model methods to account for structural errors in groundwater models (Neuman, 2003; Neuman and Wierenga, 2003; Bredehoeft, 2003; Carrera et al., 2005; Poeter and Anderson, 2005; Refsgaard et al., 2006). Using multi-models, a range of prediction can be obtained using the average predictions from a

set of plausible models (Bredehoeft 2005; Ye et al. 2004, 2008, 2010). This is accomplished by assigning weights or applying statistical criteria to each model and then combining individual model predictions (Poeter and Anderson 2005; Rojas et al. 2008).

While multi-model methods have been frequently used to account for conceptual uncertainty in a groundwater model (Bredehoeft, 2005; Rojas et al. 2008), their applications in SWI modeling is limited. Chitsazan et al. (2015) used this approach to account for errors in conceptualizing hydro-stratigraphy structure using chance-constrained programming coupled with Bayesian model averaging. Their work was however limited to only three conceptual models. Chitsazan and Tsai (2015) further used a hierarchical Bayesian model averaging (HBMA) method to prioritize sources of uncertainty in predicting Chloride concentration in a faulted aquifer. They evaluated the variance of model prediction from individual sources of uncertainty including model parameters, fault permeability architecture, variogram model, grain-size method, and boundary head value. Their findings showed that prediction uncertainties are more affected by structural errors than by uncertain model parameters.

2.4.2   *Uncertainty in model parameters*

Understanding a SWI system depends fundamentally on the input data coupled with an adequate knowledge of hydrology and hydrogeology of the system to create a representative conceptual model including SWI processes. The conceptual model of SWI requires detailed data about aquifer characteristics, such as hydraulic properties, geological borders, boundary conditions, dispersivity (dispersion and molecular diffusion), and

30

sources and sinks, that will aid in understanding groundwater dynamics (Bakalowicz 2005).

Cases studies of SWI with detailed data are rare. One of the few exceptions is the study of

Post et al. (2018) that reported SWI with exceptionally detailed hydrogeological data. In

most aquifers, the complexity of subsurface conditions often leads to scarcity in field-data

describing the hydrogeological system, which will result in uncertainties with model

predictions (El-Fiky 2010). Simmons (2005) listed a few challenges that can mislead

modelers in understanding variable-density systems, stressing at high dependency of SWI

models to field-data about heterogeneity, hydrodynamic coefficients and sources/sinks. As

such, modeling efforts should be invariably dedicated to exploring and reducing

uncertainties around their predictions if they are used for decision support (Keating et al.,

2010).

A number of modeling efforts has been dedicated to reducing (or quantifying) SWI

prediction uncertainties through: (1) inverse modeling, or parameter estimation, that can be

used to estimate (calibrate) the properties of an aquifer system that are important to model

predictions (Doherty et al. 2010); (2) stochastic modeling that can be used to quantify the

prediction uncertainties by the forward propagation of the remaining uncertainties

associated with parameters after model inversion (Tonkin and Doherty 2009); and (3)

collecting additional field-data to be used as calibration dataset for increasing reliability of

model prediction (Moore and Doherty 2005).

2.4.2.1   Inverse modeling

In an inverse groundwater model, parameter estimates (e.g. hydraulic conductivity) constitute the inverse solution of the groundwater flow and/or solute transport equations best consortiums with the available observed dependent variable value (e.g. hydraulic head, flow or concentration) (Alcolea et al., 2006). Carrera et al. (2005) provided a review of various techniques to solve the inverse problem of parameter identification in groundwater modeling. While model inversion techniques have been applied regularly to groundwater models (Werner et al., 2013), the use of inverse modeling for variable-density flow and solute transport is rare (Sanz & Voss, 2006) (Table 2). One of the main reasons is that the governing flow and solute transport equations should be coupled through the dependence of water density on salinity concentration in order to model a variable-density SWI system (Guo & Langevin, 2002). This severely increases the computational burden of a SWI inversion, which often limits the estimation of parameters to the inverse solution of constant-density groundwater flow equation. In addition, the parameter estimation requires information about salinity concentration, aquifer bottom topography, and initial conditions (Carrera et al., 2010), which are not usually available for most costal aquifers. Another challenge in the SWI model inversion is the lack of knowledge about the input parameters that highly affect the predictive performance of a SWI model and the optimal types of observed dependent variables that should be used to estimate such parameters (Sanz & Voss, 2006; Shoemaker 2004; Carrera et al., 2010). In the following, we introduce these parameters and their required observation data for model calibration.

A fundamental understanding of dispersion mechanisms (longitudinal and transverse dispersivity) and molecular diffusion is critical for evaluating the width of the steady-state transition zone in homogeneous coastal aquifers (Shoemaker 2004; Paster & Dagan, 2006). While the dispersivity parameters have similar impact on the width of the transition zone (Abarca & Clement, 2009), the transverse dispersion is also a controlling factor to determine the amount of seawater entering an aquifer (Abarca et al., 2007). Dispersivity parameters are ideally determined from laboratory or field experiments. Werner et al. (2013) argued that dispersion coefficients obtained from laboratory or field experiments cannot reproduce thick mixing zones that are found in the field. In most cases, the values of longitudinal and transverse dispersivity coefficients are determined by calibrating a model rather than actual measurements. Abarca and Clement (2009) estimated the values of dispersion coefficients using the width of a (laboratory-based) mixing zone as an observed data during model calibration. Similarly, Shoemaker (2004) indicated that salinity observations at depths is more important than head observations when estimating dispersivity. Interestingly, the molecular diffusion can be estimated using the salinity log concentration (Sanz & Voss, 2006). The logarithm of salinity concentration can also be used as an observed data for calculating porosity (Sanz & Voss, 2006) that is a factor influencing the spread of intrusion.

The extent of the intrusion is mainly controlled by freshwater inflow as well as the horizontal hydraulic conductivity. The freshwater inflow rate highly affects the calculation of submarine groundwater discharge. The horizontal hydraulic conductivity mainly controls the penetration length of the interface and the amount of seawater entering an aquifer (Abarca et al., 2007). Both the freshwater inflow and the horizontal hydraulic conductivity

can be estimated using head and salinity observation data (Sanz & Voss, 2006). However, concurrently calibrating hydraulic conductivity and freshwater inflow using only head and salinity observations leads to high correlation between these parameters, which prohibit unique estimates of their values. Using flow observations perpendicular to the shoreline can reduce this correlation, further resulting in unique estimation of the hydraulic conductivity and freshwater inflow parameters (Shoemaker, 2004).

Compared with other model parameters, the hydraulic conductivity can vary considerably over small distances in highly heterogeneous geologic systems (e.g. Karst) and thus its spatial heterogeneity can control the flow pattern and salinity migration. A review of various inversion techniques (pilot points parameterization, Monte Carlo variant of the representor, sequential self-calibration, moment equations, zonal calibration and non-iterative semi-analytical) to estimate the hydraulic conductivity in highly heterogeneous systems has been provided by Hendricks Franssen et al. (2009). The geostatistical method of pilot point parameterization was recognized as a more physically representative approach for characterizing geologic heterogeneity compared with other methods. In the pilot points parameterization, the geology is represented using a set of discrete-locations (pilot points) by enforcing a spatial interpolation from the pilot points to the model grids (Alcolea et. al., 2006). Model calibration is then used to adjust the values of pilot points through an iterative process by minimizing an objective function measuring the misfit between computed results and observed data (e.g. head, flow and salinity concentration) (Doherty et al., 2010; Sanz & Voss, 2006).

Several SWI studies have determined the spatial heterogeneities in the hydraulic conductivity of a coastal aquifer using the pilot points parameterization approach (Langevin

& Zygnerski, 2013; Baalousha, 2016). In these studies, the number of pilot points needed for a representative heterogeneous system was defined much larger than the number of available observations. After the calibration, the model outcomes fitted reasonably well to field measurements. Moore and Doherty (2005) argued that even a perfectly calibrated pilot-point model may still exhibit high levels of parameter uncertainty after model inversion in a highly heterogeneous aquifer. This is because, in field practice of heterogeneous aquifers, observation data (e.g. hydraulic head) are usually sparsely distributed over a geologic domain in an arbitrary fashion whereas the spatial geologic domain (hydraulic conductivity) is continuous and should be parameterized by introducing many model parameters (large parameter dimensionality) (Nilsson et al., 2007; Yeh et. al., 2015). Estimating more parameters of interest than the number of observations is not reasonable resulting in data being "spread too thin" (Uusitalo et. al., 2015). In such cases, the solution of the estimation problem is non-unique (Doherty, 2015). Such models that almost always suffer from the lack of a unique solution for parameter estimation are commonly referred to as "ill posed" models (Doherty et al., 2010). This non-uniqueness requires a different approach in model calibration than those used with well-posed models.

Regularization mechanisms have been repeatedly used to stabilize a parameter estimation process when the solution of the estimation problem is non-unique (Doherty, 2015). For example, the Tikhonov regularization can be used to minimize the deviation of parameters from the user specified preferred condition that is often determined based on expert knowledge about the hydrogeological variability (i.e. heterogeneity) in the system (Doherty et al., 2010). This variability is often expressed by an expected value and a covariance function (or a variogram). White et al. (2010) showed that the use of Tikhonov

regularization highly affects the predictive ability of a calibrated SWI model for a heterogeneous coastal aquifer. Although the use of Tikhonov regularization often results in parameter fields that are geologically realistic, the calibration process requires the estimation of the pilot points that are inestimable on the basis of the calibration dataset. This may induce numerical instability when model outcomes are fitted to field measurements (Doherty et al., 2010). Recently, several studies used subspace methods to attain more numerical stability by subtracting inestimable parameters and/or inestimable parameter combinations from the calibration process (Tonkin & Doherty, 2005; Aster et al., 2013). This is achieved through singular value decomposition (SVD) of the weighted Jacobian matrix that represents the sensitivity of model results in response to variations in model parameters (for details see e.g. Doherty at al., 2010). Model parameter combinations that correspond to singular values larger than a user-defined truncation value are deemed to be estimable on the basis of a calibration dataset. These parameter combinations span the calibration solution space. In contrast, the inestimable parameter combinations span the calibration null space and retain their initial values during the calibration process. Few studies calibrated a SWI model by concurrently using Tikhonov regularization and SVD through model inversion. Meyer et al. (2018) combined SVD and Tikhonov regularization to increase the reliability of data fit in a SWI model applied to understand the impact of regional flow. Similarly, Herckenrath et al. (2011) used both SVD and Tikhonov regularization to increase the stability of parameter estimation in a highly parameterized synthetic model. Although the numerical stability increased significantly during the model inversion and the calibration results were generally satisfactory in these studies, a level of

36

uncertainty remained in the calibrated results, leaving predictions of salinity migration uncertain.

The uncertainty of a calibrated model leads to uncertainty in model predictions (Werner et al., 2013). The predictive performance of a calibrated model can be assessed by evaluating the sensitivity of the calibration dataset and model predictions to estimated parameters (Hill & Tiedeman, 2007). If model predictions are sensitive to the parameters that are poorly informed by the calibration dataset, there will be large uncertainties in model predictions. Uncertain predictions can be still useful for management purposes since they provide reasonable approximations of the real-world systems (Safi, Vilhelmsen, et al., 2018). However, it is imperative to analyze the uncertainties with model predictions when they are used for decision support (Vilhelmsen & Ferre, 2017).

Table 2-2 Reported studies related to inverse modeling of SWI

Reference	Uncertain parameter	Observation type	Note
Post et al. (2018)	Horizontal and vertical hydraulic conductivities, porosity, horizontal longitudinal, vertical longitudinal, and transverse	Head	Parameters were estimated using zonal calibration with extensive observation data points.
Baalousha (2016)	Hydraulic conductivity	Head	Spatial heterogeneities in hydraulic conductivity was parameterized using 1,500 pilot points representing hydraulic conductivity ranging from 0.1 to 200 m/days in the regional-scale coastal aquifer of Qatar.
Nofal et al. 2015	hydraulic conductivity, recharge and dispersivity values	Head and salinity	Parameters were estimated using zonal calibration manual calibration.
Langevin and Zygnerski (2013)	Hydraulic conductivity	Head	Spatial heterogeneities in hydraulic conductivity was parameterized using an irregular distribution of pilot points with a high density of points near the pumping wells and an ordinary kriging with an isotropic exponential variogram.
Lu et al. 2013	hydraulic conductivities, specific and yield storage, diffusion coefficients,	Flow, head and chloride concentrations	Flow observations were used to calibrate the transport parameters while head and concentration observations were used to estimate hydraulic properties of aquifer. Parameters were estimated using zonal calibration. During calibration vertical hydraulic conductivity was estimated as 10% of the horizontal hydraulic conductivity and the horizontal longitudinal dispersivity was set as 10% of the transverse hydraulic conductivity.
Walther et al. 2012	Hydraulic conductivity, upstream inflow, and aquifer extraction	Steady-state head	PEST was used for parameter estimation. The ranges of hydraulic conductivity upstream inflow, and aquifer extraction were set 1.1%–1000%, 5%–500%, and 0%–400%, respectively.
Sherif et al. 2012	Hydraulic conductivity and specific yield	Transient head	Limited available data about the chloride concentration collected at a distance of about 5km from the shoreline was used to validate the calibrated results.
Rasmussen et al. 2012	Vertical hydraulic conductivity of the clayey till, horizontal hydraulic conductivity of the sand and the upper chalk layer, and hydraulic conductivity near the drains.	Transient head	The calibrated model was validated against geochemical and geophysical data from borehole logs and an airborne transient electromagnetic survey. They found that the calibrated results cannot be improved significantly by further calibration due to the lack of enough transient head data, groundwater abstraction at the level of waterworks, and homogeneity assumption.
Sulzbacher et al. 2012	Hydraulic conductivity	hydraulic, hydrological and geophysical data, spatial HEM, local monitoring data	A good agreement was observed between measured and computed hydraulic heads, total dissolved solids data for both the entire freshwater lens on a large scale and in the area of the well fields on a small scale.
Herckenrath et al. (2011)	Hydraulic conductivity	Head	Spatial heterogeneities in hydraulic conductivity was parameterized in a synthetic model of Henry's problem.
Sanz and Voss (2006)	Hydraulic conductivity, freshwater inflow, molecular diffusivity, and porosity	Head, salinity and flow	Hydraulic conductivity and freshwater inflow were estimated from only pressure or concentration observations. Hydraulic conductivity, freshwater inflow, solute molecular diffusivity, and porosity were estimated using observations of only the logarithm of concentration.

2.4.2.2   Stochastic modeling

Past efforts in the uncertainty analysis of SWI predictions revealed that uncertainties with input parameters can highly affect the knowledge gained from modeling of the current and future states of salt/fresh water interface (Herckenrath et al., 2011). Prediction uncertainties were mainly evaluated in response to uncertainties with hydraulic conductivity, groundwater pumping rates, recharge rate, SLR, and temperature (Table 3). Several studies showed that the prediction of SWI is affected more by groundwater abstraction rate than by any other source/sink parameters (Loaiciga et al., 2012; Felisa et al., 2013; Stratis et al., 2016). Moreover, the uncertainties with climate change processes (e.g. SLR) have negligible impact on SWI predictions compared with the impact of uncertain groundwater abstraction rates (Zhao et al., 2013). Others reported that the uncertainties with the hydraulic conductivity can produce large uncertainties in SWI predictions (Lecca & Cau, 2009; Herckenrath et al., 2011; Pramada & Mohan, 2015). Interestingly, the uncertainties with both the hydraulic conductivity and pumping rates have similar impacts on SWI (Kerrou et al., 2013). The uncertainty with the spatial distribution of hydraulic conductivity however has more impact than that of pumping rates (Kerrou et al., 2013).

The main challenge with a groundwater model is hence to quantify prediction uncertainty while maintaining a good fit with observed field-data (Keating et. al., 2010). Guillaume et al. (2016) argued that the model prediction should involve exploration of alternative systems in the hope that one may represent the real-world system sufficiently. Moore and Doherty (2005) indicated that the model predictions of a groundwater system always contain errors particularly those that depend on the hydraulic conductivity. Extensive efforts were dedicated to provideg estimates of prediction uncertainty in a groundwater model by evaluating

the uncertainties with the spatial heterogeneity in hydraulic conductivity (e.g. Liu et al., 2007; Sidiropoulos & Mylopoulos, 2015; Peña-Haroa et al., 2011). Sanchez-Vila et al. (2006) provided a review of methods to estimate the spatial distribution of hydraulic conductivity in heterogeneous aquifers. They indicated that many possible solutions for hydraulic conductivity should be suggested to obtain a solution that can represent the geology of an aquifer reasonably well. These solutions are used to produce a range of predicted values. Herckenrath et al. (2011) represented the variability of the predicted values of SWI in response to spatial variabilities of hydraulic conductivity by a probability distribution function with a mean that provides an approximation to the prediction of minimum error variance, and a standard deviation that characterizes the uncertainty of the model prediction.

The methods for stochastic modeling of groundwater systems have been reviewed (Dagan, 2002; Li et al., 2003). At present, the most popular and feasible uncertainty analysis techniques in groundwater modeling are based on Monte Carlo (MC) simulation (JiChun & XianKui, 2013) that allows evaluating and quantifying prediction uncertainty in highly heterogeneous systems (Dagan, 2002). Examples of such MC-like techniques include the Markov Chain Monte Carlo (MCMC) methods (Harvey & Gorelick, 1995), the generalized likelihood uncertainty estimation (GLUE) (Beven & Binley, 1992), calibration-constrained Monte Carlo methods (Tavakoli et al., 2013; Kitanidis, 1996; Woodbury & Ulrych, 2000; Carrera et al., 2005), and the null-space Monte Carlo (NSMC) method (Tonkin & Doherty, 2009). Using these techniques leads to generating a range of predictions obtained using random realizations that each allows the model outcomes fit reasonably well to field measurements. Random realizations are generated from a prior probability distribution that is ideally determined from expert knowledge of the system state. by generating a range of predicted values obtained

using different parameter sets that each allow the model to match the observation data sufficiently well (multiple calibrated fields).

The applications of MC-like techniques are limited in SWI modeling, and hence their limitations, controlling factors, computational demands, and required prior information are not fully known. Zeng et al. (2016) evaluated the pollution risk of a groundwater source field in a shallow coastal aquifer (thickness of <20m). They used MCMC to quantify uncertainties with the prediction of Chloride concentration obtained from a SEAWAT model, and DREAM(ZS) as a sampling algorithm. Although their findings demonstrated the applicability of MCMC in SWI systems, the small range of parameters used for uncertainty analysis (e.g. hydraulic conductivity of 0.1 to 20m/day) and assumption of aquifer homogeneity seem to severely reduce the model run-time. Lacca and Cau (2009) used MC simulation to quantify the impact of the heterogeneity on the salinity dispersion process in a confined aquifer. They used a Gaussian distribution to create random fields of log hydraulic conductivity using HYDRO_GEN code (Bellin & Rubin, 1996). Similarly, Pramada and Mohan (2015) used MC simulations to evaluate the uncertainties with the prediction of the penetration length of the interface due to uncertainties with heterogeneity in the hydraulic conductivity. They created random fields of the log hydraulic conductivity using a Gaussian distribution with the mean and standard deviation obtained based on the calibration results. The range of hydraulic conductivity (i.e. heterogeneity) was however very small (~53 to 65m/day), which resulted in a fast model convergence. Rajabi and Ataie-Ashtiani (2014) attempted to decrease the simulation time of MC simulation for a SWI system by changing the sampling strategy. They illustrated that the use of optimized Latin hypercube sampling strategies instead of the simple random sampling and Latin hypercube sampling strategies can significantly reduce the computational demand of a MC simulation in a SWI

system. However, their work was limited to the application of the Henry problem. In actual applications, the large run-times of (particularly transient) SWI simulations make additional computational burden to the MC simulation. Rajabi et al. (2015) further proposed the use of non-intrusive polynomial chaos expansions as a means to accelerate MC uncertainty analysis in SWI predictions in highly non-linear systems.

Previous studies indicate that the use of MC-like techniques for uncertainty analysis of SWI prediction is prohibitively time consuming in highly parameterized systems due to long model runtime, large number of required model-runs, and the mathematical complexities of inverse methods (Herckenrath et al., 2011). Compared with other MC-like techniques, the NSMC method is less demanding computationally (Tonkin & Doherty, 2009). In this method, a set of random parameter fields is generated from a prior probability distribution using e.g., Sequential Gaussian Simulation (SGS) method. The expected value and the spatial covariance function (or semivariogram) of the distribution are determined from prior information or from the calibrated results of a pilot-point model. The random fields are projected onto the null-space and adjusted through model re-calibration. The calibration-constrained fields are then used to compute model predictions (for details see Tonkin & Doherty, 2009). Among the limited applications of NSMC in SWI modeling, Herckenrath et al. (2011) used this methodology to generate calibration-constrained fields of the hydraulic conductivity for quantifying uncertainties with the prediction of the penetration length of the interface in a synthetic case (Henry problem). They found that the estimated uncertainty of the model prediction using the NSMC was slightly smaller than that calculated using the linearized method. In their study, the random fields were generated from a known lognormal distribution (i.e. detailed prior information) using SGS. Such detailed prior information is not usually available in a real aquifer system. Moreover, although

42

NSMC has computational advantages over other MC-like techniques, it also requires a detailed prior probability distribution, and does not account for impression pertaining to prior information during the randomization process.

Our review of the existing MC-like techniques reveals that all the techniques require a geologic prior information to infer the required statistics for MC simulations. Such detailed prior information involves the specification of an expected field value (i.e. mean values of starting points) and a covariance function (or semivariogram) of the parameter distribution. The choice of the expected field value, and/or the variogram type (spherical, exponential, or Gaussian) and parameters (nugget effect, sill, and range) can influence strongly the estimated range of the prediction uncertainty (Bardossy et al., 1990). Such prior information is typically prone to uncertainty in many coastal aquifers. Fuzzy set theory can provide an intuitive approach to the quantification of imprecision pertaining to prior information (Zadeh, 1965). In this theory, a real scalar value corresponding to an imprecise parameter changes into a set of fuzzy values using a fuzzifier (or membership function) that can be defined based on the limited (rough) knowledge of the system (for details see e.g. Bardossy et al., 1990). Although the application of fuzzy set theory has been demonstrated in various fields of science (Sunitha & Mathew, 2013), it has not received enough attention in SWI modeling. Rajabi and Atae-Ashtiani (2016) used a fuzzy (MCMC) Bayesian inference to incorporate imprecise prior information into the prediction uncertainty analysis. Zhao et al. (2013) evaluated the prediction uncertainty of a SWI system by introducing longitudinal and transverse dispersivity coefficients as two fuzzy numbers and hydraulic conductivity as a randomly generated parameter.

While few studies were reported to analyze and reduce SWI prediction uncertainties in actual case studies, a large level of uncertainty has often been common (e.g. Zhao et al., 2013;

Rajabi & Atae-Ashtiani, 2014; Zeng et al., 2016). Large uncertainties in model prediction may cause undesirable management decisions (Werner et al., 2013). To avoid such situations, it is imperative to constrain prediction uncertainty when a model is used for decision support. This can be done by additional monitoring in order to increase the reliability of conceptual models (Safi et al., 2018b).

Table 2-3 Reported studies related to stochastic modeling of SWI and methods applied to quantify prediction uncertainties

Reference	Uncertain parameter	Note
Stratis et al. (2016)	Pumping rate	Impact of parameter uncertainty on the model prediction was analyzed using the ALOPEX stochastic optimization algorithm (Harth and Tzanakou 1974) coupled with Gyben-Herzberg equation.
Zeng et al. 2016	Hydraulic conductivity	MCMC was used to quantify uncertainty with the prediction of Chloride concentration in monitoring wells.
Pramada and Mohan (2015)	Hydraulic conductivity	Uncertainty with the prediction of the penetration length of interface was analyzed using Monte Carlo method in a two-dimensional SWI case study
Rajabi and Atae-Ashtiani 2014	Hydraulic conductivity	Several strategies were evaluated to reduce the computational time of MCMC in SWI uncertainty analysis.
Felisa et al. 2013	Pumping rate, wells distances for the coastline, and the distance between wells	The impacts of uncertainties with parameters on the prediction of salinity were analyzed in the vegetation capture zone.
Zhao et al. 2013	SLR, different amplitudes of tide, seasonal variance of influx, annual variance of the pumping rate	The impacts of uncertainties with drivers of SWI, and combinations of different parameters were analyzed.
Kerrou et al. (2013)	Pumping rate and hydraulic conductivity	Impacts of uncertainties with pumping rate and hydraulic conductivity on the model prediction were analyzed separately and jointly.
Loaiciga et al. 2012	Groundwater abstraction and SLR	A linear uncertainty analysis was used to evaluate the impacts of drivers for SWI on the intrusion.
Herckenrath et al. (2011)	Hydraulic conductivity	Uncertainty with the prediction of the penetration length of interface was analyzed using NSMC in a synthetic case (Henry problem).
Naji et al. 1999	Geometry	Prediction uncertainty was analyzed using a combination of several uncertainty analysis techniques.
Lecca, P. Cau. 2004	Aquitard conductivity	Uncertainty with the prediction of salinity was analyzed using MC simulation in a multi-layered coastal aquifer.
Lecca and Cau 2009	Hydraulic conductivity	Uncertainty with the prediction of the penetration length of interface was analyzed using Monte Carlo method.

2.4.2.3 Data acquision strategy

Monitoring involves designing a strategy and methods for the most effective field surveys towards obtaining the most reliable data for improving conceptual models. Data should be ideally collected in all spatial directions for creating or improving a 3D SWI model. In reality, financial constraints and/or spatial limitations often reduce the ability to directly measure/collect data (Hartmann, et. al. 2014). Using inverse modeling, the value of a parameter can be estimated using the value of an indirect observation data, e.g. measurements of hydraulic head, flow and/or salinity concentration (Hoeksema & Kitanidis, 1984). Dausman et al. (2010) argued that measuring salinity concentration at depths is important to understand the movement of interface. Salinity should be collected close to interface, and mainly from the deep parts of an aquifer. Hemond and Fechner (2013) recognized the hydraulic head as the most common type of observation data that is used to estimate hydraulic properties. Both head and salinity concentration data can be monitored using observation wells or nearby existing supply wells (Sen, 2015). In practice, the sampling locations and type of additional data are often determined based on expert opinion (Vilhelmsen & Ferre, 2017). However, there is no guarantee that sampling locations can contribute to optimal reduction in uncertainties, particularly over a 3D heterogeneous domain. Given the high cost of data collection, it is imperative to identify the precise locations for monitoring data using an optimal design (OD).

In this context, several OD methods have been reported to guide the hydrogeological field-investigation (Tiedeman et al., 2003; Reed et al., 2000; Cieniawski et al., 1995; Wagner, 1999; Andricevic & Foufoula-Georgiou, 1991; Loaiciga 1989; Rouhani & Hall, 1988). Wagner (1999) developed an optimization method to minimize uncertainties in model predictions for designing a sampling network within the context of groundwater management. A cost design algorithm to guide data collection to reduce uncertainties in

model predictions was developed using Kalman filters by Rizzo et al. (2000) and Kollat et al. (2011). Tiedeman et al. (2003) presented a statistical approach (value of improved information statistic) to identify parameters most important to model predictions and Tiedeman et al. (2004) developed another statistical approach (observation-prediction statistic) to assess the impact on model predictions by adding or removing observations. Moore and Doherty (2005) and Christensen and Doherty (2008) developed a method that can be used to evaluate the influence of adding a new observation well to an existing calibration dataset on the predictive performance by calculating the variance of prediction uncertainty/error. The main advantage of this method is that the actual values of observations are not used in the OD; hence, observations can be existing or future observations (Wöhling et al., 2016). In this method, the "worth" of adding a new observation (subsequently referred to as data worth (DW)) to the existing calibration dataset is determined by either (1) starting with no observation and then adding an observation one at a time (Wöhling et al., 2016), or (2) beginning with a large set of (synthetic) observations and then removing observations one at a time (Vilhemson & Ferre, 2017). Further extensions of the DW-based OD include the selection of multiple observations (Walis et al., 2014) with different types (Wöhling et al., 2016) targeting uncertainty reduction in multiple prediction variables (Vilhemson & Ferre, 2017). Recently, Safi et al. (2018b) carried out yet another extension to optimize the allocation of observation wells that effectively measure multiple hydrogeological data at different depths. They used Bayesian model averaging to account for non-linearity and genetic algorithms to conduct a location search for new sampling locations in 3D systems. Past efforts have resulted in designing monitoring networks to sample groundwater quality for different objectives such as minimizing the variance of model prediction (Asefa et al., 2004; Nunes et al., 2004a, 2004b; Herrera & Pinder, 2005; Ammar et al., 2008; Chadalavada & Datta, 2008; Dokou & Pinder, 2009; Chadalavada et al., 2011), detecting contaminant

37

concentration (Montas et al., 2000; Reed et al., 2000, 2003; Reed & Minsker, 2004; Kollat & Reed, 2007; Kollat et al., 2008), and minimizing mass of contamination (Montas et al., 2000; Reed & Minsker, 2004; Wu, 2004; Wu et al., 2006; Kollat & Reed, 2007).

Despite numerous OD studies in groundwater modeling, the OD has rarely been examined in the context of SWI systems. Dhar and Datta (2009) developed a methodology for monitoring of SWI based on the minimization of the sum of normalized absolute deviations between the computed concentration and a targeted concentration corresponding to a management strategy. This is realized by constraining the computed concentration using the inverse distance weighted (IDW) interpolation method. Shoemaker (2004) demonstrated that head and salinity observations should be located close to the toe of the interface. Flow observations are effective in areas near the coastline where ground water is discharged to Sea. Dausman et al. (2010) applied the DW-based OD on the Henry problem to define the optimal locations of salinity concentration and temperature that would reduce uncertainty with the prediction of the displacement of salt/fresh water interface. Their work was however limited to a two-dimensional case, and a single observation well. The findings of Safi et al. (2018b) highlighted the importance of considering three-dimensionality in the design of a monitoring network for SWI systems. They concluded that the worth of collecting head and salinity measurements to reduce uncertainty of interface prediction depends mainly on their spatial distance from the shoreline although the depth of measurement is important.

2.5   Existing gaps and future needs

Despite more than a century of research in the modeling of SWI, much remains in terms of improving the predictive performance of SWI models that are used as decision support tools for management purposes. The literature indicates that the greatest shortfall in research on SWI modeling is the lack of uncertainty analysis studies. We provide below a

framework towards increasing the reliability of SWI models and enhancing their predictive

performance (Figure 2-6).
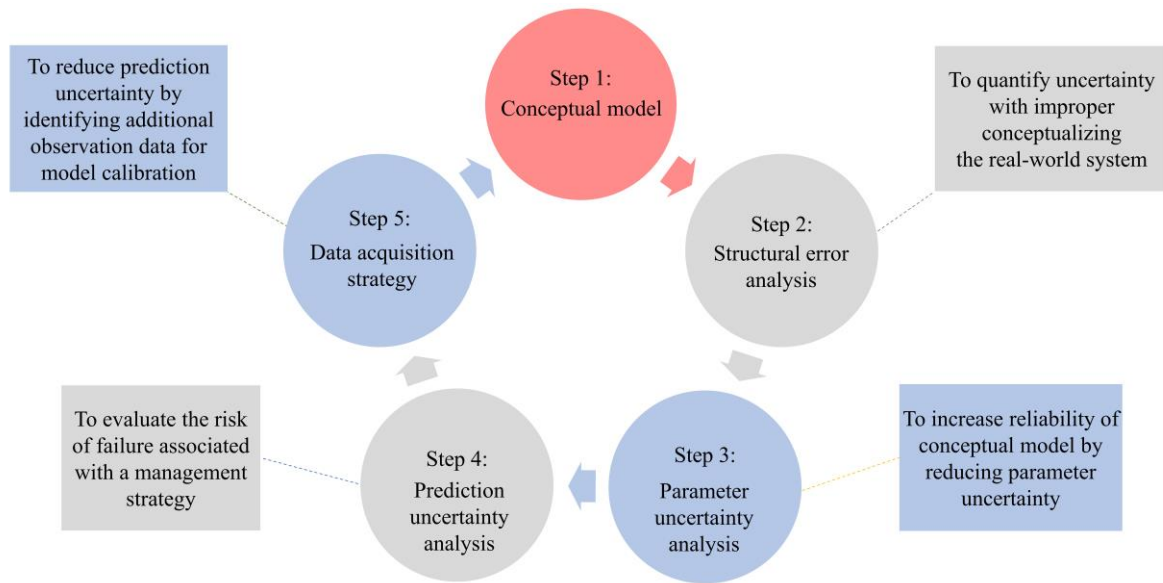
Figure 2-6 Proposed framework for enhancing the performance of SWI models for management purposes

We relate the main scientific challenge in SWI research to the application of

knowledge gained from SWI models into management practices (Figure 2-7a to Figure 2-7e

and Table 2-4). The number of research papers that use SWI models as decision support tools

is growing at an ever-increasing rate. The main issue concerning the proposed conceptual

models in these papers is the overconfidence of modelers to consider a single conceptual

model for a SWI system. While multi-model methods have been frequently used to account

for structural errors in the conceptual models of groundwater systems, their applications in

SWI modeling is limited to a few studies (e.g. Chitsazan et al. 2015) (Figure 2-7a). More

research is needed to recognize and combine multiple competing models representing

different types of seaside boundary condition, number of geologic layers, bottom elevation of

aquifer, aquifer geometry, fracture and fault orientation, conduit characterization methods,

and initial salinity profile in the system. The impacts of different statistical criteria for

weighting alternative conceptual models on the predictive performance of a SWI model should be also investigated.
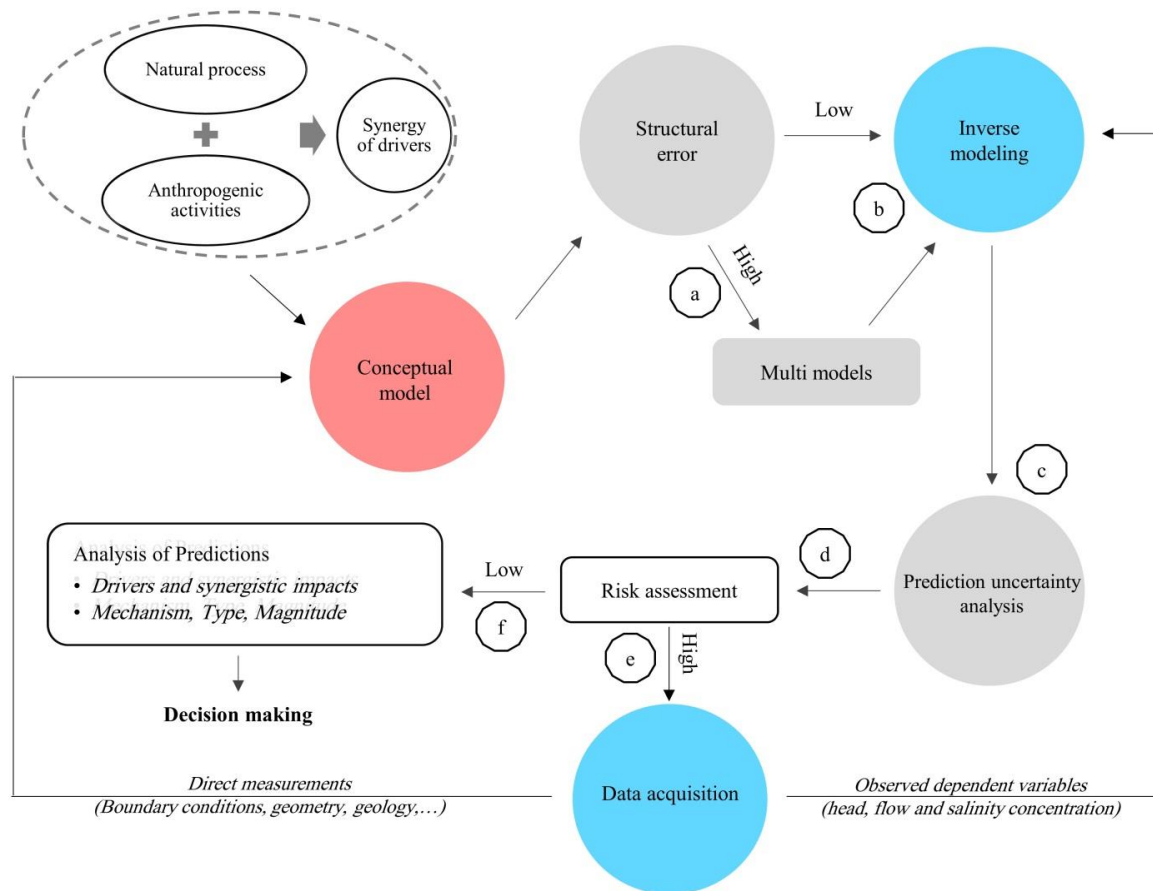
Figure 2-7 Proposed modeling/management framework for improving and applying the knowledge gained from modeling into management practice

Our review of literature showed that a concern regarding the structural error is related to its impact on the calibration results and prediction (Figure 2-7b and Figure 2-7c). In this context, perhaps the main research gap is to evaluate the impacts of geologic simplification and vertical mesh refinement on the calibration and prediction of the mixing zone (Figure 2-7b). For example, the predicted results gained by using a zonal calibrated model can be compared with those obtained using a pilot point parameterized model with coarse/fine and/or regular/irregular pilot points distribution over a geologic domain. The impact of vertical discretization or grid refinement along the coast on the resolution of the computed mixing zone should be further explored through a sensitivity analysis.

Table 2-4 Future needs for prediction uncertainty analysis and decision making in SWI modeling

Element	Future need
Structural error	– Use of multi-model methods for analyzing errors in conceptualizing boundary and initial conditions, aquifer geometry, and geologic structure
	– Impact of structural error on the calibration results and model predictions
	– Impact of grid refinement on the model predictions
Inverse modeling	– Required type of observation data for model calibration
	– Evaluating possible correlations among calibration parameters that are estimated using the same type of observation
	– Variable-density model inversion
	– Computational demand of SWI model inversion in highly heterogeneous coastal aquifers
	– Application of regularization mechanism on the calibration results in highly heterogeneous coastal aquifers
Stochastic modeling	– Incorporating parameter uncertainty and imprecision in its prior information simultaneously into the prediction uncertainty analysis
	– Computational demand of SWI prediction uncertainty analysis due to including many uncertain parameters
	– Application of NSMC to real-world highly heterogeneous case studies
	– Application of MC-like techniques to deep coastal aquifers
	– Impact of large prediction uncertainties on decision making
Data acquisition	– A cost-effective methodology to guide field-data collection in coastal aquifers
	– Considering three-dimensionality and model non-linearity during the network monitoring design
	– Design a monitoring network for multi observation types and multi prediction variables
SWI predictions	– Understanding the dynamics of SWI in response to the synergy of its drivers
	– Understanding the mechanisms and type of SWI in real-world case studies
	– Examining opportunities for adaptation plans in SWI systems
	– Evaluating the effectiveness of management plans in alleviating SWI

Comprehensive modeling efforts to analyze and reduce parameter uncertainties are a key factor for future research in modeling of SWI (Figure 2-7b). A comprehensive research is lacking to determine the impact of each type of common observed data (e.g. temporal and steady state head and salinity concentration, flow, width of interface, etc.) on the estimation of parameters in a SWI model during model inversion. While a few studies have been dedicated to assess the impacts of various types of observation data on the estimation of SWI parameters, much remains to evaluate the correlations that are incurred between the calibration parameters (e.g. diffusion, storativity, hydraulic conductivity, recharge, etc.) due to the use of a specific observation type (e.g. head, salinity or flow) as well as the impact of these correlations on the predictive performance. Such knowledge will aid in effectively optimizing model parameters using an available calibration dataset.

Limited attempts have been dedicated to the parameter estimation of highly heterogeneous coastal aquifers through the application of pilot point parameterization

approach (Figure 2-7c). In this context, the impact of increasing/decreasing the density of pilot points within the mixing zone or near pumping wells on the model prediction has not yet been evaluated. The main reason for lacking such studies is the high computational demand of SWI model inversion in highly parameterized systems. Much effort is needed to improve the computational burden of SWI inversion, for example, through code parallelization. Moreover, the application of regularization mechanisms is very limited in SWI model inversion, and thus their impact on the reduction of prediction uncertainty is not fully known. When using SVD, the computed model prediction is reliable only if the starting values of the null-space located pilot points that are critical to prediction reflect reasonable estimate of the real-world geologic system. Initial values are typically assigned based on prior information (Doherty et al., 2010). In cases where the prior information is imprecise, the computed model prediction may not encompass the truth. Research is needed to evaluate the impact of improper initializing the pilot points on the uncertainties with the prediction of SWI.

A large body of knowledge has been accumulated by developing, reviewing and applying methods for analyzing groundwater prediction uncertainty in the past thirty years. Prediction uncertainty associated with a SWI model has been rarely quantified (Figure 2-7c), and thus management decisions are often made without consideration of the failure risks associated with a management strategy that is evaluated using the uncertain modeling results (Figure 2-7d). More and more case studies are needed to understand the impacts of parameter uncertainties induced by field-data deficit on the predictive performance of a SWI model in different geological settings using the existing techniques (i.e. MC-like techniques). The uncertainty analysis of SWI prediction meets significant challenges including higher requirements for convergence tolerance, mesh refinement to increase vertical resolution of the transition zone, high computational demand for simulating SWI especially in large scale

coastal aquifers, and lack of prior information to infer the required statistics (Kerrou et al. 2013; Zhao et al. 2013). Moreover, combining all sources of parameter uncertainties such as abstraction rates, hydraulic conductivity, boundary condition, etc., requires additional computational loads, which makes it impossible to perform a prediction uncertainty analysis (Kerrou et al. 2013).

Our review of existing prediction uncertainty analysis methods (e.g. NSMC) revealed that there is still room for criticism and improvement of these techniques for their application to SWI modeling in the real-world systems (Figure 2-7b). Existing methods fall short of simultaneously incorporating parameter uncertainty and imprecision in its prior information into the prediction uncertainty analysis (Figure 2-7c). There is a host of future opportunities to develop further methodologies that provide flexibility concerning required prior information, computational demand, and degree of aquifer heterogeneity. Such methodologies can be particularly useful to quantify prediction uncertainty in deep coastal aquifers because the estimated prediction uncertainty can be highly dependent on prior information from the deep geologic layers, for example prior information about an expected field value and/or covariance function. Such prior information is typically imprecise in many heterogeneous aquifers. Limited to no attempt has been made to analyze the impact of the imprecision pertaining to geologic prior information on the estimated range of uncertainty with the predictions of SWI (Figure 2-7c). This is an area of worthy further investigation because many coastal aquifers worldwide lack hydrogeological data about their deep layers where the interface is often located.

Mathematical modeling has been rarely used to design field-investigation in SWI studies (Figure 2-7-d). Limited previous OD studies for a SWI system are based on two-dimensional examples such as the Henry problem or linear models. An exception is the study by Safi et al. (2018b). Although those investigations provide insights into the development of

mixing-zone, the application to field conditions requires further consideration of three-dimensionality in future field measurements and field-scale heterogeneity. Moreover, there are potentially significant improvements to be made from evaluating the influence of various types of measurements (e.g. hydraulic conductivity, hydraulic head, and salinity concentration) on the uncertainty reduction of SWI predictions. In addition, the applications of the existing design methods (e.g. DW-based OD) are largely restricted to steady-state field-measurements due to the short model runtime required to simulate steady-state simulations. Research is needed to identify the locations of observation wells with transient measurement in SWI systems.

Further research is needed to evaluate the impacts of prediction uncertainties on management decisions that are made based on modeling predictions (i.e. risk assessment) (Figure 2-7d). For example, input model parameters corresponding to the anthropogenic activities (water consumption, population growth rates, land-use change and urbanization) and climate change (precipitation, temperature and SLR) are typically prone to uncertainty (Werner et al. 2013). Their impacts on SWI should be examined by analyzing the dynamic of SWI in response to uncertainties with these input parameters (Safi et al. 2018a). While coupling anthropogenic activities and natural stressors has a synergistic effect that aggravates the intrusion beyond the sum of the individual impacts (Safi et al. 2018a), the magnitude of their synergistic impacts has been rarely evaluated in SWI studies (Figure 2-7f). The impacts of anthropogenic activities on the timing and magnitude of climatic cycles and events should be further explored. Equally important is to assess the impact of climate change on increasing the impact of anthropogenic activities e.g., increasing the freshwater demands due to increased temperature.

A general understanding of SWI mechanism has been attained primarily by numerous applications of the Henry problem (e.g. Abarca et al., 2007). Well-documented

studies addressing the impacts of SWI drivers on the mechanism of SWI are however lacking for real case studies (Figure 2-7f). The occurrence of passive SWI in coastal aquifers has been widely documented in many research papers. However, the mechanisms of active and passive-active SWI are not fully understood and recognized using case studies (Werner 2016). Moreover, much of the reported literature in transient modeling of SWI focuses on the lateral displacement of salt/fresh water interface owing to a change in the inflow rate or groundwater abstraction. The controlling factors influencing the vertical mechanism of intrusion are not fully known.

The effectiveness of adaptation plans in alleviating SWI are limited to a few studies (Ergil, 2001; Fatoric & Chelleri, 2012; Georgpoulou et al.2001; Kaleris & Ziogas, 2013). More studies that critically evaluate the effectiveness of management plans in alleviating SWI are needed to reduce the gaps between SWI knowledge and management practice (Figure 2-7f). The potential role of planned adaptation strategies in alleviating saltwater intrusion should be further explored to inform policy making on sustainable management of urban coastal aquifers.

CHAPTER 3

STOCHASTIC MODELING OF SALTWATER INTRUSION IN HETEROGENEOUS COASTAL AQUIFERS UNDER FIELD-DATA DEFICIT: COUPLING NSMC WITH SGS AND FUZZY PARAMETER SETS

Abstract

This paper demonstrates an approach for a reliable quantification of the uncertainties associated with model predictions of saltwater intrusion in heterogeneous coastal aquifers for which the deep hydrogeological characteristics are poorly known. In this approach, a pilot point calibrated model is used to assess the sensitivities of calibration dataset and model predictions to model parameters. Based on the sensitivity analysis, the model parameters are subdivided into Subset (i) that is informed by the calibration dataset, subset (ii) that is poorly informed but to which the predictions are sensitive, and Subset (iii) to which both the calibration data and the predictions are insensitive. Subsequently, the Sequential Gaussian Simulation (SGS) is used to generate random realizations for subset (i), while Fuzzy SGS is used to generate realizations of subset (ii); subset (iii) parameters are not randomized but kept at their initial values. Fuzzy SGS is conducted using a wide range of fuzzy expected field values as well as a range of "sensible" fuzzy kriging variograms. The prediction uncertainty is finally assessed using the null-space Monte Carlo (NSMC) method that is used to recalibrate the generated random fields. The performance of the proposed method was examined using the SEAWAT model and data from a heterogeneous coastal aquifer with limited field-data. The estimated range of the prediction uncertainty was compared with the prediction uncertainty obtained using the traditional NSMC methodology with the SGS and a

single calibrated model. The estimated prediction uncertainty was more realistic for the proposed method than for the traditional methodology.

3.1 Introduction

Groundwater constitutes a main source of drinking water in many coastal urban areas in arid or semi-arid regions. In coastal aquifers, a transition mixing zone is formed at the saltwater and freshwater interface by maintaining the hydrostatic pressure between the two fluids near the coast (Paniconi et al., 2001). Prolonged decrease of the groundwater level will increase the landward encroachment of saltwater into the aquifer; this process is generally known as saltwater intrusion (SWI) (Bear et al., 1999). The extent of SWI is often driven primarily by an imbalance between groundwater abstraction and aquifer recharge caused by mismanagement or lack of regulatory enforcement (Sophiya & Syed, 2013). While anthropogenic activities, particularly groundwater abstraction, often play the major role in the encroachment of salinity, zones of high hydraulic conductivity (e.g. fissure zones) along the coast may intensify and expedite this process (Werner et. al., 2013), widen the saltwater-freshwater mixing zone, decrease the transition depth, and increase the potential for upward leakage of saltwater in groundwater wells near the coastline (Bear et al., 1999).

Enforcing a firm strategy that aims towards the protection of groundwater resources requires an adequate understanding and control of the SWI dynamics in response to drivers forcing the intrusion (Quevauviller et al., 2016). For this purpose, mathematical modeling of flow and solute transport in the subsurface environment can provide substantial information about the impacts of these drivers on the intrusion (Cobaner et al., 2012). Modeling requires the characterization of the subsurface environment and the definition of its hydrogeological properties by relying on considerable field data (Bakalowicz, 2005). If such data are not

available, inverse modeling can be used to estimate (calibrate) these properties and thereby improve the reliability of model predictions (Alcolea et al., 2006). For an effective SWI model inversion, it is important to identify parameters that affect the predictive performance of SWI as well as the type, number, and location of observed data (e.g. temporal and steady-state head, salinity concentration, flow, etc.) that can be used to estimate those parameters (Safi et al. 2018b). The hydraulic conductivity has been widely recognized as the main factor controlling the amount of saltwater entering an aquifer (Abarca et al., 2007). Often, it is estimated using observations of head, flow and/or salinity concentration in SWI systems (Rasmussen et al. 2012; Nofal et al. 2016; Post et al. 2018). The logarithm of salinity concentration can be used as an observed data for calculating porosity (Sanz and Voss 2006), while storage can be estimated using the observations of the transient head (Rasmussen et al. 2012). Freshwater inflow affects submarine groundwater discharge and similar to the hydraulic conductivity, it can be estimated using observations of head and salinity concentration (Sanz and Voss 2006). Dispersivity parameters are critical for evaluating the width of the mixing zone (Abarca and Clement 2010) and can be estimated using observations of salinity concentration along the depth and within the mixing zone (Shoemaker 2004; Dausman et al. 2010).

The performance of a calibrated SWI model is highly dependent on the quality and quantity of available observation data and how these data correlate to model forecasts (Safi et al. 2018b). One concern regarding available observed data is that they often contain measurement errors/noise, particularly for models representing pre-development conditions in a coastal aquifer (Walther et al. 2012). Ignoring large measurement errors force the input parameters to be adjusted to compensate for structural error during model calibration, potentially resulting in biased model predictions (Doherty et al. 2010). Another concern is that observation data are usually sparse in many coastal aquifers due to financial constraints,

spatial limitation and/or scale of the study area, for example in large-scale urbanized coastal

aquifers (Baalousha 2016). The use of sparse observation data often results in model

simplification (e.g., homogeneity assumption) during the calibration process. Case studies of

SWI with extensive observation data are rare. One of the few exceptions is the study of Post

et al. (2018) who estimated homogeneous hydraulic conductivity fields in a SWI model for

an island with detailed salinity concentration data. Similarly, Huizer et al. (2016) estimated

the homogenous hydraulic conductivity in a regional model for a Dutch coastal aquifer using

a large number of head and TDS concentration data. In these studies, heterogeneity in the

hydraulic conductivity was excluded from the calibration process. Kerrou and Renard (2010)

argued that heterogeneity in the hydraulic conductivity affects the penetration length of

interface in 3D systems, and thus its estimation is crucial for predicting the interface

displacement in heterogeneous coastal aquifers (Houben et al. 2017; Yang et al. 2018).

A review of various inversion techniques indicated that the pilot point

parameterization is a more physically representative approach for characterizing geologic

heterogeneity compared to the other methods (for details see Hendricks Franssen et al. 2009).

Several SWI studies have determined the spatial heterogeneity of hydraulic conductivity in

large-scale coastal aquifers using the pilot points parameterization approach (Sanford and

Pope 2010; Langevin and Zygnerski 2013; Baalousha 2016). In these studies, the number of

pilot points needed for a representative heterogeneous system was invariably much larger

than the number of available observations. After the calibration, the model outcomes fitted

reasonably well to field measurements. Moore and Doherty (2005) argued that even a

calibrated pilot point model with perfect correspondence between measurements and model

outputs can still exhibit a high level of parameter uncertainty when modeling a heterogeneous

aquifer. In this case, model calibration provides multiple plausible outcomes, indicating that

there will be uncertainty in model predictions (Ye et al., 1997). Large uncertainties in a

model prediction will limit its value towards the sustainable protection and management of water resources (Post, 2005).

Groundwater modeling efforts aim to explore and quantify the uncertainties of their predictions, while maintaining a good model fit to the observed field-data (Keating et al., 2010). Several Monte Carlo (MC)-like techniques have been developed for this purpose by generating a range of predicted values obtained using different parameter sets that each allow the model to match the observation data sufficiently well (multiple calibrated fields). Examples of such methods include the Markov Chain Monte Carlo (MCMC) methods (Harvey & Gorelick, 1995), the generalized likelihood uncertainty estimation (GLUE) (Beven & Binley, 1992), and calibration‑constrained Monte Carlo methods (Tavakoli et al., 2013; Kitanidis, 1996; Yeh et al., 1996; Woodbury & Ulrych, 2000; and Carrera et al., 2005). However, these methods can be prohibitively time consuming to apply for SWI modeling in highly parameterized systems due to long model runtime, large number of required model runs, and the mathematical complexities of inverse methods (Herckenrath et al., 2011).

Compared with the above methods, the null-space Monte Carlo (NSMC) method (Tonkin & Doherty, 2009) is less demanding computationally. In this method, a set of random parameter realizations is first generated from a probability distribution defined on the basis of prior information; for hydraulic conductivity the lognormal distribution is often used. The expected value and the spatial covariance function (or semivariogram) of the distribution are either determined from a-priori information or can be estimated from independent data through model calibration. The Sequential Gaussian Simulation (SGS) method can be then used to generate random fields (Tonkin & Doherty, 2009). The generated random parameter realizations are subsequently projected onto the null-space and adjusted through inexpensive re-calibration resulting in a set of stochastic realizations that respect the calibration

constraints. Finally, these realizations are used to produce model predictions (for details see Tonkin & Doherty, 2009).

The application of the NSMC for quantifying uncertainties with groundwater model predictions is limited. Keating et al. (2010) used a highly nonlinear groundwater model to compare the performance of the NSMC with the MCMC and reported that the two methods gave similar results. The NSMC has been rarely used in SWI modeling, and hence its limitations, controlling factors, and required prior information are not fully known. Herckenrath et al. (2011) made the only formal uncertainty analysis using the NSMC in SWI systems. They used SEAWAT on a synthetic case and generated stochastic realizations using the NSMC to represent the spatial variability of the hydraulic conductivity. The uncertainty of model predictions was estimated based on the stochastic realizations, and then compared with the prediction uncertainty calculated using linearized analysis. The estimated uncertainty of the model prediction was slightly smaller for NSMC than for the linearized method. In their study, the SGS was used to generate random fields from a known lognormal distribution for the hydraulic conductivity. In practice, expert knowledge does not usually derive precise prior probability distributions because the expected value and/or covariance function are usually poorly known from field measurements (Rajabi and Atae-Ashtiani 2016). In such cases, both uncertainty and imprecision exist simultaneously. In the present context, imprecision refers to the vagueness (or ignorance) in the prior information about an uncertain parameter. In the NSMC method, if the prior information is imprecise, the random fields can be generated as Fuzzy parameter realizations (Bardossy et al., 1990) that can be used in combination with the SGS to generate random fields, which is referred to as Fuzzy SGS in this study. To our knowledge, limited to no attempt has been made to combine Fuzzy parameter realizations with SGS for the NSMC analysis in groundwater modeling.

Despite the relatively early theoretical development of the Fuzzy set theory (Zadeh 1965) to cope with imprecise prior information, this theory has been rarely used in the prediction uncertainty analysis of SWI systems, and thus the imprecisions often omitted entirely from the analysis (e.g., Pramada and Mohan 2015; Kerrou et al. 2013; Lecca and Cau. 2004, 2009; Pool et al. 2015; Zeng et al. 2016; Michael et al. 2016). One of the few exceptions is the study of Rajabi and Atae-Ashtiani (2016) who proposed the use of fuzzy Bayesian inference based on MCMC for incorporating imprecision into the prediction uncertainty analysis. However, the application of their method was limited to homogeneous aquifer systems. The magnitude of the impact of the imprecision on the estimated range of uncertainty with predicting the interface is not known in heterogeneous SWI systems. In the coastal aquifers, the interface can be located in the deep geologic layers and thus its prediction is dependent on prior information from those layers. Compared with other hydraulic properties, the heterogeneity in hydraulic conductivity has been recognized as the main factor controlling the development of the interface in highly heterogeneous coastal aquifers because it can enhance the dispersion significantly (Abarca et al. 2007; Kerrou et al. 2013; Herckenrath et al. 2011). Therefore, its uncertainties can highly affect the prediction of the interface. Quantifying prediction uncertainties is important for modeling SWI in deep heterogeneous coastal aquifer systems, because their subsurface environment can be very complex to characterize, e.g. the presence of fracture zones. Such heterogeneity can seldom be identified from the available data, which usually calls for model simplifications during the calibration process, further influencing the quantification of uncertainties associated with the predictions of the interface movement.

To our knowledge, a formal analysis for estimating uncertainties in model predictions of SWI in deep heterogeneous groundwater systems has not yet been reported. As such, this study aims at providing an approach for quantification of uncertainties around SWI

model predictions in heterogeneous aquifer systems with limited hydrogeologic data and imprecise prior information. It combines the NSMC method with SGS and fuzzy SGS for uncertainty quantification. In what follows, we first explain the theory underpinning the proposed approach. Then, we define the SWI problem in deep heterogeneous coastal aquifer systems by presenting an actual SWI field example. Following that, the proposed approach is applied to the SWI example. Finally, we evaluate and discuss the performance of the proposed approach to quantify prediction uncertainties associated with the actual SWI example.

3.2 Methodology

The methodological framework (Figure 3-1) consists of sequential steps related to the modeling of flow and solute transport. The first step includes parameterization and subsequent parameter estimation. In the second step, a sensitivity analysis is performed to subdivide the parameter set into the three subsets depending on the parameter's influence on the simulations corresponding to either the calibration data or the predictions. Next, we generate a large set of calibration-constrained parameter realizations using an NSMC by combining unconstrained parameter subset realizations into a full parameter set realization (Tonkin & Doherty, 2009). Then the combined realization is projected onto the solution null space and the projected realization is recalibrated to fit the data. Finally, we quantify model prediction uncertainties by estimating predictions based on calibration-constrained realizations. The following explains each step in more detail.
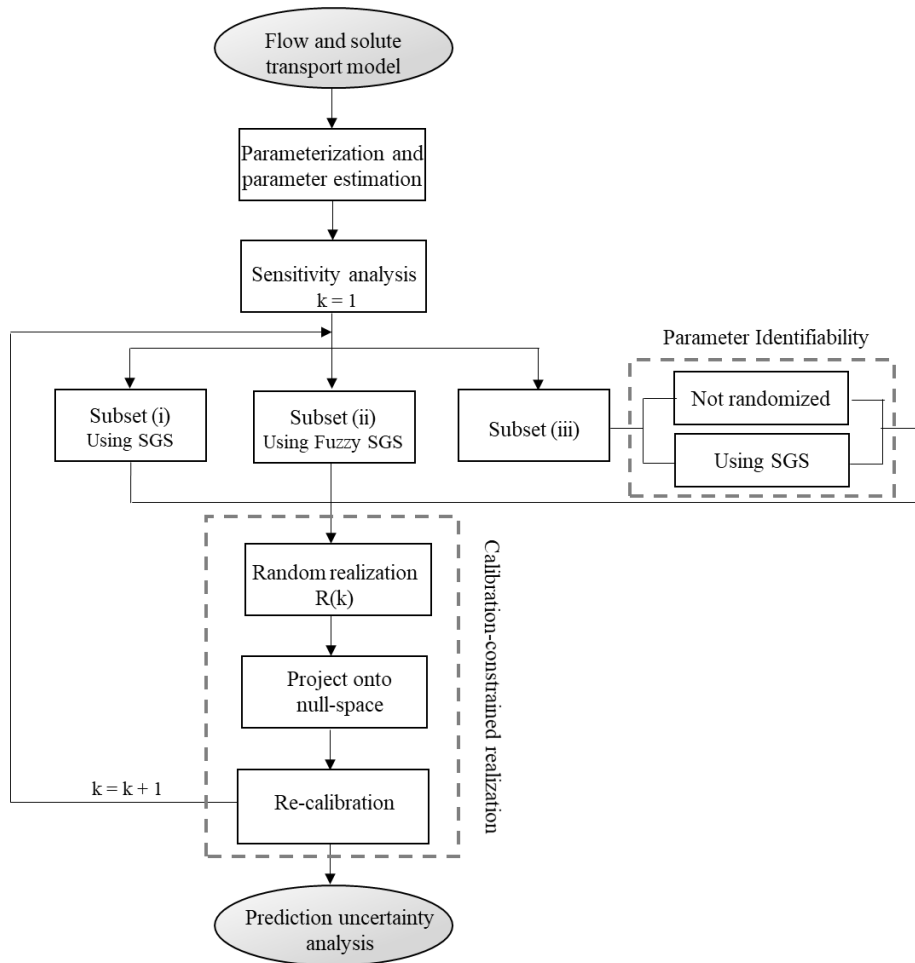
Figure 3-1 Methodological framework: K is the number of realizations, R(k) is the kth realization, and SGS stands for Sequential Gaussian Simulation

3.2.1 *Flow and solute transport model*

Past efforts resulted in the development of several codes providing numerical solutions for the flow and solute transport in porous media. Such codes are commonly used to predict SWI from sea/ocean into fresh groundwater in response to a change in recharge or groundwater abstraction. SWI models are generally categorized into either variable-density (e.g., Essaid, 1990; Oldenburg & Pruess, 1995; Guo & Langevin, 2002; Ye et al., 2016) or sharp-interface models (Mehdizadeh et al., 2014). The latter are based on the assumption that the width of the saltwater-freshwater mixing zone is much smaller than the thickness of the

aquifer. Therefore, freshwater and saltwater are assumed to be immiscible fluids separated by a sharp interface (Bakker et al., 2013). The variable-density approach considers the saltwater-freshwater interface as a wide transition zone due to strong hydrodynamic dispersion, which provides a physically better representation of SWI than the sharp interface approach (Huyakorn et al., 1987; Lu et al., 2009). The variable-density modeling approach is preferable when concentration data are to be used for calibration, and it is required if the model predictions are concentration dependent. The proposed methodology requires a SWI code that can simulate variable density flow and solute transport in a coastal aquifer. The most frequently used variable-density codes include SEAWAT (Guo & Langevin, 2002), SUTRA (Voss 1984), FEFLOW (Diersch 1996), FEMWATER (Lin et. al., 1996), MOCDENSE3D (Oude Essink, 1998), SWI (Bakker et al. 2013), FAST-C (Holzbecher, 1998), FEMFAT (Yeh et al. 1996), and CODESA-3D (Gambolati et al., 1999).

3.2.2 *Parameterization of heterogeneous hydraulic conductivity field*

In heterogeneous aquifers, the hydraulic conductivity can vary considerably over small distances and it often controls the flow pattern, velocity, and salinity migration (Boulding 1996; Murphy and Morrison 2002; Houben et al. 2017). Hence, the use of only a few zones to represent the hydraulic conductivity field may not represent the flow conditions adequately (Murphy & Morrison, 2002). The use of a highly parameterized model is therefore preferred to reduce the structural noise incurred by lumping real-world parameters (Doherty & Welter, 2010). As such, instead of using zones of constant value, the hydraulic conductivity field is controlled and estimated at a number of discrete-locations (so-called pilot points) distributed throughout each geologic zone by undertaking a spatial interpolation

from the pilot points to the model grid for a cell-by-cell parameterization (Doherty et al., 2010).

3.2.3 *Parameter estimation*

In highly parameterized models, the number of pilot points needed for a representative heterogeneous system is usually much larger than the number of available observations. In such cases, the solution of the estimation problem is non-unique. As such, parameter estimation must be stabilized by including one or more regularization mechanisms. For example, the Tikhonov Regularization can be used to minimize the parameters' deviation from the user specified preferred condition that is often defined from expert knowledge about the hydrogeological variability in the system (Doherty et al., 2010). Such variability is often expressed by an expected value and a covariance function (or a variogram). With the Tikhonov regularization, the pilot point values are estimated by minimizing an objective function representing both the misfit between computed and observed data (called model-to-measurement misfit) and the deviation from the preferred condition (Doherty, 1998).

Further constraints can be added to the inversion through truncated singular value decomposition (TSVD) of the normal matrix (for details see e.g. Doherty at al., 2010). Model parameter combinations that correspond to singular values larger than a user-defined truncation value are deemed to be estimable on the basis of a calibration dataset. These parameter combinations span the calibration solution space. In contrast, the inestimable parameter combinations span the calibration null space and retain their initial values during the calibration process. Hence, it is important that the initial values of such pilot points reflect physically reasonable values of the geologic system. Initial values are typically assigned either on the basis of expert knowledge of geology or through estimation of lumped

parameters on a global basis (i.e. zonal calibration) (Doherty et al., 2010). The latter is used in the following demonstration.

3.2.4   Sensitivity analysis - Definition of parameter subsets

The calibration results are subsequently assessed by computing the Composite Sensitivity (CS) of each pilot point parameter from the Jacobian matrix. Columns of the Jacobian matrix represent the model parameters, while the observations and predictions are identified by rows. The CS value quantifies the cumulative sensitivity with respect to a parameter of all simulated values corresponding to the calibration data (Doherty, 1998). A high or low CS value indicates that the calibration data inform well or poorly about the corresponding parameter value respectively. Similarly, the sensitivity of each model prediction is calculated with respect to each pilot point parameter. A high sensitivity indicates that the pilot point parameter is important to the prediction. The sensitivity results are then used together to subdivide the pilot point parameters into three subsets: *subset (i)* includes the parameters that are informed by the calibration data set, *subset (ii)* has the parameters that are poorly informed but to which a prediction is sensitive, and *subset (iii)* to which both the calibration data and the predictions are insensitive. This subdivision is used in the section 3.2.5.

3.2.4.1   Parameters correlation

The correlation among parameters from different subsets makes it difficult to include or exclude a specific parameter from a subset. This is because changes in one parameter (e.g., from subset (i)) can be offset by changes in other parameters (e.g., from subset (iii)). Although the CS provides information about the impact of calibration dataset on

the parameters, it does not account for the parameter correlation and the level of structural noise within a calibration dataset (Hunt et al., 2006). A statistic that incorporates parameter correlation (particularly helpful for use in highly-parameterized models) is parameter identifiability (Doherty and Hunt 2009). Parameter identifiability varies between 0 and 1 and is defined as the square of the cosine of the angle between a parameter and its projection onto the calibration solution space (Doherty 2015). A value of 1 indicates that a parameter is completely informed by the calibration dataset and the measurement noise is the only responsible term for any possible uncertainty with the estimation of that parameter (ideally *subset (i)*). Therefore, the deficit in the number of observations in the calibration dataset does not have an impact on the uncertainty of that parameter. An identifiability of 0 indicates that a parameter cannot be informed by the available observations due to the information deficit in the calibration dataset (e.g., *subset (iii)*). A parameter that has an identifiability between 0 and 1 is not unique. The information provided for that parameter by the calibration dataset is shared with other parameters (Doherty 2015). In this study, we calculated the identifiability of parameters using the IDENTPAR utility of PEST while setting the truncation value at 5.0E-6 (Doherty et al. 2010). The identifiability of parameters is used in following.

3.2.5   Calibration-constrained realizations using NSMC

A random realization of hydraulic conductivity is generated for each subset of pilot point parameters (Tonkin & Doherty, 2009). The generated realization for all subsets is then combined into a realization containing the full set of parameters. The combined realization is subsequently projected onto the solution null-space, and the projection is added to the set of calibrated parameter values. This parameter set is finally adjusted through model re-

calibration to respect calibration constraints and the process is repeated for a large number of combined realizations.

Subset (i) uses SGS to generate the corresponding parameter values. For SGS, the previously calibrated pilot point values are used to determine the mean hydraulic conductivity value, while a pre-defined (from expert knowledge) covariance function is used to generate correlated random noise that is added to the mean value to obtain the (unconstrained) subset realization values of subset (i). An alternative option for generating random fields is using the posterior covariance from the calibration based on the Schur Complement which is a linearized form of Bayes rule (e.g. the PREDUNC utilities in PEST) (see e.g., Fienen et al. 2010). Subset (ii) is generated similarly, except it uses fuzzy SGS to generate the parameter realization whereby 1) the mean is generated from a probability distribution that can for example be triangular, trapezoidal, or uniform; and 2) the noise is generated by using a fuzzy covariance function (e.g. from an exponential variogram) for which the range are generated from a distribution that can for example be Gaussian, triangular, trapezoidal, or uniform. In subset (iii), the parameter values are kept fixed at the initial values if they have low identifiability. Note that holding the parameter subset (iii) at starting values does not mean that they are known perfectly. They retain their initial values because they do not influence the model prediction and parameters of subset (i). If subset (iii) parameters have high identifiability, the parameter values are randomized using SGS (similar to subset (i)).

3.2.6   *Prediction uncertainty analysis*

The uncertainty of a prediction is finally quantified from the range of model-predicted (simulated) values obtained using the generated calibration-constrained realizations.

3.3 Problem statement: an example

3.3.1 Description of study site

The study site consists of a heterogeneous geologic structure underlying Beirut city and its suburbs (Lebanon), a highly urbanized metropolitan area recognized for water shortage challenges and high dependency on groundwater resources (

Legend

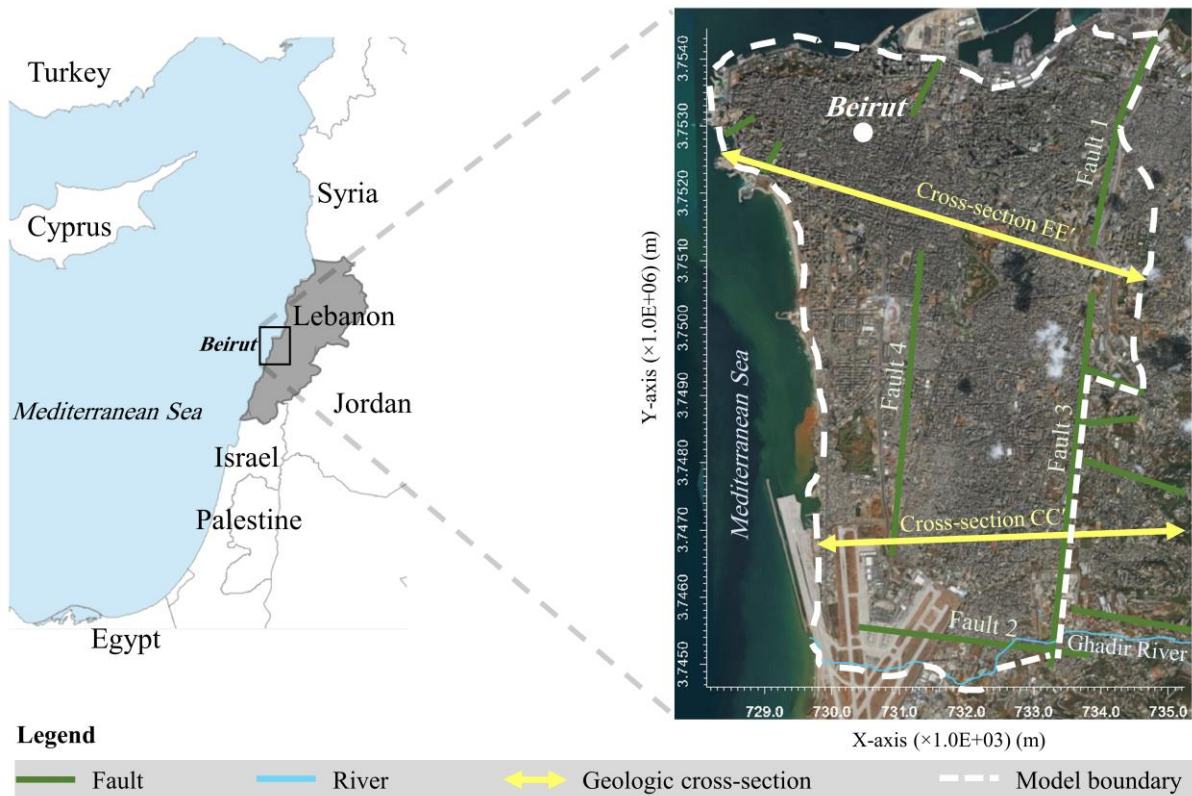| — Fault | — River | ⟷ Geologic cross-section | --- Model boundary |

Figure 3-2). The coastal aquifer stretches midway along the Eastern Mediterranean with 16.5 km of diverse shorelines including rocky beaches, sandy shores and cliffs, covering an area of ~48km^2. It is bounded by the Mediterranean Sea to the west and north, by two faults and an aquitard to the east, and by a fault and a river to the south.
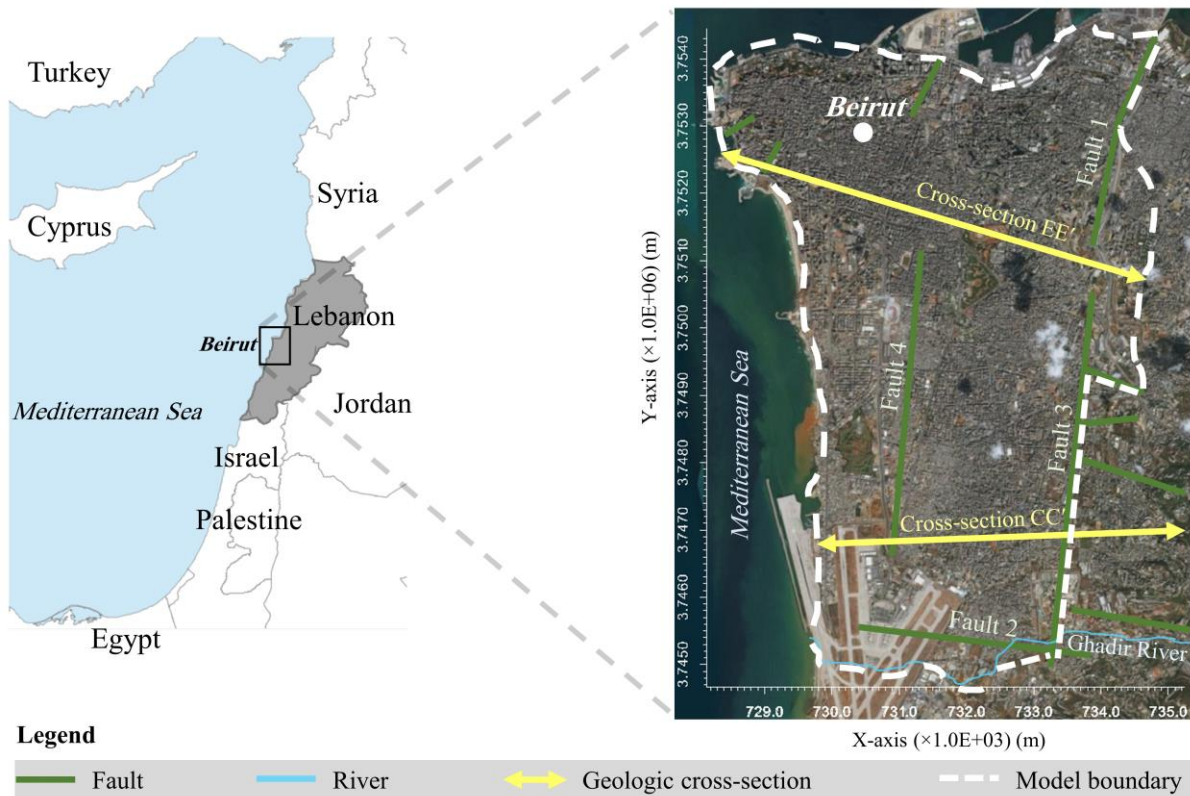
Figure 3-2 Location and surface geology of the pilot aquifer

The exposed rocks in the area are of Cretaceous and Quaternary ages with pockets of Tertiary deposits (Peltekian, 1980). The Cenomanian-Quaternary (carbonates-unconsolidated alluvial plain deposits) formations constitute a ~700m thick aquifer/aquitard system, consisting mainly of hard and compact limestone and dolomite with chert and marl intercalations (Khair, 1992). The aquifers are characterized by a relatively high transmissivity but low storativity, particularly in the Cenomanian formations. The infiltration rates can be high due to the presence of weak or partial cementation between grains of sand and poorly consolidated conglomerates in the quaternary deposits allowing for moderate permeability (Khair, 1992). It is likely that recharge has gradually decreased from 30% in 1969 (Ukayli, 1971) to near nil in 2018 due to urban sprawl (Safi et al., 2018a). The rock sequence of the Cenomanian-Turonian age (Walley, 1997) is divided into 3 subunits, each exhibiting a

61

different lithology and thickness (
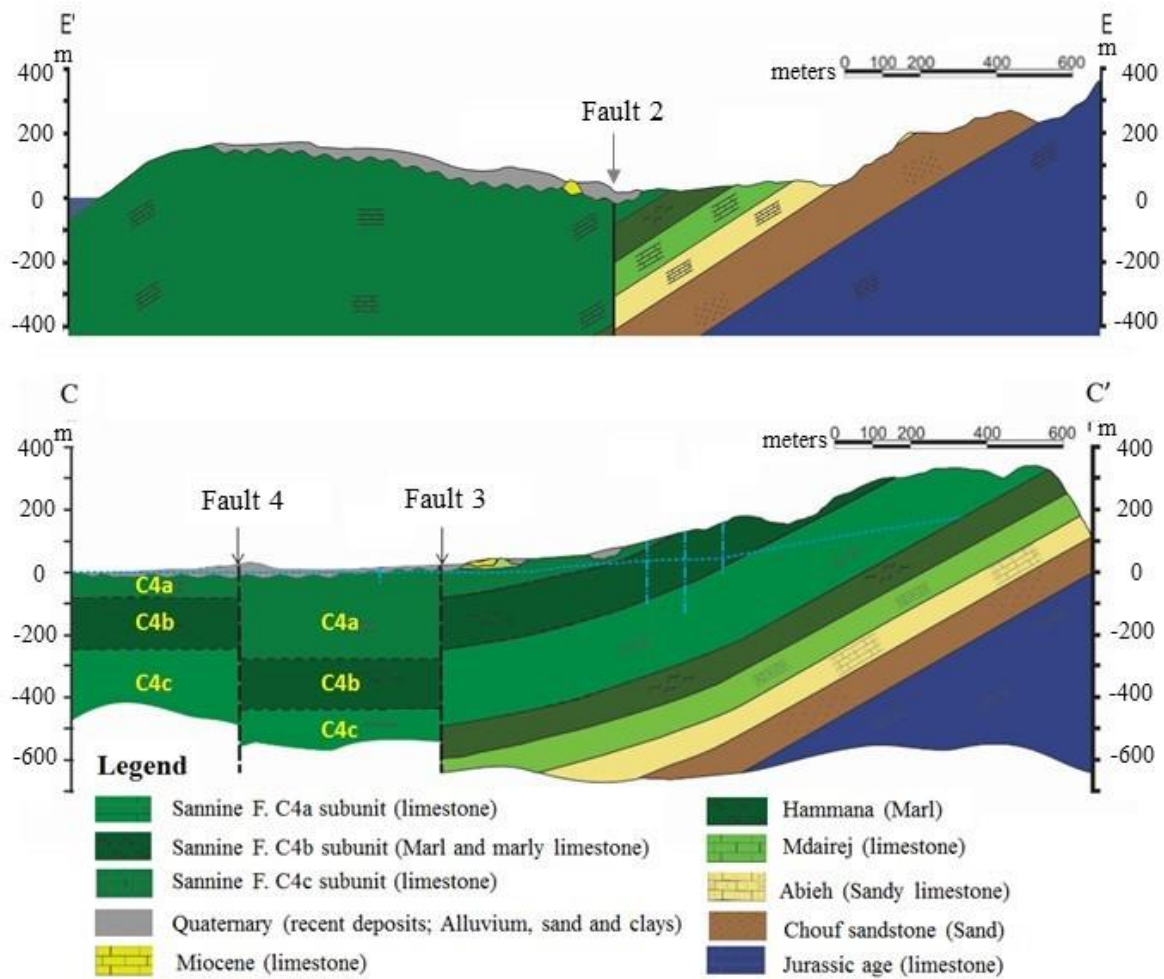
Figure 3-3) referred to in ascending stratigraphic order (Ja'ouni, 1971) as 1) Afqa

Dolomite member, 2) Aaqoura member, and 3) Mnaitra member. These same members are

also known from oldest to youngest as C4a, C4b and C4c respectively (Saint Marc, 1974;

Walley, 1997; Khadra, 2003). The C4a is 200 m thick and consists of crystalline, dolomitic,

marly dolomitic and reefal limestone (Ja'ouni, 1971; Khadra, 2003; Nader, 2000). The C4b is

a ~125 m thick a sequence of thinly bedded limestone, marly limestone, dolomite and marly

dolomite strata, whereas the C4c has an average thickness of ~180 m, and is composed of

thick and compact limestone and fossiliferous strata with several chert bands and nodules

across different horizons.
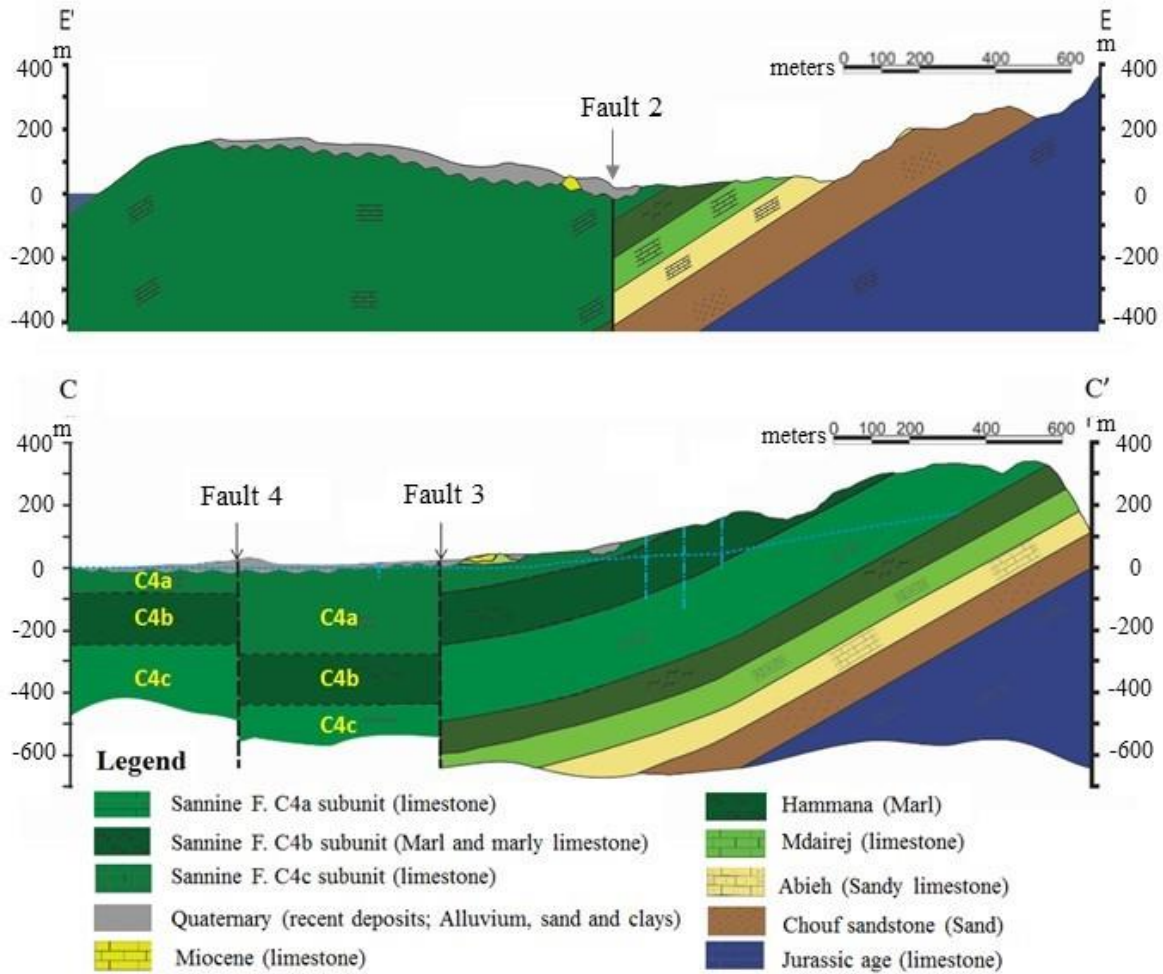
Figure 3-3 Geologic cross-section CC′ and EE′

3.3.2   Need for mathematical modeling

Nearly 4,500 small-scale wells are reportedly tapping the upper aquifer (i.e. Quaternary and a part of Cenomanian), complementing the limited supply provided through the municipal network water supply to nearly 1 million individuals (Safi et al., 2018a). The upper aquifer has been reported as increasingly vulnerable to SWI (Safi et al., 2018a). Moreover, the increasing trend of salinity over time (Rachid el al., 2017, 2015) is expected to limit the accessibility of the shallow freshwater resources in the near future (Safi et al., 2018b). The limited remaining freshwater resources in the upper aquifer is likely to encourage authorities to start tapping the deeper part of the system. Therefore, it is imperative

for decision makers to determine the volume of freshwater resources at depths using a combination of field monitoring and mathematical modeling. In this context, information and data about hydraulic conductivity, heterogeneity, fractured networks, hydraulic head and the current position of the interface are almost non-existent for the deep parts of the system. As such, large uncertainties are expected in any modeling effort limiting the value of the model to serve as a planning tool for decision makers to assess the risk of failure associated with a given management strategy. Under the existing conditions, where the shallow data is scarce while the deep data is almost non-existent, the risk assessment is dependent on quantifying the prediction uncertainty.

3.4 Model set up and details of uncertainty analysis

3.4.1 Set-up of flow model

In this study, we set up the model using SEAWAT (Guo & Langevin, 2002) to solve the variable-density groundwater flow problem. We considered a set of criteria in the code selection process centered on the ability of code to: 1) simulate the 3D nature of the vertical and lateral encroachment of salinity in confined and unconfined aquifers, 2) characterize various types of time-dependent boundary conditions, 3) simulate steady-state and long-term transient flow and solute transport with the least numerical instability, 4) link to an inversion code to quantify uncertainties, and 5) contain reasonable computational resources. The model domain (~42km^2) is bounded to the west and to the north by a Dirichlet boundary along the shores; to the east by a no-flow boundary (faults 1 and 3); and to the south, partially by a no-

flow boundary (fault 2), partially by a local river (Ghadir) (

Legend

——	Zone boundary	——	Specified head boundary condition	▲	Head observation
——	Fault	——	River	●	Pumping well
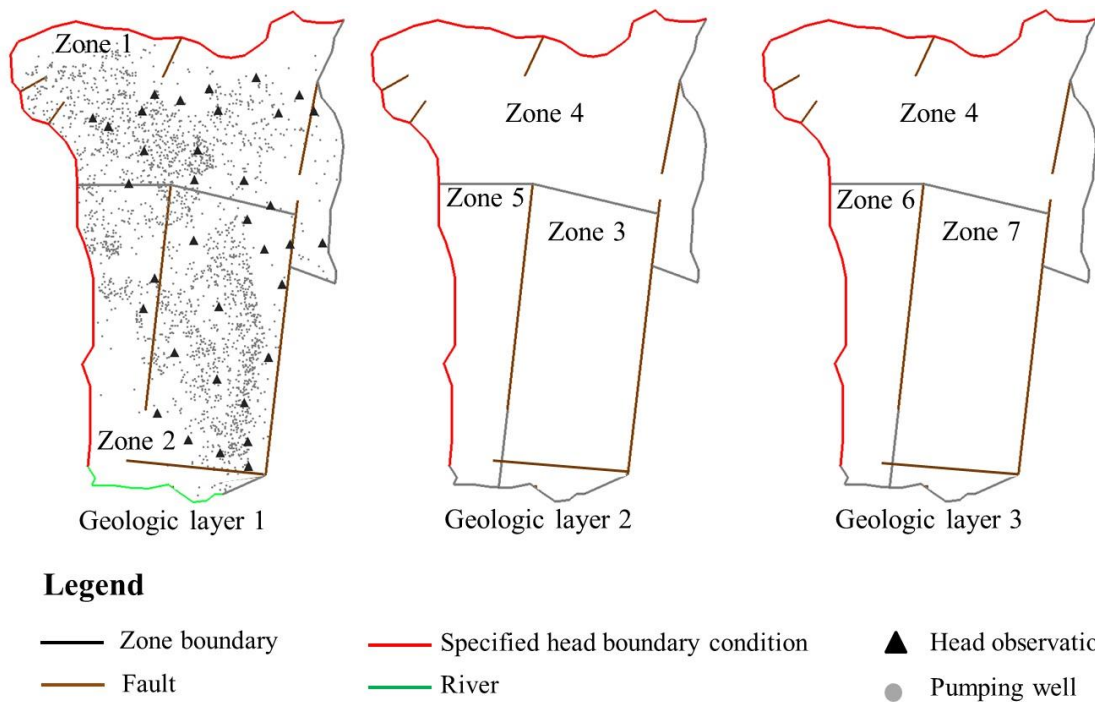
Figure 3-4). The river is simulated as a drain channel (

Legend

—— Fault   —— River   ↔ Geologic cross-section   ┄┄ Model boundary
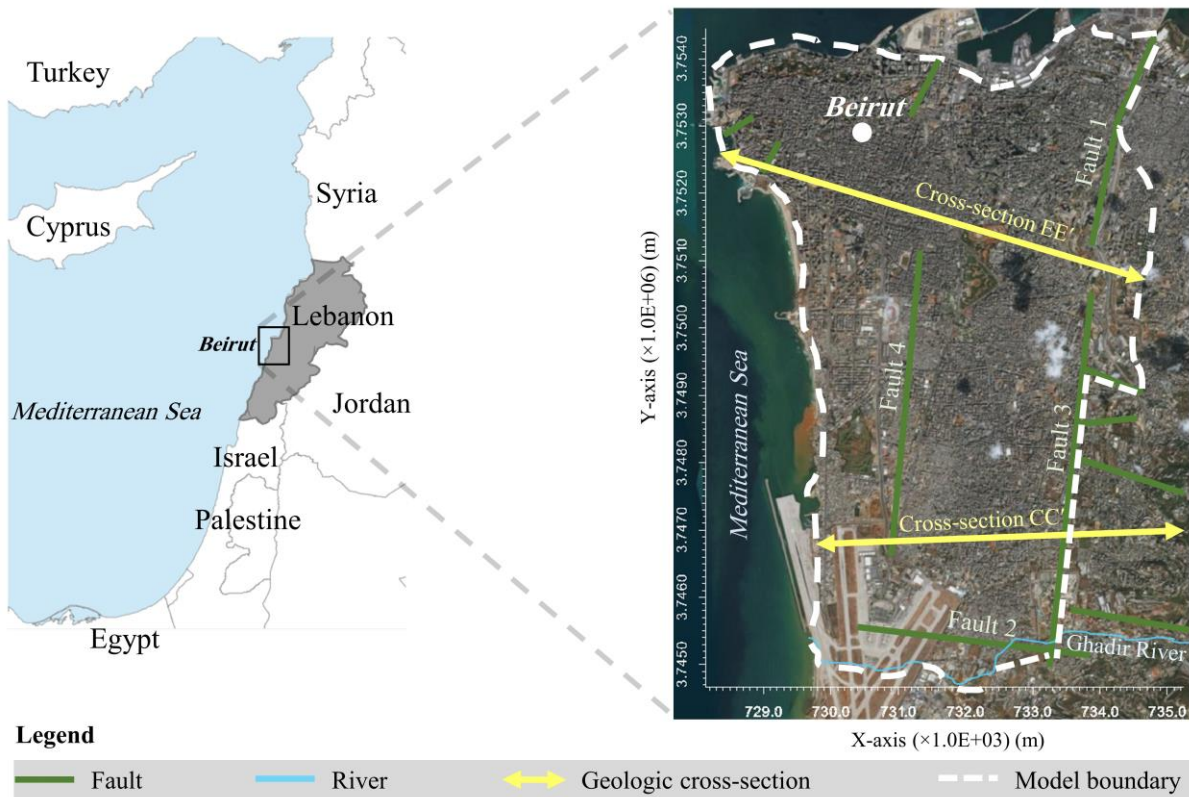
Figure 3-2) because it is mostly dry but with occasional flow from groundwater influx e.g. during winter rainfall events. Due to lack of data, the drain conductance is

assumed to be 1,000 (m2/day/m) (Yager, 1993). The model was discretized horizontally into 4,251 active cells of 100 by 100 meters designed in 115 rows and 75 columns.

The model comprises a transient period of 50 years subdivided into 50 stress periods of one-year duration (from March 1969 to March 2019). The first stress period (1969) is specified as steady state with the aim of providing a stable hydraulic head and salinity distribution at the beginning of the transient period as described below. The recharge rate of the system is set to 30% of average annual precipitation in 1969 (Ukayli, 1971), which gradually decreases to nil in 2019 (Safi et al., 2018a). At a 1.75% population growth and a domestic consumption rate of 180 liter per capita per day (MoEW, 2010), groundwater abstraction is estimated to increase from ~7.8 in 1969 to ~40 MCM in 2019 distributed among 2368 pumping wells (

Figure 3-4). Due to lack of historical information about the spatial distribution of groundwater abstraction from 1969 to 2019, the number of wells is assumed to be constant, equal to the number and distribution recorded in 2013 (Safi et al., 2018a).

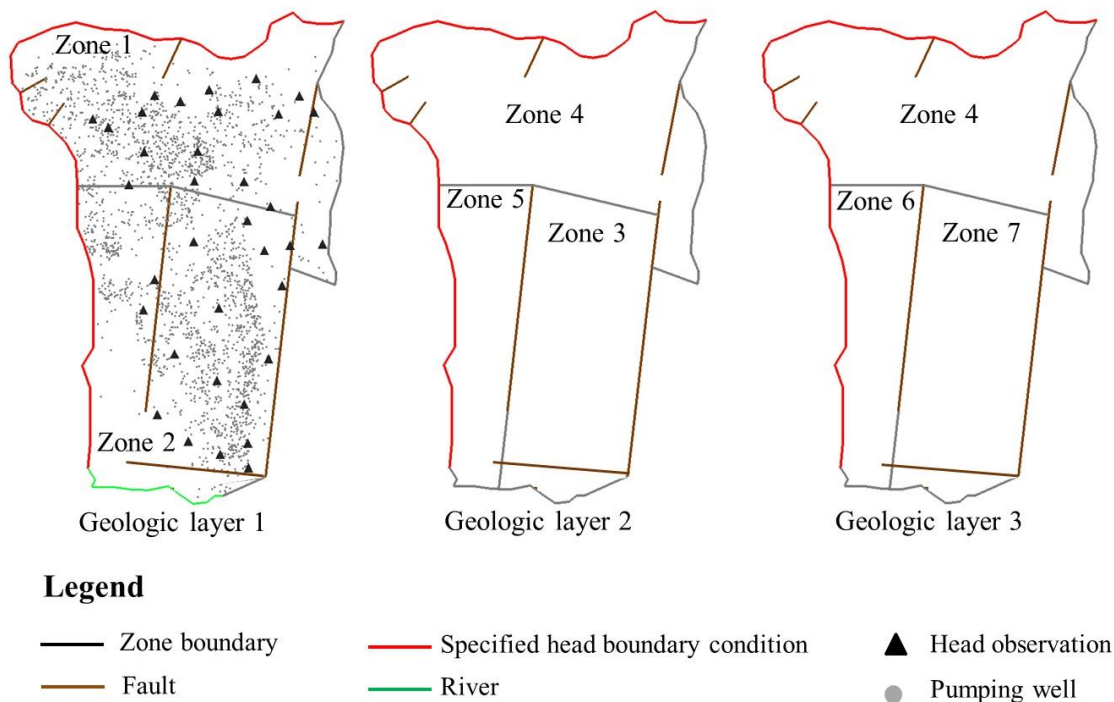The geology of the system is divided into seven zones, together covering three layers

(

Geologic layer 1   Geologic layer 2   Geologic layer 3

Legend

—— Zone boundary	—— Specified head boundary condition	▲ Head observation
—— Fault	—— River	● Pumping well
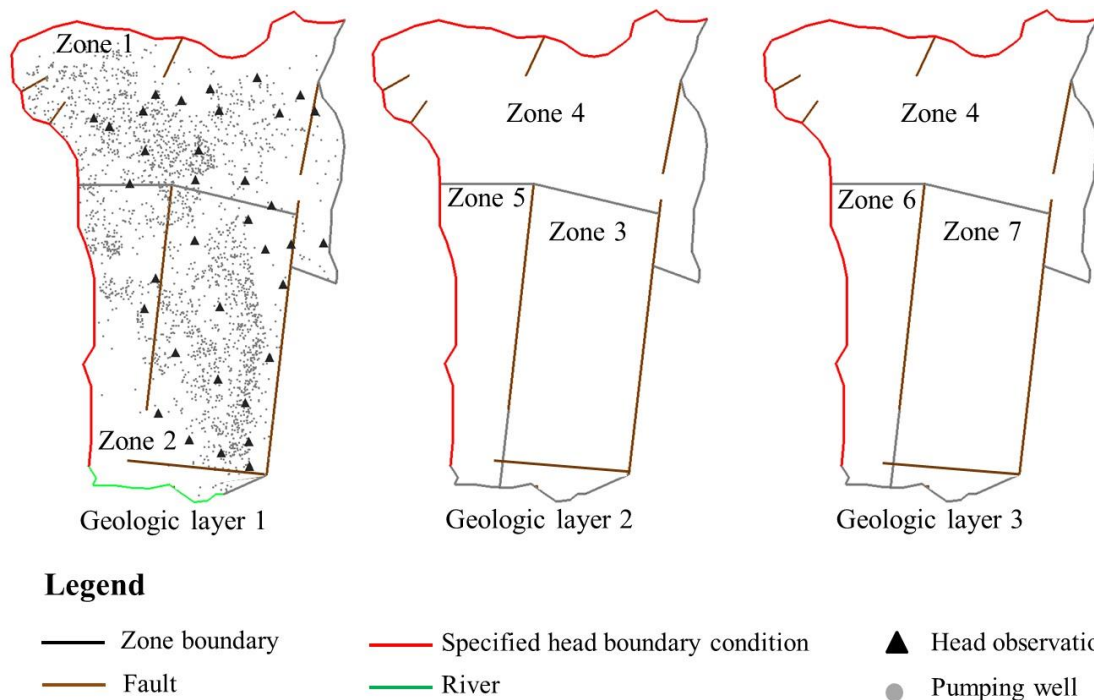
Figure 3-4). The first geologic layer, with a thickness between 100 and 150 meters,

covers the Cenomanian-Quaternary aquifer system. It is divided into two zones: zone 1

consists of a mix of C4c and Quaternary in the north, while zone 2 is a mix of the C4a and

Quaternary formations in the middle and to the south. The middle layer has an overall

thickness of ~150 meters and is divided into zone 3, which is the C4a formation (aquifer) to

the east, zone 4 which is the C4c formation (aquifer) in the north, and zone 5 which is the

C4b formation (aquitard) along the western coastline. Similarly, the third layer with a

thickness of ~250 meters contains zone 4, which is the deeper part of the C4c formation

(aquifer) in the north, zone 6 that is the deep C4c formation (aquifer) along the western

coastline, and zone 7 that represents the deep C4b formation (aquitard) to the east (Table 1).

The top of the layers as well as the bottom of the deepest layer were adjusted using

topography data (ground elevation) and bottom elevation data along cross-sections,

respectively.
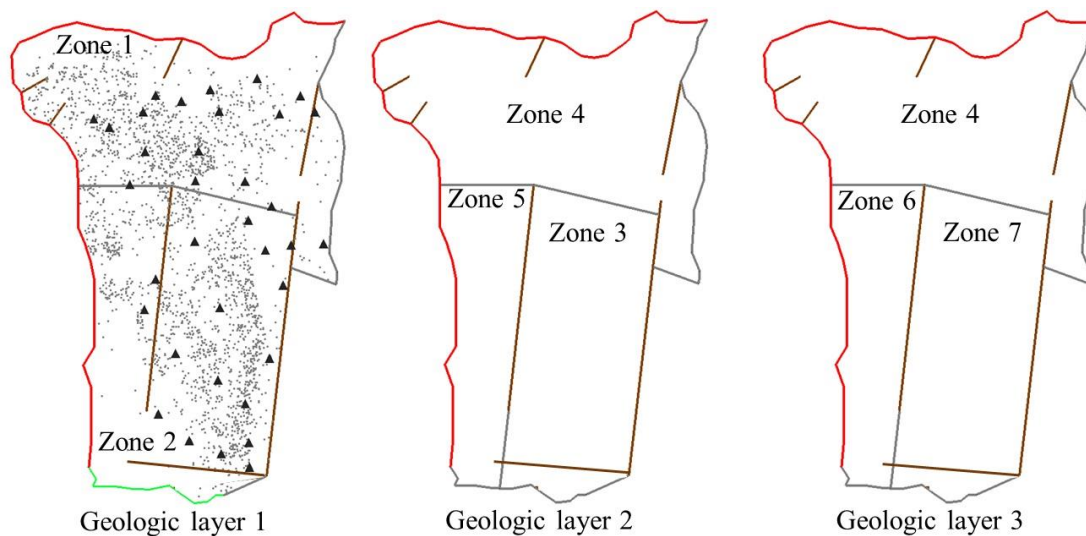
67

Figure 3-4 Geologic layers, aquifer/aquitard zones, boundary conditions, locations of head observations (18 wells in zone 1 and 17 wells in zone 2) and licensed abstraction wells in the top layer, in the shallow aquifer. The pilot points distribution is identcal for all layers.

Horizontal anisotropy and vertical anisotropy ratios were estimated based on the dips and strikes of the faults (Peltekian, 1980) and ranged from 0.8 to 1.3 and from 7 to 15, respectively. Specific storage was set to 10-5 m^{-1} for all zones (as suggested by Ford & William, 2007 for karstic regions). The Cenomanian formation and the Cenomanian-Quaternary system are reported to be permeable with a specific yield of ~0.03 and 0.15, respectively (UNDP, 1970). If the head drops below the top surface of a layer, specific yield is used rather than specific storage. Thus, all layers are defined as confined-unconfined (convertible) in the flow model.

3.4.2   Set-up of solute transport model

The estimated hydraulic conductivity using pilot points (described below) was used to define the hydraulic conductivity field of the solute transport model (
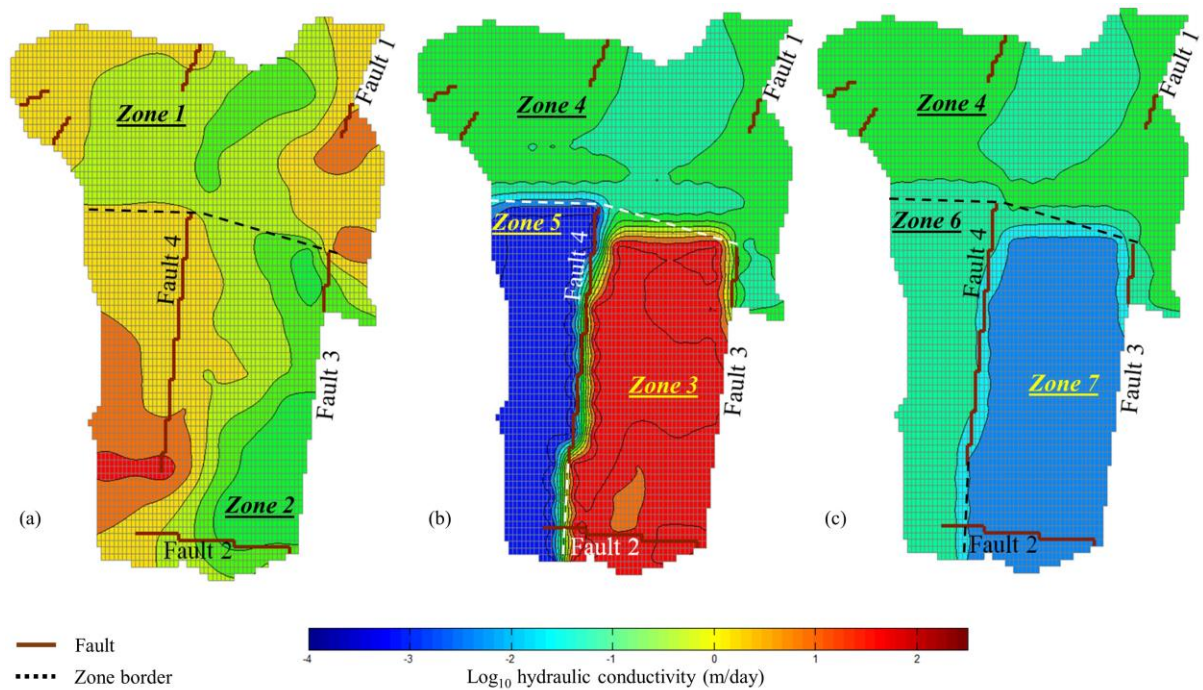
Figure 3-7). Compared to the flow model, the number of transport model layers was increased for the second and third geologic layers to achieve a more accurate simulation of the salt/fresh water interface (Guo & Langevin, 2002) because the thicknesses of these layers were large. For transport simulations, layers 2 and 3 were thus subdivided into 6 and 7 sublayers, respectively. For the Dirichlet boundary condition along the shores, we used a TDS concentration of 35 g/l (Masciopinto, 2013). The molecular diffusion coefficient, the longitudinal dispersivity (αL), and the slope of density over concentration were set at $10-6$ m^2/s, 50 m, and 0.7143, respectively (Guo & Langevin, 2002; Cobaner et al., 2012; De Filippis et. al., 2016). For the purpose of obtaining steady-state with SEAWAT and defining the initial condition for transient transport, the solute transport (MT3D) model was run under transient conditions with steady-state (MODFLOW) hydraulic head until a steady-state concentration distribution was achieved (as suggested by Guo and Langevin 2002). We ran SEAWAT to steady state using pumping rates from 1969. Prior to steady-state simulation, the

starting salinity distribution for the solute transport model was set to an entirely freshwater

aquifer (Werner et al. 2013). The steady-state condition of the solute transport model was

then evaluated by calculating the total mass of salinity entering to the aquifer during the

simulation (as suggested by Guo and Langevin 2002). It was assumed that the solute

transport model was constrained at the beginning of the transient simulation using this

approach. The resulting salinity distribution was used as initial condition for the 50 years of

transient simulations giving two model predictions: (i) the mass encroachment of saltwater

(in megatonne) into fresh groundwater; and (ii) the volume of fresh groundwater stored in the

deep aquifer (i.e. in zone 6 described below) with a TDS concentration less than 1.5 g/l at the

end of simulation period. The latter is shortly called "volume of freshwater" in the following.

3.4.3   *Parameterization and parameter estimation*

The model parameters were defined to be hydraulic conductivity at 564 pilot points (
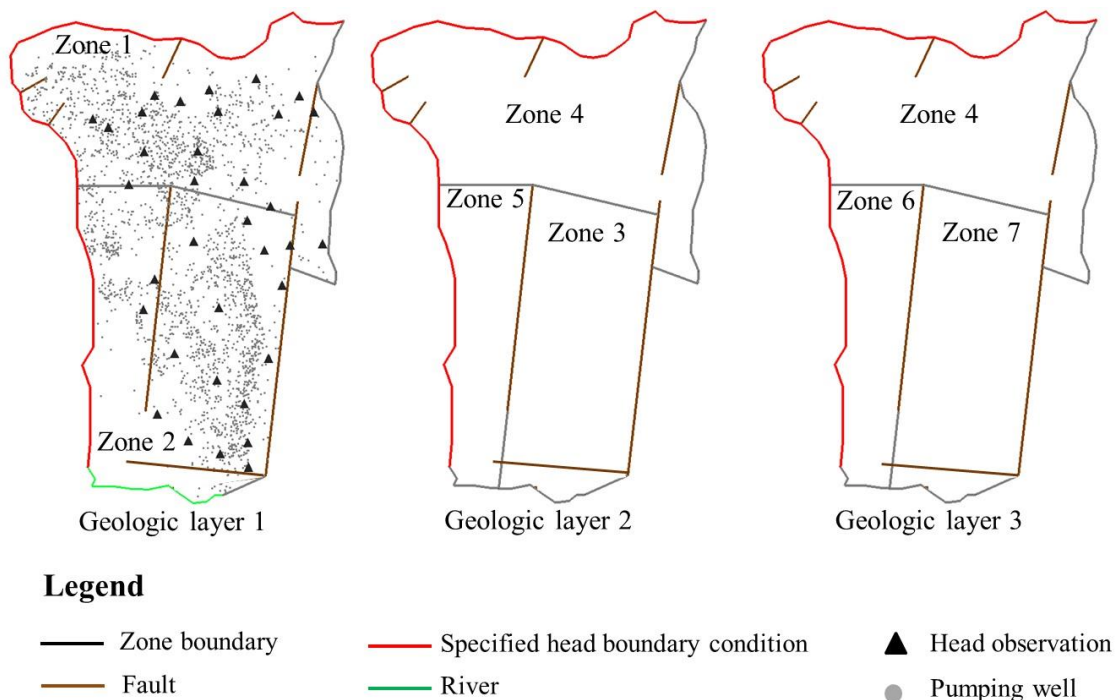
Figure 3-4). Each geologic layer consisted of 158 pilot points uniformly distributed over the domain. Pilot points were placed within a 500m distance from each other to avoid large spatial gaps (Doherty et al., 2010). The final distribution confirmed that at least one pilot point was placed between two head observations along the flow direction. Limited information exists about the hydraulic conductivity of the geologic zones (Table 1). Therefore, the hydraulic conductivity values of the geologic zones were first estimated using simple zonal calibration (constant hydraulic conductivity within each zone). The estimated hydraulic conductivity values were then used as initial values for the pilot points within the respective zones. Using PEST, the pilot points values were estimated using the existing head observations and Tikhonov regularization in combination with SVD (Doherty, 2015). Only 35 head observation wells were available for calibration, and their values were only specified in 5m intervals. This interval is associated with a standard deviation of 2.5m, representing the measurement noise (error) associated with the head observations. From this, we estimated that a value of 250 m^2 for the measurement objective function (i.e. for ___ in equation 1) was a reasonable target. This was based on multiplying 35 (observations) by the squared standard deviation of 2.5m (as suggested by Fienen et al., 2009). We used a weight of 1.0 for all observations. To implement the Tikhonov regularization, the interpolation from the pilot points to model grid used an exponential variogram with a range of 500 meters, corresponding to the separation distance between the pilot points (Doherty et al., 2010). The sill and nugget were set as 0.1m^2 and 0, respectively.

3.4.4 *Prediction uncertainty analysis*

As shown later, from the sensitivity analysis, we found parameter subset (i) to include pilot points in zones 1 to 4. For this subset, realizations of $\log_{10}$ hydraulic

conductivity were generated using SGS and an exponential variogram with a sill of 1m/day

and a range of 500m (i.e. the distance between the two pilot points). For subset (ii), which (as

shown later) constitute pilot points in zone 6, we generated the realizations by Fuzzy SGS

using a trapezoidal distribution as membership function for the log mean hydraulic

conductivity as shown in Eq. (2):

$$\overline{}$$

(2)

$$\overline{}$$

where   is the membership degree of the element   (here log mean hydraulic

conductivity) to the fuzzy set A. The definition of a, b, c and d is depicted in Figure 3-5. The

selection of a trapezoidal membership function was based on our existing prior information

about the geology of zone 6. In general, the membership degree   reflects the grade (or

degree) of membership of the element x to the fuzzy set A. The membership degree of 0

means that the element x is not a member of the fuzzy set. The membership degree of 1

indicates that the element x is fully a member of the fuzzy set (e.g. the most expected (or

measured) range of parameter value). This element is bounded by a lower (b) and an upper

(c) support limit. In this work, we considered two scenarios with different lower and upper

support limits. The first scenario was developed to represent a worst-case scenario, whereby

we assumed very limited prior information on the expected mean values of the $\log_{10}$

hydraulic conductivity. Thus, the membership value of 1 was assigned to a wide range of

$\log_{10}$ hydraulic conductivity from 1 to 2 m/day (i.e. b and c in Figure 3-5-a) (Kahdra et al.,

2017). In the second scenario, we used expert knowledge to define a tighter range where the

membership function equals 1 between 1.5 and 2m/day (Figure 3-5-b). Given that the $\log_{10}$

mean hydraulic conductivity values may also occur beyond the highest membership degree

limits, we allowed the membership values to decrease linearly to approach a lower (a) and an

upper (d) bounds of -1.7 and 2.69m/day, respectively for both scenarios. Furthermore, for the Fuzzy SGS we used a Gaussian membership function to generate a set of fuzzy values for the range of the exponential variogram for both scenarios. The central value and standard deviation of the variogram's range were defined as 500m and 75m, respectively (Figure 3-5-c). The fuzzy variograms were used to generate fuzzy covariance matrices. Using the FIELD GENeration (FIELDGEN) utility in PEST (Doherty, 2008), stochastic fields of hydraulic conductivity were generated for model grids based on the fuzzy mean hydraulic conductivities and fuzzy covariance matrices. The PPSAMP utility of PEST was then used to assign random values to the pilot points through sampling of stochastic fields (Doherty et al., 2010). During the randomization process, the sill of the variogram ($0.1m^2$) was adjusted ($0.07m^2$) based on a trial-and-error matching to generate random values of pilot points within the expected range for the $\log_{10}$ hydraulic conductivity (Table 1) in zone 6.
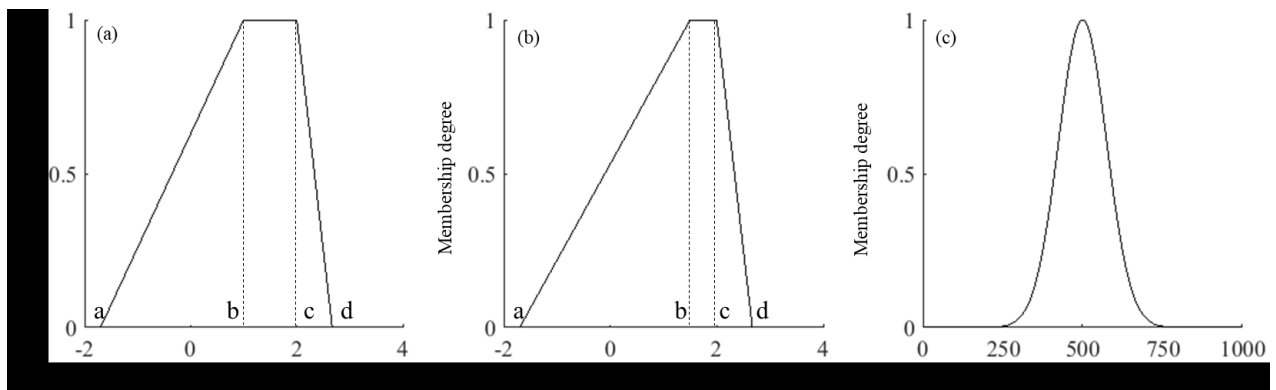
Figure 3-5 Fuzzy SGS membership functions corresponding to: a) log mean value of hydraulic conductivity in scenario 1 (poor prior information); b) log mean value of hydraulic conductivity in scenario 2 (improved prior information); and c) the variogram range defined for both scenarios.

Finally, in scenario 3, we evaluated the proposed Fuzzy SGS approach by quantifying prediction uncertainties when instead of using Fuzzy SGS for subset (ii), we used the same kind of SGS as for subset (i). We assumed no prior information exists about the mean hydraulic conductivity of subset (ii), and hence the starting values of pilot points prior

to the prediction uncertainty analysis were assigned through estimation of lumped parameters using zonal calibration (Doherty et al., 2010). The estimated range of prediction uncertainty is then compared to the prediction uncertainty results obtained using the suggested Fuzzy approach.

Despite focusing on the estimates of hydraulic conductivity, the proposed methodology is not limited to the uncertainty with this input variable. Additional uncertainties related to other input variables (such as dispersivity coefficients, recharge/discharge rates, boundary conditions …) could be incorporated in the framework. Depending on the sensitivity of predictions to parameters, including other sources of uncertainties would likely result in an increased prediction uncertainty. In the present case, the prediction uncertainty analysis is limited to the hydraulic conductivity due to the large run-time of the model.

We carried out the parameter estimation and the NSMC analysis using PEST as a model independent tool. We created additional code functionality to cover the limitations of PEST to implement our methodology for the prediction uncertainty analysis. This is largely limited to the generation of the fuzzy SGS inputs, which were implemented in Python.

3.5   Results and discussion

3.5.1   Parameter estimation

Using the 35 head observation points, the hydraulic conductivity values of the geologic zones were first estimated by applying the zonal method, and afterwards by applying the pilot points approach. The scatter plots of computed versus observed head

values for each of the calibration methods are depicted in

(a) Zonal calibration   (b) Pilot points parameterization
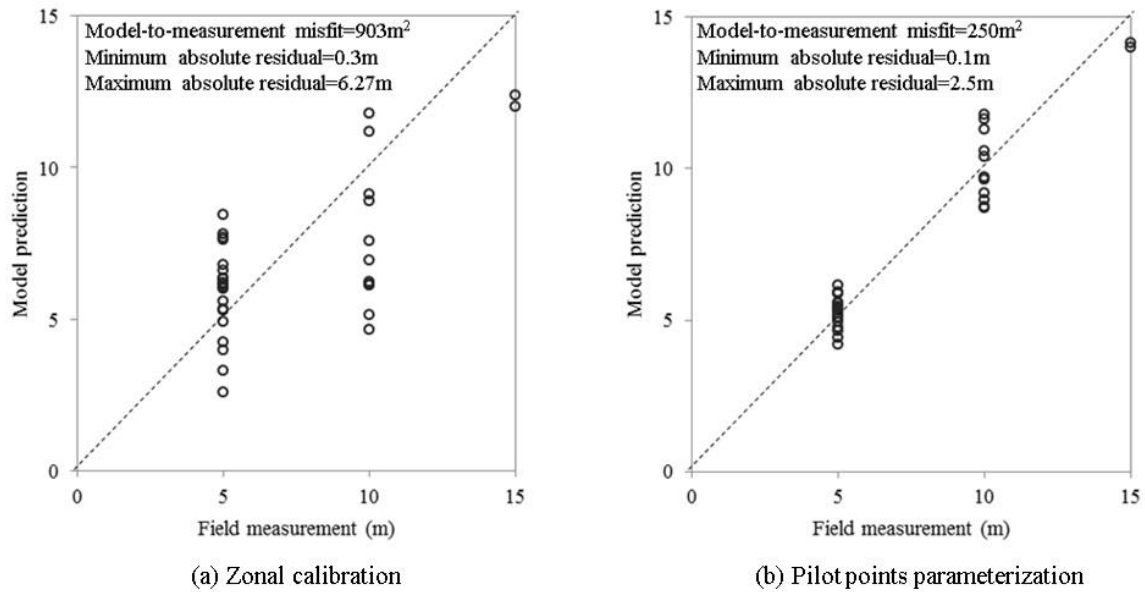
Figure 3-6. Using the zonal method, the residual absolute errors ranged from 0.3 to 6.27m with an average of ~2m, and the model-to-measurement misfit could be reduced to 903m^2. Using the pilot point parameterization, both the range of the residual absolute errors and the model-to-measurement misfit decreased by ~70% compared to the zonal estimation. This is because the pilot point parameterization approach was capable of better representing the heterogeneous hydraulic conductivity field and thereby to simulate a more detailed (or

variable) field (
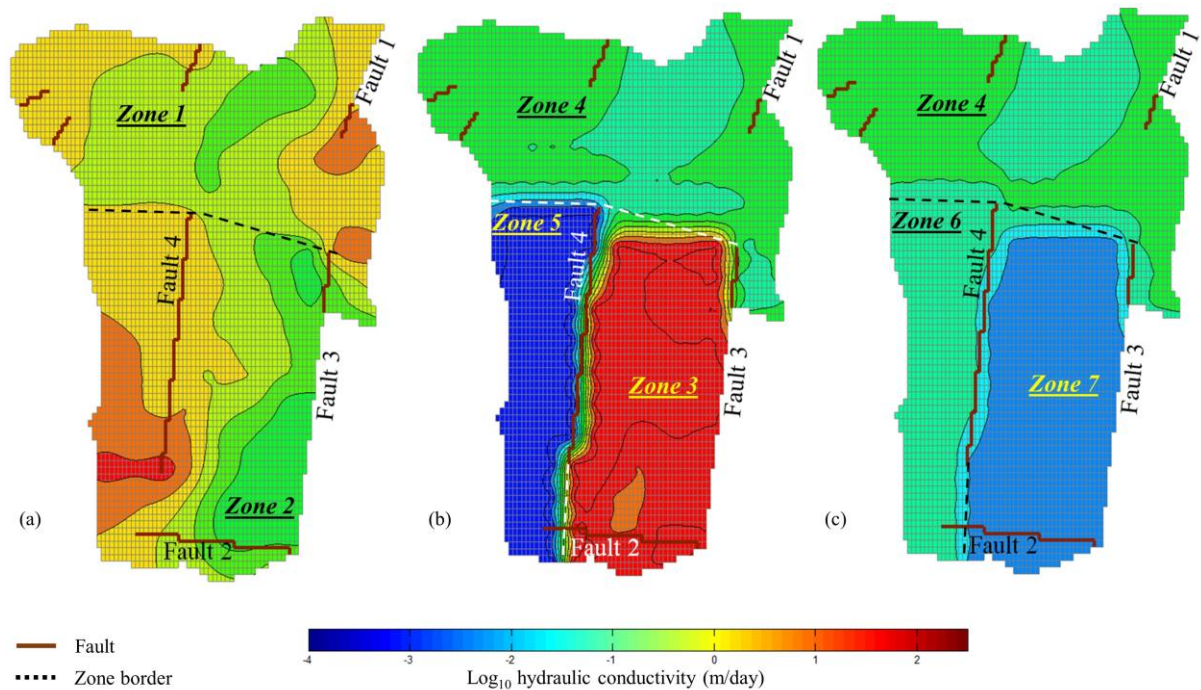
Figure 3-7). The computed model-to-measurement misfit value was 250 m^2, which corresponds well with the head observation errors. The model-to-measurement misfit however, did not drop below the targeted value ($\sim$250m^2) due to the use of the Tikhonov regularization to constrain the parameter estimation process. Combining the Tikhonov regularization with the truncated SVD (Tonkin & Doherty, 2005) further increased the stability of the process by removing the inestimable combinations of pilot points from the calibration process. Using the SVD, the parameters belonging entirely to the null-space (C4b in layers 2 and 3, and C4c in layer 3) retained their starting values (i.e. zonal values) during the parameterization (Table 1). Due to the lack of hydrogeological information, the starting values of all pilot points were assigned an initial estimation of lumped parameters using zonal calibration as suggested by Doherty et al., 2010.

(a) Zonal calibration (b) Pilot points parameterization
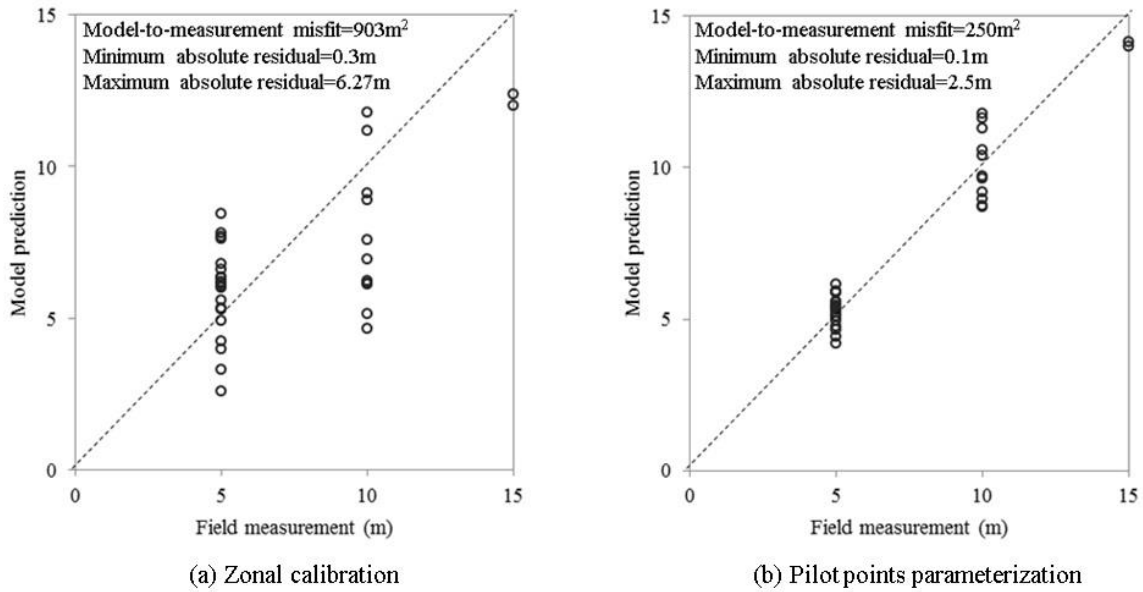
Figure 3-6 Model-to-measurement misfit for the 35 head observations with measured values at 5, 10, and 15 meters

Note that both calibration methods resulted in the estimated hydraulic conductivity values falling within the expected ranges (Table 3-1). Using the pilot points parameterization, the largest estimated hydraulic conductivity values were located between faults 2 and 4 in the upper layer and between faults 3 and 4 in the middle layer (
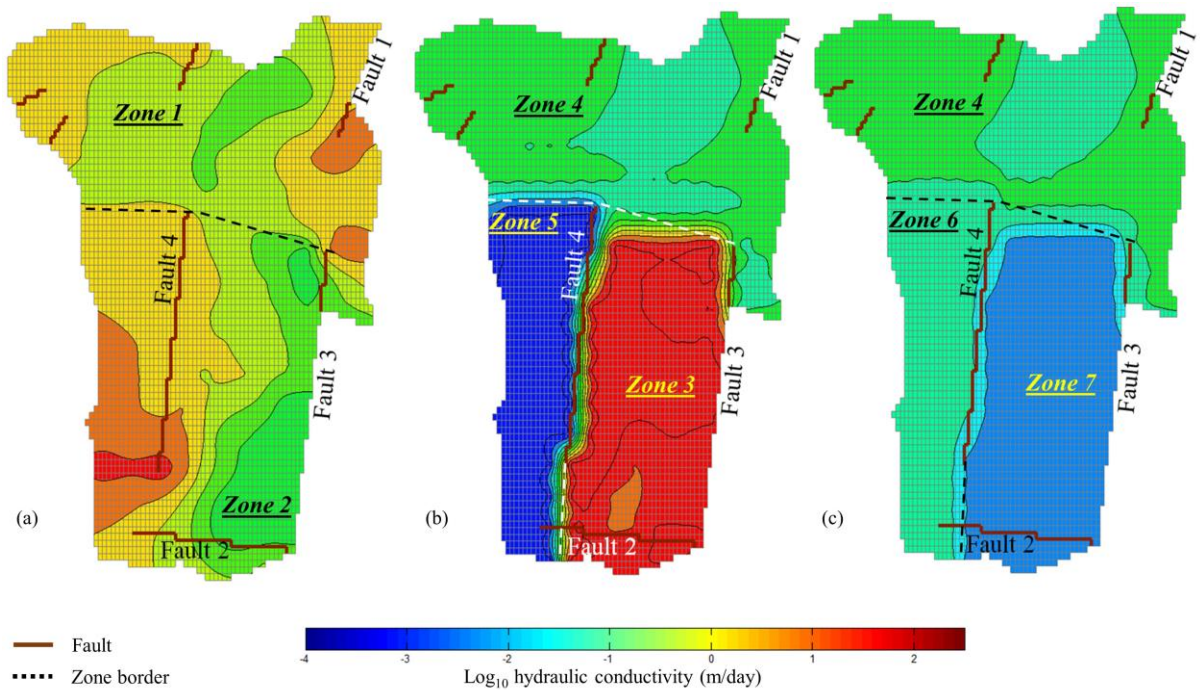
Figure 3-7 and Table 3-1). The degree of heterogeneity of the estimated hydraulic

conductivity field was very low in zones 5, 6, and 7 (
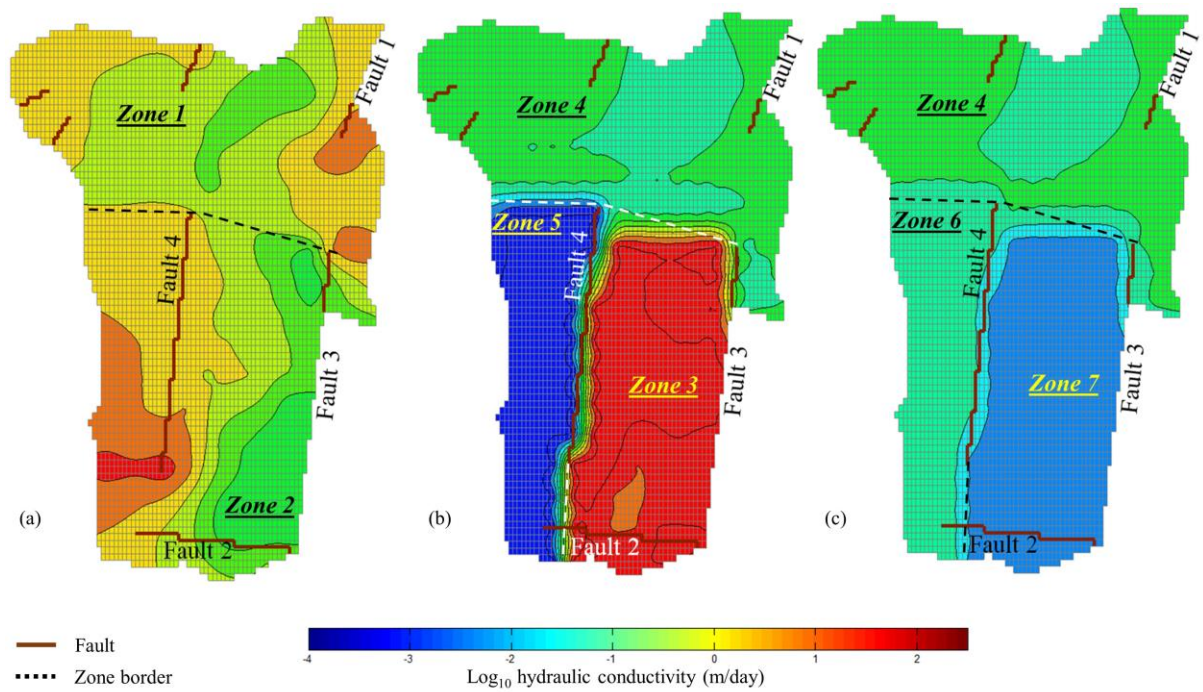
Figure 3-7).

Table 3-1 Geologic formations within model layers with corresponding range of hydraulic
conductivities (Ukayli, 1969; Petekian, 1980), and estimated hydraulic conductivity bound values for the
various geologic formations

Model domain	Geologic formation	Type	Zone	Expected range for $\log_{10}$ Hydraulic conductivity (m/day)	Estimated $\log_{10}$ value using zonal approach (m/day)	Estimated $\log_{10}$ value using pilot points parameterization (m/day)	Parameter subset
Layer 1	C4C-Quaternary	Aquifer	1	-1.7 to 2.7	0.3	-0.8 to 1.5	*Subset (i)*
	C4a-Quaternary	Aquifer	2	-1.3 to 2.7	1.4	-0.7 to 2.7	*Subset (i)*
Layer 2	C4a	Aquifer	3	-1.3 to 2.7	2.5	0.4 to 2.7	*Subset (i)*
	C4c	Aquifer	4	-1.7 to 2.7	-0.6	-1.7 to 1.6	*Subset (i)*
	C4b	Aquitard	5	-5 to -3	-3	-3	*Subset (iii)*
Layer 3	C4c	Aquifer	4[a]	-1.7 to 2.7	-0.6	-1.7 to 1.6	*Subset (i)*
	C4c	Aquifer	6	-1.7 to 2.7	-1.7	-1.7	*Subset (ii)*

C4b	Aquitard	7	-5 to -3	-3	-3	*Subset (iii)*

[a] The same zone is used to characterize the C4c in the second and third layers
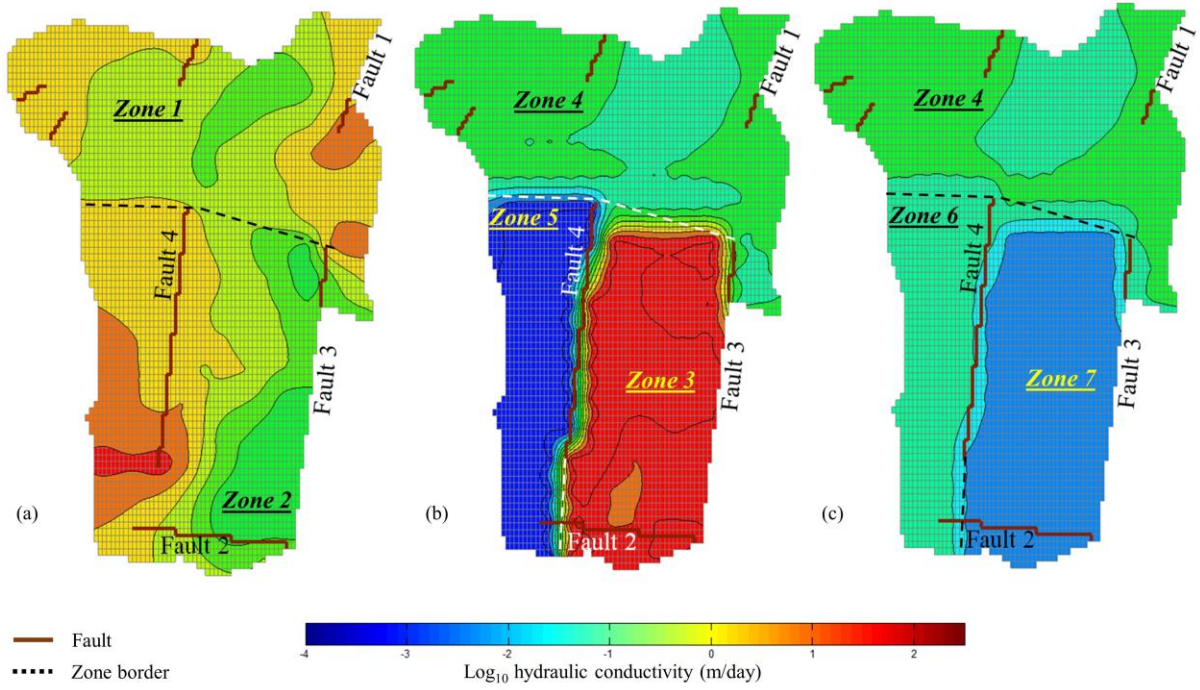
Figure 3-7 Calibrated results of log hydraulic conductivity using pilot points parameterization; (a) geologic layers 1, 2 and 3 are shown in plots (a), (b), and (c), respectively.

3.5.2   Simulations of salt/fresh water interface

79

Figure 3-8 illustrates the model grid of the transport model as well as the steady state

distribution of salinity simulated (in 1969) using pumping rates from 1969. Simulation of the

salt/fresh water interface under steady state conditions confirms that the interface is mainly
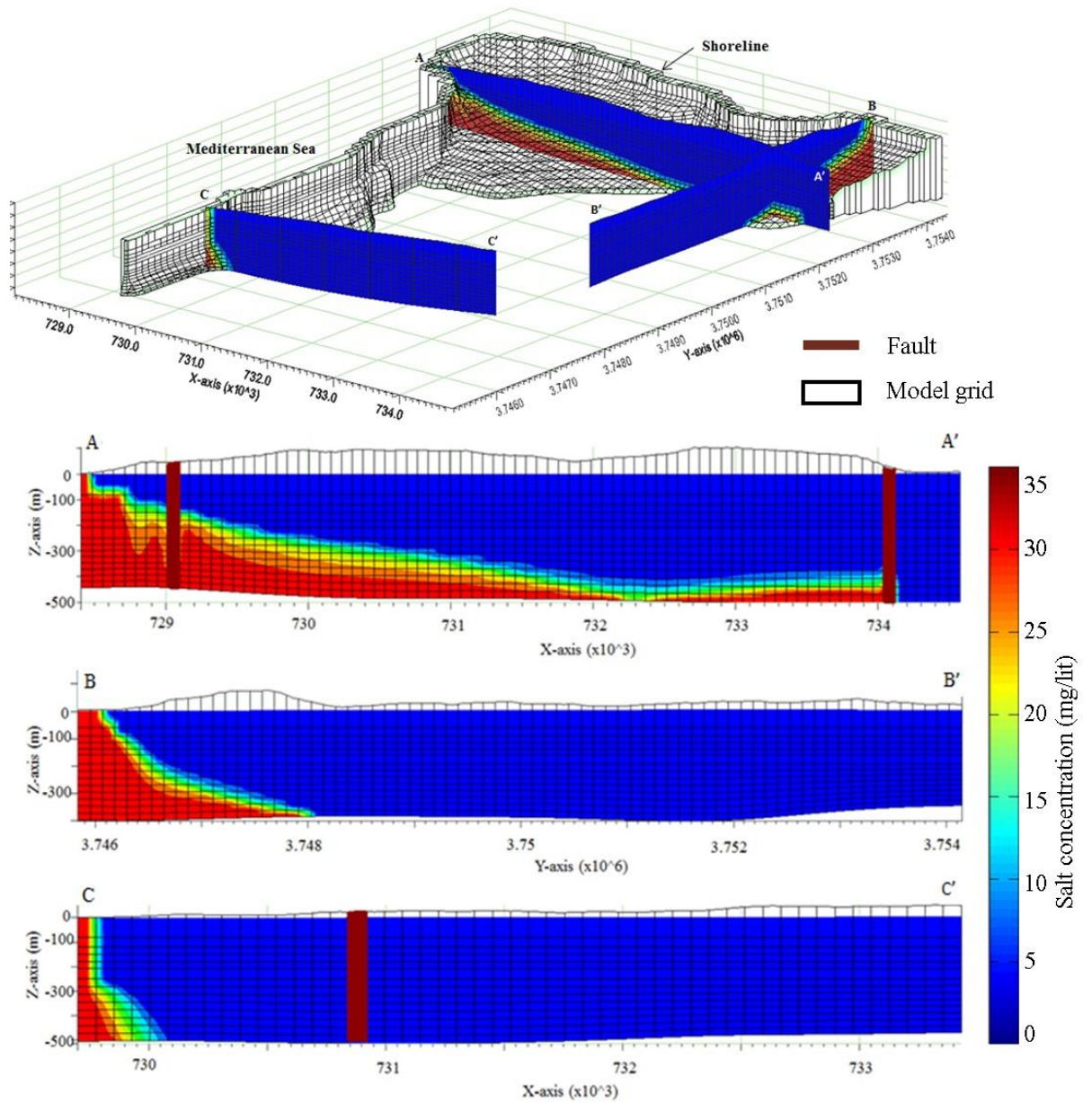
located in the deep geologic layers (
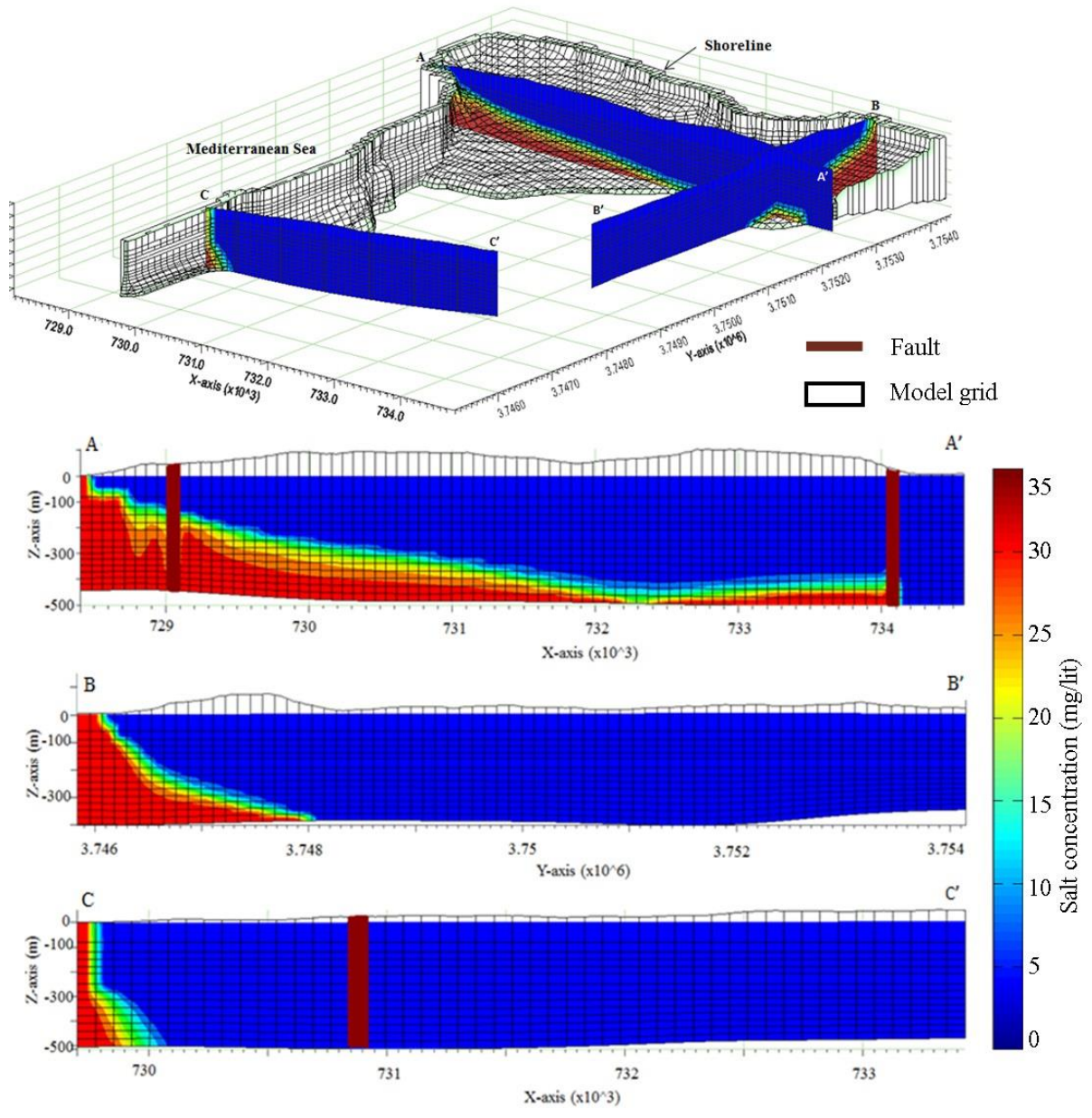
Figure 3-8). At steady state, the toe of the salt/fresh water interface reaches a local
fault in the northwest (cross-section A,
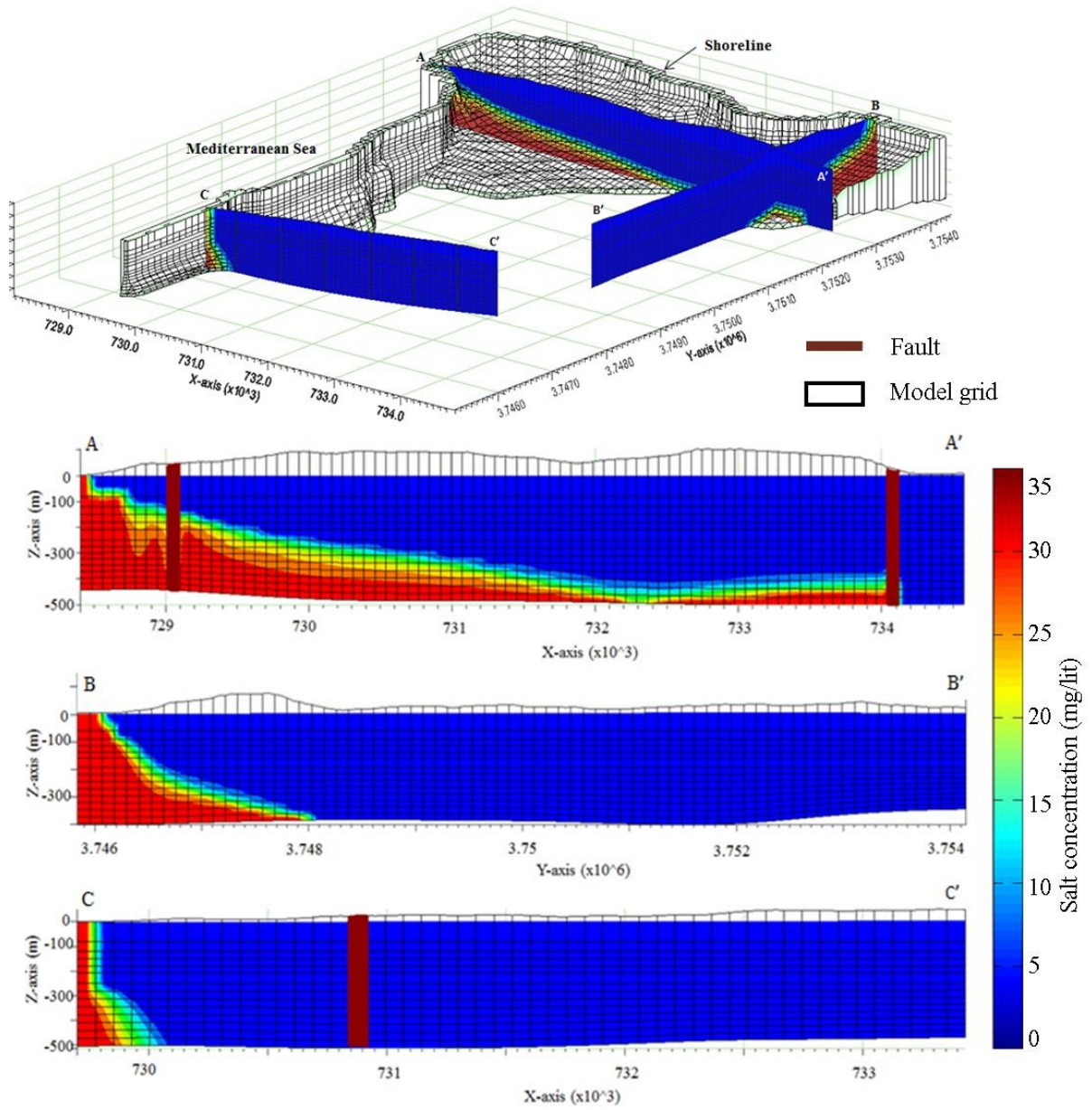
Figure 3-8). In contrast, a deep interface is formed at the western coastline (cross-section CC′,
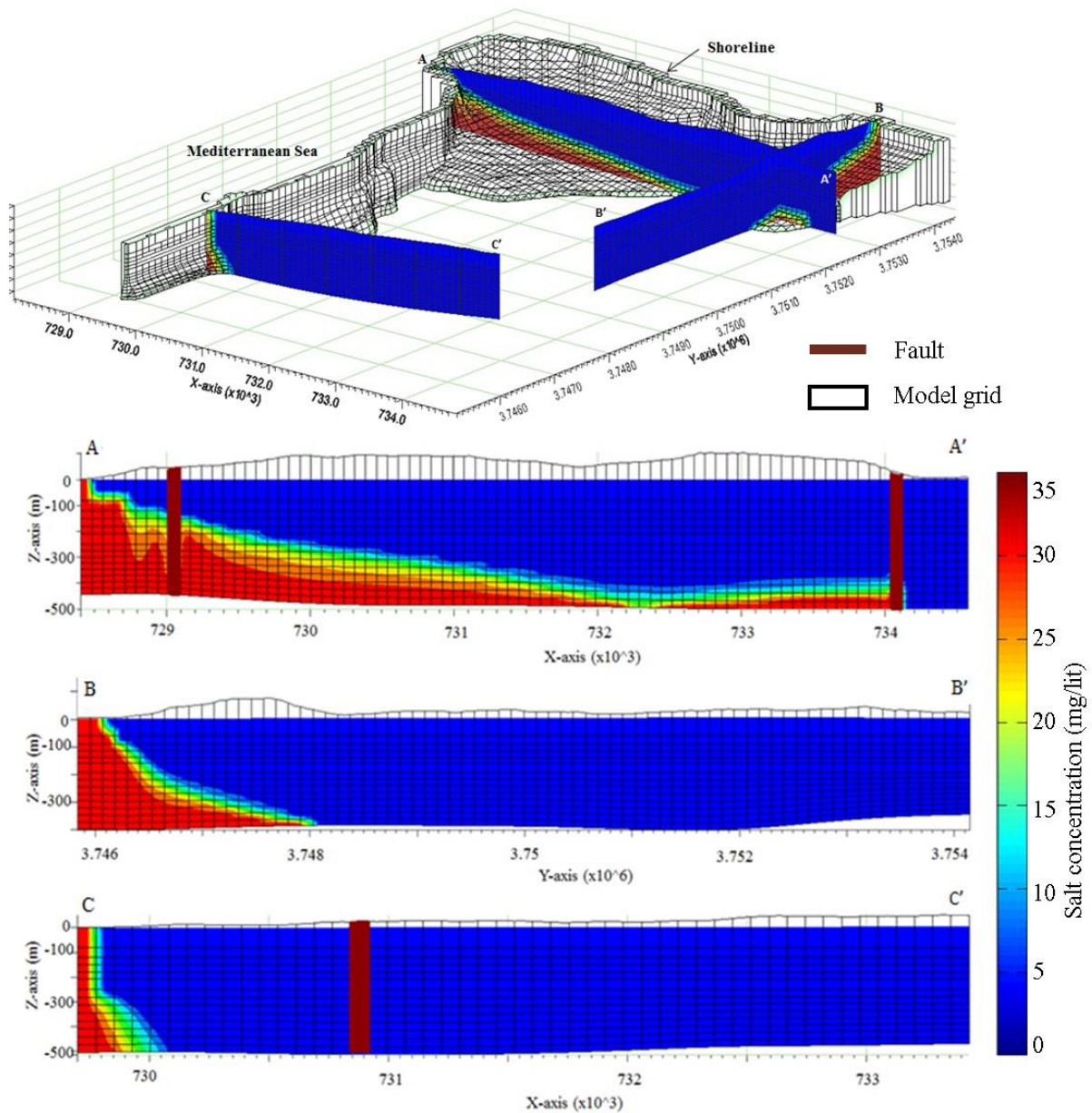
Figure 3-8) due to the low hydraulic conductivities of C4b (the aquitard represented by zone 5). The low values prevent the landward displacement of the interface into the aquitard (the middle numerical layers). The intrusion from the western interface therefore occurs in the deep aquifer (C4c), where the hydraulic conductivities are 2 to 3 orders of magnitude higher than in the overlying aquitard (Table 3-1). Unlike the western coastline, a

wide zone of intrusion is observed in the aquifer along cross-section BB′ (
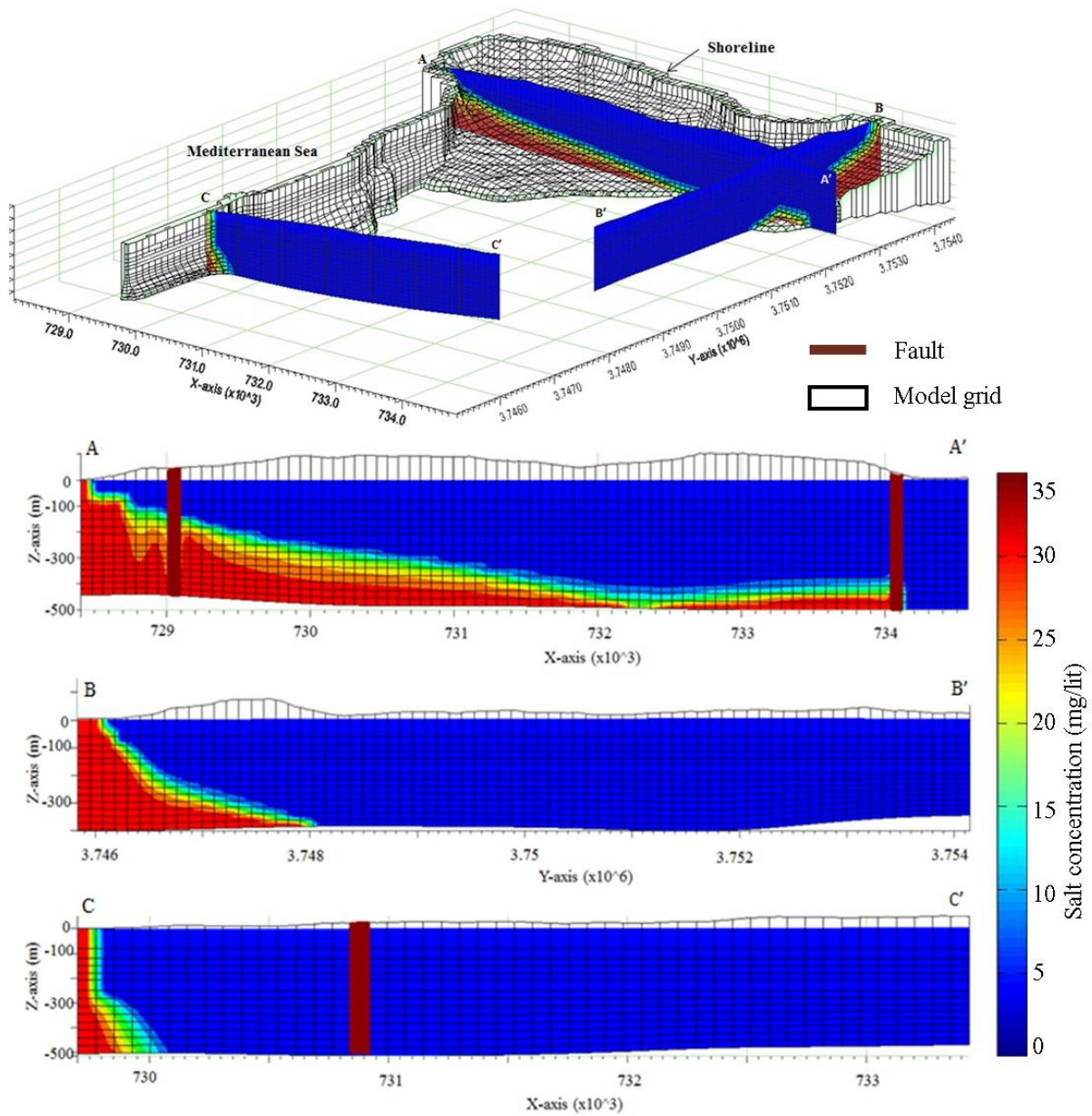
Figure 3-8) because there is no aquitard separating the shallow and deep aquifers.
The steady state salinity is used as initial condition for the transient simulation, which is
carried out to achieve the model prediction values. Transport simulations to predict for the
following 50 years were undertaken based on the pilot point calibrated results. The model

prediction results are shown as deterministic results in
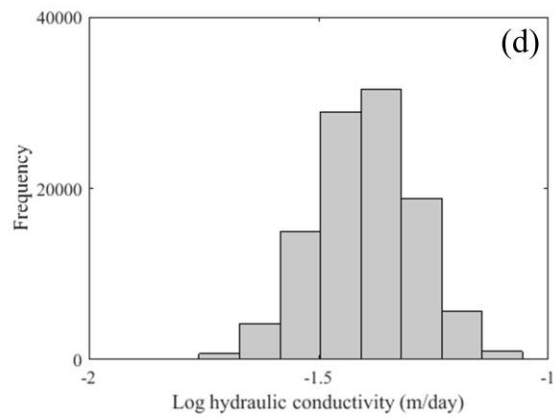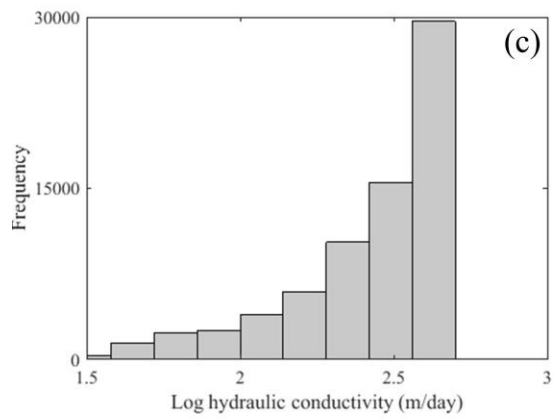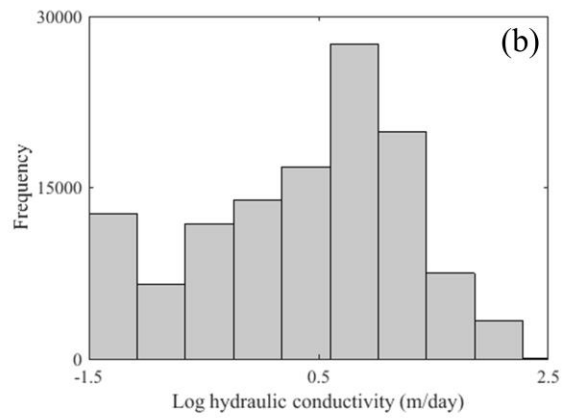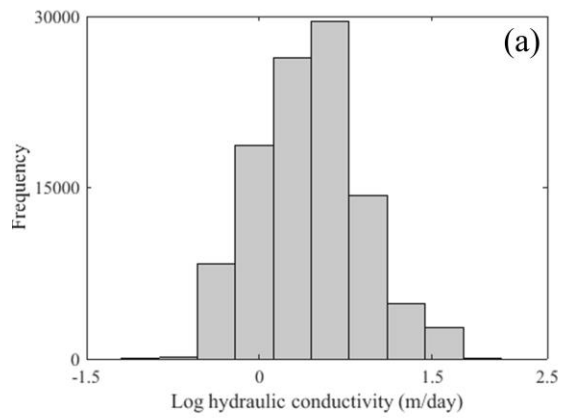
Figure 3-12h and
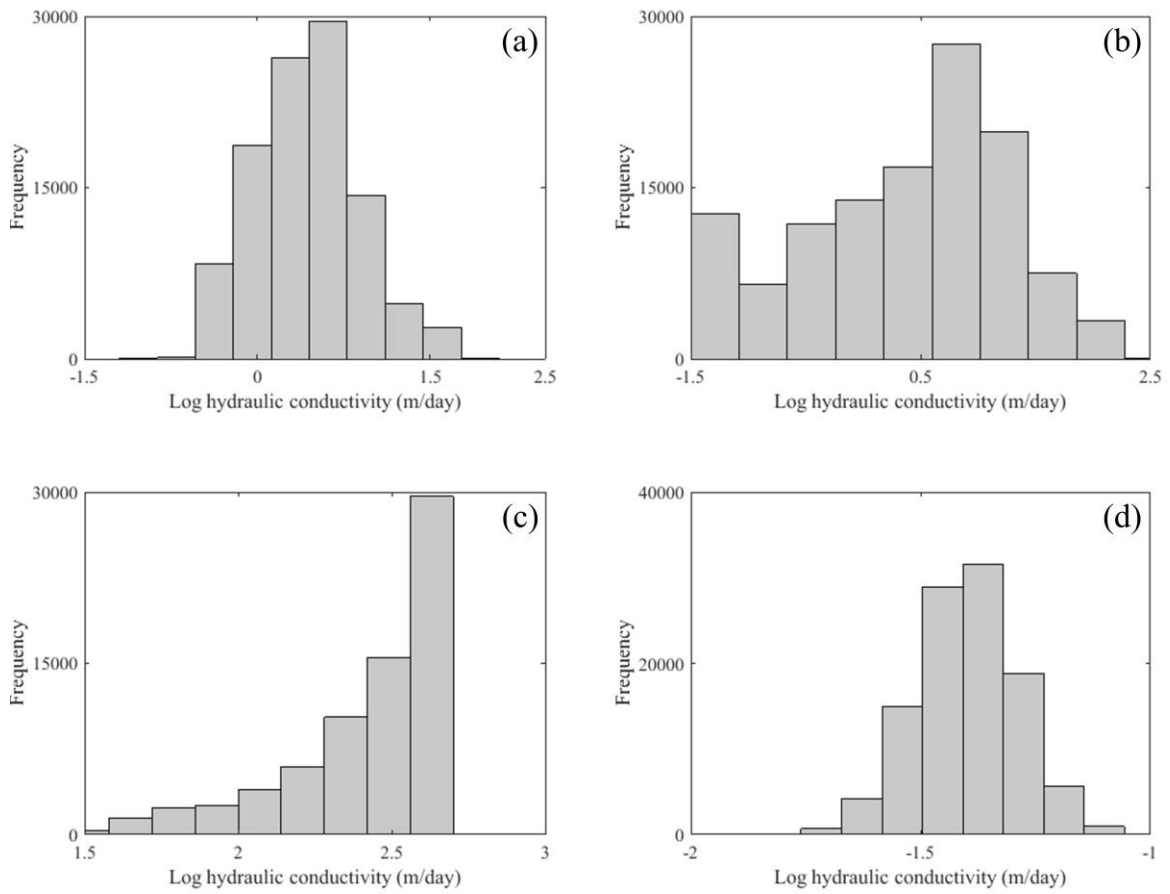
Figure 3-12i. The total mass of salinity increased by 5% due to 50 years of groundwater abstraction, and the remaining volume of freshwater was estimated as being 1.86km^3 after such abstraction.
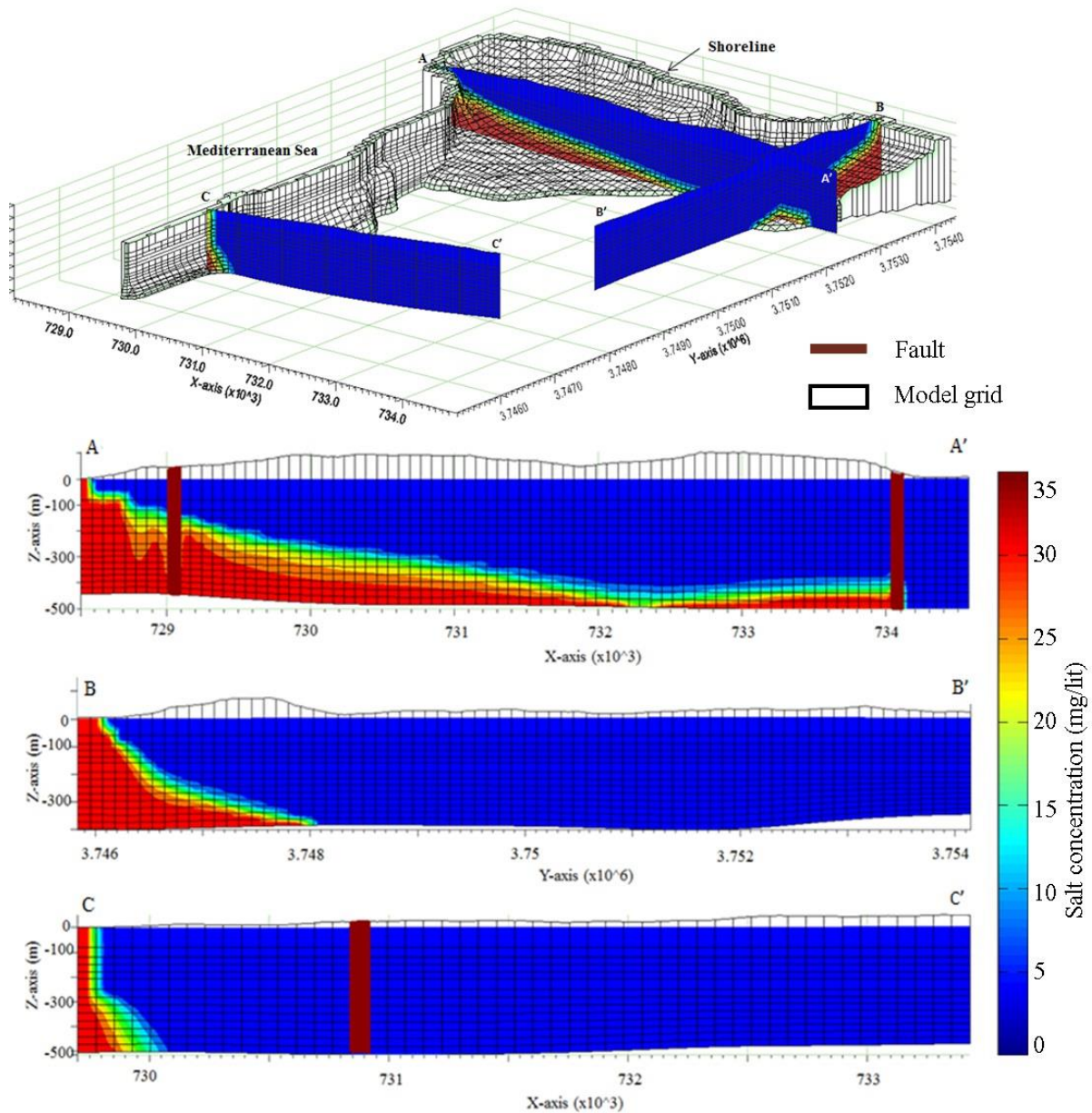
Figure 3-8 Steady-state salinity concentration along three transects simulated when using 1969 pumping rates (with isoline of 35 gr/lit). This result is used as initial condition for the 50 years of transient simulation of transport. The uneven white cells in the top of each transect illustrate the topographic relief.

3.5.3 Sensitivity analysis - Definition of parameter subsets

The calibration results were evaluated by calculating the composite sensitivity (CS) of observations to the estimated values at the pilot points. The sensitivity analysis revealed that pilot points located in the upper and middle aquifers are informed by the calibration

dataset (i.e. high CS) (
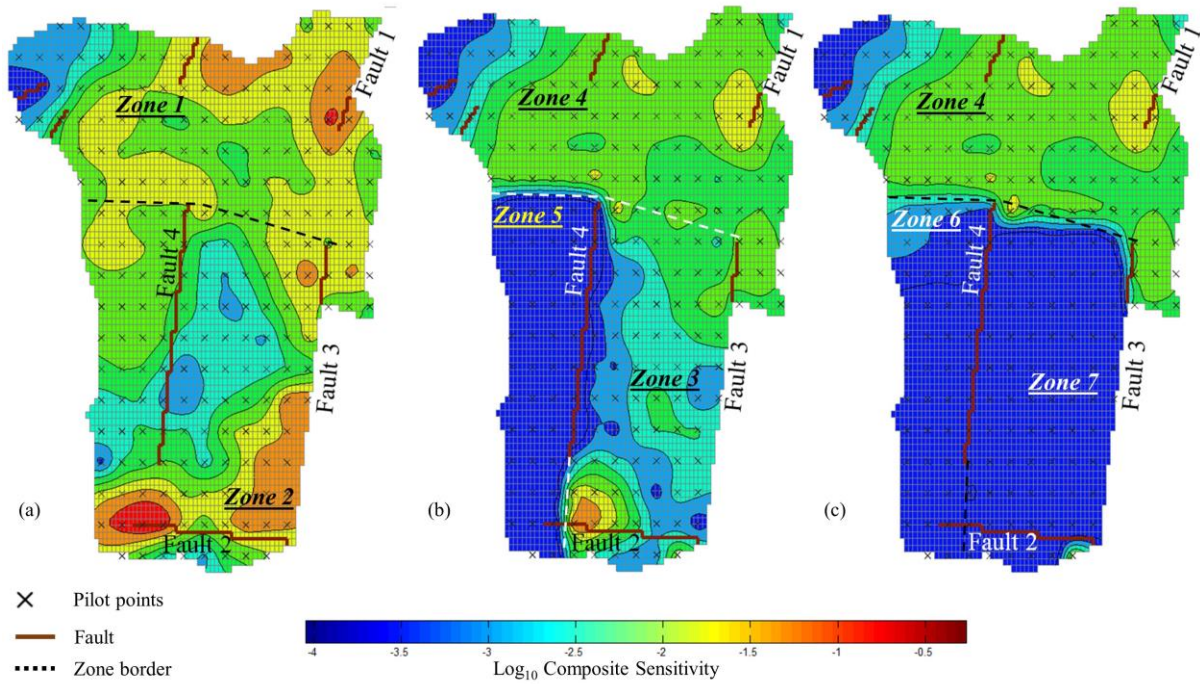
Figure 3-9), which is not surprising since the existing head observations are obtained

from the upper layer (
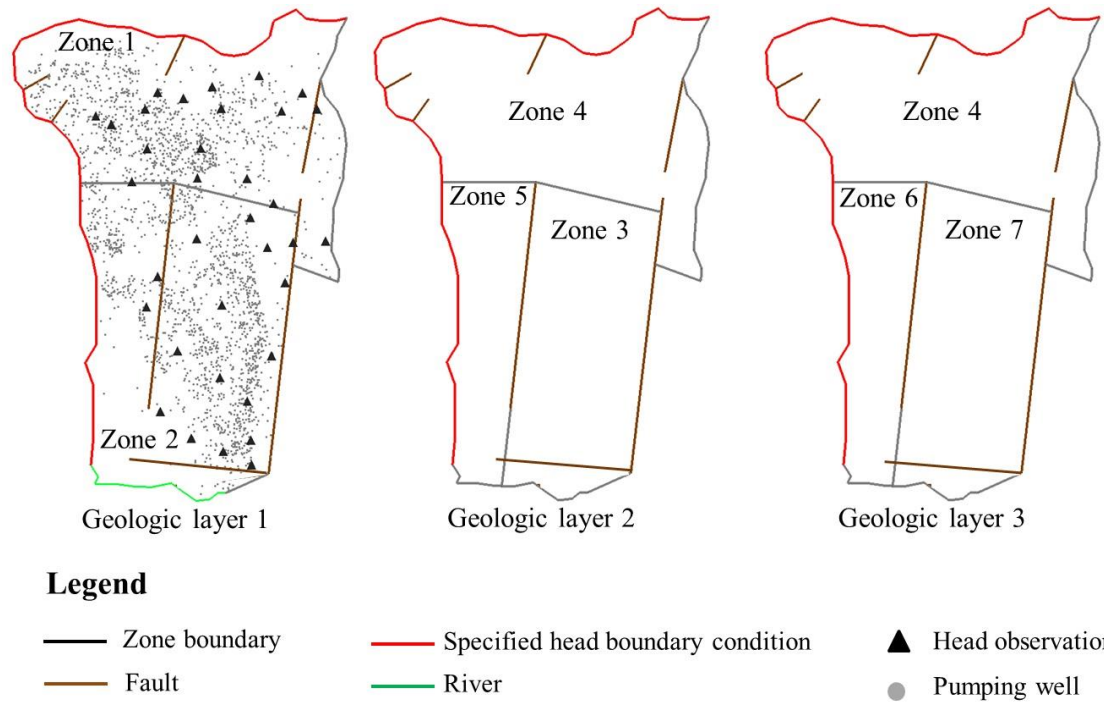
Figure 3-4). The parameter Subset (i) thereby defined the pilot points located in

zones 1, 2, 3, and 4. The highest CS values are at the pilot points located in the southwest of

zone 2, where there is high seaward flow between faults 2 and 4. The CS values decrease from the top layer (e.g. zone 1) to the deeper layers (e.g. zone 4). The CS values also decrease when moving southwards from zone 4 to zone 3 in the second layer. The lowest CS values are for the pilot points of aquitards in zones 5 and 7 and in the deep western aquifer in zone 6, indicating that the hydraulic conductivity in these zones cannot be determined from existing head observations.

Transport simulations for the following 50 years allow the evaluation of the sensitivity of the salinity predictions with respect to the hydraulic conductivity values (
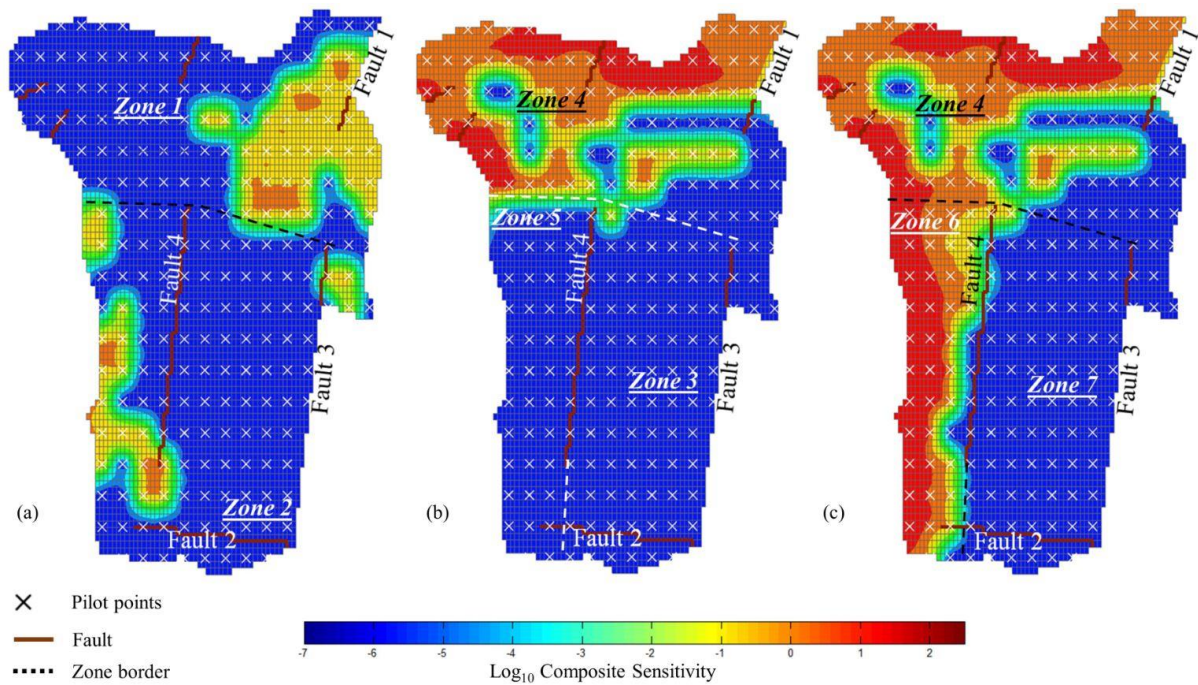
Figure 3-10). This information identifies pilot points belonging to subsets (ii) and (iii) whereby
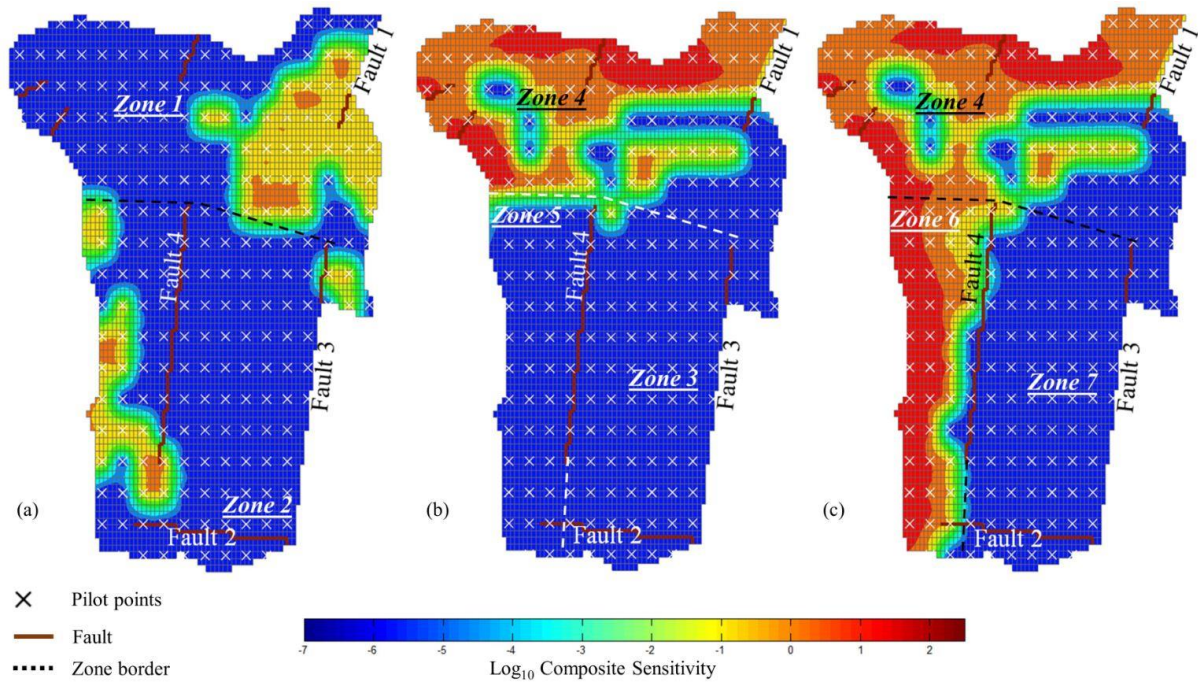
Figure 3-10 indicates that the pilot points in zone 6 (C4c formation) have a high impact on the 50-year displacement of the interface. As a result, these pilot points are defined as belonging to subset (ii). In contrast, low sensitivities are observed with respect to pilot points in zones 5 and 7 for observations (
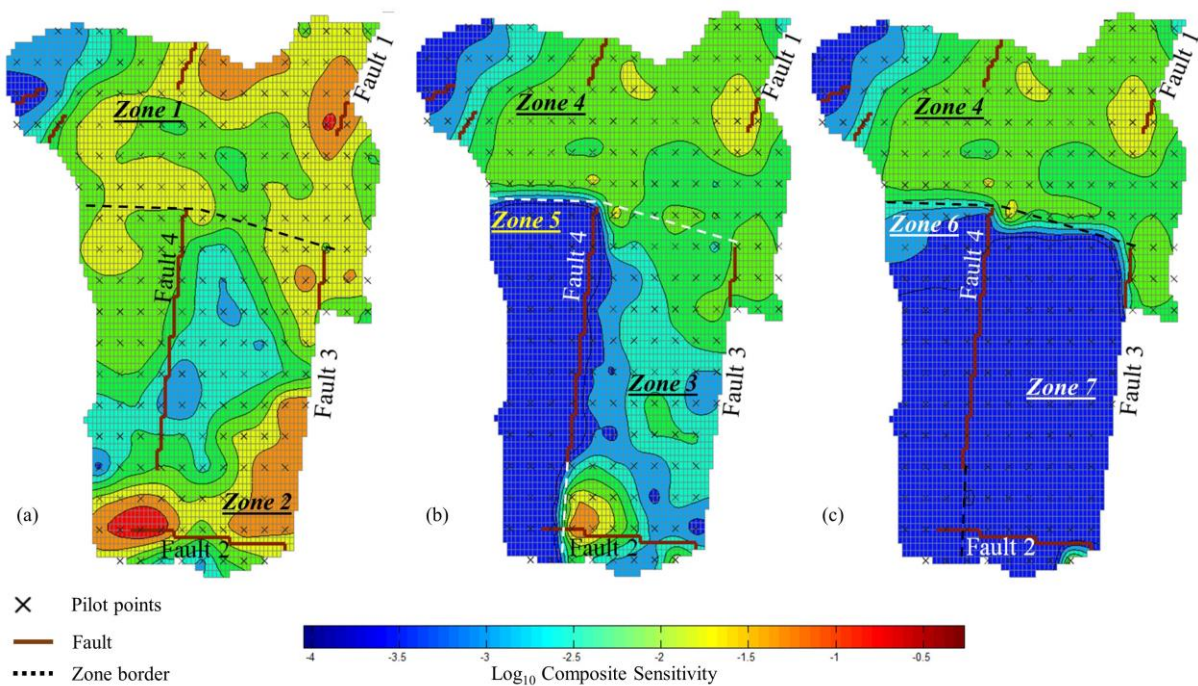
Figure 3-9) and predictions of salinity change (
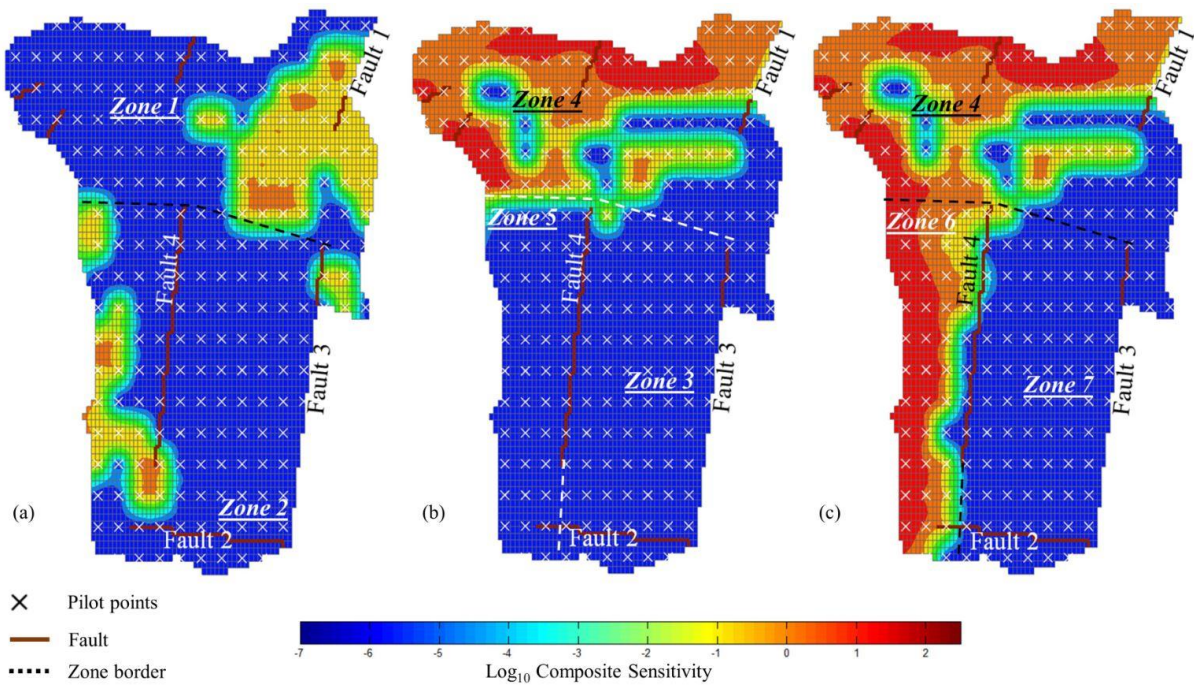
Figure 3-10). The pilot points of these zones are therefore included in parameter

subset (iii).
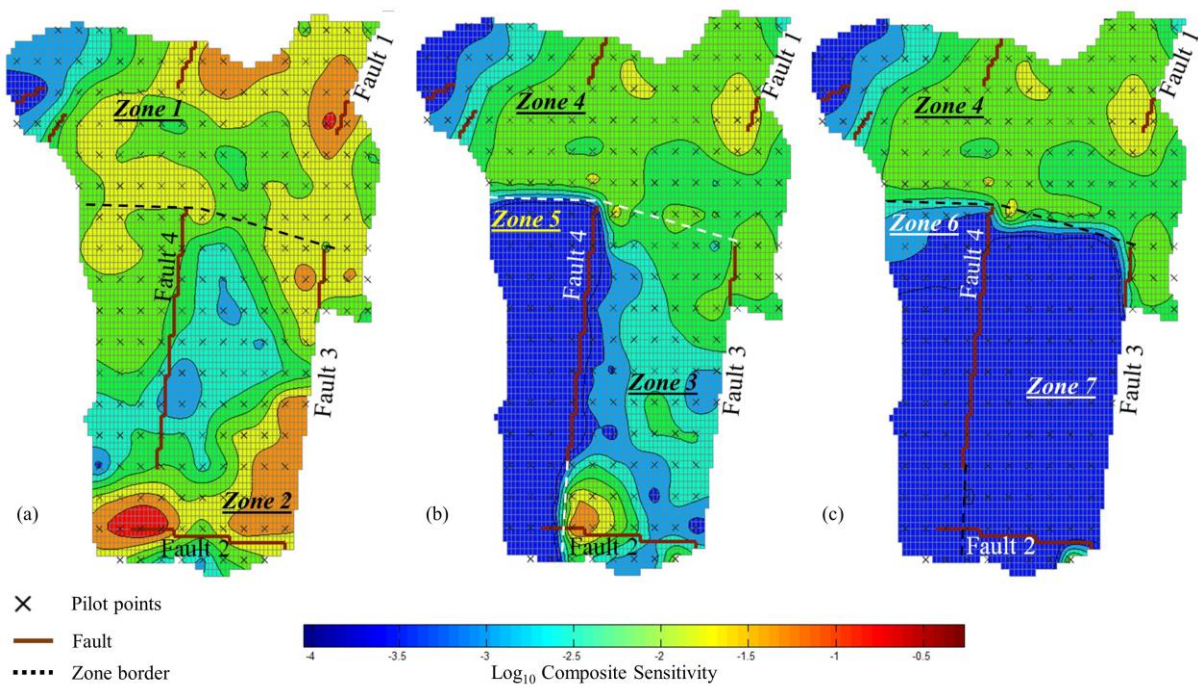
Figure 3-9 Log10 Composite Sensitivity (CS) of head observations to the pilot points values; (a) geologic layers 1, 2 and 3 are shown in plots (a), (b), and (c), respectively.
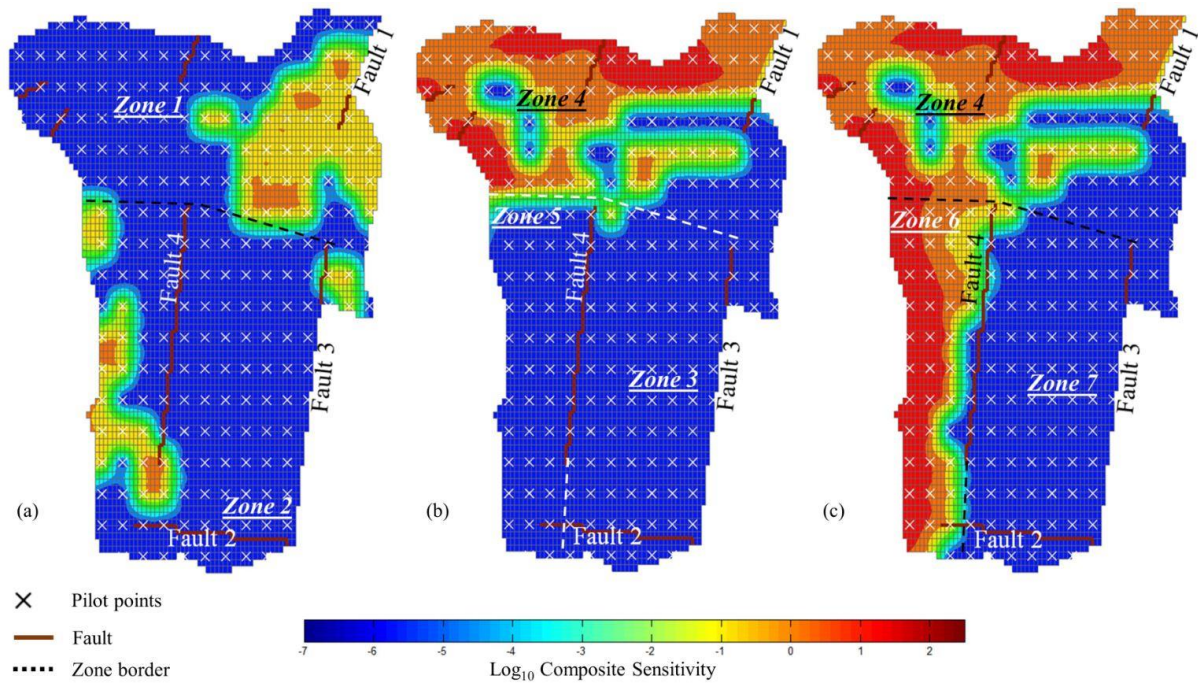
Figure 3-10 Log10 Composite Sensitivity (CS) of model prediction of change in mass of salinity to the pilot point values; (a) geologic layers 1, 2 and 3 are shown in plots (a), (b), and (c), respectively.

3.5.4   Parameters correlation

Figure 3-11 shows the identifiability of parameters along with the locations of head observations and pilot points. The highest identifiability belongs to the pilot points that are located near the head observations in the upper layer (zones 1 and 2), indicating that the values of these pilot points can be estimated within a low level of uncertainty (Figure 3-11a). The identifiability of parameters decreases by 3 orders of magnitude from the top layer (zones 1 and 2) to the deep layer (zones 5, and 6). In the middle layer, the results of parameter identifiability revealed that the estimation of the pilot points values was not unique in zones 3 and 4, and their information is shared with other pilot points located in the top layer (Figure 3-11b). In contrast to other zones, it is clear that the hydraulic conductivity in zones 5, 6, and 7 cannot be informed by the calibration dataset (Figure 3-11c). In zones 5 and

7, the very low identifiability indicates that the changes in the values of parameters in *subset (iii)* cannot offset the changes in other parameters' values in *subset (i)* during the calibration. Therefore, we did not change the subdivision of parameters.
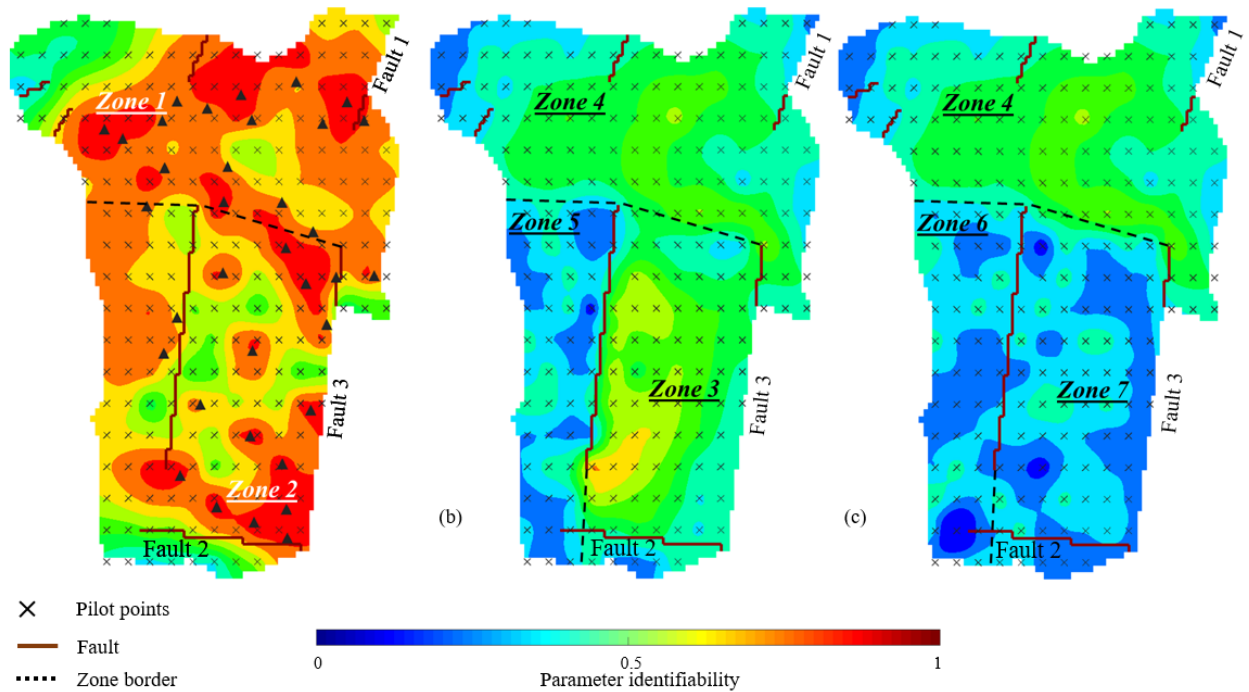
Figure 3-11 Parameter identifiability in the geologic layers; (a) geologic layers 1, 2 and 3 are shown in plots (a), (b), and (c), respectively.

3.5.5 *Calibration-constrained realizations*

One thousand calibration-constrained realizations were generated for the hydraulic conductivity field. For subset (i), the histograms for calibration-constrained $\log_{10}$ hydraulic

93

conductivities are shown in

Figure 3-12. The histograms show that the hydraulic conductivity values of zones 1, 2 and 4 approached the lognormal distribution. The distribution of $\log_{10}$ hydraulic

conductivity in zone 3 was left skewed
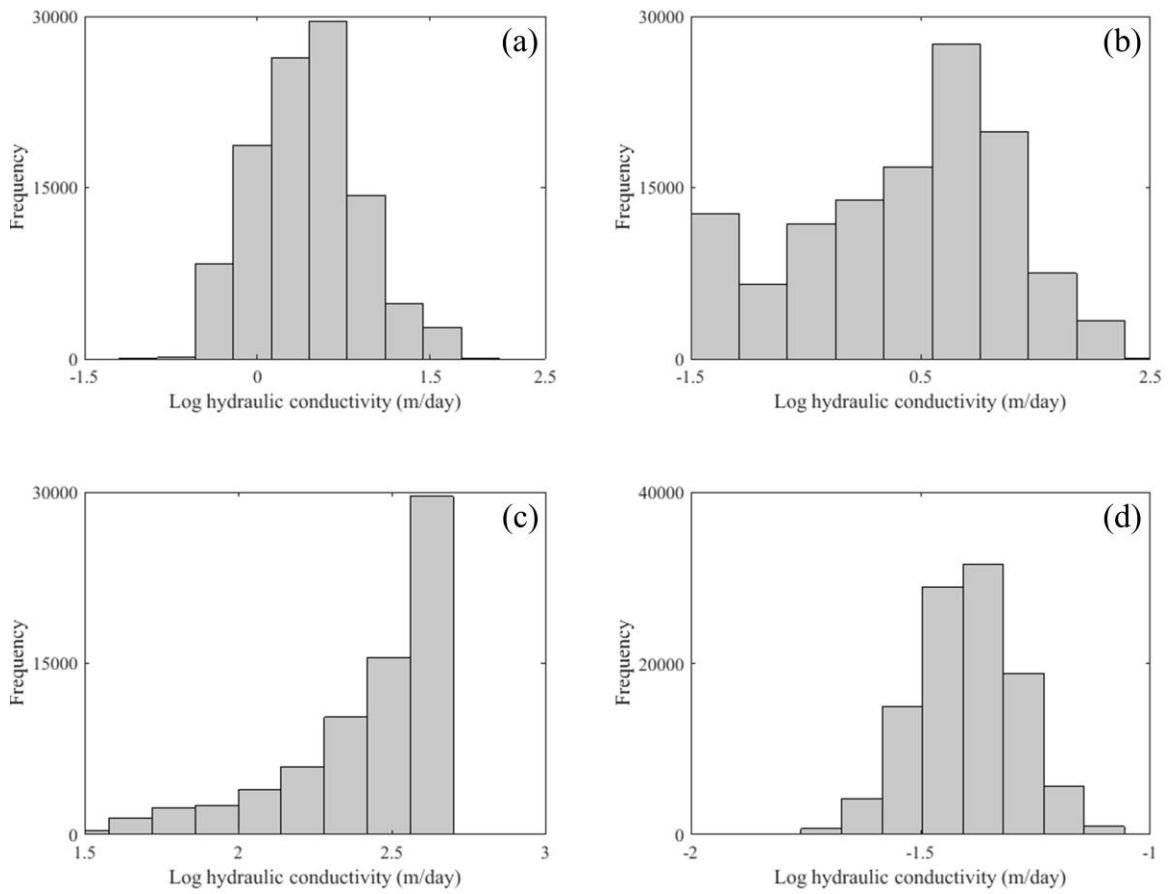
Figure 3-12c) because the initial values of most starting pilot points were high (and close to the upper bound of the expected range) prior to the parameter randomization process

(
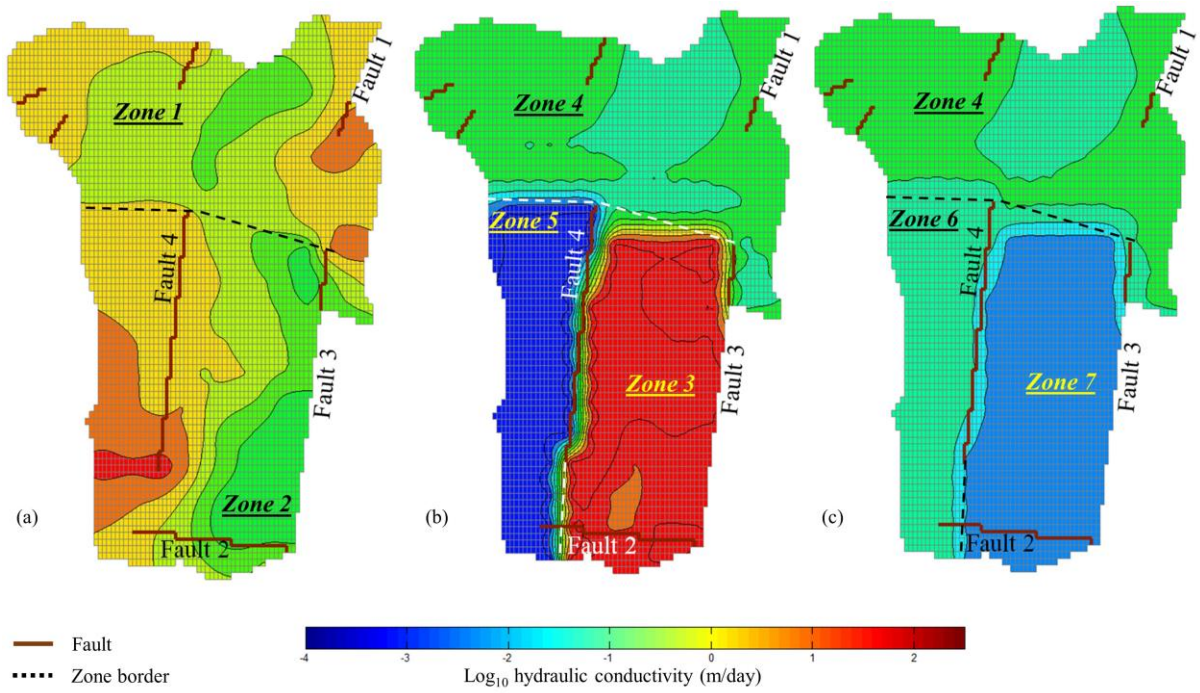
Figure 3-7 and Table 3-1). The spread of the histogram (or heterogeneity) in the calibration-constrained $\log_{10}$ hydraulic conductivities decreases with depth from layer 1 (zones 1 and 2) to layer 2 (zones 3 and 4). This is due to the higher variations in the starting pilot points values in zones 1 and 2 compared with those in zones 3 and 4 (
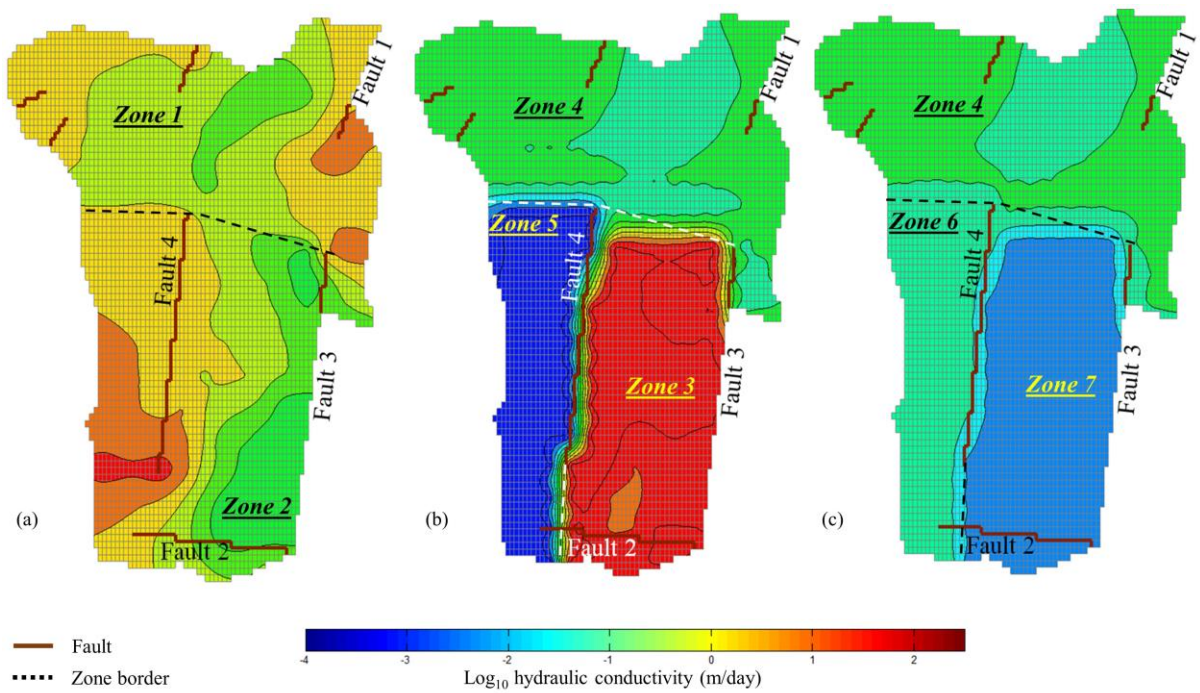
Figure 3-7 and Table 3-1). For subset (ii), the generated fuzzy values of the log

mean hydraulic conductivity and the range of Kriging variogram were used for the Fuzzy

SGS, generating the 1000 realizations of log hydraulic conductivity with the histograms

shown in Figure 3-14a and Figure 3-14d for both scenarios (1 and 2) that were considered

with regards to the limits set on the trapezoidal distribution that was used as the membership

function for the log mean hydraulic conductivity. The shape of the histograms is similar to

the shape of the membership function shown in Figure 3-5. The difference between the two

histograms primarily comes from the difference between the respective log mean hydraulic

conductivity distributions defined for the two scenarios (Figure 3-5a and Figure 3-5b).
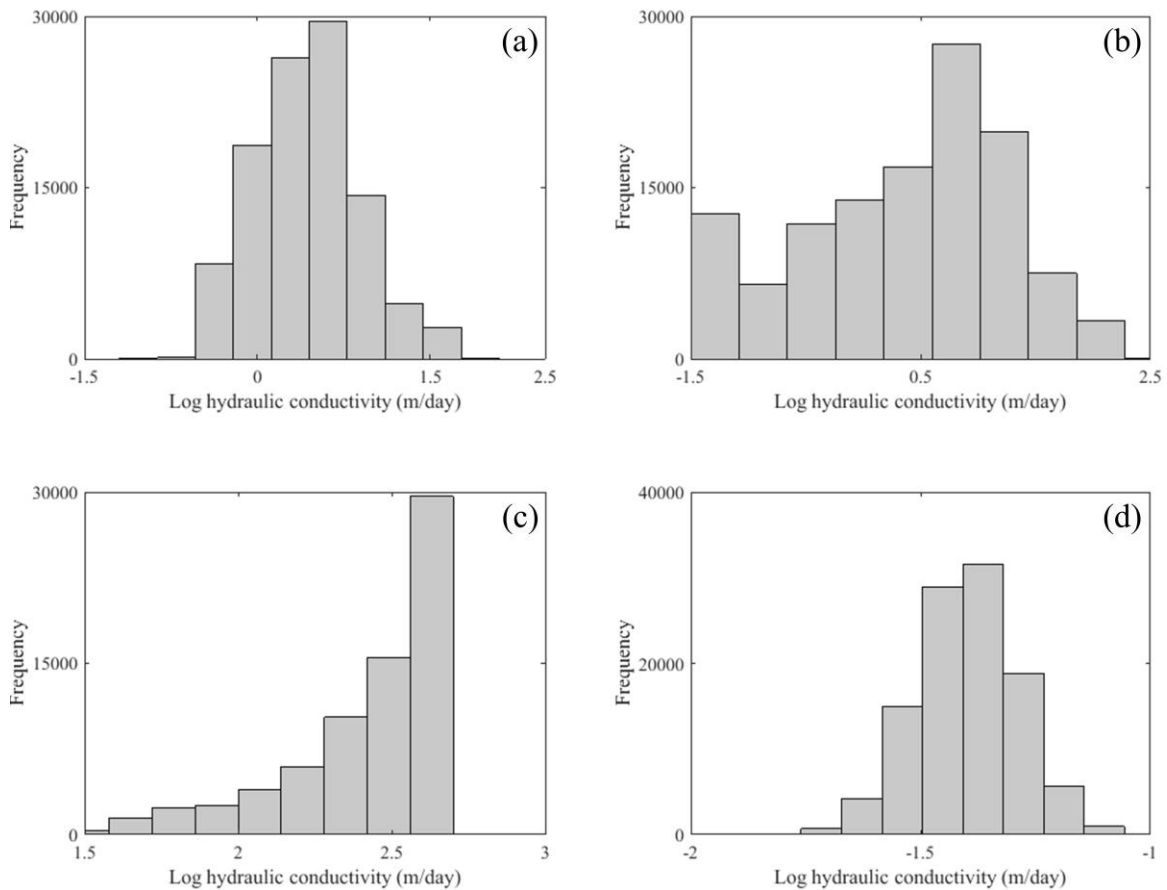
Figure 3-12 Histograms for generated calibration-constrained log10 hydraulic conductivity in (a)
zone 1; (b) zone 2; (c) zone 3; and (d) zone 4

3.5.6 Prediction uncertainty analysis
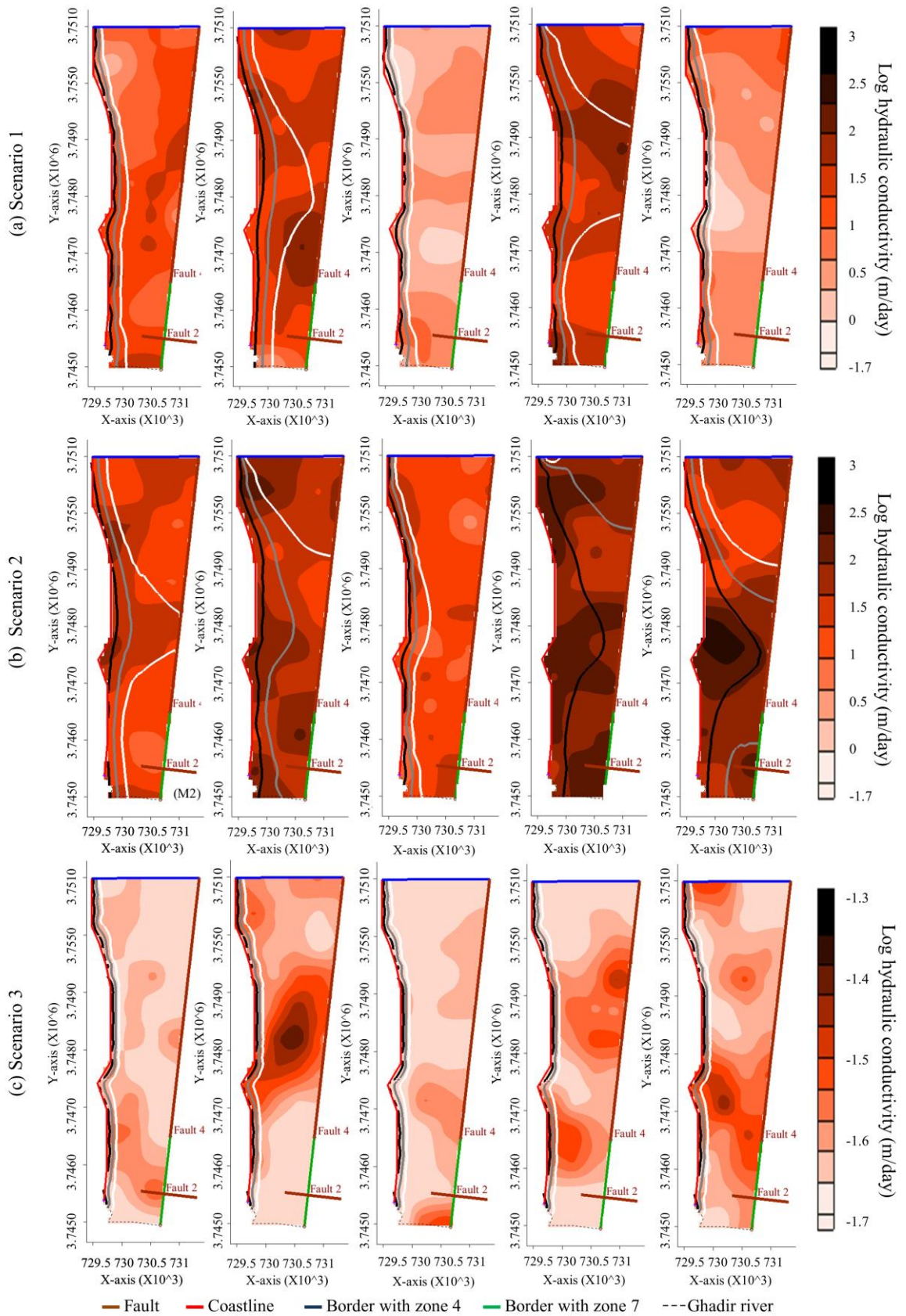
Figure 3-13 shows the calibration-constrained log$_{10}$ hydraulic conductivity fields

along with the position of the salt/fresh water interface after a 50-year simulation in some

randomly selected realizations. The $\log_{10}$ hydraulic conductivity fields are only shown for

zone 6 where different scenarios were used to generate hydraulic conductivity fields. The

uncertainty with the estimated $\log_{10}$ hydraulic conductivity had a noticeable impact on the

estimation of the position of the interface in scenarios 1 and 2 (
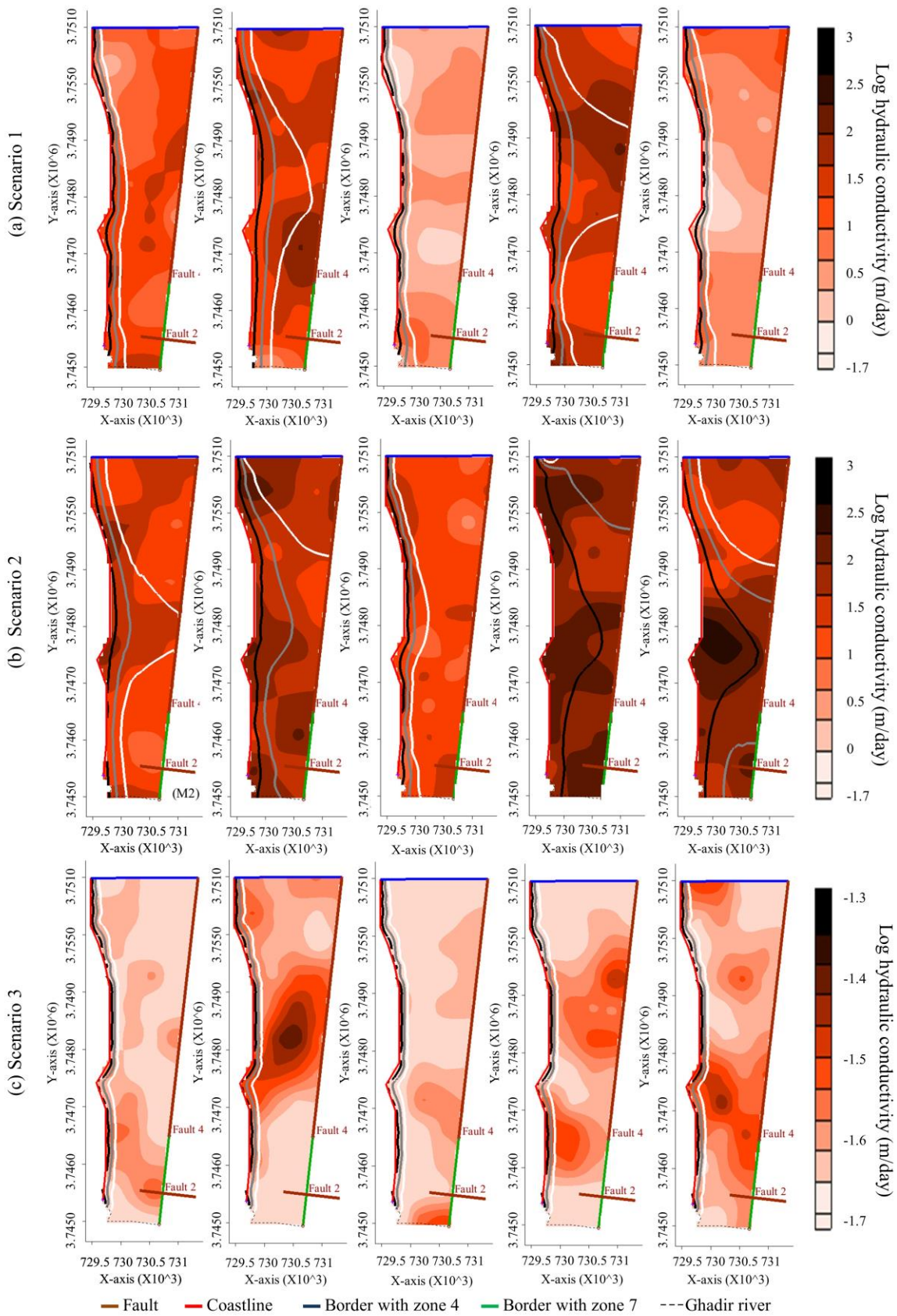
Figure 3-13a and
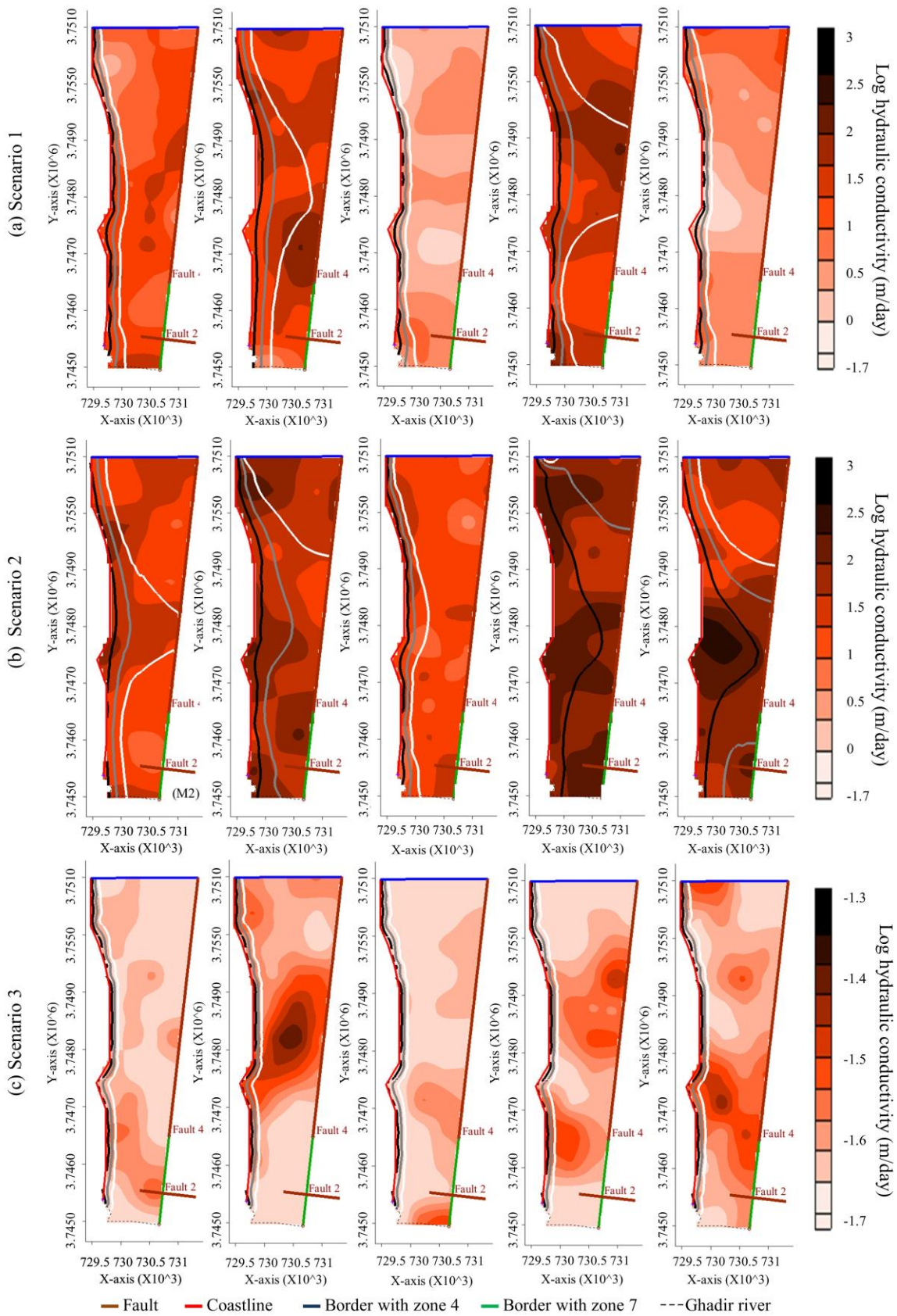
Figure 3-13b). It is apparent that the high hydraulic conductivity values tended to exacerbate SWI and move the interface landward. In both scenarios, variabilities in the estimated $\log_{10}$ hydraulic conductivities produced large variabilities in the prediction of the position of interface. In scenario 1, the variability in the model prediction is larger than that in scenario 2 due to the larger variabilities in the $\log_{10}$ hydraulic conductivity values among the

realizations (
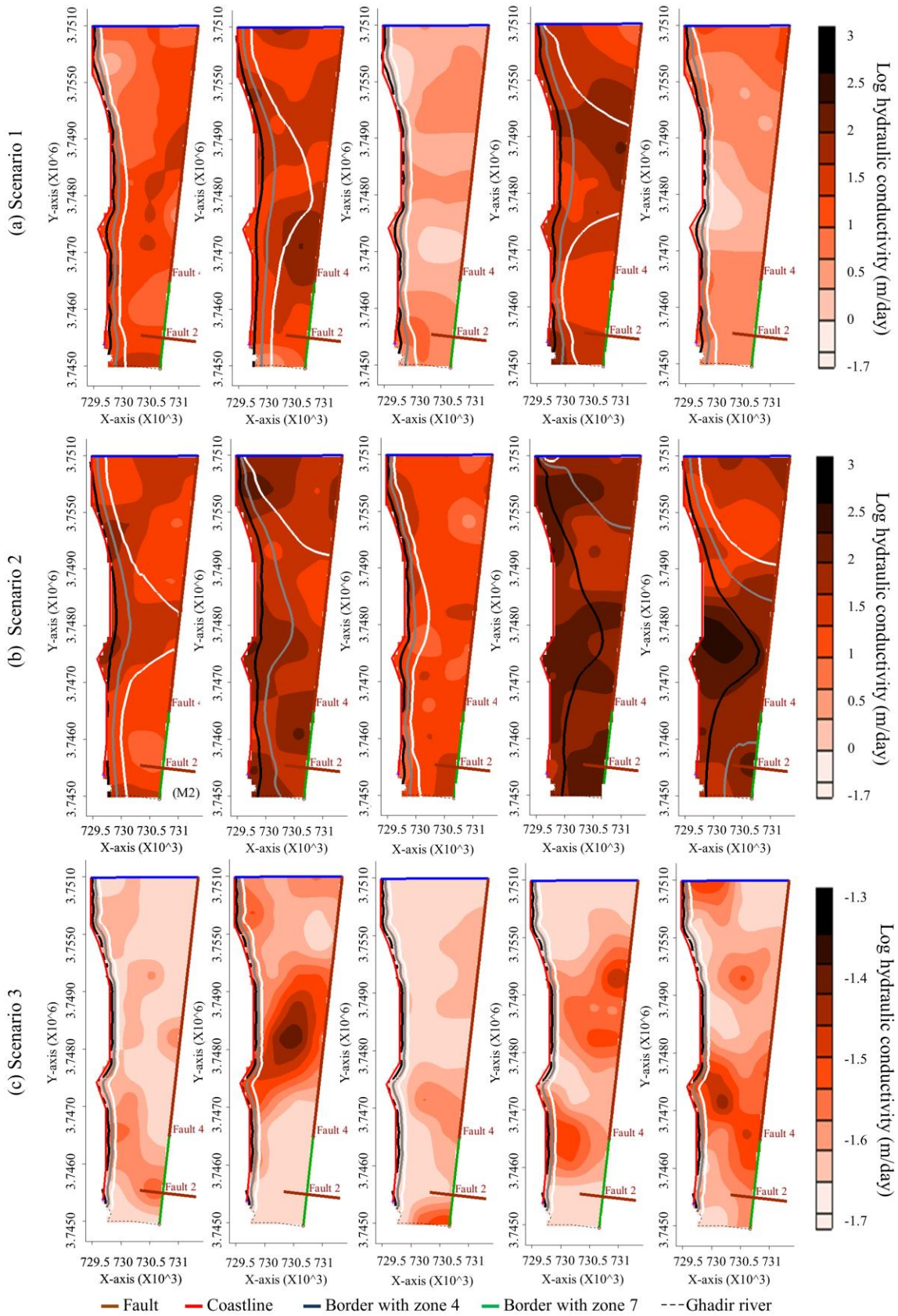
Figure 3-13a vs.
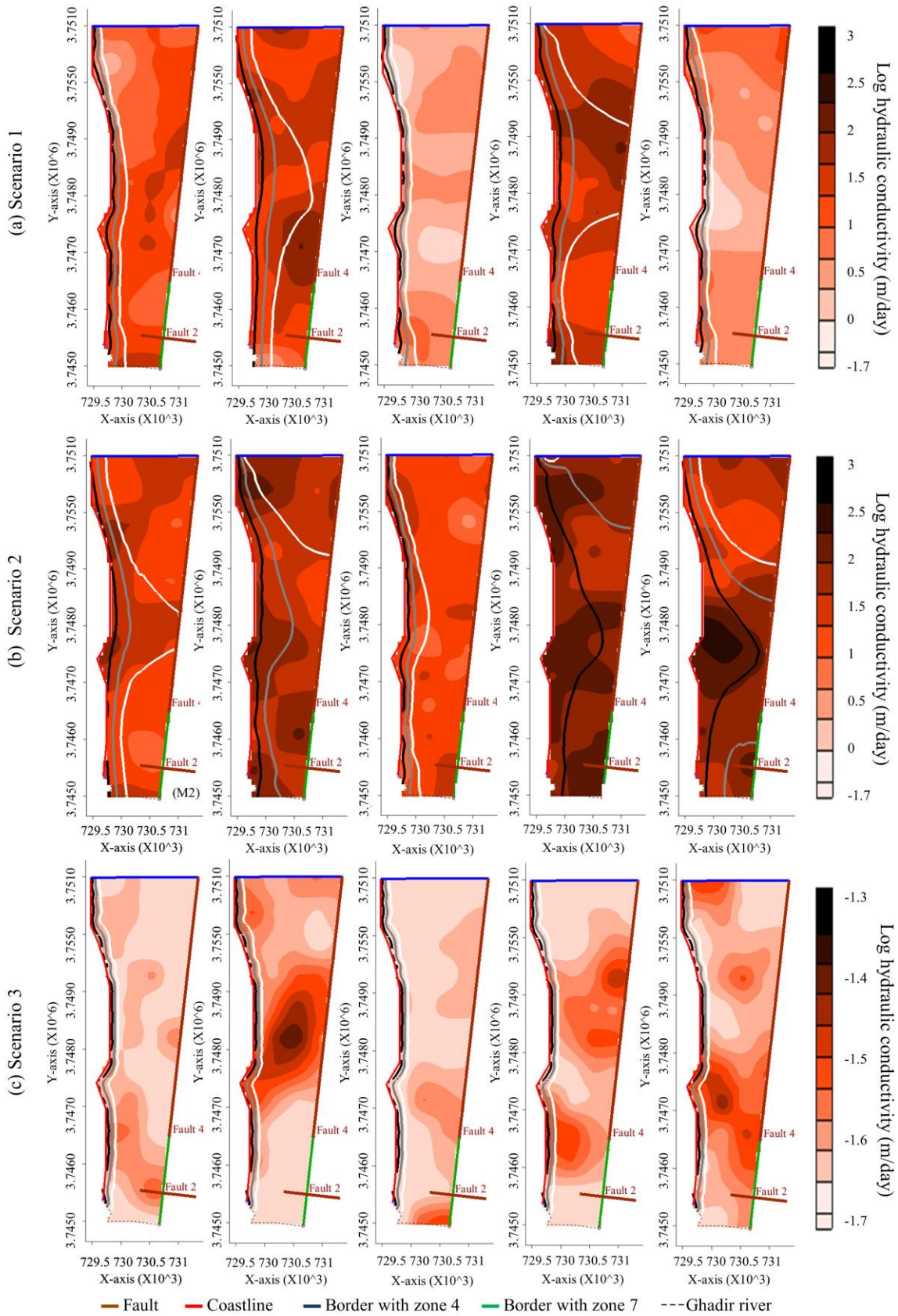
Figure 3-13b). In scenario 3, the $\log_{10}$ hydraulic conductivity values were low along the coastline, and therefore the landward displacement of the interface caused by groundwater abstraction was small as compared with those in other models in scenarios 1 and

2 (

Figure 3-13c vs.

107
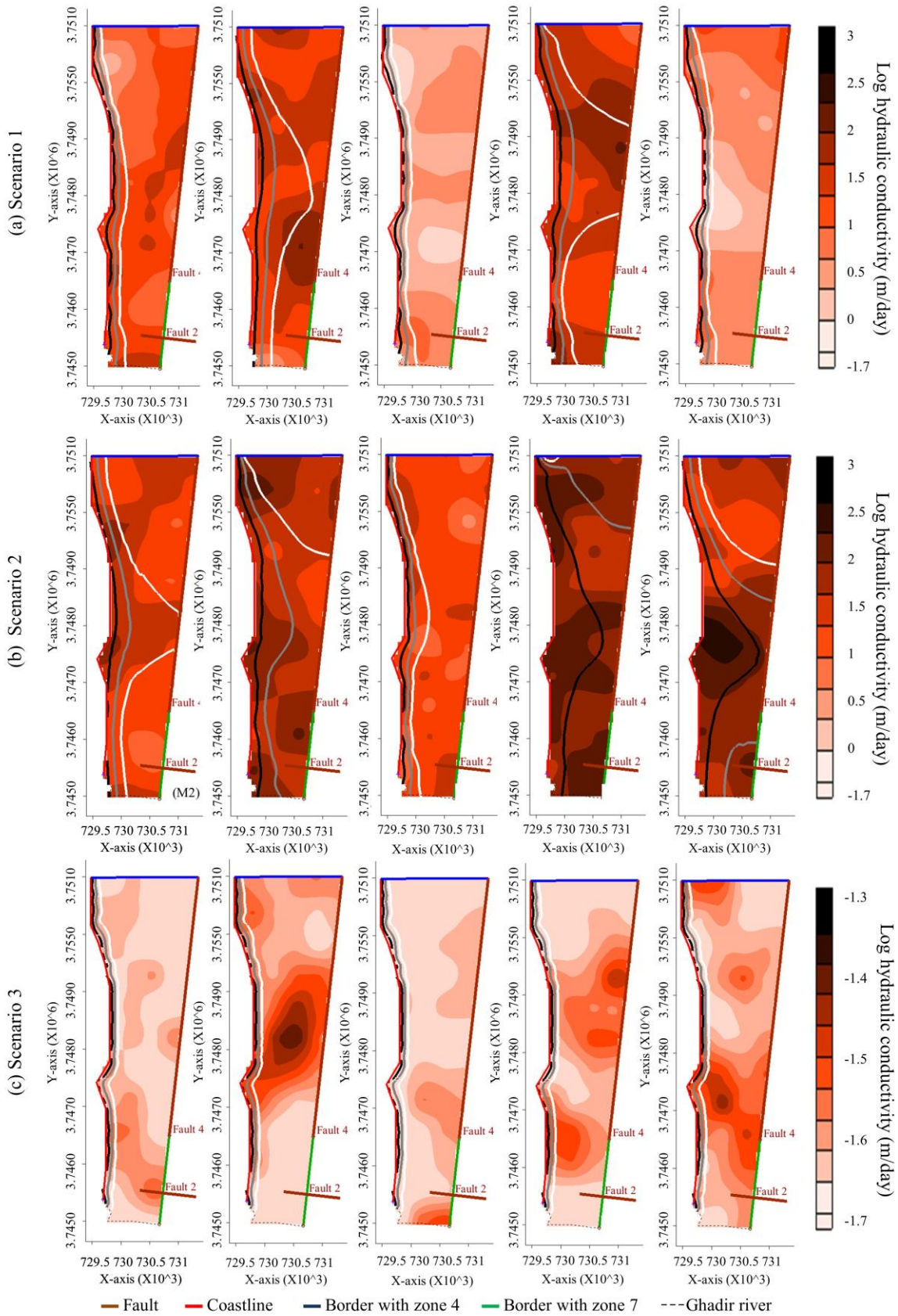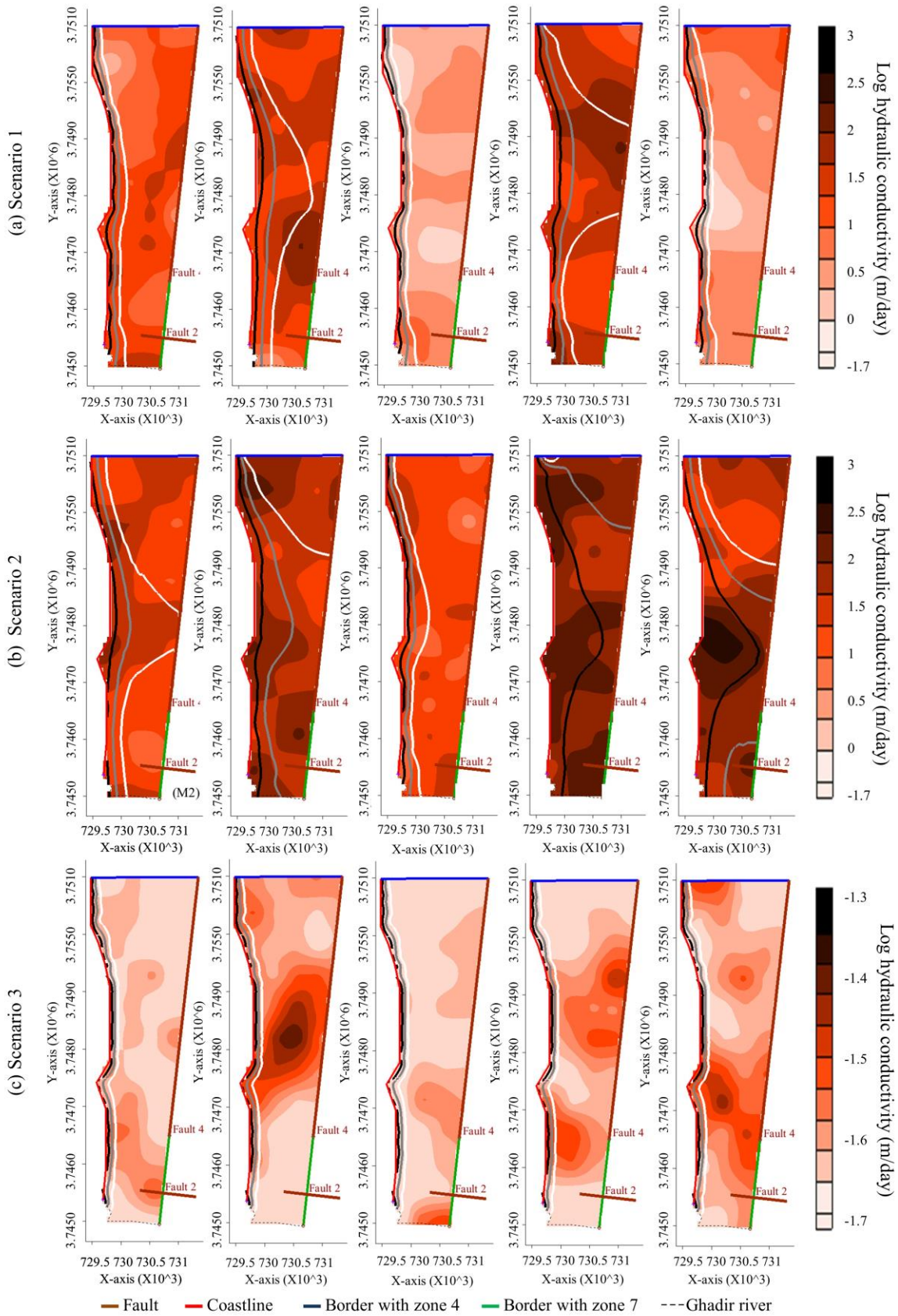
Figure 3-13a and

Figure 3-13b). In this scenario, the variability in the computed salt/fresh water

interface was very small among the generated realizations (
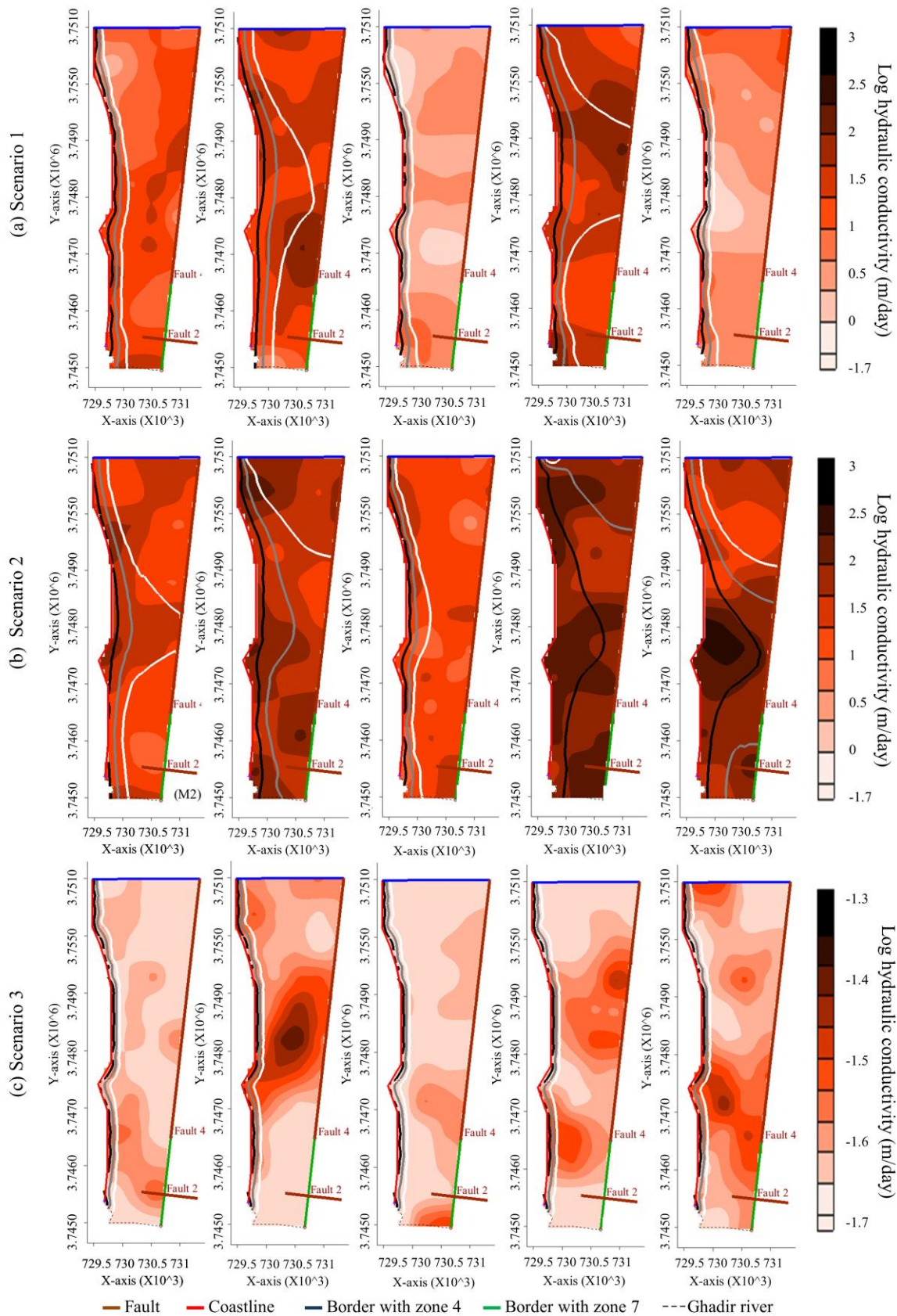
Figure 3-13c).
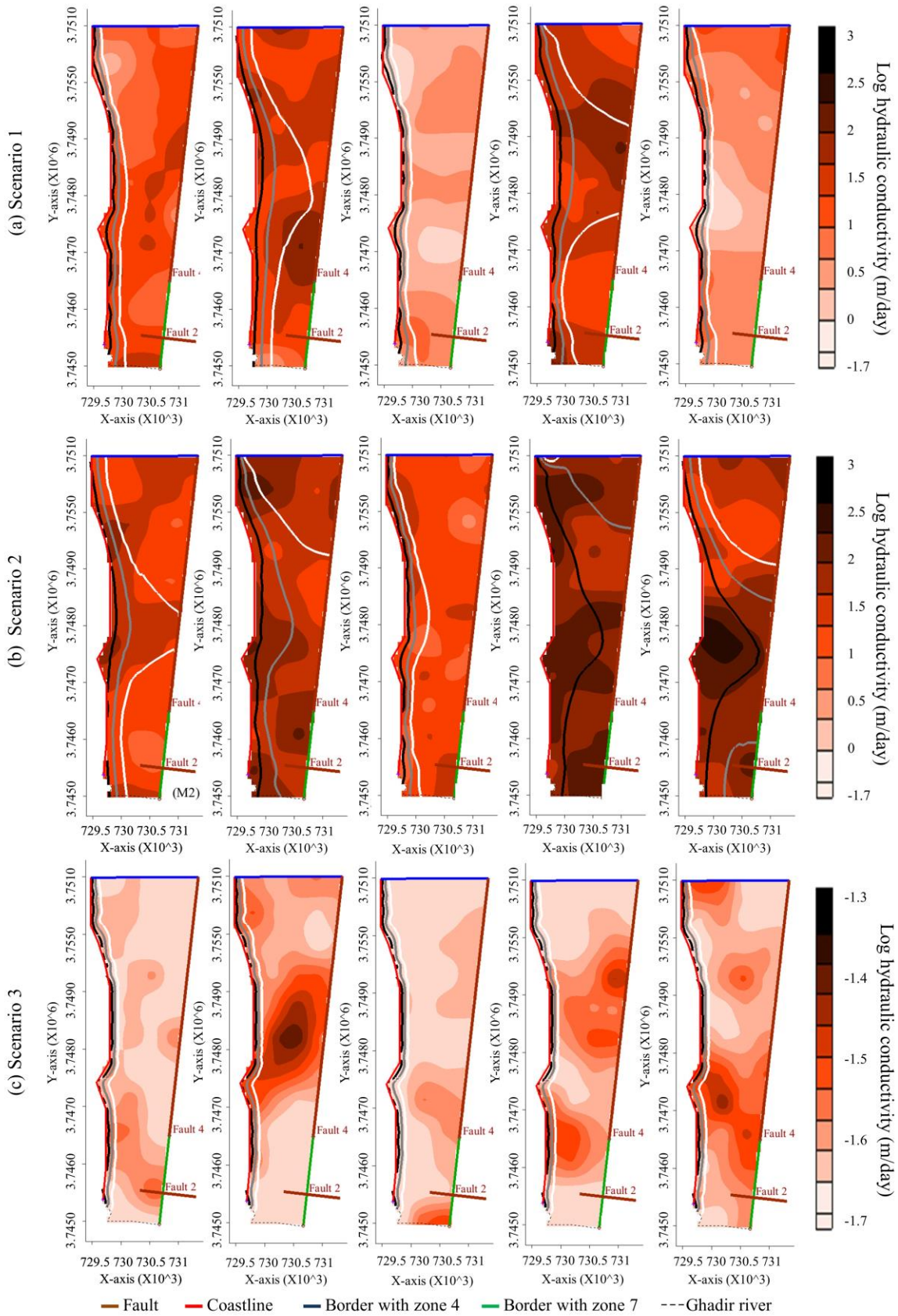
Figure 3-13 Map view of Log10 hydraulic conductivity distribution for zone 6 along with the position of the interface with 75% (black), 50% (gray), and 25% (white) of sea water concentration (35gr/l) after 50

Figure 3-14 shows histograms generated from one thousand predictions from 1969 to 2019. As can be seen, the realizations of the log hydraulic conductivity showed a large variability with regards to the scenarios that were defined with regards to the limits set on the trapezoidal distribution that was used as the membership function for the log mean hydraulic conductivity (Figure 3-14). The prediction histograms have a shape similar to that of the underlying membership function for the log of the mean hydraulic conductivity value in the deep zone 6 (Figure 3-14 vs. Figure 3-5). In scenario 1, the histogram for both predictions exhibits a large range of variability, with the predicted percent increase in total mass of salinity over the 50 years simulation period ranging from 5 to 80%, while the values ranged from 1.3 to 1.9 km3 when it came to predicting the remaining volume of freshwater due to 50 years of abstraction (Figure 3-14b and Figure 3-14c). For scenario 2, with a more informed prior distribution (i.e. less imprecision), the estimated ranges of prediction uncertainty narrowed significantly (Figure 3-14e and Figure 3-14f). Over the 50 years simulation period, the predicted percent increase in total mass of salinity ranged from 40 to 80% in scenario 2, while the predicted values for the remaining volume of freshwater values ranged from 1.3 to 1.5 km3. The difference between the corresponding prediction histograms of the two scenarios underlines the importance of using informed priors to reduce prediction uncertainty for systems, when the hydrogeological parameter values are poorly identifiable from the available calibration data (compare Figure 3-14b and Figure 3-14e, or Figure 3-14c and Figure 3-14f). The predictions in scenario 2 are more realistic than those in scenario 1, because we improved our prior information about the geology of zone 6. By reducing the imprecision of prior information about the $\log_{10}$ mean values (scenario 2 vs. scenario 1), the lower support limit increased by 50% (from 1 to 1.5m/day) (Figure 3-5b vs. Figure 3-5a). As a result of such improvement in prior information, the range of uncertainties with the model

predictions decreased by 55% and ~65% when predicting percent increase in total mass of

salinity and the remaining volume of freshwater, respectively (Figure 3-14e vs. Figure 3-14b

and Figure 3-14f vs. Figure 3-14c), clearly indicating that the imprecision in geologic prior

information has high impact on the estimated range of prediction uncertainty in SWI systems.

When the same kind of SGS for subset (i) was used for subset (ii) instead of the

proposed Fuzzy SGS approach, we found that the calibration-constrained values in zone 6

ranged between 0.02 and 0.035 m/day (Figure 3-14g). The values appear to be different and

much smaller than the range estimated using the Fuzzy approach. Moreover, the range of

predictions was also found to be much smaller (Figure 3-14h and Figure 3-14i) as compared

to the ranges obtained using the Fuzzy approach. The prediction ranged from ~0 to 20% for

the increase in the total mass of salinity and from 1.7 to 1.9 km3 for the remaining volume of

freshwater. Comparing the predicted results in scenario 3 (Figure 3-14h and Figure 3-14i)

with the predicted result of the single pilot point calibrated model (shown by red rectangles in

Figure 3-14h and Figure 3-14i) indicates that the estimated range of prediction uncertainty is

skewed towards the predicted result of the single calibrated model. This is because the

calibration-constrained values were near the lower bound of hydraulic conductivity in zone 6

and similar to the estimated hydraulic conductivity in the calibrated model (Figure 3-14g vs.

Table 3-1). It is apparent that the estimated range of prediction uncertainty strongly depends

on the initial values of starting pilot points. Note that since the initial values used for the

pilot points in zone 6 were not reliable (as they were determined from pure zonal calibration),

large biases are expected for model predictions. This is indeed the case when one compares

Figure 3-14h and Figure 3-14i to the prediction ranges obtained under scenarios 1 and 2

(Figure 3-14b, Figure 3-14c, Figure 3-14e, and Figure 3-14f). One can thus conclude that

generating parameter realizations using SGS with a Gaussian distribution with a poorly

defined mean is not a reliable option for quantifying prediction uncertainty. Using this

approach can lead to severely biased and narrow ranges of prediction.
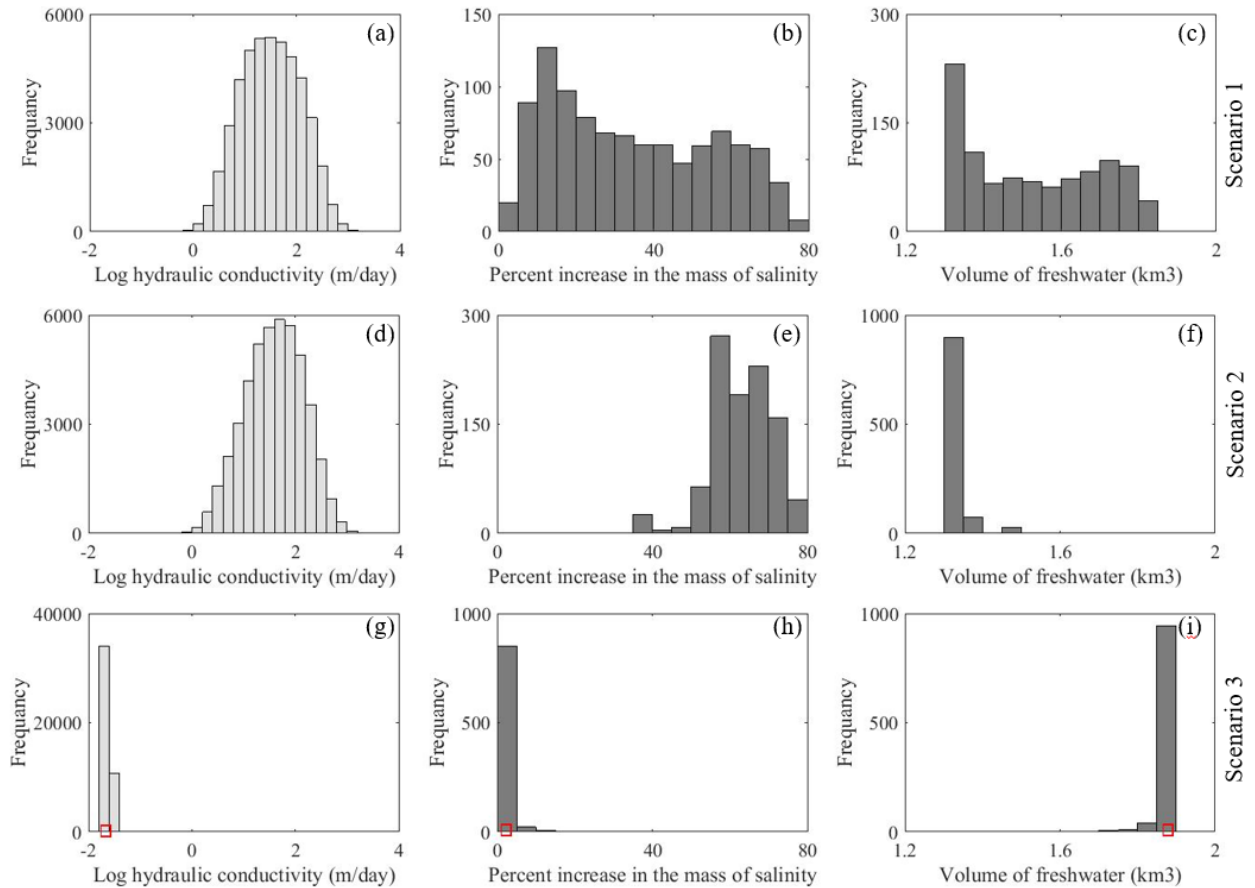
Figure 3-14 Histograms for 1000 realizations of log10 hydraulic conductivity for zone 6 (light gray) and for the corresponding model predictions (dark gray), respectively: Scenario 1 with vague prior information (a, b and c), Scenario 2 with strong prior information (d, e and f); and Scenario 3 using SGS instead of Fuzzy SGS for zone 6 (g, h and i), Bin widths of 0.2, 5 and 0.05 are used for the histograms (a, d and g), (b, e and h), and (c, f and j), respectively. □ represents the calibrated log_{10} hydraulic conductivity for zone 6 and predicted values using the deterministic model (i.e. the single calibrated pilot-points model)

While the nature of the real-world systems involves imprecise geologic prior

information due to doubtful, biased or limited field-measurements, the traditional NSMC

methodology requires precise and "crisp" information to infer the required statistics for MC

simulations. Using the traditional methodology, the estimated range of prediction uncertainty

can contradict the findings gained from the sensitivity analysis when predicting the interface

movement in SWI systems. For the present example, the model prediction exhibited small

uncertainties when using the traditional NSMC methodology (scenario 3 in Figure 3-14) whereas the sensitivity analysis asserted that large prediction uncertainties would occur when predicting the displacement of the interface (Figures 9 and 10). This contradiction is caused by forcing the use of a crisp prior probability distribution about the geology of deep layers during the uncertainty analysis instead of realistic and basic soft information that are often available. We found that the choice of the expected field value (i.e. starting values of the pilot points) can influence strongly the estimated range of the prediction uncertainty using the NSMC (Figure 3-14a and Figure 3-14d vs. Figure 3-14g). We demonstrated that if the expected value is set equal to the zonal calibrated result when it is not known a-priori (as suggested by Doherty & Welter, 2010), the stochastic predictions of SWI can be biased towards the predicted results from the single pilot point calibrated field, which can contradict the results of the sensitivity analysis (Figure 3-14g). This can be the case in deep heterogeneous coastal aquifers because, in field practice, observations data are usually distributed within the upper parts of a geologic domain due to financial or spatial constraints (e.g. through existing pumping wells). Therefore, the hydraulic conductivity of the deep layers cannot be properly informed by observations. If the calibrated hydraulic conductivity is used as the expected field value (i.e. starting values of the pilot points), the estimated range of the prediction uncertainty does not encompass the truth. In such cases, the expected field value is invariably determined from limited hydrogeological evidence or expert knowledge that often provides vague, ambiguous and basic information about the geology of the deep layers in a real-world system. Our findings highlighted that the imprecision in the expected mean value of the hydraulic conductivity in the null-space pilot points located in the deep geologic layer can strongly affect the estimated range of uncertainty with the prediction of the interface in a coastal aquifer (scenario 1 and 3 vs. scenario 2).

The gap between the results of the traditional methodology and sensitivity analysis can be reduced if the imprecise nature of real-world systems can be realistically and simply incorporated into the prediction uncertainty analysis. Our proposed Fuzzy SGS approach can be used to express both uncertainty and imprecision simultaneously in the prediction uncertainty analysis. Using this approach, the belief of an expert on the likelihood of the occurrence of a value in the field can be simply expressed using a membership function and subsequently incorporated into the uncertainty analysis. For practical applications in deep heterogeneous SWI systems, we suggest considering a wide range of fuzzy expected values for the null-space pilot points that are located in the deep layers to inform predictions. Similarly, the imprecision of the variogram can be quantified and incorporated into the prediction uncertainty analysis by calculating a wide range of "sensible" values for the unknown parameters of the variogram (nugget effect, sill, and range) using fuzzy membership functions. Using Fuzzy SGS, a normal (prior probability) distribution is created to generate random log hydraulic conductivity field by coupling a fuzzy expected field value with a fuzzy variogram. The final distribution of multiple calibration-constrained log hydraulic conductivity fields contains a large number of "sensible" prior probability distributions with different means and variances, instead of a single crisp prior probability distribution that is obtained using the traditional NSMC methodology. This approach can lead to a more realistic estimation (or maximum level) of prediction uncertainty (e.g. scenario 2 in this study) than the traditional methodology.

In the current application, the complexity of the subsurface conditions led to a paucity in data describing the geology as a factor controlling SWI, which resulted in large uncertainties in model predictions. Such uncertainties can make it difficult for water resources managers and decision makers to plan a management strategy to secure the quantity and quality of groundwater in the pilot aquifer. However, uncertainties are only relevant if

115

they encapsulate an unwanted situation. A decision can be made based on highly uncertain results as long as it lies outside the uncertainty bound; otherwise, it is necessary to evaluate the risk that the decision may fail when its planning relies on uncertain model predictions. For the present prediction example, if a decision seeks a resource with the freshwater volume of $<1.2km^3$, the high uncertainty with the model prediction does not influence the decision. On the other hand, there is a risk that the decision fails if planning for freshwater volumes greater than $1.3km^3$. Ignoring imprecision in prior information can lead to an overestimation of the available volume of fresh groundwater (i.e. scenario 1 vs. scenario 2); which in turn misinforms decision making about freshwater volumes in excess of $1.5km^3$. Interestingly, the estimated predictions using the traditional methodology (i.e. scenario 3) can completely mislead decision makers if a decision seeks a freshwater resource with a volume of greater than $1.7km^3$. Using the traditional methodology, a large volume of freshwater (i.e. ~1.7 to $1.9km^3$) is estimated compared to scenario 2 (i.e. ~1.3 to $1.5km^3$). In short, if a decision lies inside the uncertainty bound, the proper estimation of prediction uncertainty can cause decision makers to invest in obtaining freshwater from other resources (e.g. deep aquifer, desalination, precipitation …) to meet the demand. Therefore, it is imperative to assess the tradeoff between the prediction uncertainty and the risk of project failure to understand the importance of proper estimating the prediction uncertainty.

3.6   Conclusion

In the present study, we developed a methodology to provide estimates of the prediction uncertainty for cases where the available calibration dataset holds limited information about (pilot points) parameters that inform the predictions of interest. Our methodology combines more or less crude geologic prior information and prediction sensitivity analysis with fuzzy set theory and the NSMC methodology. The sensitivity

analysis is used to identify the parameter subspace of the model, which are informative of model predictions but uninformed by the calibration dataset. This subspace is critical for making prediction uncertainty estimates. Expert knowledge proved to be an important information that was used to constrain the subspace through a set of fuzzy variables and probability density functions. By combining these different methodologies together in what we call Fuzzy SGS, we were able to make estimates of the variabilities in the underlying hydraulic conductivity fields. Using the proposed Fuzzy SGS method, limited prior knowledge about hydrogeological parameter values can be represented by a set of membership function with e.g. a Gaussian, a triangular, a trapezoidal or a uniform distribution to generate random hydraulic conductivity fields. These fields form the input to the NSMC method.

We have compared this methodology to the uncertainty estimates obtained through the traditional NSMC methodology employing traditional SGS. In this method, generating a set of random fields for the hydraulic conductivity requires multiple starting (pilot points) parameters and a (lognormal) probability distribution defined on the basis of prior information. If the probability distribution is poorly known from prior information, it can be estimated based on the calibrated results of pilot points. Our findings show that combining NSMC with only pure SGS (i.e. the traditional NSMC methodology) can increase the risk of underestimating the prediction uncertainty. Underestimation of the prediction uncertainty may lead to results that can misinform decision makers, and thereby cause undesirable management decisions.

The methodology was demonstrated on a case located along the Eastern Mediterranean (Beirut, Lebanon). The pilot aquifer is a fractured heterogeneous coastal aquifer that is highly affected by SWI from its upper parts. We used a SEAWAT model to examine the availability of freshwater resources in the deep parts of the aquifer characterized

by limited geologic information. The available head observations from the upper parts could not provide information about the geology of the deeper parts to which the predictions were sensitive. We showed that the prediction uncertainty is underestimated using the traditional NSMC method for cases similar to this aquifer. Using our methodology, we made a quantification of the prediction uncertainty in response to the uncertainty with the heterogeneity in the hydraulic conductivity under such poor prior information. The uncertainty related to the deep part of the system could best be constrained by using crude prior information to carry our Fuzzy SGS.

In the present application, we limited the prediction uncertainty analysis to the influence of uncertainties with the heterogeneity in the hydraulic conductivity due to its higher impact on the prediction of the interface in comparison to other model parameters. Incorporating further prediction uncertainties including the uncertainties related to dispersivity coefficients, recharge and discharge rates, spatial distribution of pumping rates and boundary conditions is recommended. Yet, the computational time associated with this endeavor is prohibitive, which was recognized as the main limitation of the present work to include all uncertain parameters during the prediction uncertainty analysis. For real-world applications, it is recommended to use the fuzzy SGS for incorporating prior information about all uncertain model parameters that are critical to model predictions because their prior information is expected to be imprecise due to the nature of real-world systems. It is expected that the estimated range of prediction uncertainties using the proposed methodology would increase the uncertainty in the final model predictions.

CHAPTER 4

DATA-WORTH ASSESSMENT FOR A THREE-DIMENSIONAL OPTIMAL DESIGN IN NONLINEAR GROUNDWATER SYSTEMS

Abstract

Groundwater model predictions are often uncertain due to inherent uncertainties in model input data. Monitored field data are commonly used to assess the performance of a model and reduce its prediction uncertainty. Given the high cost of data collection, it is imperative to identify the minimum number of required observation wells and to define the optimal locations of sampling points in space and depth. This study proposes a design methodology to optimize the number and location of additional observation wells that will effectively measure multiple hydrogeological parameters at different depths. For this purpose, we incorporated Bayesian model averaging and genetic algorithms into a linear data-worth analysis in order to conduct a three-dimensional location search for new sampling locations. We evaluated the methodology by applying it along a heterogeneous coastal aquifer with limited hydrogeological data that is experiencing salt water intrusion (SWI). The aim of the model was to identify the best locations for sampling head and salinity data, while reducing uncertainty when predicting multiple variables of SWI. The resulting optimal locations for new observation wells varied with the defined design constraints. The optimal design (OD) depended on the ratio of the start-up cost of the monitoring program and the installation cost

of the first observation well. The proposed methodology can contribute toward reducing the uncertainties associated with predicting multiple variables in a groundwater system.

4.1   Introduction

Groundwater models are commonly used in conjunction with field monitoring to assess the physical processes representing subsurface flow and solute transport. Such models simulate the groundwater dynamics in an aquifer by translating its physical, chemical, and biological characteristics into mathematical equations with simplifying assumptions (Holzbecher and Sorek 2006). These equations require adequate representative data about aquifer characteristics such as hydraulic properties, geological borders, boundary conditions, sources and sinks, amongst others, towards understanding groundwater dynamics (Bakalowicz 2005). However, the complexity of subsurface conditions can preclude at times having adequate data about control parameters, which will result in increased uncertainties with model simulations (El-Fiky 2010). Under an incomplete knowledge coupled with the uncertainty in predictions, it is not feasible for water resources managers and decision makers to plan a management strategy to secure the quantity and quality of groundwater (Tribbia and Moser 2008). Therefore, many aquifer systems remain not well protected or are poorly managed because of the lack of both monitoring and the appropriate decision support tool such as a well-calibrated groundwater model (Comte et al. 2006). Hence, it is imperative to design a monitoring network that would alleviate prediction uncertainties (Storck 1997). In this context, models can be used as a test bed to design for new (optimal) monitoring locations that would increase the reliability of model simulations. This technique is generally referred to as optimal design (OD) with several reported methods to guide the design of

monitoring networks towards reducing uncertainties in model predictions (Tiedeman et al. 2003; Herrera et al. 2000; Reed et al. 2000; Cieniawski et al. 1995; Wagner 1995; Andricevic and Foufoula-Georgiou 1991; Loaiciga 1989; Rouhani and Hall 1988).

A recently developed method by Moore and Doherty (2005), and later extended within the Bayesian context by Christensen and Doherty (2008), evaluated the variance of prediction uncertainty using a linear propagation of uncertainties associated with parameters that are formulated for distributed models. Using this method, an existing calibration dataset is augmented by adding new observations. The worth of such an addition (subsequently referred to as data worth (DW)) to reduce model prediction uncertainty is then evaluated. Dausman et al. (2010) applied the DW-based OD on the Henry problem to define the optimal locations of salinity concentration and temperature that would reduce uncertainty of predicting the displacement of a salt/fresh water interface caused by a change in the inflow to the system. Wallis et al. (2014) extended the DW-based OD for selecting multiple observations and Wöhling et al. (2016) extended it further by using a genetic algorithm (GA) to incorporate multiple new observations of head and/or hydraulic conductivity to decrease the predictive uncertainty. Vilhelmson and Ferre (2017) carried out yet another extension to simultaneously select multiple new measurements targeting multiple forecasts of interest. Note that the applications of the DW-based OD are largely restricted to a single or multiple observation location(s) in two dimensions. The simultaneous DW-based optimization of monitoring design with measurements in three dimensions has not been reported. Expanding the DW approach into three-dimensional space is particularly important for monitoring contaminant concentrations and to design a solute transport system.

In practice, groundwater contamination distribution varies spatially and vertically over a geologic domain. In order to understand and predict the contaminant transport, it is

imperative to sample concentrations along all spatial directions. An optimal design in three dimensions allows the identification of the optimal locations for monitoring contaminant concentration both in space and across depth. The best example of such systems is saltwater intrusion (SWI) where the spread of the intrusion typically occurs in three dimensions through the lateral and vertical displacement (or upconing) of the interface. In modeling of SWI, neglecting three-dimensionality in geologic input data can result in large uncertainties with regards to model predictions (Werner et al. 2013), influencing both the magnitude and the trend of the intrusion (Kerrou and Renard 2010). It can also lead to overestimation of the toe penetration length (Lu et al. 2009), and subsequently misevaluating the DW of a proposed design when the OD target is predicting the future position of the interface. In such cases, geologic data should be collected through the direct observations of hydraulic conductivity values in all spatial directions in order to reduce prediction uncertainty. However, financial constraints and/or spatial limitations (e.g. in urbanized aquifers) usually limit the accessibility to direct measurement of hydraulic conductivity from the deep parts of an aquifer (Hartmann, et. al. 2014). Using inverse modeling, hydraulic conductivity values can be estimated through the inverse solution of the groundwater flow and/or solute transport equations for the value of an observed dependent variable (or an indirect observation) such as hydraulic head and/or contaminant concentration (Hoeksema and Kitanidis, 1984). Dausman et al. (2010) recognized that the measurements of salinity are of greater worth than other measurements in proximity to the interface at locations where the interface moves because salinity concentration defines the interface. The cost and utility of monitoring head and/or salinity depend on the operation, implementation and start-up costs of monitoring, the types of monitoring equipment, the resolution of monitoring data, and data processing costs (Hericks et al. 2017). In practice, nearby existing supply wells are usually used as observation wells to

monitor head and/or contaminant concentration data (Sen 2015). This can avoid extra cost for drilling a new observation well.

Moreover, the DW methodology assumes that an initial baseline can be established using historical data and available information about the main hydrogeological characteristics of the aquifer under study (i.e. boundary conditions, and source/sinks). This initial baseline is expected to provide an adequate insight into the overall water flow system and serves as a testbed to estimate hydraulic heads, conduct model simulations and calculate the sensitivity of head and predictions to model parameters. However, uncertainties in model predictions are common when attempting to predict beyond the range of available data. This is particularly the case for highly parameterized models with more unknown parameters than observations. In such nonlinear models, the estimation of the variance of prediction uncertainty depends on the actual values of measurements, which are unknown prior to collection (Leube et al. 2012). If the model non-linearity is high, it may lead to multiple plausible results for a proposed observation location. Hence, the entire range of possible values for measurements should be considered during the OD (Leube et al. 2012), such that one can calculate a wide range for sensitivities of observations and predictions to parameters.

Several Monte Carlo (MC) based techniques have been developed to account for model uncertainty. MC techniques can be used to generate a range of measurement values obtained by using different parameter sets (multiple realizations) that are conditioned by the calibration dataset (Keating et al. 2010). Compared with other techniques such as the Markov Chain Monte Carlo (MCMC) method (Harvey and Gorelick, 1995), the generalized likelihood uncertainty estimation (GLUE) (Beven and Binley, 1992), and calibration constrained Monte Carlo methods (Tavakoli et al., 2013), the subspace technique for calibration constrained Monte Carlo analysis referred to as the null space Monte Carlo

(NSMC) method (Tonkin and Doherty 2005) requires less computational time for generating a large number of calibration-constrained parameter fields, which is suitable for groundwater modeling in highly parameterized systems due to the long model runtime and large number of required model runs (Herckenrath et al. 2011). In this method, a set of random parameter realization is first generated from a probability distribution defined based on available prior information. The generated random realizations are then projected onto the null-space, and adjusted through model re-calibration resulting in a set of calibration-constrained realizations (for details see Tonkin and Doherty 2009). For the OD, calibration-constrained realizations can be ranked and assigned weights according to their goodness of fit with observed data. Using Bayesian model averaging (BMA), model weights are determined via Bayes' theorem from the likelihood that the calibration dataset are generated by realizations (Hoeting et al. 1999). During the OD, the optimal location of a new observation can then be determined by making average over all possible locations obtained using calibration-constrained realizations (Freeze et al. 1992). In this way, uncertainties with model parameters and predictions are considered in designing a monitoring network using the DW methodology when taking an uncertain baseline for an OD.

A DW-based OD should hence provide flexibility concerning model dimensionality, allow for any desired task-oriented formulation targeting any measurement type (direct and indirect), account for various sources of uncertainty (e.g. geologic structure, heterogeneity, boundary condition, and source/sink) while constraining cost of data collection to remain at a minimum. Existing DW-based OD methodologies fall short of simultaneously provide these criteria for the design of a monitoring network in a groundwater system.

In this study, we extend the DW-based OD to optimize simultaneous measurements with different depths at a single and multiple spatial location, while constraining cost to

remain at a minimum and considering non-linearity through a Bayesian model averaging (BMA) framework. The cost is constrained by obtaining adequate hydrogeological information with a minimum number of observation wells. In what follows, we describe the theory underpinning the design methodology followed by the design method and an actual application to find the optimal locations within the model domain at which data acquisition would be most effective to reduce uncertainty in the simulation of saltwater intrusion.

4.2   Methods and materials

The proposed methodology involves a Bayesian model averaging (BMA) framework with a three-dimensional data worth (DW)-based optimal design (OD) analysis, and selection of an optimal observation dataset with respect to reducing model uncertainty (Figure 4-1).

1) Bayesian Model Averaging (BMA): Calculate K stochastic models (M_k), k=1,2…K and calculate model weights → For each M_k: Form matrices of X_{old}, $Y = \begin{bmatrix} y1 \\ \vdots \\ yn \end{bmatrix}$, C(e), C(P), $X = \begin{bmatrix} Y \\ X_{old} \end{bmatrix}$ → Calculate ∂_{base}^2

(2) Define new monitoring locations at: n locations = $L1…, Ln$; m depths = $D1…, Dm$; for l parameters = $P1…, Pl$ → Form sensitivity matrix for the location across multiple depths $X_{new} = \begin{bmatrix} L1 \\ \vdots \\ Ln \end{bmatrix}$, where $Li = \begin{bmatrix} D1p1 & \cdots & D1pl \\ \vdots & \ddots & \vdots \\ Dmp1 & \cdots & Dmpl \end{bmatrix}$ $i = 1, …n$

Add X_{new} to X_{old}, and calculate the sensitivities in X using PEST, and then remove X_{new} from X_{old}

k=1, N=1

(3) Genetic Algorithm (GA): Population size of P; Design size of N (i.e. number of new observations); Model M_k; i=1

P combinations of N rows from X_{new}; For each selected row from X_{new}; Add rows of X_{new} to X_{old} → Proposal design for size N; Calculate Value Index (VI) of design → **(4)**

Define: Mutation, Crossover, retain and random select → Design criteria met? No / Yes → D_k: Proposed design of size N selected from model M_k

k=k+1 (if k<K)

(4) Calculate VI of the proposed design using all models M_k → Assign model weights to calculated VI → Get an average estimate of VI for the proposed design

(if k=K) Select the D_k (k=1,… K) with the highest averaged VI

(5) Cost-effective design: Calculate VI/Po, N → N=N+1 **(3)** → Select the design size with the highest VI/Po

Figure 4-1 Optimal Design framework

M_k: stochastic simulation models; X_{old}: Sensitivity matrix of existing observations to parameters; Y: Sensitivity matrix of predictions to parameters; C(e): Covariance matrix of measurement noise (e); C(P): Covariance matrix of parameters (P) innate variability; X: Jacobian matrix; is the base predictive uncertainty variance; X_{new}: Sensitivity matrix of new observation wells to parameters; L: Sensitivity matrix of an observation well with measurements at multiple depths to parameters; k is the model number; N is the size of design (i.e. number of new observations); GA is Genetic Algorithm; VI is Value index; D_k is a proposed design using model M_k; and Po, N is operation cost of a monitoring project for N new observations

4.2.1 Bayesian model averaging (BMA) framework

We denote a set of distributed groundwater models M_k: k=1, …, K for predicting flow and/or solute transport over a geologic domain. Each model is a probability distribution model comprising the likelihood function of the observed data h_0 and the model

parameters P_k (e.g. hydraulic conductivity). The posterior predictive distribution of the forecast of interest Δ is determined as a weighted averaged individual prediction as expressed in Equation 1 where weights can be determined using Bayes' theorem on the basis of the likelihood that the observed data h_0 is generated using equation 2 (Hoeting et al. 1999):

$$ \tag{1} $$

$$ \tag{2} $$

where   is a probability mass function over the model   . The use of a defuse prior   is a neutral choice when there is no subjective preference for any of the model   (Wöhling et al. 2015). One can further normalize the weights by summing over the weights:

$$ \overline{\hspace{3cm}} \tag{3} $$

where   is the likelihood of observing the calibration dataset h_0 under model M_k . It can be determined based on its prior parameter distribution using equation 4:

$$ \tag{4} $$

where   is created by generating random parameter fields that meet calibration constraints. We use the subspace technique for calibration constrained Monte Carlo analysis called the null space Monte Carlo (NSMC) method (Tonkin and Doherty 2005) to create random parameter fields (   ). Compared with other techniques for example the Markov Chain Monte Carlo (MCMC) method (Harvey and Gorelick, 1995), the generalized likelihood uncertainty estimation (GLUE) (Beven and Binley, 1992), calibration constrained Monte Carlo methods (Tavakoli et al., 2013), deformation methods (Gómez Hernández et al., 1997), and the method of stochastic equations (Rubin and Dagan, 1987), the NSMC requires less computational time for generating a large number of calibration-

constrained parameter fields, which is suitable for groundwater modeling in highly

parameterized systems (i.e. large   ) due to the long model runtime and large number of

required model runs (Herckenrath et al. 2011). Prior to use the NSMC method, the hydraulic

conductivity field is parameterized by defining a large number of pilot points (   ) covering

the geologic domain. The model is then calibrated to estimate the values of pilot points. The

extent to which a pilot point parameter can be informed (identified) by the existing

observations can be measured by a singular value decomposition of the Jacobian matrix that

represents the sensitivity of observations to the pilot points parameters (for details see e.g.

Doherty and Hunt 2010). Pilot points parameters corresponding to the singular values that are

larger than a given user-defined "truncated" value (5.0E-6 in this work) span the calibration

solution space. These pilot points are deemed to be estimable on the basis of existing

observations. In contrast, those that contain low or zero singular values span the calibration

null space, and are considered as being inestimable. Using the NSMC method, a set of

random values is first generated from a prior probability distribution of hydraulic

conductivity fields. The random values are placed on the pilot points (which is called a

random realization). The generated random realization is projected onto the null-space

through differencing the random values and the calibrated pilot points values, and the

projected difference re-added to the calibrated values. The projected parameter set is then

adjusted through a model re-calibration in order to respect calibration constraints made by

existing observations. The result is a calibrated-constrained realization that respects both

stochastic variability of hydraulic conductivity field as well as calibration constraints (for

details see Tonkin and Doherty 2005). The posterior probability distribution of model

predictions is then computed on the basis of generated calibrate-constrained realizations.

4.2.2 *Linear model calibration*

We assume that each Bayesian model M_k is a linear model that defines a relationship between its parameters and its predictions using equation (5) (Doherty 2015):

$$M_k: \qquad\qquad\qquad\qquad\qquad (5)$$

where   denotes a   vector of head observations comprising the calibration dataset that are contaminated with noise   (i.e. error in field measurement),   represents a   vector of model (pilot points) parameters in the conceptual model, and   is the action of model or model sensitivity (or Jacobian matrix). The unknown model parameters can be then estimated by minimizing an objective function that is defined based on the sum of the squared weighted residuals between the model results and (potential) observed data (or model-to-measurement misfit) using equation 6:

$$(6)$$

where h is a   vector of potential head observations,   is the vector comprising of unknown parameters (or parameter estimates), T stands for the matrix transpose operation, and   is a diagonal matrix with squared observations weights (   ) that is defined to be proportional to the inverse of the covariance matrix of observations noise. The parameter vector minimizing the objective function (in equation 6) can be determined using equation 7:

$$(7)$$

where   is the matrix with squared (calculated) weights of observations. The potential wrongness (or error) of the estimated parameters   compared with the true parameter fields   can be evaluated by equation 8:

$$(8)$$

where I is the identity matrix. Let us further assume that   denotes a true model prediction. Then, the relationship between   and   is estimable using equation 9:

$$(9)$$

where   is a   vector representing the sensitivity of prediction to model parameters. If   is a model prediction that is computed from   using equation 9, the potential wrongness of computed prediction is hence expressed by equation 10:

$$(10)$$

However, the true parameter fields ( ) and prediction ( ) are unknown. Therefore, none of the potential wrongness of (or error in) estimated parameter (in equation 8) and computed prediction (in equation 10) is calculable. Let us assume that   and   are independent and their covariance matrices are known. Thus, the covariance of parameter error can be expressed by equation 11:

$$(11)$$

where   is a   parameter covariance matrix representing innate parameter variability which can be created using a Kriging variogram that is defined to represent the spatial distribution of the hydraulic conductivity fields,   is a   matrix of measurement noise   ,   is so-called the resolution matrix that describes the relationship between estimated and true parameters,   .

4.2.3   Prediction uncertainty variance

Combing the equations 10 and 11 leads to the expression of the variance of model prediction uncertainty as described by equation 12 (Christensen and Doherty 2008):

$$(12)$$

The first term on the right side of this equation is the prediction uncertainty. The second term shows the decrease in prediction uncertainty by calibrating a model against observation data.

4.2.4   *Data Worth (DW) analysis (prediction of single variable)*

The variance of the model prediction uncertainty does not account for parameters, measurements or prediction values. Instead, it comprises only the sensitivities of model observations and predictions to parameters, that are included in the   and   matrices, respectively. For the purpose of an optimal design, the change in the prediction uncertainty can be evaluated when a new observation (set) is added to the existing calibration dataset. In general, when adding an observation, the larger the reduction in model prediction uncertainty, the higher the DW this observation has in the calibration dataset. The DW is measured using equation 13 (More details can be found in Vilhelmsen and Ferre 2017):

$$\overline{\quad\quad}\tag{13}$$

where the   is the decrease in the prediction uncertainty when adding a new observation point, and   is the predictive uncertainty pertaining to the existing calibration dataset. The DW ranges between 0 and 1 and shows how the base predictive uncertainty reduces when augmenting the calibration dataset by adding a single or multiple observations. The DW of 1 denotes that the prediction uncertainty is completely diminished by adding new observations whereas the DW of 0 indicates that new observations do not have any impact on the prediction uncertainty reduction.

4.2.5   *Value Index (VI) analysis (prediction of multiple variables)*

The DW for an observation point can be further evaluated if the optimization target

is to minimize the uncertainty with predicting multiple variables in a groundwater system,

e.g. forecasts of stream flow reduction, flow velocity, or contaminant migration. For this

purpose, the DW is first calculated for each prediction variable. A weight is then defined for

each variable, and subsequently applied to each DW. The weighted DWs are then combined

into a single value index (VI) indicating the value of monitoring each observation well

according to the priority of prediction variables (equation 14) (More details can be found in

Vilhelmsen and Ferre 2017):

$$\tag{14}$$

where j corresponds to an observation set, n stands for the number of prediction

variables,   is the weight of the ith prediction variable , and   is the *DW* of jth

observation set to ith variable. Weighting prediction variables is a subjective choice of

modeler/manager, and can be based on various factors related to model predictions such as

economic worth of making predictions, or prioritizing a prediction when making

management plans.

4.2.6   *Data Worth (DW)-based 3D optimal design (OD)*

As outlined in Figure 4-1, the methodology consists of five interrelated steps

outlined below. (1) For each model M_k, a series of matrices are formed to represent the

sensitivity of the existing calibration dataset to model parameters (X_{old}); the sensitivity of

predictions to model parameters (Y); the innate parameter variability C(p); the measurement

noise C(e); and Jacobian matrix X that consists of Y and X_{old}. These matrices are used to

calculate the base predictive uncertainty. In the present work, the PREDUNC program in the PEST suites of utilities was used to calculate the base predictive uncertainty (Doherty 2015).

(2) A set of arbitrary 3D locations for potential (yet to be collected) observations is specified and used as input to the DW analysis. In order to perform a 3D design, we create an X_{new} matrix containing the spatial locations of observation wells, where each row of matrix represents a single observation location. Each observation location (i.e., an element of the X_{new} matrix) contains a corresponding sensitivity matrix L with m rows and l columns, where m is the maximum number of measurement depths and l is the number of model parameters. The L matrix comprises the sensitivity of a single observation location to all model parameters with respect to its measurement depths. Each row of this matrix contains the sensitivity of a measurement at a certain depth to model parameters. Each column includes the sensitivity of a certain parameter to a measurement at multiple depths. All new measurements pertaining to the L matrices are added to the X_{old}, and subsequently the sensitivities to parameters are estimated by calculating the Jacobian matrix X using PEST (Doherty 2015). The new measurements are then detached from the X_{old}.

Note that for temporal monitoring design, the X_{new} matrix can be simply expanded by additional L matrices corresponding to different model stress periods. For this purpose, a L_i matrix is generated for each model stress period.

(3) The third step is to find an optimal set of n potential observation wells. Combinations of n rows are selected from the X_{new} matrix. The Genetic Algorithm (GA) selects multiple rows corresponding to the combinations in the X_{new} matrix (for details about GA see Wohling et al., 2016). A p $\times$ 1 vector of randomly sampled N rows is generated, where p is the user defined population size (p=50 in this work). This vector forms the initial population of designs (i = 1). Each element of this vector contains a random combination of n rows of X_{new}. The L matrices pertaining to these n rows are added to the X_{old}, and

subsequently VI of combinations is evaluated using PREDUNC. Note that each combination comprises n number of new observation locations, and each new observation contains measurements at multiple depths. Therefore, the X_{old} matrix is expanded by adding the maximum measurements. In the next step, a new population of design (size N) is generated by applying the standard GA selection schemes, i.e. selection, mutation, and crossover (Wohling et al., 2016). In the present study, we retained 40% of the population for the next generation (i = i + 1), muted 5% of population (which was allowed to increase if the population was too uniform), and allowed a 15% chance of selecting outside of the admissible location (similar to Vilhelmsen and Ferre 2017 and Wohling et al., 2016). The new proposal design is then compared with the previously generated designs. We ended the loop when the highest VI and the proposed designs were similar in the last ten subsequent trials. We allowed a maximum of 1,000 trials to re-populate the designs in order to achieve convergence. The converged design is recorded as the proposed design of size N (i.e. D_k) for model M_k.

(4) The X_{old} matrix is amplified by the proposed design (D_k) of size N obtained using a model M_k. The reduction in prediction uncertainty is then evaluated in all models M_k using the amplified X_{old} matrix, and subsequently the VI is calculated for each model. The estimated VIs are multiplied by models weights (estimated through the BMA), and then it is averaged. The averaged VI is the impact of the proposed design (D_k) on the prediction uncertainty reduction with respect to model non-linearity.

The proposed design of size N is re-created for all models M_k (k<K). Subsequently the averaged VI is calculated. Among all proposed designs for models M_k (k=1,2…K), the design that has the highest averaged VI is selected as the optimal design for placing N observations with respect to the uncertainty of the model input.

(5) A cost-effective analysis can finally be performed to find the most economic size of the design (i.e. number of new observation wells). A design is cost-effective when the reduction of prediction uncertainty (i.e. increase in DW) exceeds its cost. The cost is herein defined by the number of required observation wells. The cost-effective analysis is accomplished by calculating the cost (Po) of each design size N and the one that can provide more information at minimal operation cost, is considered the optimal design. This is estimated in terms of the ratio of DW/Po. The design that has the highest DW/Po ratio is the most cost-effective design.

4.3   Application

4.3.1   Description of study area

The performance of the proposed method is evaluated by simulating flow and solute transport in an actual aquifer system. Located along the Eastern Mediterranean (Figure 4-2), the pilot aquifer (covering an area of approximately 48 Km^2) underlies Beirut city (Lebanon) and its suburbs. The study area has a 16.5 km of shorelines encompassing rocky beaches, sandy shores, and cliffs. It is bounded by several faults from the east and south, and partly by an intermittent river from the south.
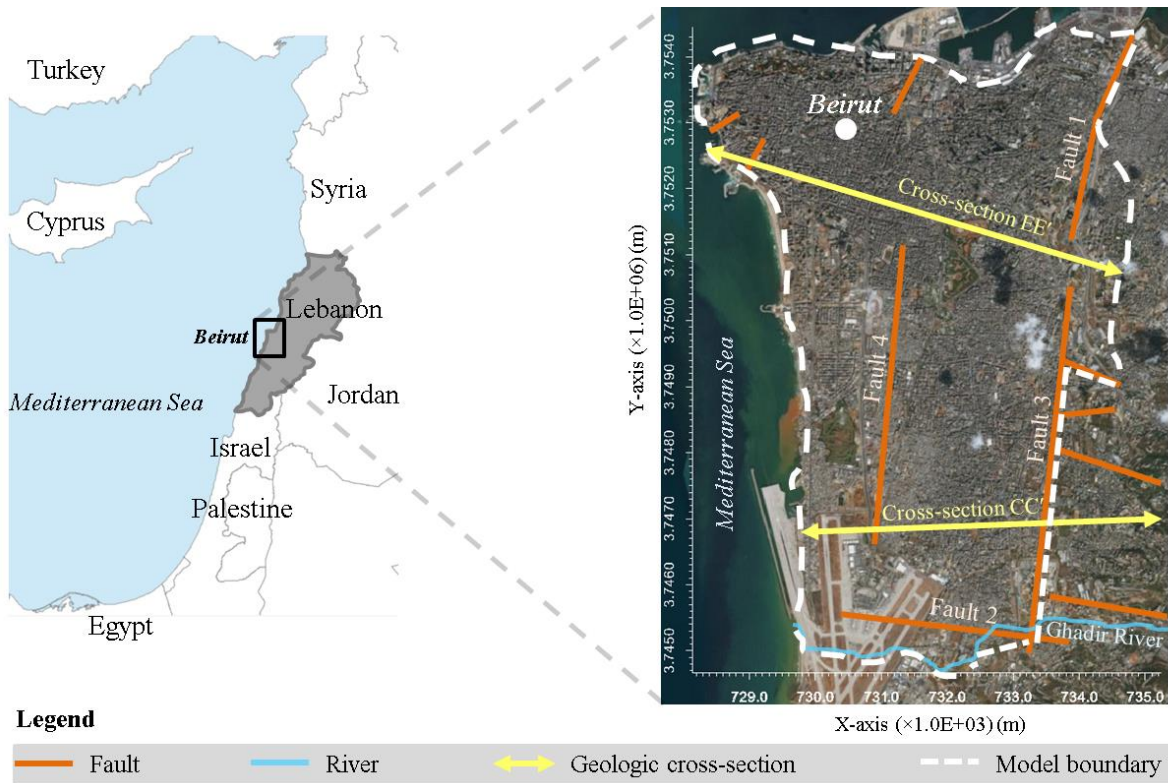
Figure 4-2 Location and surface geology of the pilot aquifer

4.3.2 Hydrogeology

The hydrogeology of the pilot aquifer consists of Cretaceous karst limestone overlaid by Upper Tertiary and Quaternary unconsolidated deposits (Peltekian 1980). The ~700m thick, fractured Cenomanian-Quaternary system is dominated by hard and compact limestone and dolomite interbedded with chert, and intercalations of marl (Kahair 1992).

136

According to the available geologic cross-section (
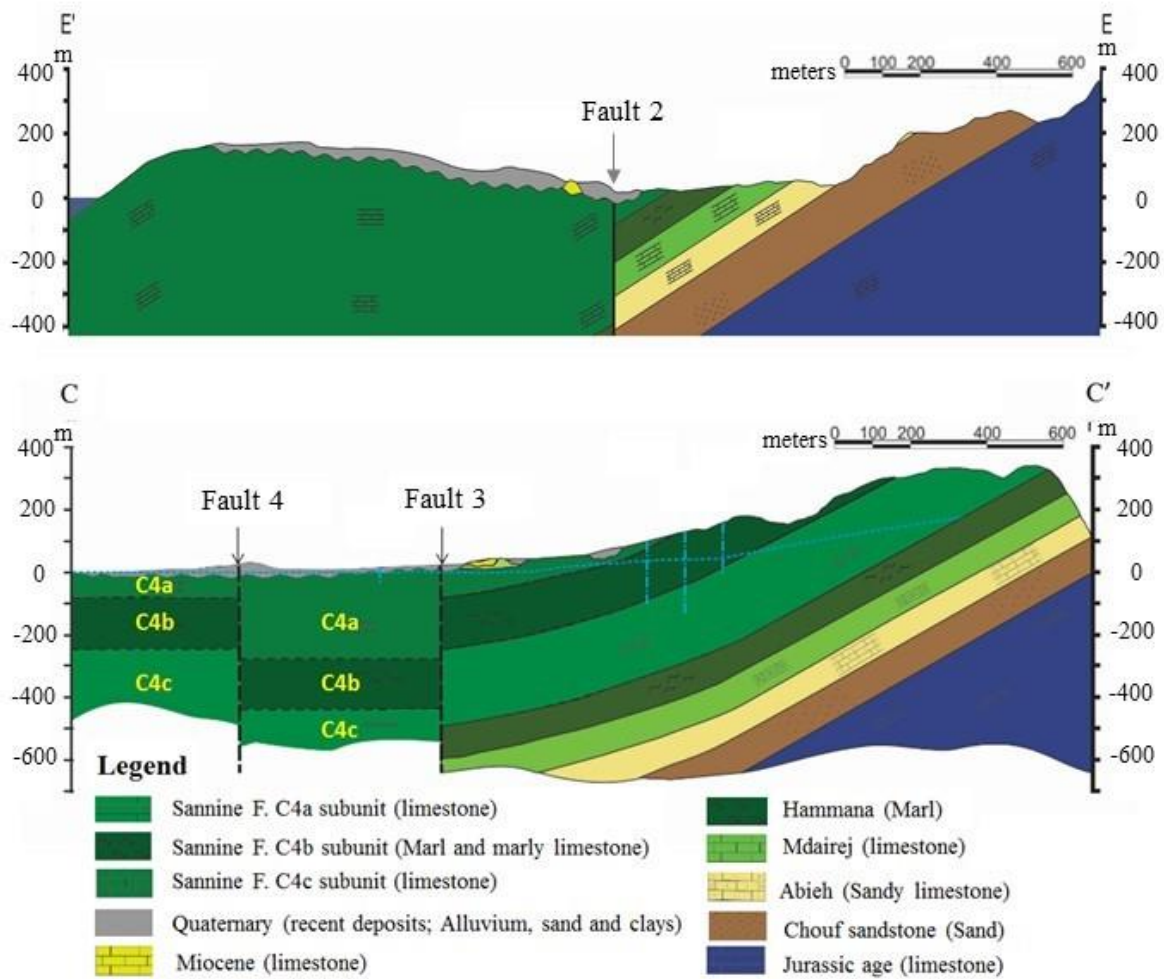
Figure 4-3), the rock sequence of Cenomanian Turonian age (Walley 1997) can be

divided into three subunits of 1) Afqa Dolomite member that consists of crystalline,

dolomitic, marly dolomitic and reefal limestone, 2) Aaqoura member that contains a sequence

of thinly bedded limestone, marly limestone, dolomite and marly dolomite strata, and 3)

Mnaitra member that composed of thick and compact limestone and fossiliferous strata with

several chert bands and nodules across different horizons. These are also known as C4a, C4b,

and C4c formations, respectively (Saint Marc 1974). The aquifer can be divided into seven

zones to describe its geologic surface and subsurface (Figure 4-4 and Table 4-1). The upper

geologic layer consists of a mix of C4c and Quaternary in the north (zone 1), and a mix of the

C4a and Quaternary formations in the middle and to the south (zone 2). The middle layer contains the C4a formation (aquifer) to the east (zone 3), the C4c formation (aquifer) in the north (zone 4), and the C4b formation (aquitard) along the western coastline (zone 5). The last geologic layer with a thickness of ~250 meters comprises of the C4c formation (aquifer) in the north (zone 4), the deep C4c formation (aquifer) along the western coastline (zone 6), and the deep C4b formation (aquitard) to the east (zone 7) (Table 4-1).

The Cenomanian formation and Cenomanian-Quaternary systems can be characterized as permeable with a specific yield of around 3 and 15%, respectively (UNDP 1970). The infiltration rates can be high in the quaternary deposits (Khair 1992). The freshwater influx to the aquifer in the year 1969 was primarily through a reportedly high recharge equivalent to 20-30% of precipitation (21% reported by UNDP 1970; 27% reported by Khair et al. 1994; and 30% reported by Ukayli 1971). The increase in urbanization since 1969 has nevertheless decreased the recharge potential to near nil in 2018 (Safi et al. 2018).
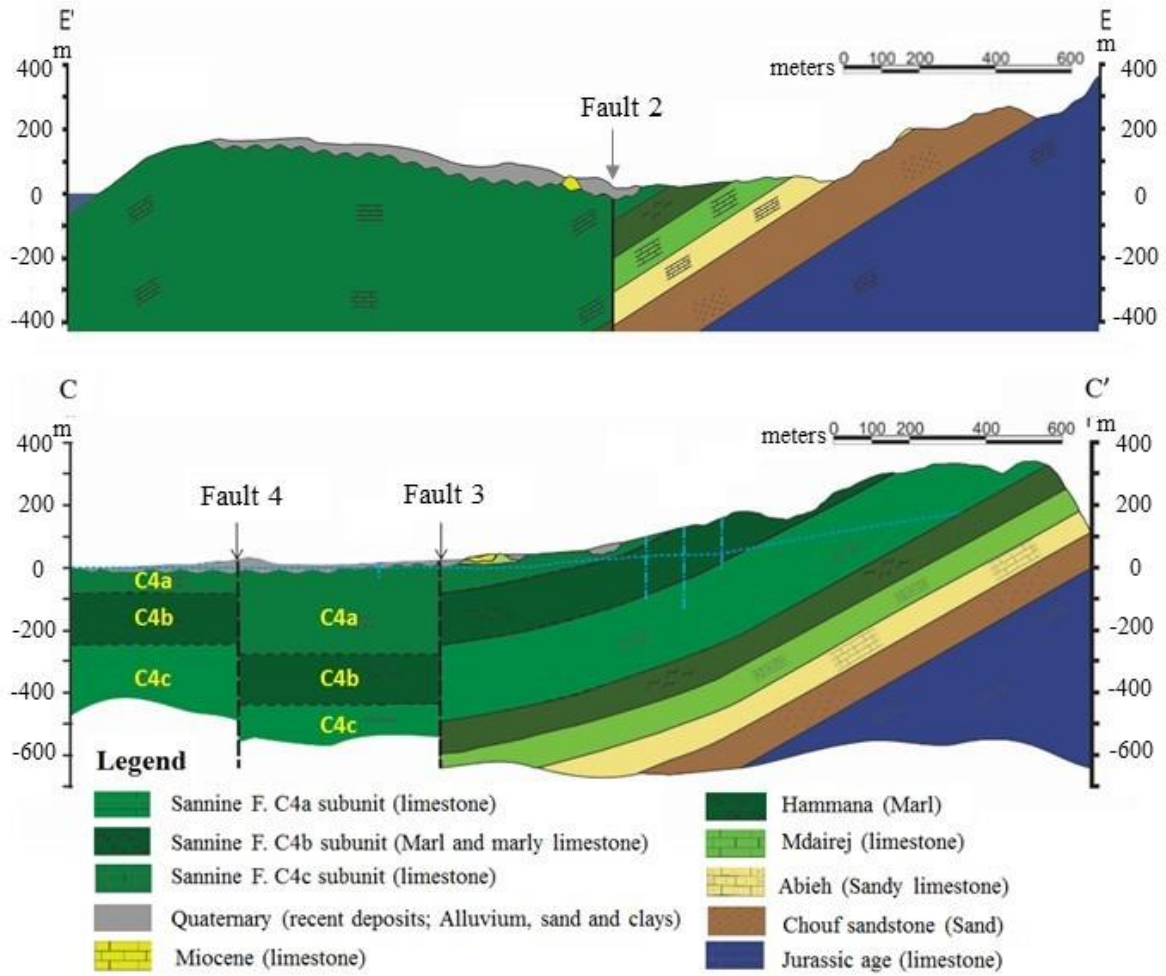
Figure 4-3 Geologic cross-sections CC′ and EE′
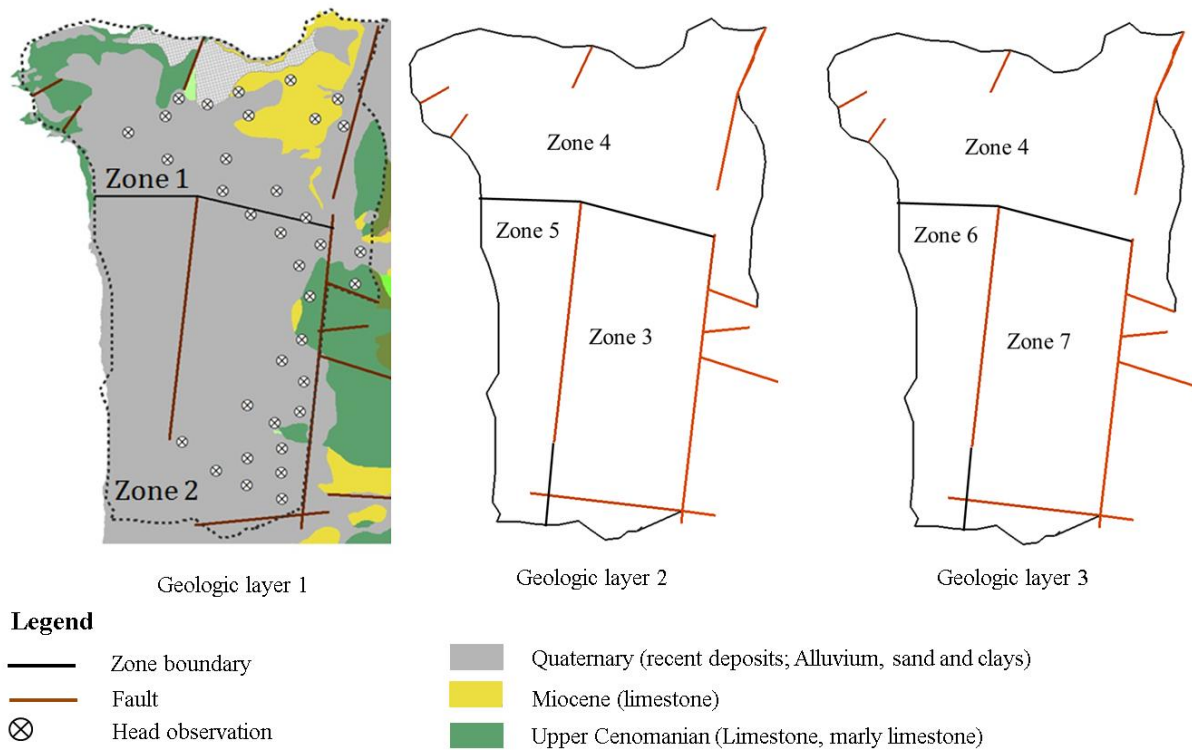
Figure 4-4 Location of historic head observations in the pilot aquifer with geologic zones

Table 4-1 Geologic formations in the pilot aquifer with corresponding hydraulic conductivity ranges (Ukayli 1969; and Petekian 1980)

Model domain	Thickness (m)	Geologic formation	Type	Log hydraulic conductivity (m/day)	Zone
Layer 1	~100 to 150	C4c-Quaternary	Aquifer	-1.69 to 2.69	1
		C4a-Quaternary	Aquifer	-1.26 to 2.69	2
Layer 2	~150	C4a	Aquifer	-1.3 to 2.69	3
		C4c	Aquifer	-1.69 to 2.69	4
		C4b	Aquitard	-5 to -3	5
Layer 3	~250	C4c	Aquifer	-1.69 to 2.69	4[*]
		C4c	Aquifer	-1.69 to 2.69	6
		C4b	Aquitard	-5 to -3	7

* The same zone used to characterize the C4c in the second and third layers.

140

4.3.3 Statement of problem and needs for a monitoring plan

The upper part of the pilot aquifer is reportedly highly vulnerable to saltwater intrusion (SWI) with many locations already experiencing high salinity because of groundwater overexploitation (Safi et al. 2018; Rachid et al. 2017), limiting its freshwater resources and forcing the authorities to consider tapping the deeper parts of the aquifer. In this context, groundwater modeling can guide decision makers towards sustainable abstraction without accelerating SWI while also protecting the deeper parts where the lack of subsurface characterization will inevitably increase uncertainties associated with model predictions. Therefore, it is imperative to design a monitoring network with optimal locations to constrain/ reduce model uncertainties.

The design of a monitoring network for the pilot aquifer requires simulating and understanding of the dynamics of saltwater intrusion in response to future groundwater abstractions from the deep parts of aquifer. Hence, emulating realistic future conditions of the pilot aquifer is an important step in the OD analysis. In the current application, a scenario was defined that assumes that the authorities will start extracting groundwater from freshwater resources in the deep aquifer zone 6 after March 2018, by 50 wells pumping at $200m^3/d$ (Figure 4-5). In this scenario, the bottom elevation of pumping wells reaches to depths of 360 meters below mean sea level (BSL) (in the middle of layer 3 in zone 6). A groundwater model was then used to simulate the future SWI in response to groundwater exploitation from the upper as well as deeper parts of aquifer. The objective of the work is to find the best locations to explore information about model prediction of: (a) the displacement of salt/fresh water interface in zone 6 caused by groundwater abstraction in entire aquifer (prediction variable 1), and (b) increase in the salinity concentration in the newly installed pumping wells in zone 6, which is caused by the landward displacement of the interface. As for the latter, salinity concentration was predicted at two points (A and B) specified in the

141

front of the pumping wells. The points A and B were located at depths of 360 meters (BSL) (similar to the bottom elevation of pumping wells in the scenario) (Figure 4-4). Salinity prediction at point A is subsequently called prediction variable 2. Similarly, salinity prediction at point B is called prediction variable 3.
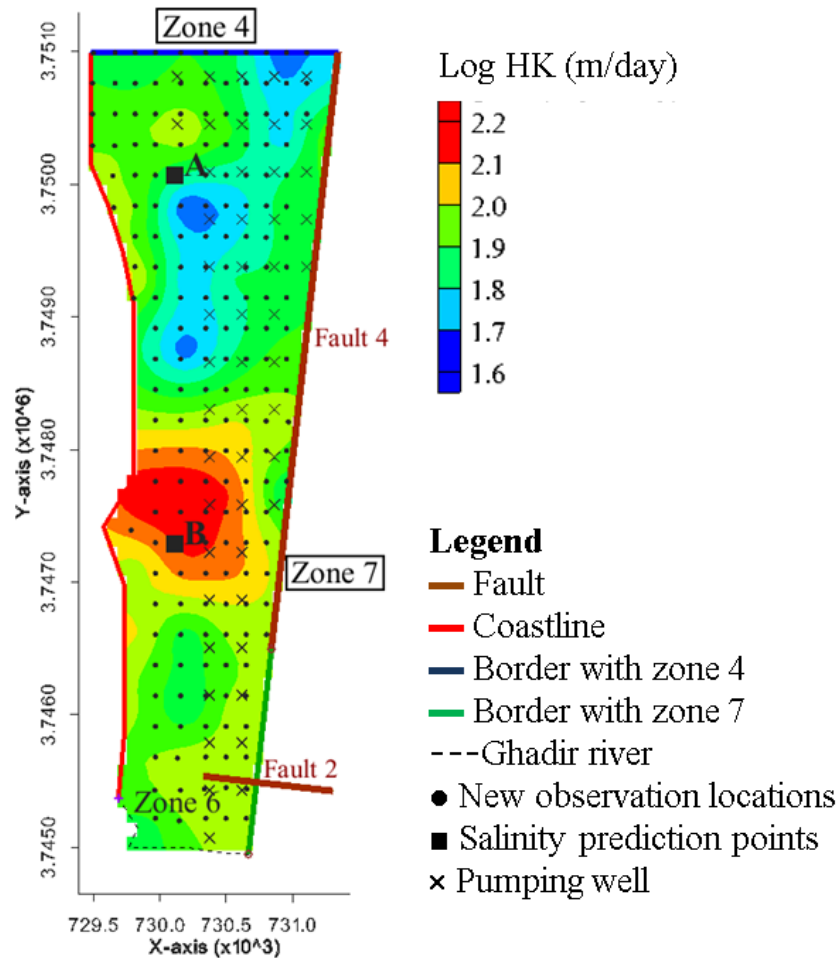
Figure 4-5 Potential new observations locations for monitoring head and salinity in zone 6, along with the locations of new pumping wells and model prediction points A and B at the depth of 360 meters below sea level – colored contours are the average of log hydraulic conductivity between all stochastic models – X and Y axes are in units of meters

4.3.4   Model set-up

SEAWAT code (Guo and Langevin 2002) was used to simulate the salinity migration in the pilot aquifer, and perform the OD in zone 6. SEAWAT is a variable density groundwater flow modeling code representing flow and solute transport processes solved by

MODFLOW and MT3D jointly. The criteria considered in the code selection process centered on its ability to: 1) simulate the 3D nature of vertical and lateral encroachment of salinity in confined and unconfined aquifers, 2) characterize various types of time-dependent boundary conditions, 3) simulate steady-state and long-term transient flow and solute transport with least numerical instability, 4) link with an inversion code (such as PEST) to quantify uncertainties, and 5) requires reasonable computational resources.

Our model comprised a transient stress period of 50 years subdivided into 50 sub-periods of one-year duration, extending from March 1969 up to March 2019 (the future state). The first stress period (March 1969) was used as the calibration-time period because the best query of calibration (head) dataset corresponded to the year 1969 with a total of 35 head

observations, tapping into the upper geologic layer (
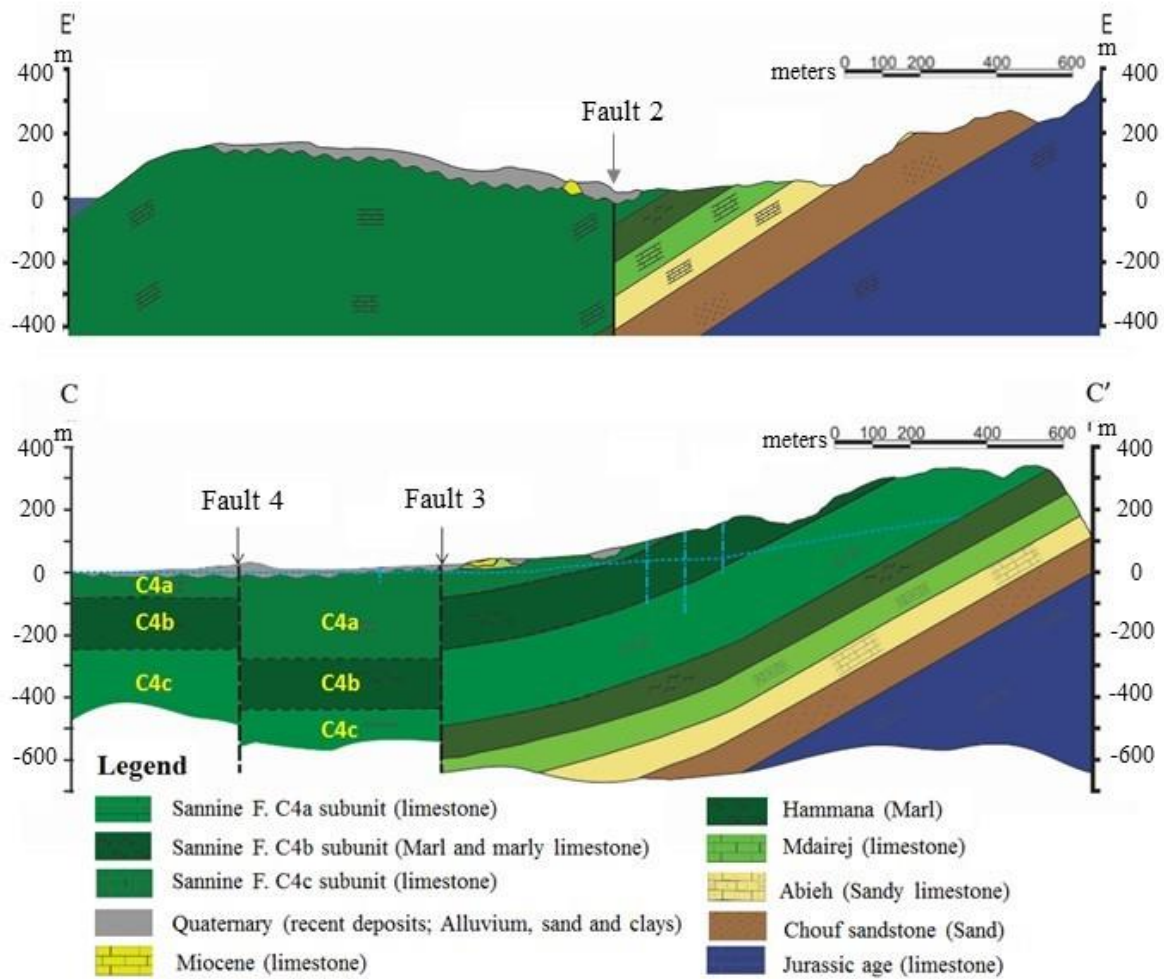
Figure 4-3).

In the set-up of the SEAWAT model, the sea boundary to the north and west is specified as a constant head and concentration boundary condition with an average salinity level of 35 gram per liter (gr/l). The eastern boundary was assumed to be a no-flow boundary due to aquitards and Faults 1 & 3 in the vicinity. The horizontal discretization contains 4,251 active cells designed in 115 rows and 75 columns where each grid cell represents a square of 100 by 100 meters (Figure 4-6). Groundwater abstraction for the upper aquifer was estimated for the years 1969 to 2019 given a 1.75% population growth and 180 liters per capita per day (l/c/d) domestic consumption rate (MoEW 2010). The population were considered to increase

from approximately 0.35 million (M) in 1969 to 1M in 2019, respectively. The freshwater

influx to the aquifer in the year 1969 was assumed to be primarily through recharge

equivalent to 30% of precipitation (Ukayli 1971). This rate was linearly decreased to zero for

2019 due to increase in impervious pavements over time (Safi et al. 2018). The lateral flow

was assumed to be zero due to the vicinity of the aquifer with faults and aquitards.
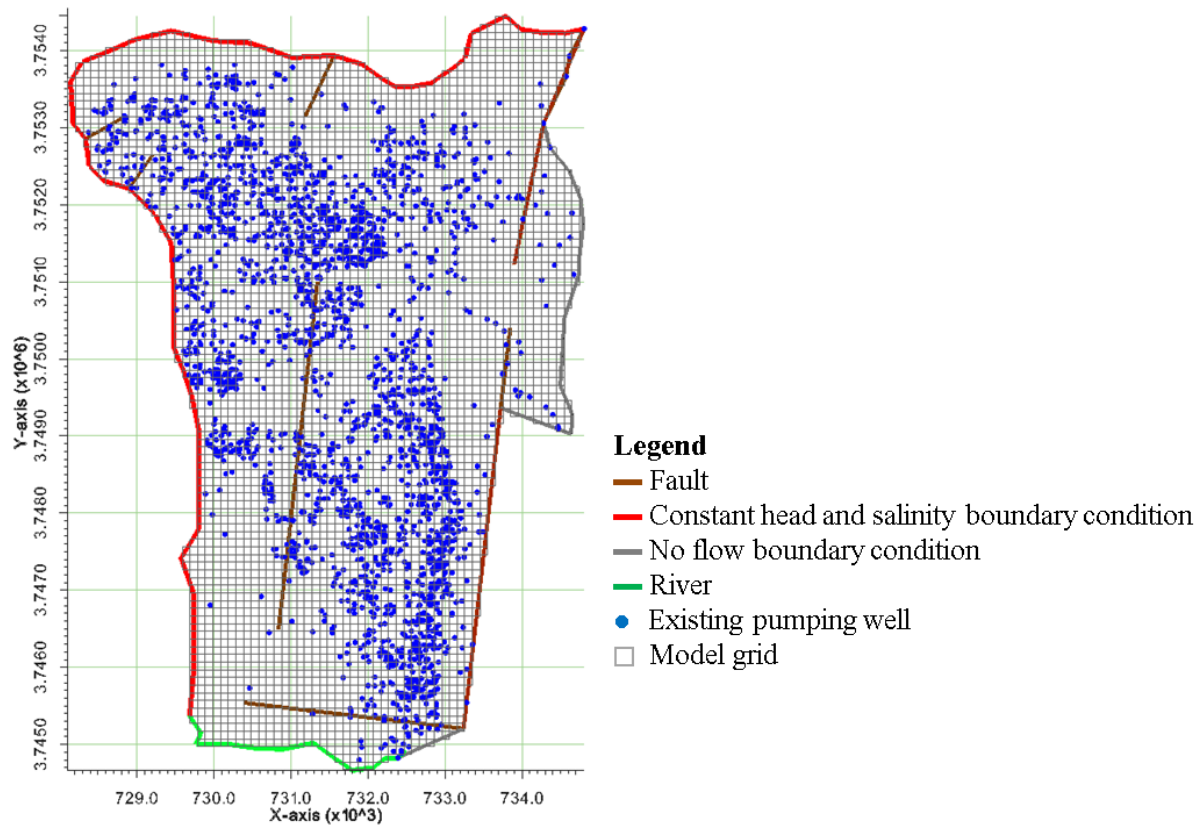
Figure 4-6 Model grids, boundary conditions, and locations of abstraction wells in the upper part of the Beirut coastal aquifer

4.3.5 Pilot points parameterization

The geology of aquifer is poorly characterized due to limited available information

about its characteristics. Its hydraulic conductivity can vary considerably over small distances

(Safi et al., 2018) and thereby the use of only a few zones to represent the hydraulic

conductivity field may not represent the flow conditions adequately. A set of pilot points was

assigned to each geologic zone to represent the spatial variability in the hydraulic

145

conductivity. Altogether, a total of 564 pilot points parameters was defined for the entire model domain (i.e. the vector P_k in the BMA). We used an exponential Kriging variogram to spatially interpolate the pilot points values over the geologic domain. The value of 500 meters (separation distances between one and two pilot points) was defined for the range of variogram (Doherty and Hunt 2010). Using PEST, the pilot points parameterization approach was used in conjunction with SVD and including regularization to estimate the values of pilot points using the existing head observations (Doherty 2015).

The calibrated pilot point model was used to calculate the sensitivities of observations and model predictions variables (1, 2 and 3) to the pilot points values. According to the sensitivity results, the pilot points parameters were categorized into three subsets: subset (i) contains the pilot points that spanned the solution space or were correlated with the pilot points that lied in the solution space (zones 1 to 4); subset (ii) includes the pilot points that lied in the null-space and did not inform the predictions (zones 5 and 7); and subset (iii) comprises of the null-space located pilot points that inform the predictions (zone 6).

4.3.6   Bayesian model averaging (BMA)

A random realization of hydraulic conductivity field was generated for each subset on the basis of the prior probability distribution of its hydraulic conductivity. The generated random realizations of all subsets were then combined into one realization that contained the full sets of pilot points parameters. The NSMC method was then used to calculate a calibrated-constrained realization on the basis of the generated random realization. This process was repeated several times to create multiple calibrated-constrained realizations.

The prior probability distributions were defined according to the available geologic knowledge of each subset: subset (i) used a probability distribution that was estimated based on the results of the calibrated pilot points model; subset (ii) did not use any probability distribution and the hydraulic conductivity value was defined constant for all the pilot points; and subset (iii) used fuzzy theory set (Zadeh 1969) to create a fuzzy probability distribution for the mean log hydraulic conductivity value due to limited expert knowledge of geology. For this subset, a trapezoidal distribution was used to define the membership functions of the log mean hydraulic conductivity value for the pilot points (for details about fuzzy set theory see e.g. Bardossy et al. 1990). Accordingly, the membership function of 1 was assigned to the range of log hydraulic conductivity from 1.5 to 2m/day, (i.e. lower and upper support limits). The membership value of zero was assigned to lower and upper limits of log mean hydraulic conductivity values which were 0.31 and 2.69 m/day, respectively.

Our BMA application encompassed the generation of only 10 calibration-constrained realizations due to the large run-time of model. The Bayesian models (M_k) constructed on the basis of realizations were then used to simulate SWI for the near future. For the purpose of model averaging, similar weights were assigned to the models (M_k) because all had almost the same sensitivity to the existing observed data after model calibration.

4.3.7   *Optimal design of new observation wells*

The OD analysis involved defining the best locations for a set of new observation wells in zone 6. The design assumed that the observation wells were available every 150 meters in zone 6 (i.e. spatial location), and a total of 192 potential locations were specified in that zone (Figure 4-5). Each observation well is assumed to contain two measurements of

147

field-data, namely: (1) the head and salinity concentration at the depth of 300 meters BSL, and (2) the head and salinity concentration at the depth of 360 meters BSL. Hence, the measurements vary spatially and vertically over zone 6 (i.e. three dimensions). The values of these measurements were extracted from the last stress period (i.e. the year 2019) of the Bayesian models, and subsequently were assigned to the observations wells.

The OD framework was then applied to define: (1) the optimal design of a single observation location with measurements of head and salinity for making all predictions under different prediction weight distribution; and (2) the optimal design for N=1, 2…,5 observation wells (i.e. multiple locations) with measurements of head and salinity at a single and multiple depths to reduce the uncertainty with the prediction of the salt/fresh water interface. Several scenarios were considered to define a variation in the predictions' weights: scenario a: w1=w2=w3=0.33; scenario b: w1=0.6, w2=0.3, w3=0.1; scenario c: w1=0.6, w2=0.1, w3=0.3; scenario d: w1=0.8, w2=w3=0.1; and scenario e: w1= 1, w2=w3=0; where wi is the weight of prediction i, and i=1, 2, and 3.

Finally, a cost-effective analysis was made to find the optimal size of the design, involving N=1, 2…,5 new observations. It was assumed that the scaled cost (Ps) of the start-up of a monitoring project can vary between 0 and 1. This cost is regardless of the number of planned observation wells. The cost of implementing the first observation well (P1) was assumed to vary between 0 and 100% of the start-up cost. This variation is shown by P1/Ps. The implementation cost decreases by 0%, 10%, 20%, or 30% for any additional observation well (P1$^+$). This variation is shown by P1$^+$/P1. A set of random values were then generated based on the above-mentioned cost criteria for implementing a given monitoring project. A uniform distribution was used to randomize the costs within their defined ranges. The reduction in predictive uncertainty in relation to the cost of monitoring the head and salinity

of measurement was evaluated by dividing the DW by the cost of project implementation for N=1, 2…,5 simultaneous observation wells.

4.4   Results and discussion

4.4.1   Bayesian models

Calibration-constrained realizations were generated for the hydraulic conductivity field. The model-to-measurement misfit ranged from 251 to $258m^2$ with an average residual absolute error of ~2m in all of the stochastic models M_k. Figure 4-7 shows the calibration-constrained log hydraulic conductivity fields along with the position of salt/fresh water interface in zone 6 after a 50 year simulation based on the 10 generated stochastic models. The stochastic results are only shown for zone 6, where the OD was performed. The uncertainty with the estimated log hydraulic conductivity had a noticeable impact on the computation of the position of interface. In four of the models (models M1, M5, M6 and M10), the log hydraulic conductivity values are low along the coastline, and therefore the landward displacement of the interface caused by groundwater abstraction was small as compared with that in other models that contained large hydraulic conductivity values. In the other models, it is apparent that the high hydraulic conductivity tends to exacerbate SWI, subsequently decreasing the depth to the interface. Since the large uncertainties in the estimated hydraulic conductivities of zones 6 can increase uncertainties in the model prediction, it is necessary to quantify the prediction uncertainty.
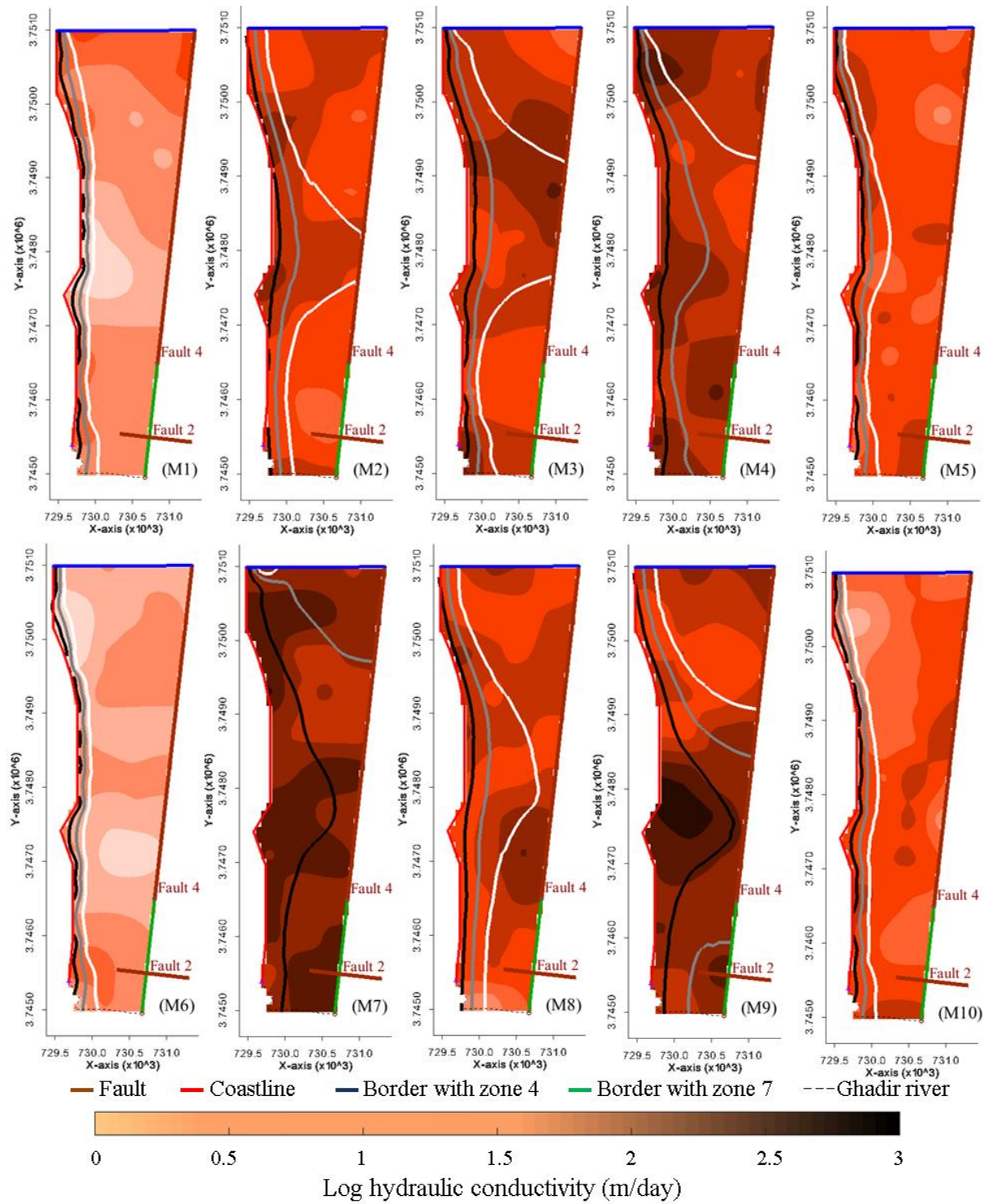
Figure 4-7 Log hydraulic conductivity distribution in zone 6 using 10 stochastic models Mk: k=1, 2 … 10; along with the position of the interface with 75% (black), 50% (gray), and 25% (white) of sea water concentration (35gr/l) after 50 years simulation

The uncertainty with predicting the displacement of salt/fresh water interface after

the 50 years simulation was quantified from the range of simulated values obtained using the

generated calibration-constrained realizations of the hydraulic conductivity. The histogram of the log hydraulic conductivity values approached near a normal distribution that ranged from 0.85 to 2.33 m/day (Figure 4-8a). The distribution is negatively skewed due to the limitations enforced on low hydraulic conductivity values through a trapezoidal membership function during the randomization process. Figure 4-8b shows the histogram of the predicted values for the displacement of the interface where the transition mixing zone is limited to 1 gr/l (threshold for drinking water). The model prediction is shown as the percent displacement of interface from its initial position to the coastline. It was computed by calculating the percent increase in the volume of salinity greater than 1gr/l caused by groundwater abstraction. The histogram for the model prediction exhibits a large level of uncertainty with the predicted percent change in the position of the interface ranging from 40 to 70% (Figure 4-8b). The prediction histogram has a shape similar to that of the log hydraulic conductivity value (Figure 4-8a vs. Figure 4-8b). This underlines the importance of the hydraulic conductivity in the deep parts of a coastal aquifer to compute the displacement of the interface.
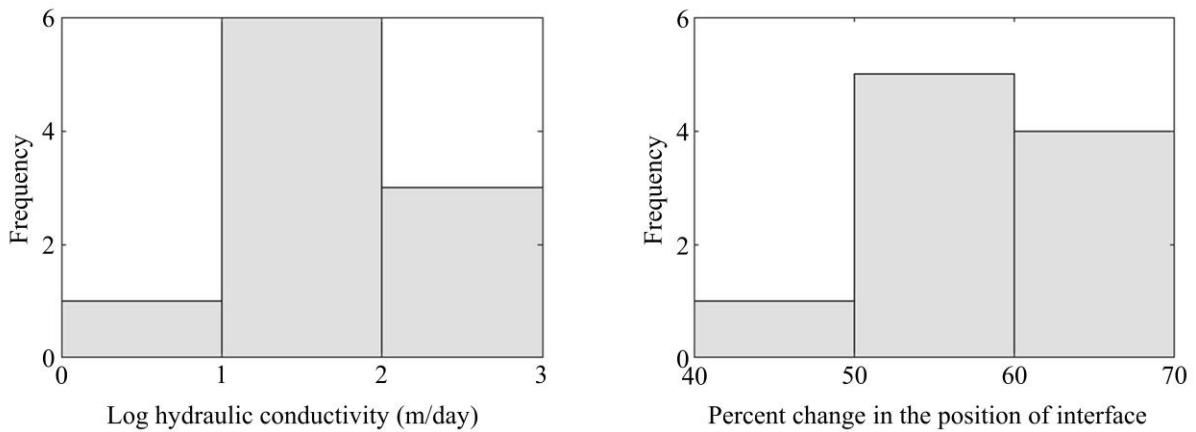
Figure 4-8 Histograms for log hydraulic conductivity values for zone 6 and for the corresponding model prediction of the percent change in the position of the 3D salt/fresh water interface with salinity >1gr/l from the coastline

4.4.2 *Optimal design for measurements with single depth at a single observation well*

The optimal design (OD) analysis determined if the uncertainty in model predictions was affected by collecting a new measurement in zone 6. For the predictions of salinity levels at points A and B, the worth of collecting head and salinity concentration data increased slightly (~20% more) when the measurement depth increased by 20% to reach the depth of the points A and B (Figure 4-9b vs. Figure 4-9e and Figure 4-9c vs. Figure 4-9f). When the depth of measurement was lower than the depth of the points (A and B), measurements made to the left of the points (closer to the interface) informed more the prediction in comparison to those made elsewhere (Figure 4-9b and Figure 4-9e). The location of a measurement with the highest DW moved landwards from the left to the right side of the points when the depth of measurement was increased (figures 9-e and 9-f). At the depth of the points A and B (360 BSL), the location of a measurement should be made prior to the locations of points and in the direction in which the interface moves landward. Compared with model predictions of salinity at points A and B, the head and salinity measurements were found to have less importance on reducing the uncertainty associated with the prediction of the interface displacement (Figure 4-9a and Figure 4-9d). For predicting the displacement of salt/freshwater interface (i.e. prediction variable 1), the most informative measurements were made parallel to the coastline and near the interface. The most informative locations moved 200 meters landward as the depth of the measurements was increased by 60 meters (Figure 4-9a vs. Figure 4-9d).

152
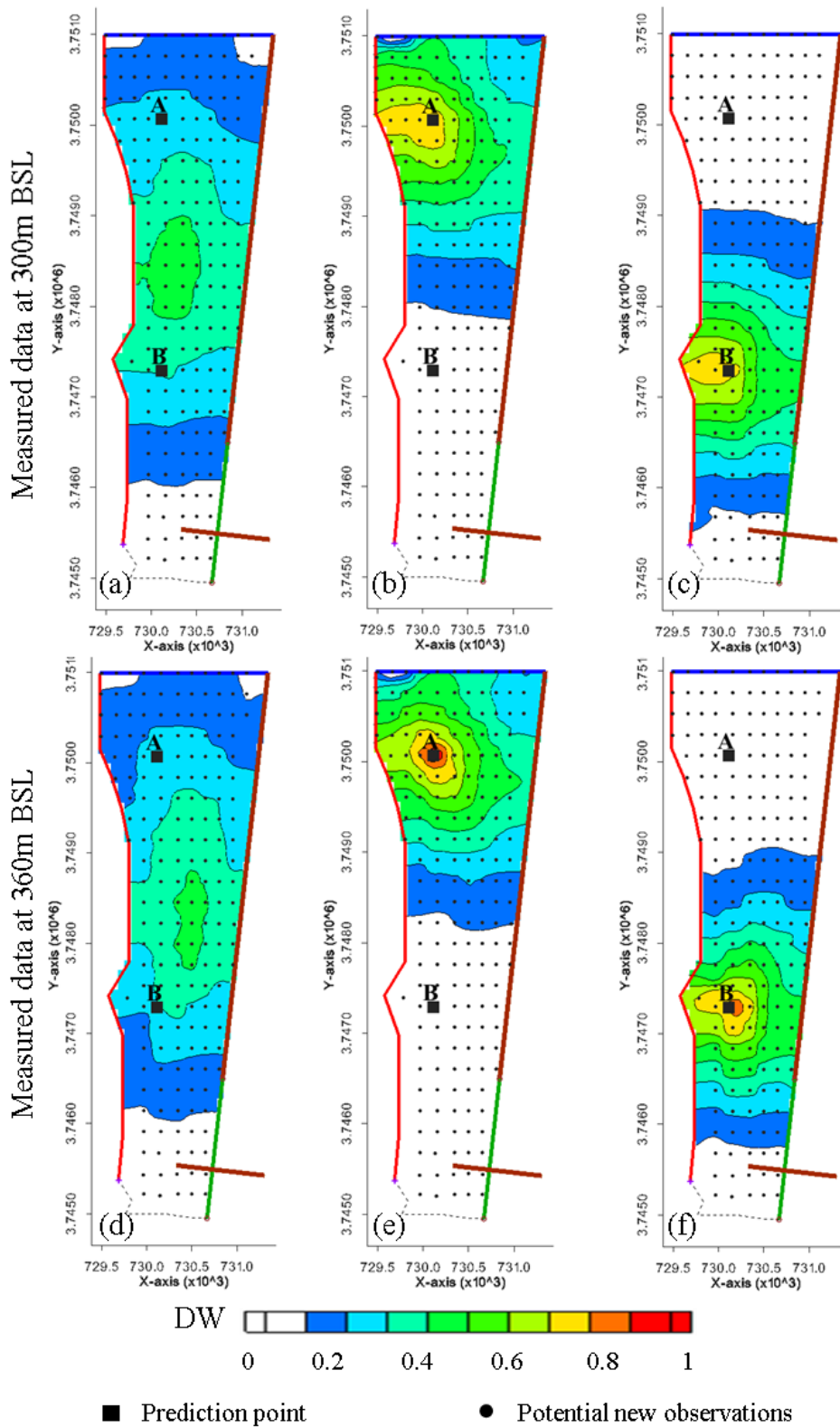
Figure 4-9 Data worth (DW) of new (yet to be collected) observation locations with measurements of head and salinity at different depths coresponding to prediction variables:
1 (interface displacement); 2 (salinity increase at point A); and 3 (salinity increase at point B)

4.4.3 *Optimal design for measurements with multiple depths at a single observation well*

The optimal design (OD) analysis determined if the uncertainty in model predictions was affected by collecting a new measurement in zone 6. Figure 4-10 shows the contoured VI averaged over the 10 models for the three prediction variables (the 3D displacement of interface, salinity levels at points A and B), given a set of specific weight distributions assigned to these three variables. Different locations were specified according to different weights of prediction variables. The optimal location of a single observation well lied close to the points A and B when a similar weight was assigned to all prediction variables (Figure 4-10a). The DW of a single observation well was higher (twice more) when predicting salinity at points A and B than that when predicting the interface displacement (Figure 4-10a vs. Figure 4-10b and Figure 4-10c). Although increasing the weight on the prediction variable 1 (w1) by a two-fold increased the VI in the observation wells located within the points A and B, the best location for a single observation still lied close to the points A and B (Figure 4-10b and Figure 4-10c). An eight-fold increase in the w1 compared with w2 and w3 shifted the best location by ~500 meters upward (Figure 4-10d). The importance of collecting head and salinity levels in making prediction of the interface displacement (variable 1) was high in the middle of zone 6 within the points A and B (Figure 4-10e) because most models showed the highest intrusion occurring mainly at the middle of the coastline (Figure 4-7). Compared with observation wells located elsewhere, the observation wells located in the middle of zone 6 sensed more concentration changes as the interface approached landward. It was apparent that the design for the location of only one observation well did not allow much reduction of the uncertainty in the prediction of the interface displacement (i.e. variable 1) with a small weight. Moreover, the uncertainty with the predictions of salinity levels at points A and B most probably approaches nil if the number of new observation wells reaches the number of prediction variables (i.e. two observation wells for two point-source prediction variables). In

contrast, more observation wells are required to provide substantial information about with the estimation of the interface displacement.
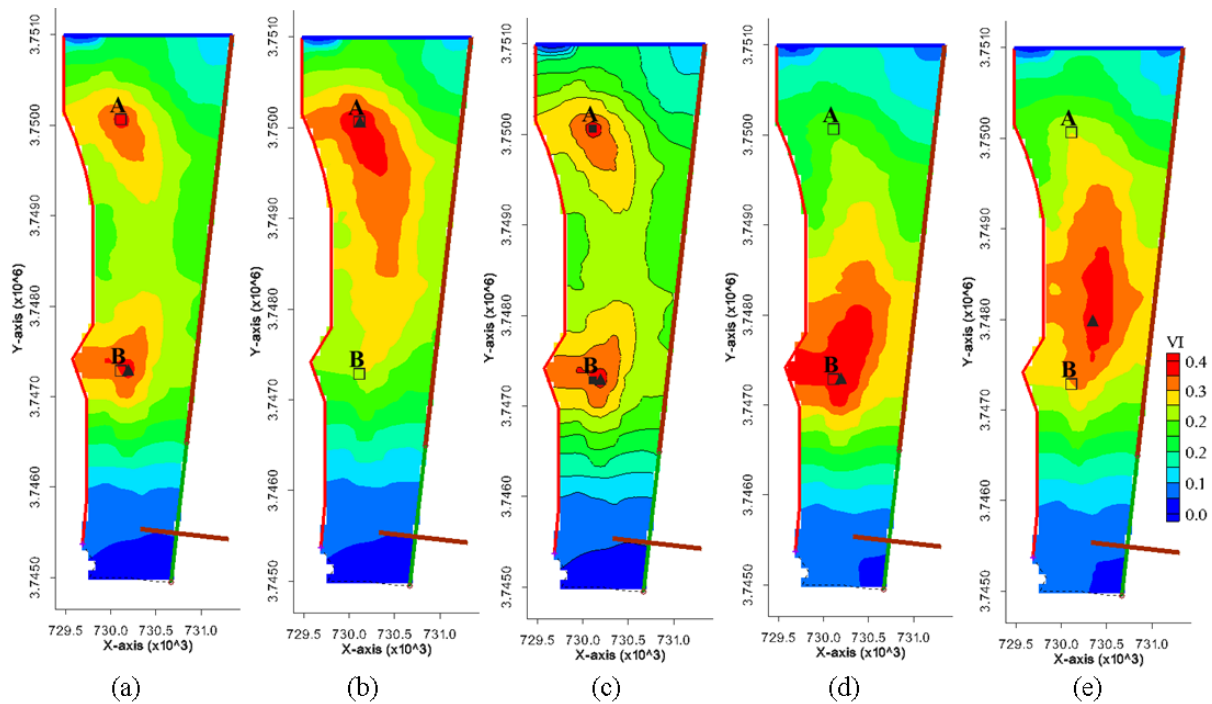
Figure 4-10 Black solid triangle represents the optimal design location for a single observation with measurement of head and salinity at multiple depths for multiple prediction variables - a) w1=w2=w3=0.33; (b) w1=0.6, w2=0.3, w3=0.1; (c) w1=0.6, w2=0.1, w3=0.3; (d) w1=0.8, w2=w3=0.1; (e) w1= 1, w2=w3=0. wi is prediction weight - colored contours are VI that was averaged over the models Mk- locations of points A and B are shown in black rectangles

4.4.4 Optimal design for measurements with multiple depths at multiple observation wells

The performance of the methodology for a larger number of observations was examined for the case where all the weight was given to the model prediction of the 3D displacement of interface (i.e. prediction variable 1). The optimal locations for N=2, … and 5 simultaneous new observations (i.e. proposed design) were specified separately at each of the 10 models M_k. Altogether, 10 designs were proposed for each size of N. Figure 4-11 shows the effectiveness of each proposed design to reduce the prediction uncertainty when considering the impact of model non-linearity. Boxplots were used as a means of comparing the proposed designs across the 10 models. For each design, the averaged DW is shown along with the estimated DW using all models. The variance of data is 10 for each boxplot

155

regardless of the number of planned new observations. Each boxplot contains 10 estimated DWs while the highest DW corresponds to the original model M_k for which the design D_k was proposed. In the proposed design for 2 observations, the mean estimate of DW ranged from ~0.52 to 0.66 (Figure 4-11a). In the proposed designs, the least and highest mean DW correspond to the designs D_3 and D_5 obtained from models M_3 and M_5, respectively. The design D_5 was selected as the best design for proposing 2 observations. It also had a small variance compared with most other designs indicating that the uncertainty with the hydraulic conductivity did not affect the best design for 2 observations significantly. The variance of D_5 however increased by increasing the design size indicating that the model M_5 is not a good candidate for the design sizes of larger than 2. In the proposed designs for 3 observations, the highest mean estimate of DW of 0.72 correspond to the designs of D_1, D_6, D_7, and D_{10} (Figure 4-11b). Among these designs, the design D_7 is affected least by model uncertainty, and hence it was selected as the best design. The design D_1 had the highest mean DW (~0.75) and relatively small variation in response to variability in hydraulic conductivity values when used for designing 4 observations (Figure 4-11c). Hence, this design was selected as the best design for 4 observations. In the proposed designs for 5 observations, the mean DW ranged from 0.68 to 0.78, and the variance of DW ranged from 0.01 to 0.05 in all designs (Figure 4-11d). We selected the design D1 that had the highest DW of 0.78, and relatively low variance of ~0.02.

In most designs, the median is higher than the mean, indicating that the DW has a left tail. The DW (i.e. additional uncertainty reduction) per additional observation decreases with increasing the number of observations. Interestingly, the spread of the DW in the designs also decreased as the number of observations was increased. The designs with larger number of observations appeared to have similar centers that exceeded those found for the designs with fewer observations. Overall, an increased number of observations reduced the

prediction uncertainty, which is not surprising, however it also increased the number of outliers, indicating that the model non-linearity can strongly affect the estimation of DW for a proposed large-size design. From the estimated DWs, we noticed that the models (M7 and M9) that caused such influence contained a very high mean log hydraulic conductivity (of > 2m/day) as compared with that in other models (Figure 4-7). In these models, the DW was very low when applying the proposed designs that were specified in other models M_k.
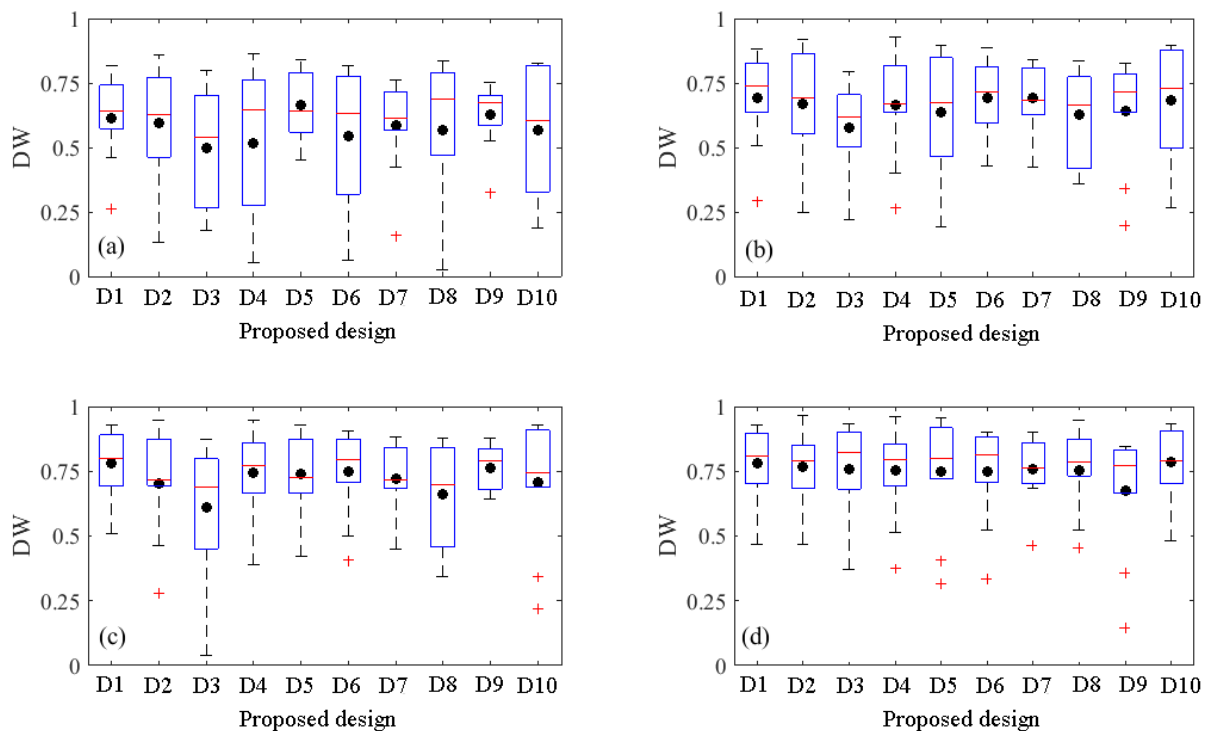
Figure 4-11 Estimated DW of proposed designs Dk from models Mk (k=1,2…10) for N=2, 3, 4, and 5 observation wells in plots a to d respectively: x-axis corresponds to a proposed design specified using a model Mk and y-axis is the estimated DW when applying a proposed design on all models – Black dot is the mean estimate of the DW and red line is the median of the estimated DWs for each design using all models.

The observation sets with the highest averaged DW for design sizes N=1,2,…,5 (Figure 4-12) showed that the proposed locations changed with the number of planned additional observations. Measurements spread from north to south parallel to the coastline with an increasing number of observations. In the small size design, the proposed locations were found to be independent of previously proposed locations. For example, the locations for the two observations did not correspond to that in the design size of 1. As a result of the spatial correlations between parameters, some correlations incurred between observations and

157

the selection of 2 observations spread out from the highest DW location for a single observation. Some proposed locations appeared to be similar when designing for larger sizes (e.g. the locations for 4 observations in the combinations of 4 and 5 observations).
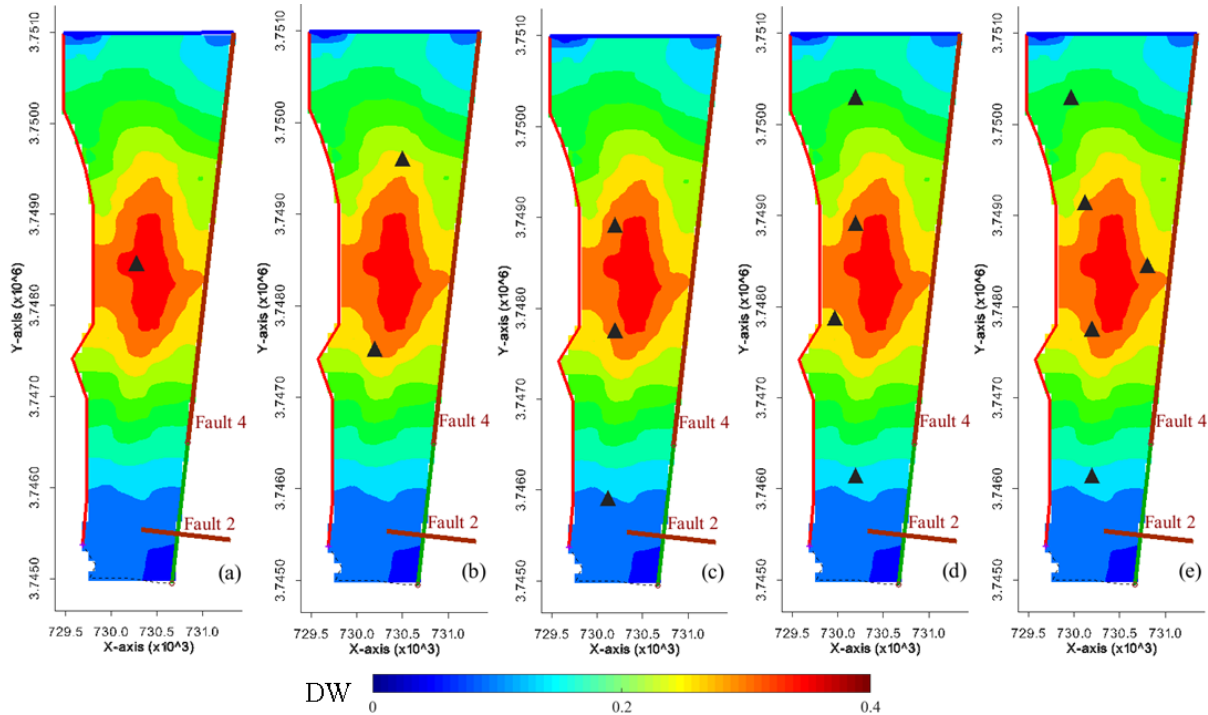
Figure 4-12 Optimal design for N=1, …5 new observations with measurement of salinity at multiple depths for predicting the displacement of the salt/water interface. ▲ is a proposed location for a new observation. The colored contours represent the DW for a single observation with measurement at multiple depths

4.4.5   Cost-effective analysis

The cost criteria was applied on the proposed design sizes of N=1,…,5 (Figure 4-13). Each point represents how the reduction of prediction uncertainty (i.e. increase in DW) exceeds its cost. The least and most cost-effective designs were the designs for 5 and 2 observations, respectively (red and green dots in Figure 4-13). This indicates that although the prediction uncertainty decreases by increasing the number of observations (Figure 4-11), the optimal design size varies according to the cost criteria. The most effective criteria was found to be P1/Ps (the cost of implementing the first observation according to the cost at start-up). An inspection of the cost-effective results shows that the optimal size of a design

should include a maximum of two observations when the cost of implementing the first observation is more than 50% of the start-up cost of the monitoring project. Under this condition, the optimal size can increase by decreasing the cost of implementing an additional observation to < 80% of the cost of operating the first observation (i.e. $P1^+/P1$). With $P1/Ps$ < 30%, the optimal size can increase by up to 4 observations if $P1^+/P1$ is <0.8. The implementation of 5 observations seems to be the most cost-effective only if the cost of implementing the first observation is much lower than the start-up cost, which may not be practically possible.
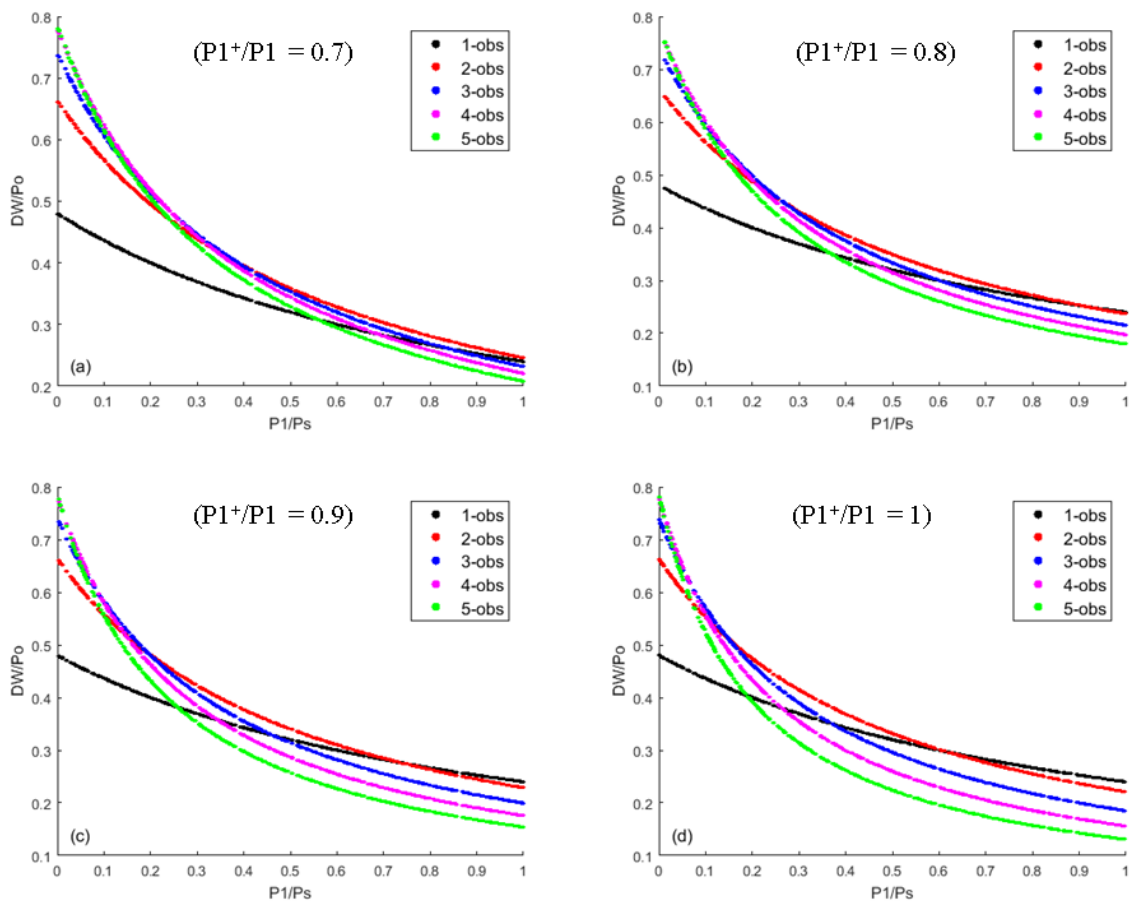
Figure 4-13 Cost-effective analysis for size of proposed design: x-axis shows the ratio of the cost of implementing the first observation (P1) to the start-up cost (Ps) (which is scaled between 0 and 1), y-axis is the reduction of uncertainty (data worth (DW)) with predicting the 3D displacement of interface to the full cost of a project (Po), dots correspond to an observation set of n=1,2…5 observations – each plot shows the different analysis according to the operation cost of an additional observation ($P1^+$) to the cost of implementing the first observation (P1) – DW is constant at each design size and only the cost of design varies

4.5   Conclusion

In this study, we extended an existing linear data worth (DW) method that optimizes multiple locations of new (yet to be collected) observations that can contribute to reducing uncertainty in predicting multiple variables in a groundwater system. Compared to previous studies that used two dimensional locations for observations, our method also optimizes simultaneous measurements with different depths at a single and multiple locations (i.e. three dimensions) at a minimum cost. We also suggested the use of Bayesian model averaging (BMA), which defines weights for each Bayesian model that contains a set of stochastic parameters. The capability to produce the calibration dataset (also considered as a model prediction) by the stochastic parameters is used to calculate the weight of each Bayesian model. The final outcome of the optimal design (OD) is a set of proposed locations for an observation set with respect to the model non-linearity.

We applied the proposed methodology on a pilot heterogeneous coastal aquifer that lacks hydrogeological information of its deep geologic layers. The target of the design was to find the best locations for placing 1, 2…,5 new observations that could contribute to the reduction of the prediction uncertainties. Two types of prediction were used as the optimization targets: capturing the increase in salinity at two points located in the deep part of aquifer and the displacement of the interface caused by groundwater abstraction. The types of observations were head and salinity with different locations in three dimensions. The following findings were deduced from the OD results of our case study:

It is important to sample data at different depths and locations if the target of a monitoring design is to predict a solute transport over a three-dimensional geologic domain.

Model non-linearity has a slight impact on proposing a single location for an observation well with head and salinity measurement. This impact increases by increasing the design size.

The DW of an observation well with head and salinity measurements depends primarily on its spatial proximity to the coastline, while the depth of measurement is secondary but also important. The proposed spatial location for an observation well moves toward the coastline when the depth of measurement decreases.

When the depth of measurement is less than the depth of a point at which the predicted salinity concentration is required, a proposed observation should be located adjacent to that point and seaward (i.e. in the direction of the sea). Conversely, when the depth of the measurement is equal or greater than the depth of the point, the observation should be located adjacent to the point and landward (i.e. further inland).

To reduce uncertainty with the future interface, observation wells should be located close to the coastline if the depth of measurement is relatively low. Conversely, observation wells can be located farther from the coast as measurement depths increase.

The proposed spatial locations for (head and salinity) observations changes with the design size. The locations become more similar by increasing the number of planned additional observations.

The optimal size for the monitoring plan depends mostly on the ratio between the start-up cost of the monitoring project and the cost of drilling the first observation well, while the implementation cost of additional observation wells is secondary but also important.

For the current application, the maximum of two observation wells is needed to obtain a cost-effective monitoring plan if the cost of implementing the first observation and monitoring data is more than 50% of the start-up cost of the monitoring project. If the cost of implementing the first observation is equal or greater than the start-up cost, only one

observation is recommended for a cost-effective design. Monitoring data from multiple observation wells is the most cost-effective if the start-up cost is much more than the cost of implementing the first observation (e.g. using nearby pumping wells as observation wells).

This study stresses that the effectiveness of the proposed methodology to secure the optimal results is hinged on the proper weighing of stochastic models when non-linearity is high. This underlines the importance of prior knowledge of the system, before designing a monitoring network to produce an effective and successful model calibration. While an increase in the number of planned observations can reduce more the prediction uncertainty during the model calibration, the cost-effectiveness of a monitoring design is contingent more on the cost of operating the first observation than any additional observation. The results of this study can be used for future field-studies to guide adaptations of sampling strategies in aquifers. Due to the large model run-times to simulate SWI, we limited the OD to steady-state measurements of head and salinity. Using transient measurements, it is expected that the proposed locations for observation wells shift landward with the movement of the interface.

CHAPTER 5

SYNERGY OF CLIMATE CHANGE AND LOCAL PRESSURES ON SWI IN COASTAL URBAN AREAS: EFFECTIVE ADAPTATION FOR POLICY PLANNING

Abstract

This article examines the relative impacts of anthropogenic interventions and global climate change on the dynamics of saltwater intrusion in highly urbanized coastal aquifers. For this purpose, simulations of the impacts of sea-level rise and abstraction scenarios for the near future were undertaken for a pilot aquifer using a multi-objective 3D variable-density flow and solute transport model. We find that sea-level rise associated with climate change has less influence on the encroachment of salinity than anthropogenic abstraction, which has a more appreciable impact on saltwater intrusion through greater sensitivity to water consumption and seasonality.

Keywords: Climate change; sea level rise; groundwater abstraction; SWI; adaptation

5.1 Introduction

Landward intrusion of seawater into coastal aquifers, known as saltwater intrusion, is primarily caused by aquifer overpumping and land-use change (Singh, 2014; Werner et al., 2013). Saltwater intrusion increasingly threatens urban coastal communities worldwide by contaminating groundwater and reducing its productive and consumptive value (Bobba,

2002; Conrads & Roehl, 2007; Fatorić & Chelleri, 2012; Park, Jang, Ju, & Yeo, 2012; Sales, 2009; Sanford & Pope, 2010; Selmi, 2013; Zhang, Savenije, Wu, Kong, & Zhu, 2011). Climate change is expected to further exacerbate saltwater intrusion due to sealevel rise coupled with higher temperatures, which would cause higher water demand, and reduced precipitation, which would reduce the surface water available for aquifer recharge (IPCC, 2007, 2014; Kumar, Carsten, & Keith, 2007).

The importance of planning to adapt to saltwater intrusion lies in protecting the biophysical elements (subsurface aquifers and groundwater quality) and curtailing associated socio-economic burdens on coastal communities (impairment of water resources, damage to soil, plants and infrastructure, etc.). However, as coastal aquifer hydrodynamics and climate change impacts remain challenging to quantify and predict (Post VEA, 2005; Sanford & Pope, 2010; Werner et al., 2013), and as the interaction between impacts of global climate change and local anthropogenic impacts remains ambiguous, coastal managers have to plan and act under incomplete knowledge to cope with these impacts and protect the economic, social and environmental security of coastal communities (Tribbia & Moser, 2008). In this context, drivers of saltwater intrusion have often been assessed using mathematical simulations that account for major hydrogeological inputs as well as temporal and spatial variations in groundwater recharge and discharge and sea-level fluctuations, through mass balance and numerical analysis (Cobaner, Motz, & Motz, 2012; El Shinnawy & Abayazid, 2011; Harbor, 1994; Purandara, Venkatesh, & Choubey, 2010; Sophiya & Syed, 2013).

Groundwater overexploitation is strongly associated with lowering the water table and the advancement of the seawater front (Cobaner et al., 2012; Ergil, 2001; Koussis, Mazi, & Destouni, 2012; Selmi, 2013; Sherif, Kacimov, Javadi, & Ebraheem, 2012), and the ability of flushing a saltwater-contaminated aquifer by stopping or reducing pumping rates or managing aquifer recharge is seldom possible. Also, the impact of sealevel rise differs

between confined and unconfined aquifers, with rising seas generally believed to first lift the entire aquifer, which would help alleviate the impacts of saltwater intrusion, before intrusion takes over again (Carretero, Rapaglia, Bokuniewicz, & Kruse, 2013; Chang, Clement, Simpson, & Lee, 2011; Werner et al., 2012). While the trends governing the physical, geological and chemical processes of interaction between the drivers of saltwater intrusion are generally similar, the rate and magnitude of these interactions remain highly context-specific (El Shinnawy & Abayazid, 2011; Melloul & Collin, 2006; Dausman & Langevin, 2005; Niang, Dansokho, Faye, Gueye, & Ndiaye, 2010; Oude Essink, 2001; Ranjan, Kazama, & Sawamoto, 2006), confirming the need for local examination in informed management and adaptation strategies. Similarly, the limited studies that examined opportunities for adaptation have showed that their effectiveness is variable and site-specific (Abarca, Carrera, Voss, & Sanchez-Vila, 2002; Ergil, 2001; Fatorić & Chelleri, 2012; Frank & Boyer, 2014; Georgopoulou et al., 2001; Kaleris & Ziogas, 2013; Masciopinto, 2013).

This study examines the additional factor of climate change impacts in comparison to local anthropogenic interventions in the occurrence and intensification of saltwater intrusion along urban coastal aquifers using a multi-objective 3D hydrogeological model responsive to the dynamics of population growth, recharge and climatic stresses. In parallel, it assesses the potential role of planned adaptation strategies in alleviating saltwater intrusion in an attempt to inform policy making on sustainable management of urban coastal aquifers.

5.2 Methodology

The methodological framework consisted of three interrelated components: characterization of the pilot aquifer study area; identification of scenarios that account for local anthropogenic interventions, climate change, and planned adaptation strategies; and

assessment of these scenarios for saltwater intrusion dynamics using a multi-objective 3D variable-density flow and solute transport model.

5.2.1 *Aquifer characterization*

The pilot area is a fractured, heterogeneous aquifer underlying Beirut City and its suburbs, a highly urbanized metropolis with recognized water-shortage challenges and high dependence on groundwater resources. The study area stretches midway along the Eastern Mediterranean, with 16.5 km of diverse shorelines, including rocky beaches, sandy shores and cliffs, over a total area of ~44 km2 (Figure 5-1). Its hydrogeology belongs to the Cretaceous and Quaternary periods, with restricted exposures of the Tertiary (Abdel Basit, 1971; Peltekian, 1980). The Cenomanian-Quaternary system (carbonate-sand) is considered one aquifer, ~700 m thick, consisting mainly of hard and compact limestone and dolomite interbedded with chert, and intercalations of marl (Khair, 1992) overlain by Quaternary recent deposits. The aquifer is characterized by accessibility and relatively high transmissivity and low storativity, particularly in the Cenomanian formations, and high infiltration rates due to the presence of weak or partial cementation between the grains of sand in the Quaternary deposits, allowing moderate permeability (Khair, 1992). It is characterized by fractured and karst systems (Masciopinto, 2013; Shaban, Khawlie, & Abdallah, 2006) and is heavily jointed and faulted (Ukayli, 1971). Nearly 4500 small-scale wells reportedly tap into this aquifer (Saadeh, 2008; SOER, 2011), complementing the network water supply to nearly a million people (CAS, 2008).
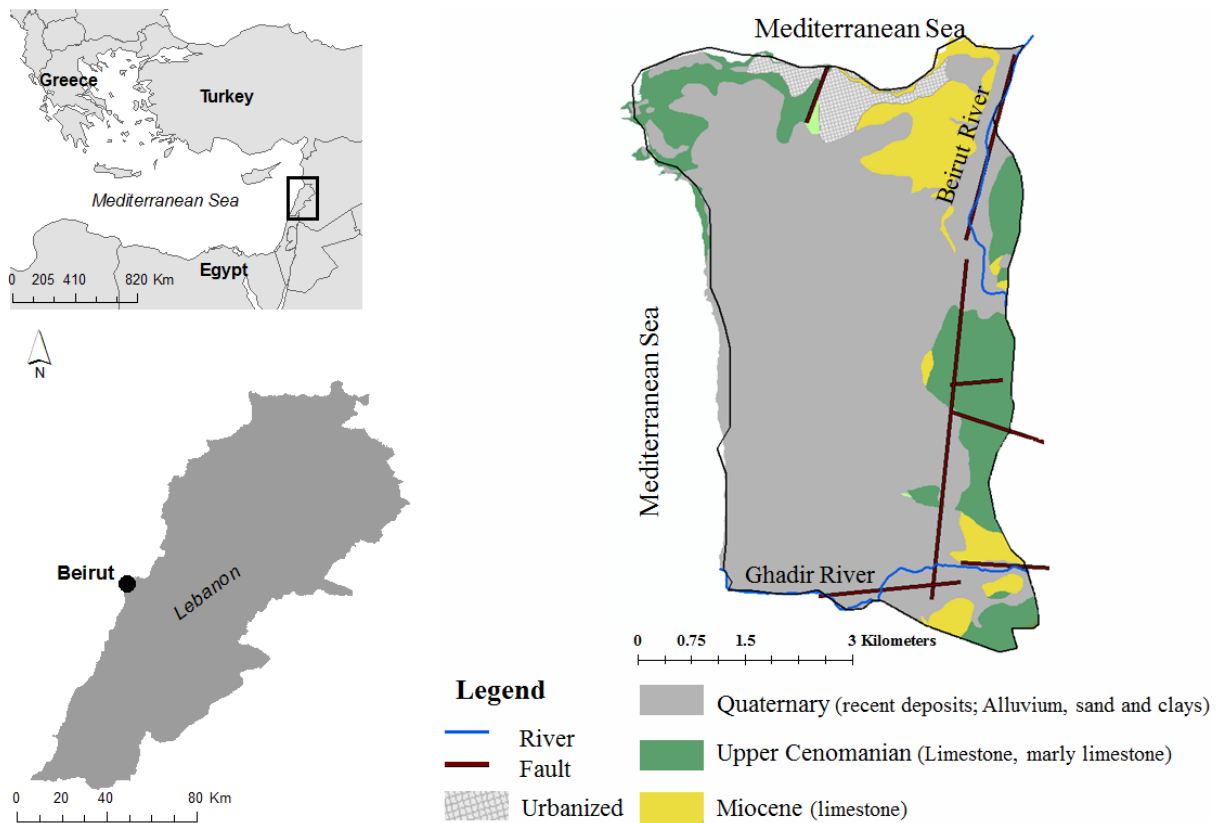
Figure 5-1 Location and surface geology of the pilot aquifer

5.2.2 Development of scenarios

Abstraction and sealevel rise scenarios were developed for the near future (2012–2032), as proxies for local anthropogenic interventions and global climate change. Groundwater abstraction was estimated based on domestic water demand rates, using population growth and per capita consumption. Two growth rates were examined: an average of 1.75% (MoEW, 2010) and a high of 2.50% (WB, 2009). Total population estimates were based on the year 2010, with ~1.2 million inhabitants in the study area (CDR/DAR, 2014). Similarly, a constant average consumption rate of 180 litres per capita per day (LCD) (MoEW, 2010) and a variable high rate of 200 LCD increasing linearly to 300 LCD (including network losses) were tested (El-Fadel, Zeinati, & Jamali, 2000; Korfali & Jurdi, 2010; Saadeh, 2008).

Table 5-1 presents levels of input variables for scenario development, with a total of 11 scenarios simulated for the period 2012–2032. Water demand and availability vary between wet and dry seasons, and this variation was considered in the scenario development, where fewer surface water supplies are expected to be available in dry seasons, when the demand for water is at its highest. Assessment of the impact of sealevel rise was based on estimates for the Eastern Mediterranean of 12–25 cm by 2030 and 22–45 cm by 2050 (Cazenave, Cabanes, Dominh, & Mangiarotti, 2001), or 30–60 cm by 2040 (SNC, 2011). Accordingly, both a low (20 cm) and a high (65 cm) sealevel rise by 2032 were assumed, using rates of 1 and 3.25 cm/y, respectively. The cumulative impact of sealevel rise and abstraction on the dynamics of saltwater intrusion was analyzed for the baseline scenario (S1) as well as the worst-case scenario (S4).

Table 5-1 Simulated scenarios with corresponding input parameters

Scenario	Population growth (%)	Consumption rate (l/c/d)	Description and details
S1	1.75	180	Baseline
S2	1.75	200 - 300	Most likely
S3	2.5	180	Modified baseline
S4	2.5	200 - 300	Worst case
S1A	1.75	180	Groundwater demand is reduced by 230,000 m^3/d as a result of adoption of adaptation/mitigation measures starting 2019
S2A	1.75	200 - 300	
S3A1	2.5	180	Groundwater demand is reduced by 350,000 m^3/d as a result of adoption of adaptation/mitigation measures starting 2019
S4A1	2.5	200 - 300	
S4A2	2.5	200-300	Abstraction is halted as demand is met as a result of adaptation/mitigation measures starting 2019
S1L	1.75	180	Sea level rise is included at 1 cm/yr i.e. rise of 20 cm by 2032
S4L	2.5	200 - 300	Sea level rise included at 3.2 cm/yr i.e. rise of 65 cm by 2032

Based on the understanding of the aquifer response to these drivers, potential adaptation strategies for mitigating saltwater intrusion were analyzed under the different scenarios. Given that the excessive spread of wells and the indiscriminate withdrawal of

groundwater are necessitated by gaps between water supply and demand, the adaptation strategies focused on reducing abstraction by reducing the demand for groundwater in general as well as reducing the gap between supply and demand. In line with the national plans (MoEW, 2010), three levels of adaptation were evaluated to analyze for effectiveness and inform decision making in sustainable aquifer management. The scenarios tested were based on the 10-year plan of the Ministry of Energy and Water (MoEW), which consisted of (a) water conservation practices tailored to reduce network losses, currently estimated at 50% (MoEW, 2010); (b) injection of treated wastewater for artificial aquifer recharge; and (c) a series of infrastructure projects, including the conveyance of water from inland to the urban area under study through a phased dam-lake project, the Beirut Awali Conveyor (MoEW, 2010). In line with the methodology, which is based on groundwater abstraction that is defined by demand, the selected adaptation strategies targeted groundwater demand and adopted the projected additional supply to Beirut from several planned projects. Adaptation Scenario A assumes additional water supply of ~230,000 m3/day, projected under Phase I (2.5–3 m3/s) of the conveyor project (MoEW, 2010); Scenario A1 assumes the additional supply ~350,000 m3/day projected under Phase II (4.5–6 m3/s) of the same project. Adaptation Strategy A2 assumes the adoption of unconventional water supplies (desalination), so that the entire demand is met through desalinated water, with no groundwater abstraction needed. Al adaptation measures were assumed to start in 2019.

5.2.3   *Model set-up and simulations*

A multi-objective 3D variable-density flow and solute transport model using SEAWAT (Langevin, Thorne, Dausman, Sukop, & Guo, 2008) was set for the target domain. Initial and boundary conditions, and sub-surface characteristics, were assigned to the mesh following the digitization of the study area. The boundary to the north and west is a specified

169

head boundary condition corresponding to the monthly stage of sea level. Two rivers bound

the domain to the north-east and the south (Figure 5-1). The southern river is dry, with

occasional flow from stormwater runoff and groundwater influx, while the north-eastern river

acts as a drain downstream and a river upstream. The influx to the system is assumed to be

primarily through recharge/runoff due to rainfall (Peltekian, 1980). In the last few decades,

the rise in urban and suburban development in and around Beirut resulted in a significant

amount of impervious surfaces. Therefore, aquifer recharge from surface runoff was

considered nil in the model simulations. A Dirichlet boundary condition was used to specify

the average salinity of the seaside boundary, with TDS of 35 g/L (Figure 5-2). The complex

hydrogeology of the subsurface environment is not well documented. Therefore, assumptions

on the aquifer's hydrogeological characteristics were made in the design of the model. The

spatial heterogeneity of groundwater abstraction and the number of supply wells (~2500)

tapping into the aquifer were assumed to be constant from 2012 to 2032. The boundary to the

east (between the two rivers) was set as a no-flow boundary due to its adjacency to the

middle Cenomanian formation (C4b), which has low hydraulic conductivity. The only

opening in the Cenomanian formation in the eastern domain was characterized by a flux

boundary condition with a low influx rate. Storativity was set at a constant of 0.3 for yield

storage and 10E-6 for specific storage. The measurements of head and salinity field

observations were considered reliable.

The model comprised a transient stress period (i.e., the computational time interval

for a simulation, here taken as 1 month) of 20 years, subdivided into 240 sub-periods of one

month each (from June 2012 to June 2032), that undergoes both steady-state and transient

conditions. The first stress period (June 2012) was specified as steady state with the aim of

providing a stable head distribution at the beginning of the transient period. Monthly

averaged head observations from June 2012 to March 2014 were used in the transient model

calibration in the Groundwater Modeling System (Version 10). The model used the advanced

pilot-points parameterization coupled with PEST (Doherty, 2007) to characterize the spatial

heterogeneity of hydraulic conductivity. The final results of model calibration suggested a

range of 8–81 m/day for the hydraulic conductivity in the first numerical layer, containing the

Quaternary, Cenomanian and Miocene formations. The hydraulic conductivity in the second

and third layers varies between 5.02 and 182 m/day. Although the calibration results were

generally satisfactory, with low model-to-measurement misfit error in terms of hydraulic

head observations, the existing geologic data were not sufficient to validate the model

calibration results for hydraulic conductivity. Therefore, expected uncertainty in estimation of

hydraulic conductivity is recognized as a limitation of the model.
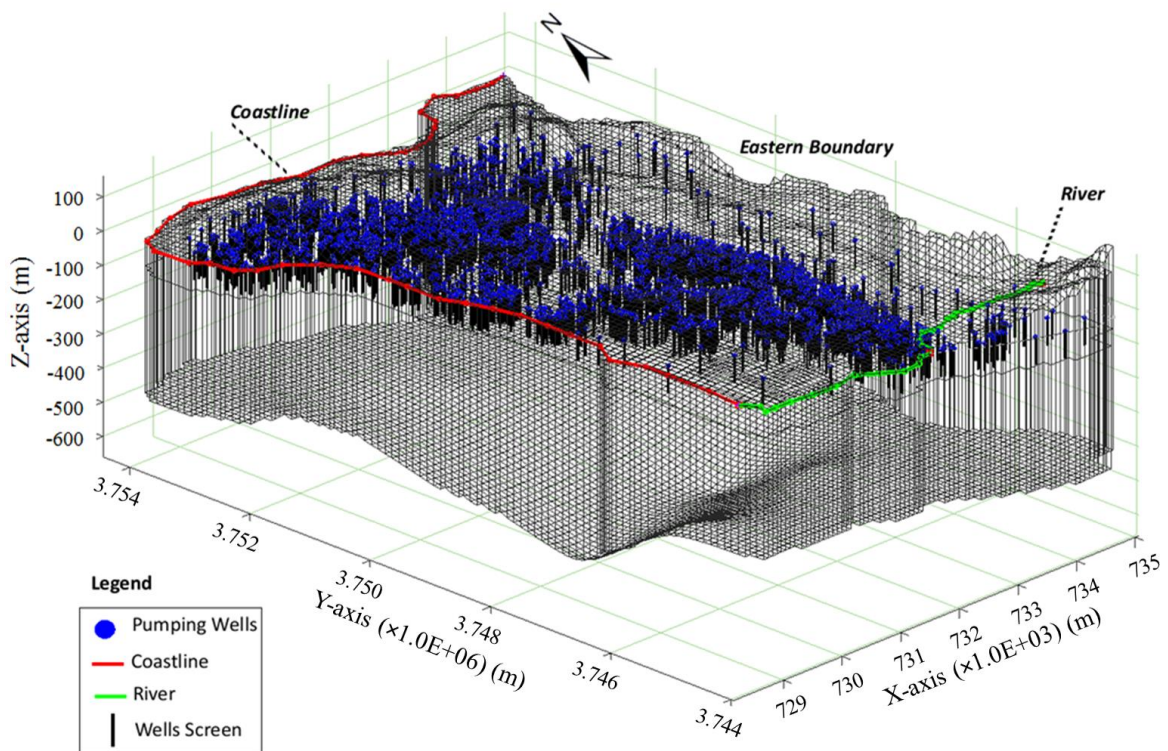
Figure 5-2 Model cells, boundary conditions and licensed wells in the Beirut aquifer (vertical magnification equals 4)

For model verification, salinity data collected during a 2013/2014 groundwater

monitoring campaign were used (Rachid, El-Fadel, Alameddine, & Abu Najm, 2015). A

steady-state MT3D model coupled with the steady-state head results of MODFLOW for June

2012 was run using the standard finite difference method with central-in-space weighting

scheme through SEAWAT. The purpose of this steady-state simulation was to adjust the

salinity distribution with the hydraulic head to estimate the initial saltwater wedge profile that

would exist in the system prior to stressors (Figure 5-3). The salinity distribution was derived

through kriging interpolation using 91 salinity measurements (in the range of 416–21,485

mg/L) collected during the groundwater monitoring programme. However, the salinity data

were not sufficiently detailed to delineate a three-dimensional distribution within the aquifer.

Since the vertical distribution was not known, the two-dimensional distribution was

interpolated with the initial saltwater wedge profile (in 2012) produced by forecasting a

historical model (which represents the water level in 1969) into 2012 (present water level).

The saltwater-freshwater interface associated with the historical model was assumed to be

under the non-intrusion condition when saltwater and freshwater were in balance.
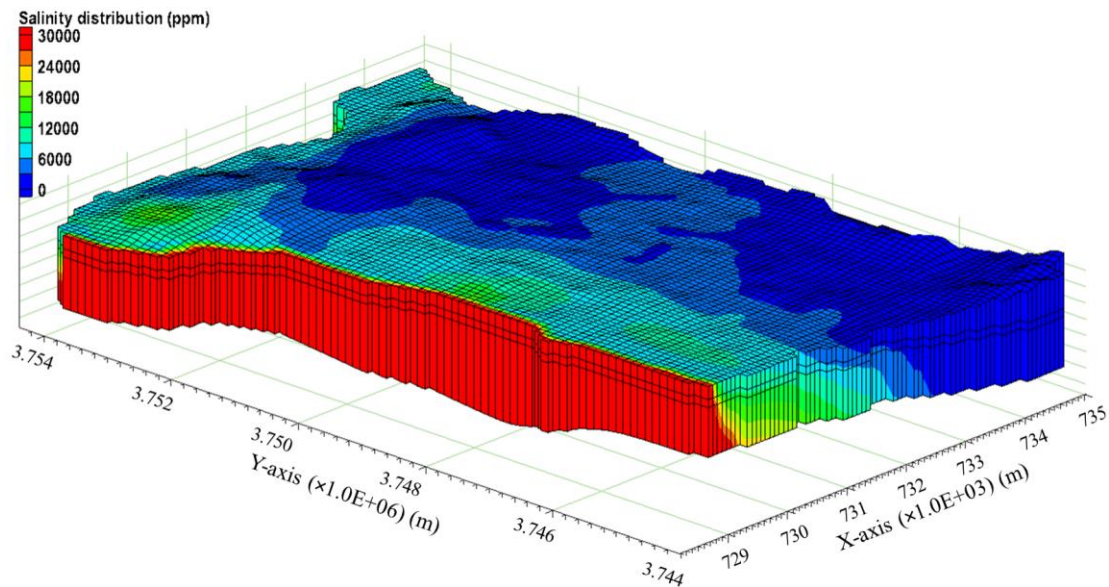
Figure 5-3 Salinity distribution in the pilot aquifer in June 2012

Analysis of SWI dynamics under the various scenarios focused on the mass

encroachment of saltwater into the fresh groundwater aquifer as well as the volumetric

displacement of the saltwater-freshwater interface over the 20 years simulation. The volumetric extent of SWI was computed using the areal extent of intrusion through vertically active cells overrun by salinity of greater than 7,000 mg/l equivalent to the threshold of brackish water. The volume of the interface with the iso-line ≥ 7,000 mg/L was estimated by multiplying the number of cells at a salinity ≥ 7,000 mg/L with the cells' volumes (length*width*depth). The mass of salinity in the entire model domain was then calculated by multiplying the volume with the porosity and salinity ≥ 7,000 mg/L.

While two main mechanisms of SWI are expected to take place[1], the geologic layer in the pilot aquifer was divided into two numerical zones to characterize the dominant mechanism of intrusion: an upper zone where supply wells are tapping and a lower zone where the toe of the interface is located.

As a measure of the relative impacts of model variables (i.e. water consumption rate, population growth and adaptation level) on the magnitude of intrusion, a Prediction Scaled Sensitivity (PSS) was conducted on scenarios of groundwater abstraction (s1A, s2, s2A, s3A1, s4 & s4A1). The PSS was defined as the percent change in the model prediction (i.e. mass of salinity and volumetric displacement of the interface) given a change in the rate of groundwater abstraction on the basis of the change in the water consumption rate, population growth and adaptation level as expressed in Equation 1 (Hill & Tiedeman, 2007):

$$ \overline{\quad\quad} \tag{1} $$

Where $\overline{\quad}$ is the derivative of the mass encroachment or volumetric displacement to the derivative of abstraction rate evaluated at the i_{th} scenario from the j_{th} baseline scenario (mg/l/m^3/yr or m^3/m^3/yr); is the magnitude of mass encroachment of salinity or volumetric

---

[1] Lateral encroachment of recent seawater due to the high degree of heterogeneity in addition to upconing due to the high vertical velocity of water as a result of low storativity

173

displacement of the interface at the j_{th} baseline scenario (mg/l or m³) ;   is the derivative of (change in) the mass encroachment or volumetric displacement in the i_{th} scenario from the j_{th} baseline scenario;   is the abstraction rate at the j_{th} baseline scenario (m³/yr);   is the derivative of (change in) the abstraction rate in the i_{th} scenario from the j_{th} baseline scenario; i corresponds to scenarios (s1A, s2, s2A, s3A1, s4 & s4A1) and j is the associated baseline scenarios (s1 & s3 for s2 & s4, respectively, and s1, s2, s3 & s4 for adaptation A & adaptation A1). For instance, if the abstraction rate increases from 10 to 12 Mm³ (17% increase) and consequently the salinity mass increases from 2000 to 2200 tonnes (10% increase), the PSS value is estimated (200 tonnes / 2 Mm³) * (10 Mm³/100) (100/2000 tonnes) = 0.5. Note that the PSS values are dimensionless. The PSS was calculated for both the mass encroachment of salinity and the volumetric displacement of the interface under seasonal conditions.

5.3   Results and Discussion

5.3.1   Impact of abstraction

The model results indicate that under the baseline scenario (S1), the saltwater-freshwater interface moves landward, indicating increased salinization of the aquifer with ~15% mass encroachment of salinity and ~20% volumetric displacement of the interface occurring in the upper zone of the aquifer within a depth of 100 m below sea-level (where most wells are tapping). Concurrently, there is >80% encroachment occurring in the lower zone of the aquifer, where the toe of the interface is located. Figure 5-4 illustrates the estimated abstraction per year over the whole simulation period for all scenarios in the absence of any adaptation measure. The results show that higher water consumption per capita results in a greater increase in abstraction (S1 vs. S2 & S3 vs. S4) as compared to that

associated with population growth rates (S1 vs. S3 & S2 vs. S4) (Figure 5-4). Increasing the

rate of water consumption from 180l/c/d to 200-300 l/c/d under S2 (the most likely scenario)

increases the total rate of abstraction by ~63% which is translated into ~60% increase in mass

encroachment of SWI and a 70% additional displacement of the interface in 20 years (by

October 2031) as compared to S1 (Figure 5-6).
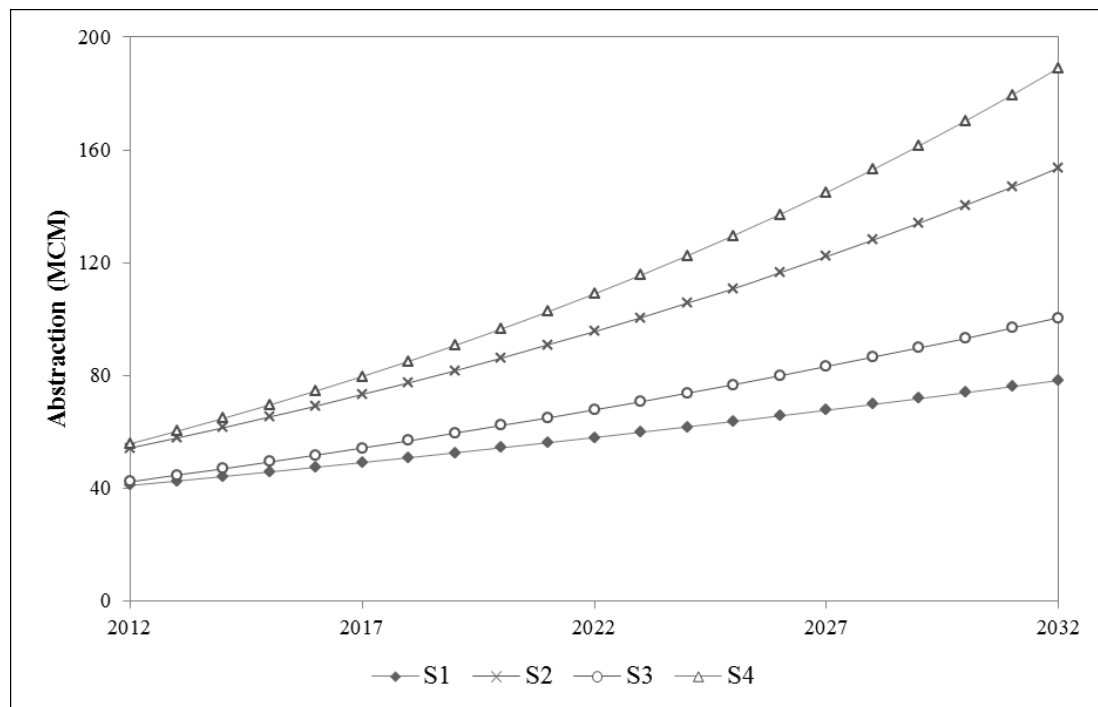
Figure 5-4 Groundwater abstraction in MCM: Variation under main simulated scenarios

The volumetric displacement of elevated concentrations at the end of the dry season

for the current state of salinity (October 2015), the beginning of adaptation scenarios

(October 2019) and the end of simulation period (October 2031) are displayed in Figure 5-5

across scenarios of groundwater abstraction. Simulations of the S3 scenario suggest that

raising the rate of population growth from 1.75% (in S1) to 2.5% (in S3) increases the

abstraction rate by 14.7% with ~12.8% exacerbation in salinity intrusion as compared to S1

suggesting that salinity encroachment is more sensitive to the existing rate of water

consumption than the rate of population growth. The coupled impact of increasing both the

population growth and the water consumption rates under S4 (the worst-case scenario) led to a 78% increase in mass encroachment, which translated into a 90% increase in the landward displacement as compared to S1. Under the scenario S4, the simulated landward displacement is 5% more than the combined predicted impact of increased population growth (S3) and consumption rates (S2) (Figure 5-6) due to the synergistic impact of both S2 and S3 scenarios on the dynamics of SWI.
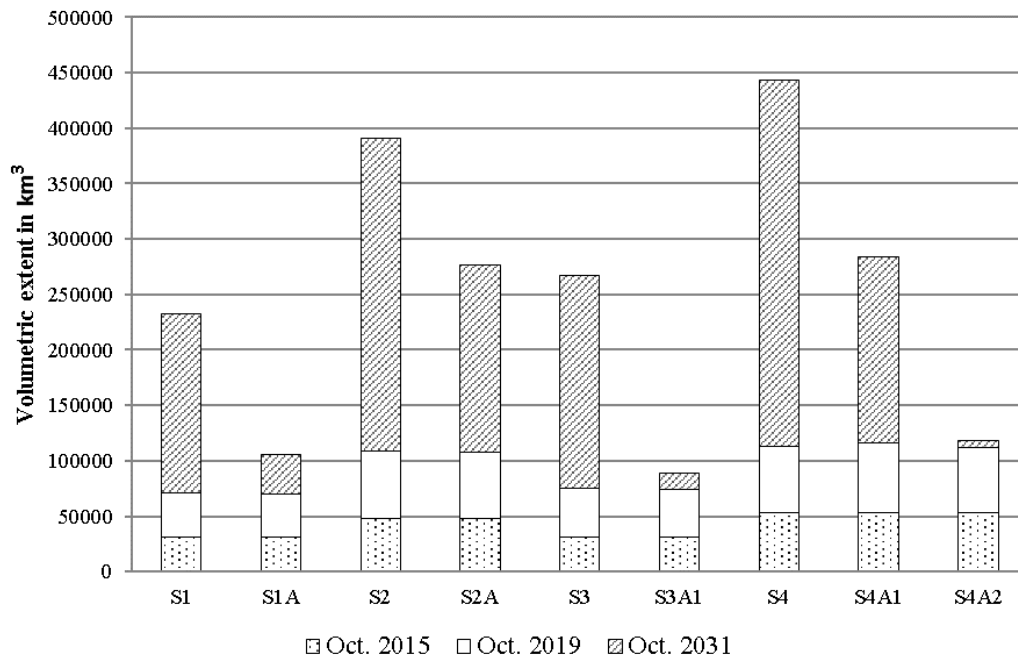
Figure 5-5 Volumetric extent of >7g/l salinity intrusion over the simulation period showing October 2015 (end of the dry season), October 2019 (beginning of adaptation scenarios) and October 2031 (end of simulation period)
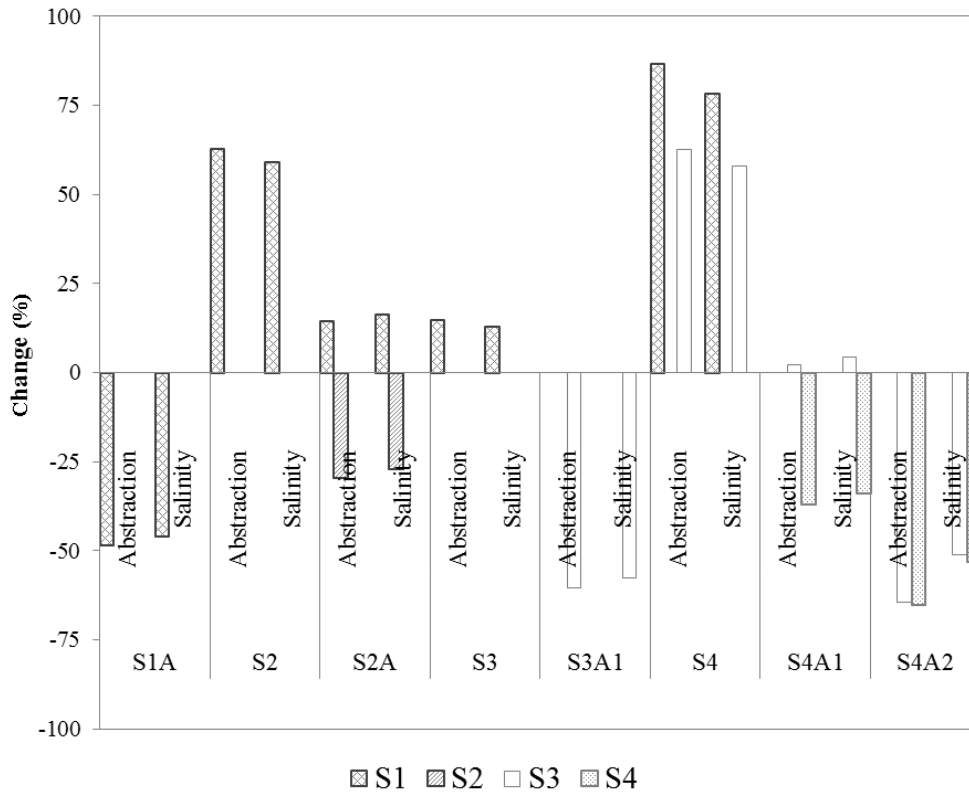
Figure 5-6 Percent change in abstraction and mass encroachment during 20 years simulation under various groundwater abstraction scenarios relative to the corresponding baseline scenarios

In the absence of adaptation measures (scenarios S1, S2, S3, and S4), it is expected that the upper zone now exhibiting SWI with elevated salinity concentrations (>7000 mg/l) will experience a volumetric intrusion that is slightly reduced from the current rate of 20% (Figure 5-7). Since elevated concentrations are encountered mainly inside the transition zone, the diminishing volumetric percentage of intrusion in the upper zone suggests that the dominant mechanism of temporal intrusion is due to lateral encroachment in the lower zone. Since groundwater abstraction increases under scenarios S2 and S4 in comparison to S1 (baseline), the volumetric percent of intrusion in the upper zone further drops (Figure 5-7) while that of the lower zone increases thus demonstrating that the movement of the interface toe is sensitive to abstraction rates. Hence, managing the abstraction rates is imperative for managing the lateral encroachment and potentially reversing the intrusion of saltwater.

177
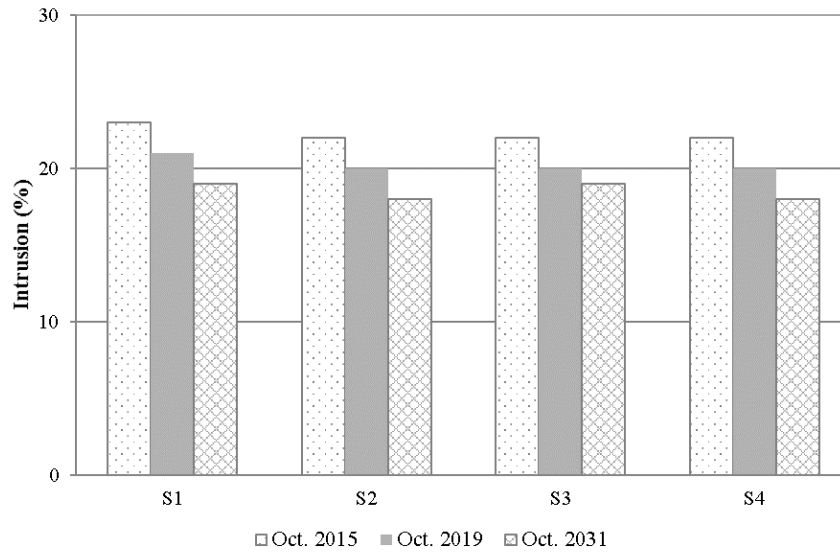
Figure 5-7 Percent volumetric extent of >7g/l salinity intrusion in upper layer of aquifer (100 m thickness)

5.3.2 *Impact of sea level rise*

The simulation of a 1.00 cm/yr SLR (20 cm by 2032) (S1L) applied to the baseline scenario (S1) resulted in a slight increase in the mass encroachment of salinity, which is equivalent to the impact resulting from a 1% increase in groundwater abstraction over the simulation period (i.e. 20 years) under similar conditions. This suggests that a sea level rise of 20 cm by 2032 has a relatively insignificant impact on SWI dynamics relative to groundwater abstraction in the study area. Similarly, a high SLR (S4L) of 3.2 cm/yr (65 cm by 2032) applied to the worst-case scenario (S4) resulted in an additional mass encroachment equivalent to the impact of only 1.7% increase in groundwater abstraction, reconfirming that the impact of a 65 cm SLR by 2032 will largely be masked by the overwhelming impact of over-abstraction. While under the analyzed scenarios of groundwater abstraction (S1, S2, S3 & S4), a SLR of 1.00 cm/yr seems to be of minimal concern due to lower magnitude of intrusion in S1 than other scenarios (S2, S3 & S4), the impact of an additional 2.20 cm/yr SLR (SLR of 3.20 cm/yr) on S1 is equivalent to the impact of a 2% increase in groundwater abstraction for the same scenario (S1). Accordingly, any adaptation strategy or management

178

measure to alleviate SWI must focus on controlling abstraction, which remains the main

driver of SWI. Note that SLR may cause potential changes to the shape of the interface,

which may increase the possibility of upconing near the coastline.

5.3.3 *Impact of adaptation scenarios*

Figure 5-8 depicts the monthly change in the magnitude of SWI upon considering

adaptation scenarios throughout the simulation period (up to 2032). For both the mass and

volumetric encroachment, trends corresponding to scenarios 1A and 4A1 suggest that

adaptation strategies under these scenarios help to reduce the demand for groundwater in the

majority of years as compared to 3A and 6A1, where the demand for groundwater remained

greater than that available supply defined in the adaptation strategies of those scenarios. For

instance, S3A1 exhibited a 60% reduction in volumetric encroachment as compared to S3,

suggesting that a reduction in demand of 350,000 m^3/d can reduce pumping rates to nil in the

wet season (for a couple of years). Note however that while total abstraction rates decrease

under various adaptation strategies (strategies A and A1), the salinity still exhibits an

increasing trend, as expected, due to the higher rate of groundwater depletion as compared to

the available replenishment particularly in the dry season. Nevertheless, adaptation strategies

A and A1 proved to be effective in decreasing the total abstraction rates and simultaneously

halt the intrusion for a significant duration before abstraction takes over again (S2A and

S4A1). Across the scenarios S2A & S4A1, the largest reduction in mass encroachment of

salinity occurred during the wet season (November to April) as the groundwater abstraction

(in some years) decreased to almost nil. In contrast, the minimal reductions were as expected

during dry season (mostly in October, the driest month of the year) because the adaptation

strategies could not meet freshwater demands.
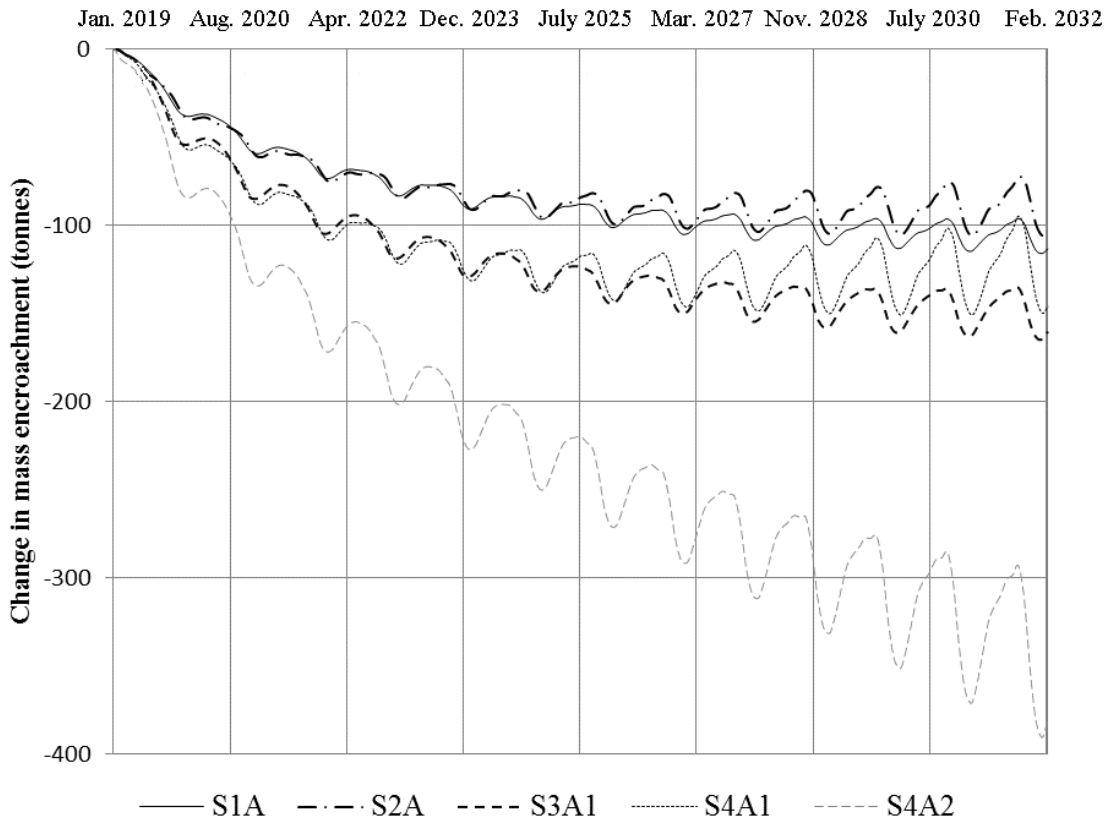
Figure 5-8 Changes in mass encroachment under adaptation scenarios S1A & S2A: Reduction in groundwater abstraction by 230,000 m3/d starting 2019; S3A1 & S4A1: Reduction in groundwater abstraction by 350,000 m3/d starting 2019.

The optimistic adaptation strategy whereby groundwater abstraction ceases by 2019 (with the demand being met through unconventional water resources - desalination) was tested under the worst-case scenario (S4) associated with assuming the highest abstraction rate and mass encroachment after 20 years (by 2032). While the simulation results showed that the mass encroachment of salinity decreased by 47% (from S4 to S4A2) over a period of 13 years (from 2019 to 2032) (Figure 5-8), the total mass of salinity in 2032 was still significantly higher (250%) than that in 2012. This asserts that while halting abstraction helps in freshening the aquifer system, a recovery period of 13 years did not revert the damage caused by 7 years of abstraction under the worst-case scenario (S4) since longer time is needed to aid the aquifer in recharge.

5.3.4 Sensitivity analysis

The sensitivity analysis suggests that the volumetric displacement of the interface, rather than the mass encroachment, is sensitive to changes in abstraction rates (Figure 5-9). Volumetric encroachment is only associated with landward displacement of elevated concentrations (> 7000 mg/l) while mass encroachment involves concentrations in the full TDS range of 0 – 35000 mg/l (seawater concentration), indicating that SWI in the aquifer is governed by concentrations of greater than 7000 mg/l. Furthermore, the results show that salinity encroachment exhibits a higher sensitivity to water consumption rates in comparison to population growth rates (S2 & S1 (Volumetric PSS = 1.08, Mass PSS = 0.94) vs. S3 & S1 (Volumetric PSS = 1.04, Mass PSS = 0.87)) (Figure 5-9). In parallel, the baseline scenarios (S1 and S3) exhibited more sensitivity to adaptation strategies (S1A & S1 (Volumetric PSS = 1.13, Mass PSS = 0.95) vs. S3A1 & S3 (Volumetric PSS = 1.1, Mass PSS = 0.95)) than S2 and S4 (S2A & S2 (Volumetric PSS = 0.97, Mass PSS = 0.91) vs. S4A1 & S4 (Volumetric PSS = 0.98, Mass PSS = 0.92)), where S1A and S3A1 highlighted a large decrease in the magnitude of intrusion with reduced water abstraction, particularly during the wet season. Nevertheless, the response to adaptation strategy A1 (reduction of groundwater demand by 350,000 m^3/d) showed higher sensitivity than with adaptation A (reduction of groundwater demand by 230,000 m^3/), despite the fact that A1 is applied to scenario S3 which involves 15% more abstraction than S1. On the other hand, further increases in water consumption (under S2A and S4A1) reduced the impact of adaptation (S2A & S2 (Volumetric PSS = 0.97, Mass PSS = 0.91) vs. S4A1 & S4 (Volumetric PSS = 0.98, Mass PSS = 0.92), particularly after a period of time where the increase in groundwater demand dominates again.
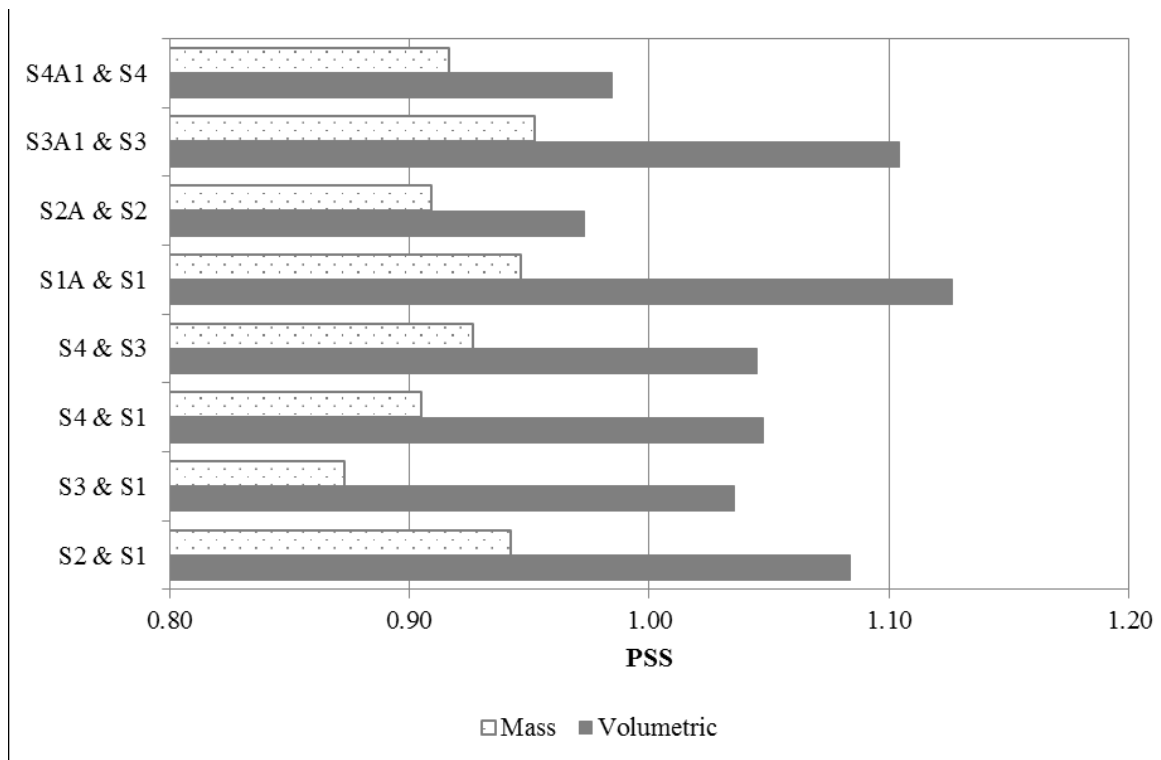
Figure 5-9 Simulated Scaled Sensitivity of various scenarios on mass and volumetric encroachment of intrusion

S1: Baseline scenario with 180 l/c/d water consumption rate and 1.75% population growth;
S2: Most likely scenario with 200 - 300 l/c/d water consumption rate and 1.75% population growth;
S3: Modified baseline scenario with 180 l/c/d water consumption rate and 2.5% population growth;
S4: Worst case scenario with 200 - 300 l/c/d water consumption rate and 2.5% population growth;
S1A & S2A: Reduction in groundwater abstraction by 230,000 m^3/d starting 2019;
S3A1 & S4A1: Reduction in groundwater abstraction by 350,000 m^3/d starting 2019;
S4A2: Abstraction in S4 is halted as demand is met as a result of adaptation/mitigation measures starting 2019;
S1L: Sea level rise is included at 1 cm/yr i.e. rise of 20 cm in S4 by 2032;
S4L: Sea level rise included at 3.2 cm/yr i.e. rise of 65 cm in S4 by 2032.

The seasonal sensitivity results indicated that the impact of adaptation strategies increased during the dry seasons when the aquifer undergoes maximum intrusion (Figure 5-10). Since the aquifer does not suffer from excessive intrusion during the wet season under the baseline scenario S1, the system exhibited the least sensitivity to the adaptation plan during the wet season (Wet PSS=0.56). This highlights the potential role of storing the excess water during the wet season for later usage during the dry season as a potential adaptation strategy to be further examined. However, the impact of adaptation on mass encroachment of salinity during the dry season was most effective under the baseline condition S1 when the PSS increased nearly four times from wet (0.56) to dry (1.73). The high sensitivity of the

182

mass encroachment to the adaptation scenario S4A1 during the wet seasons indicates the vulnerability of the aquifer during the wet-season to increases in the population and water consumption rates (PSS=0.9). While this higher sensitivity to population growth (PSS=0.9) rather than water consumption (PSS=0.8) during the wet seasons (S3 vs. S2) is in contrast to the yearly sensitivity analysis results (where PSS is 0.87 for S3 & 0.94 for S2), it is due to the fact that water consumption varies per season but population growth mainly carries a constant ratio over a given year. This highlights the need for seasonal/monthly simulations to address the impact of seasonal change in the rates of groundwater abstraction on the seasonal state of SWI for proper analysis of the impact of adaptation or mitigation strategies aimed at halting the intrusion.
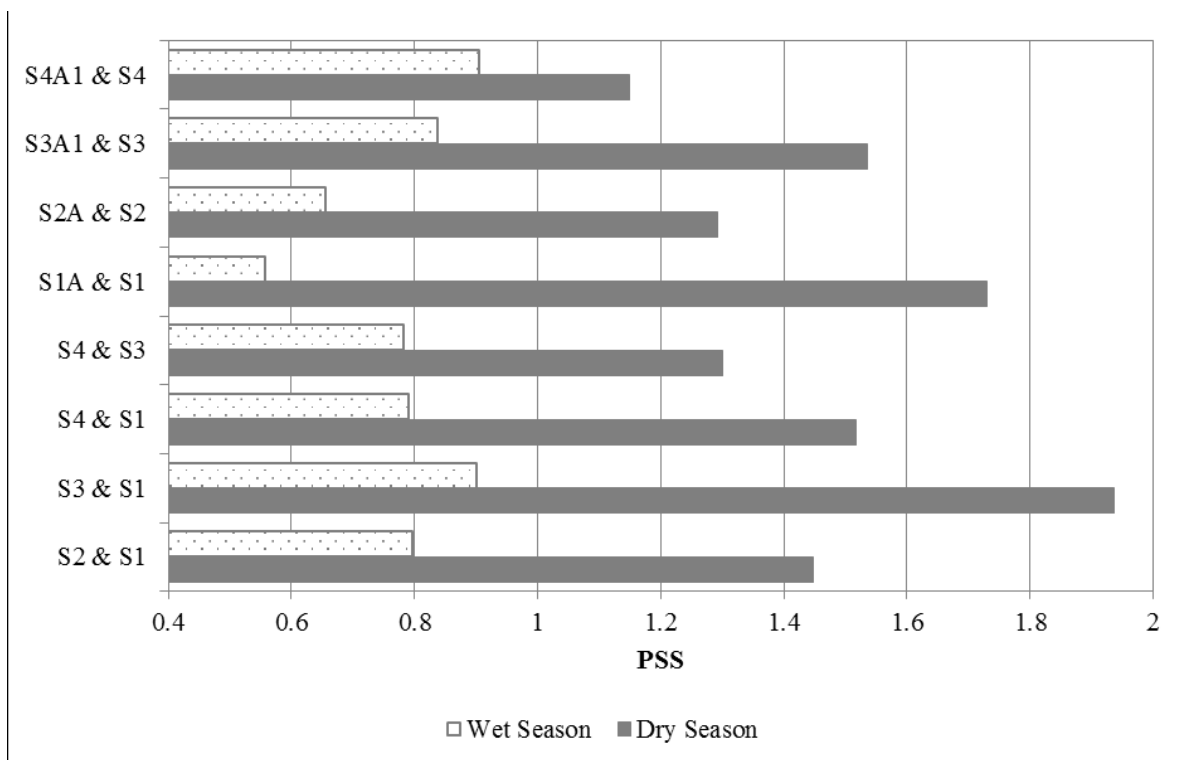
Figure 5-10 Seasonal PSS of simulated scenarios on the mass encroachment of intrusion
S1: Baseline scenario with 180 l/c/d water consumption rate and 1.75% population growth;
S2: Most likely scenario with 200 - 300 l/c/d water consumption rate and 1.75% population growth;
S3: Modified baseline scenario with 180 l/c/d water consumption rate and 2.5% population growth;
S4: Worst case scenario with 200 - 300 l/c/d water consumption rate and 2.5% population growth;
S1A & S2A: Reduction in groundwater abstraction by 230,000 m³/d starting 2019;
S3A1 & S4A1: Reduction in groundwater abstraction by 350,000 m³/d starting 2019;
S4A2: Abstraction in S4 is halted as demand is met as a result of adaptation/mitigation measures starting 2019;
S1L: Sea level rise is included at 1 cm/yr i.e. rise of 20 cm in S4 by 2032;
S4L: Sea level rise included at 3.2 cm/yr i.e. rise of 65 cm in S4 by 2032.

5.3.5 *Adaptation / mitigation framework*

While adaptation strategies can be very successful in slowing SWI even under scenarios of high population growth rates, high water consumption rates must be controlled for this purpose. Scenarios of high consumption rates render adaptation strategies ineffective after an average period of 14 years as the increase in demand for groundwater masks the benefits of the adaptation. In this context, adaptation strategies should be planned together with mitigation measures in a comprehensive framework for effective SWI control and sustainable aquifer management. While only three adaptation strategies were simulated, designing the adaptation framework necessitates examining all measures that can potentially reduce the water deficit, which is the main driver for groundwater abstraction, through targeting both demand and supply management options incorporated in national water plans in close coordination between relevant institutional and community stakeholders (Figure 5-11). In this context, the Ministry of Energy and Water (MoEW) and its Regional Water Establishments (RWE) are the main entity governing the water sector in coordination with other regulatory bodies such as the Ministries of Public Health (MoPH) and Environment (MoE) that are responsible for health and environmental protection and setting standards for water quality monitoring. The Ministry of Interior and Municipalities (MoIM) is involved in executing and monitoring of small-scale municipal works that relate to water infrastructure as well as enforcing regulations / penalties levied by other institutions. In practice, these ministries are also supported at times by the Council for Development and Reconstruction (CDR) through funding large-scale water supply projects such as dams from international organizations (MoE/UNDP/ECODIT 2011) and the Ministries of Finance (MoF) and Economy and Trade (MoET) through setting tariff structures and ensuring consumer protection.

Supply Side Management Strategies	Institutional Stakeholders	Demand Side Management Strategies
− Storm water collection along coastal areas	MoEW REW MoE MoPH MoIM CDR MoF MoTE	
− Dams (in or out of basin)		− Conservation appliances at the household level
− Desalination		− Smart Metering
− Water harvesting (building level)	Consumer at the building level Commercial and Industrial NGOs	− Tariff restructuring
− Water reuse (gray water and wastewater)		− Supply network efficiency (leaks / unaccounted for water)
	Community Stakeholders	

Figure 5-11 Adaptation framework

MoEW: Ministry of Energy & Water RWE: Regional Water Establishments
MoPH Ministry of Public Health MoE: Ministry of Environment (MoE)
MoIM Ministry of Interior & Municipalities CDR: Council for Development and Reconstruction
MoF: Ministry of Finance MoET Ministry of Economy and Trade

Smart metering, tariff restructuring, promotion of water conservation practices as well as incentives for water saving appliances are important demand side management measures indispensable for sustainable water consumption and proper resource management. On the other hand, reducing unaccounted-for-losses in the water supply network, currently estimated at 50% (MoEW, 2012), remains a priority supply management measure that can minimize groundwater abstraction as well as save invaluable surface water resources. Rainwater harvesting, benefiting from surface runoff (storm water) along coastal areas, as well as reuse of treated gray water and wastewater, despite associated sensitivity in terms of social acceptance, can also be incorporated in the framework. Other supply management methods, discussed in the national plans (MoEW, 2012), including the construction of a series of dams as well as conveying water from rural areas, could prove viable in the medium to long term when population growth and high consumption rates require boosting of available water resources. The latter should be considered in parallel to demand management strategies and other supply management measures such as unconventional sources (i.e. desalination, water harvesting, and water reuse etc.). This framework should be managed

concomitantly with a monitoring program that continuously assesses the response of the aquifer system to groundwater extraction. Naturally, the framework needs to be implemented in a wise and timely manner where different measures are gradually undertaken at critical milestones to support and boost strategies that may grow ineffective and maintain aspired performance.

5.4   Conclusion and way forward

The impact of global environmental change and local anthropogenic interventions on the intrusion of saltwater in a coastal urban aquifer was analyzed using a multi-objective variable density model through analysis of groundwater abstraction and sea level rise scenarios. The results of annual simulations showed that while the aquifer system is highly sensitive to both water consumption rates and population growth rates, a ~50% increase in the rate of water consumption leads to at least four times more volumetric displacement of the interface than a similar increase in population growth rate after 20 years. Interestingly, coupling of both has a synergistic effect that aggravates the displacement beyond the sum of the individual impacts. On the other hand, the aquifer system revealed a relatively limited sensitivity to sea level rise (induced by climate change) whereby the impact on SWI of a 65 cm rise by 2032 is masked by 2% increase in abstraction rates under the baseline scenario although other climate change impacts. Note however that the additionality factors associated with the decrease in precipitation and increase in temperature (hence increase in the net water demand) induced by climate change, is indirectly embedded in water consumption rates.

The analysis of adaptation strategies indicated considerable effectiveness in the ability to slow the rate of SWI. While the adaptation strategy of halting abstraction could not cause system-recovery or reverse the SWI damage, it succeeded in stopping the intrusion. The effectiveness of adaptation strategies to secure the aspired results is hinged on proper

planning in terms of timing, duration, capacity and context. This underlines the importance of understanding the aquifer system and its seasonal response as well as its interaction with drivers, before selecting an adaptation strategy for successful and sustainable aquifer management.

This study contributed to the understanding of the response of coastal aquifer systems to local and global stresses as well as the role of adaptation strategies in alleviating SWI. It forms a platform for effective local adaptation planning, providing informed policy and decision making for sustainable aquifer management.

CHAPTER 6

THESIS SUMMARY

6.1   Summary and findings

Worldwide, many heterogeneous coastal aquifers remain poorly managed because of the lack of reliable hydrogeological models with minimal uncertainty as decision support tools. Based on a comprehensive review about the state of the knowledge on the mechanisms, types and drivers of SWI, its mathematical modeling including sources of uncertainty in predicting SWI as well as applied methods to address such uncertainties, we defined the main limitations, controlling factors, computational demands, and required prior information of existing techniques to quantify and reduce uncertainties. We equally identified existing research gaps and future needs with a framework to fill in some gaps. In this context, the greatest shortfall in SWI modeling is related to: (1) the prediction uncertainty analysis, which meets significant challenges including high computational demand for simulating SWI especially in large scale coastal aquifers as well as a lack of precise prior information to infer the required statistics for Monte Carlo (MC) simulations; (2) the use of mathematical modeling to design a field-investigation in a cost-effective manner towards reducing prediction uncertainties; and (3) the application of the knowledge gained from SWI models into management practices.

As such we presented a method for a reliable quantification of uncertainties associated with model predictions of SWI in heterogeneous coastal aquifers that are poorly characterized due to field-data deficit. Compared with the existing Monte Carlo (MC)-like

methods, the proposed method can use crude prior information to quantify prediction uncertainties. Moreover, it incorporates both uncertainty with a parameter and imprecision in its prior information into the prediction uncertainty analysis. In particular, it can be used in deep hydrogeological systems that lack geologic field-data. The proposed method is based on the combination of various uncertainty analysis techniques such as NSMC, SGS, and Fuzzy set theory. The efficiency of the proposed method in quantifying the prediction uncertainty was demonstrated by simulating SWI into the Beirut coastal aquifer, a fractured karstic aquifer that has been increasingly reported to be vulnerable to SWI with a need for a mitigation plan that is curtailed by inadequate characterization of the subsurface environment. A 3D variable density groundwater flow and solute transport model (SEAWAT) was set-up to simulate SWI in the aquifer. The model comprised a transient period of 50 years subdivided into 50 stress periods of one-year duration (from March 1969 to March 2019). Initial and boundary conditions, as well as subsurface characteristics were assigned as input into the model. The model predictions were introduced as the displacement of the salt/fresh water interface caused by 50 years of groundwater abstraction as well as the remaining volume of freshwater stored in the aquifer due to such abstraction. The latter is important for decision makers because the limited remaining freshwater resources in the upper parts of the aquifer is likely to encourage authorities to start tapping the deeper part of the system in the near future. The model was used to (1) describe and predict flow and solute transport processes in the aquifer; (2) assess the potential role of inversion techniques in reducing parameter uncertainties; and (3) evaluate the efficiency of the proposed method in quantifying uncertainties with the model predictions of SWI. To achieve the latter, the estimated range of the prediction uncertainty was compared with the prediction uncertainty calculated using the traditional NSMC methodology with the SGS and a single pilot point calibrated model.

The spatial variability in the hydraulic conductivity played a major role in controlling the flow direction, matching the computed hydraulic head with observed data, and predicting the SWI in the pilot aquifer. The calibration dataset mainly informed about the hydraulic conductivity of the upper layers whereas the estimation of the model prediction was highly dependent on the hydraulic conductivity of the deep layers. The sensitivity analysis confirmed the large uncertainties in model predictions. The estimated range of the prediction uncertainty did encompass the truth using the traditional methodology. Using the proposed method led to a more realistic estimation of the prediction uncertainty than the traditional methodology. The prediction uncertainty ranged from 1.3 to 1.5km^3 for the remaining volume of freshwater stored in the aquifer, and from 40 to 80% for the increase in the total mass of salinity caused by 50 years of groundwater abstraction.

We developed a methodology to guide in locating monitoring stations for additional head and salinity observation data towards reducing the uncertainties with the predictions of the volume of freshwater stored in the deep parts of the aquifer. The proposed method optimizes simultaneous measurements with different depths at multiple spatial locations. It is an extension to an existing linear data-worth (DW) analysis method from the suite of PEST utilities with a global optimization method for an optimal design of groundwater monitoring networks. Our methodology combines the DW analysis with Bayesian model averaging (BMA) and a genetic algorithm (GA) for a 3-D location search. The BMA is used to perform the analysis under non-linear conditions. In the design for monitoring new head/salinity observation wells, the impact of model non-linearity increased with increasing the number of observation wells. The importance of the head and salinity measurements at a certain location with three dimensions changed with respect to the position of the interface. The proposed spatial locations of observation wells became somewhat similar by increasing the number of planned additional observations. The precision of the proposed location depended on the

weighing of stochastic models through the BMA. The optimal size for the monitoring plan depended primarily on the ratio between the start-up cost of the monitoring project and the cost of drilling the first observation well, while the implementation cost of any additional observation well was less significant.

We finally examined the relative impacts of local pressures and global climate change, and their synergistic impacts on the dynamics of SWI in highly heterogeneous urbanized coastal aquifers. For this purpose, input parameters corresponding to the groundwater abstraction (water consumption and population growth rates) and climate change (temperature and sea level rise (SLR)) were assumed to be uncertain. Several scenarios of groundwater abstraction were defined by varying the rates of water consumption and population growth based on the literature reported values. Similarly, SLR scenarios were defined by varying the sea level according to the reported values for future SLR along the Mediterranean coast. Simulations of SWI for the near future (2012 to 2032) were then undertaken at the Beirut aquifer. In line with the national plans, three levels of adaptation were evaluated to analyze the effectiveness and informed decision making towards sustainable aquifer management in the aquifer. Groundwater abstraction was recognized as the main driver forcing the intrusion. As expected, SWI was sensitive to both water consumption and population growth rates used to estimate groundwater abstraction. Nevertheless, the water consumption rate had at least four times more impact on SWI than population growth rate. The synergistic effect of both rates aggravated SWI beyond the sum of the individual impacts. The uncertainty with predicting the spread of SWI revealed a limited sensitivity to the uncertainty of the SLR rate compare with that of the abstraction rate. The impact of a high uncertainty (~220%) with SLR was masked by only a 2% uncertainty with groundwater abstraction rates. Adaptation strategies could alleviate the SWI pending proper planning in terms of timing, duration, capacity and context. This underlines the importance of understanding the aquifer system and its seasonal

response as well as its interaction with drivers, before selecting an adaptation strategy for successful and sustainable aquifer management.

6.2   Study limitations and recommendations for future work

The complex hydrogeology of the subsurface environment that controls water flow and solute transport as well as input recharge/discharge parameters were not fully known in the Beirut aquifer. Due to the limitation in available field-data, some simplifying assumptions were invariably made in the set-up of the SEAWAT model as outlined below.

- Population growth and water consumption rates used to estimate groundwater abstraction rates for the near future (2012-2032) were 1.75% and 180 l/c/d, respectively. Uncertainties with these parameters were not considered due to scarce data.

- Spatial heterogeneity of groundwater abstraction and the number of supply wells (~2500 wells) tapping into the Beirut coastal aquifer did not vary over time (from 2012 to 2032).

- The supply wells receive water mainly from the Quaternary formation within the depth of 10 to 100 meters below the sea level. Recent query of the database reported bottom elevation for only 100 (out of 2478) wells in Beirut. In the model set-up, top screens of the 2478 supply-wells were adjusted based on the topography while their bottom screens vary spatially as to the available dataset for the 100 wells (Annex B). Moreover, only licensed supply wells were considered due to lack of data about the distribution of illegally drilled wells in the aquifer.

- The specified flux boundary condition had a minor impact on the hydraulic head due to its low influx rate and short length along the eastern border of the domain. The groundwater table in 1969 was found to be similar at both sides of the eastern border in the

Beirut aquifer and its adjacent aquifer (Annex D). Since the adjacent aquifer is also a costal aquifer, the direction of flow is expected to be seaward and parallel to its border with the Beirut aquifer. Hence, influx to the Beirut aquifer was considered nil in 1969.

• The rest of the boundary to the east (between the Beirut and Ghadir rivers) was considered a no-flow boundary due to the vicinity with the middle Cenomanian formation (C4b) and faults 1 and 3. These faults were assumed to play a no-flow boundary role in the hydrogeological system of the Beirut aquifer.

• The flow interchange between the pilot aquifer and the adjacent aquifer is negligible beneath the Ghadir River due to the seaward direction of flow in both aquifers.

• The Beirut River was not included in the conceptual model because it was transformed from a riparian river to a concrete canal in 1968.

• Groundwater table uniformly received recharge by infiltration of precipitation in 1969 due to lack of land-use data for that year. This amount slightly decreased to nil in 2019 due to increase in the impervious pavements over time.

Despite considerable efforts made to fill knowledge gaps in SWI uncertainty analysis, much remains to be desired in terms of improving the predictive performance of SWI models towards informed decision making for management purposes. Future efforts may address the following:

1) Uncertainty analysis:

• Analyze the impact of structural errors on SWI predictions by combining multiple competing models representing different types of seaside boundary conditions, number of geologic layers, bottom elevation and geometry of aquifers, fracture and fault orientation, conduit characterization, and initial salinity profile.

- Evaluate the impacts of geologic simplifications and vertical mesh refinements on the calibration and prediction of the mixing zone.

- Determine the impact of each type of common observed data (e.g. temporal and steady state head and salinity concentration, flow, width of interface, etc.) on the estimation of parameters in a SWI model during the model inversion.

- Evaluate the impact of correlations among calibration parameters (e.g. diffusion, storativity, hydraulic conductivity, recharge, etc.) on the predictive performance of SWI models.

- Analyze the impact of increasing/decreasing the density of pilot points within the mixing zone or near pumping wells on model predictions.

- Examine the impact of regularization mechanisms on the reduction of prediction uncertainty.

- Understand the impacts of parameter uncertainties induced by field-data deficit on the predictive performance of a SWI model in different geologic settings using existing techniques (i.e. MC-like techniques).

- Measure the level of complexity in characterizing geologic structure in a SWI model.

- Assess the impact of including/excluding variable density in head observed data on model calibration.

- Evaluate the effect of change in the boundary between the solution space and null space on prediction uncertainty

- Improve the computational burden of SWI inversion.

- Evaluate the synergistic impacts of uncertainties with geologic parameters and input recharge/discharge parameters on prediction uncertainty

- Evaluate the impact of model discretization on prediction uncertainty

- Analyze SWI prediction uncertainty in response to uncertainties related to dispersivity coefficients, recharge and discharge rates, spatial distribution of pumping rates, and length and rate of boundary conditions.

2) Field monitoring:

- Evaluate the efficiency of a proposed design method by collecting field-data from the suggested locations in the aquifer

- Examine the application of the proposed method in identifying the optimal locations for water injection (i.e. artificial recharge) into an urban coastal aquifer towards alleviating SWI

- Evaluate the influence of various types of measurements (e.g. hydraulic conductivity, hydraulic head, and salinity concentration) on the uncertainty reduction of SWI predictions using the proposed method.

- Identify the locations of observation wells with transient measurements in SWI systems.

3) SWI dynamics and drivers:

- Evaluate the coupled effects of dispersive processes and geologic heterogeneity on the thickness of the transition mixing zone in real-world systems

- Discern the impact of geologic simplification on the estimation of possible saltwater

upconing by characterizing the 3D nature of upconing in a real-world system

- Evaluate the impacts of prediction uncertainties on management decisions that are adopted based on model predictions (i.e. risk assessment).

- Examine the magnitude of synergistic impacts of drivers on SWI.

- Recognize controlling factors influencing the vertical mechanism of intrusion in real case studies.

6.2.1   *Application of the model for management practice*

The aim of a groundwater model is typically to support policy makers and stakeholders with the impact assessment of their decisions towards the protection of an environmental system. However, groundwater models often fail to predict accurately the flow direction and rate of solute transport primarily given that: (1) a significant amount of field-date is required to characterize the complex subsurface environments (e.g. fractured aquifers). Such data does not fully exist in any aquifer; (2) parameterizing a complex hydrogeological system (e.g. Karst) always contains errors due to lack of an accurate methodology to characterize such systems; (3) including all complexities of the real-world system into the conceptual model is not practically possible; and (4) increasing the complexity of the conceptual model (e.g. using very fine horizonal and vertical model grids) can significantly increase the computational burden of model simulations and dependency of the conceptual model on field-data. As such, large uncertainties are always expected in any modeling effort, which can mislead decision makers, and thereby cause undesirable management decisions. Although the risk of failure associated with a management decision that is tested and planned using uncertain modeling outputs can be assessed by quantifying prediction uncertainties (as

discussed in chapter 3), combining and including all sources of prediction uncertainty in a model (such as abstraction rates, hydraulic conductivity, boundary condition, etc.) requires additional computational loads, which makes it impossible to perform an uncertainty analysis (also discussed in chapter 2). For these reasons, models are usually constructed individually for each management decision/purpose. Such models are so-called fit-for-purpose models.

The objective of a fit-for-purpose model is determined by the consultation between decision makers, the modeler, and stakeholders to define what is needed from the modeling output and what can be achieved according to the available data. A fit-for-purpose model is then constructed (usually on the basis of an existing simple model) by answering the following questions: What prediction variable corresponds to a decision made by stakeholders/managers? What modeling tools/codes can be used to estimate the predictions? Which conceptual model of the system is likely to produce better predictions? Which elements/parameters of the conceptual model (e.g. heterogeneity in hydraulic conductivity, recharge distribution, boundary conditions, etc.) highly affect the predictions? What is the required level of complexity/simplicity of the conceptual model (e.g. spatial and temporal variations of parameters) in order to achieve reliable predicted results? Are the available data sufficient enough to represent the required complexity of the real-world system (i.e. is there any parameter uncertainty due to lack of data)? Are the parameters uncertainties reduced by calibrating the model using the available observed data? Do the remaining uncertainties lead to large uncertainties with the predictions? Where should additional data be collected to improve the predictions?

In the present research, two fit-for-purpose SWI models were constructed to (1) assess the impacts of national adaptation plans on alleviating SWI in the Beirut coastal aquifer in order to support policy makers with the impact assessment of their decisions towards the protection of groundwater quality in this aquifer (Chapter 5), and (2) determine

the remaining volume of freshwater stored in the deep parts of the aquifer in order to support policy makers with future decisions towards the protection of the freshwater resources in the aquifer (Chapter 3). The latter was later used for a related objective (Chapter 4) to specify where additional data should be collected to improve the reliability of the modeling output. The application of the model for other (or future) management decisions (which have not been addressed in this research) requires the assessment whether the presented model is fit for a new purpose, by evaluating the ability of the model to answer the (abovementioned) questions posed by new modeling objectives. The assessment can be based on whether or not each stage of the model conceptualization has been undertaken in a manner that is appropriate for a stated modeling objective (i.e. a decision) and whether it has resulted in a predictive tool that can be used with an agreed level of confidence. For instance, if the managed aquifer recharge is practiced as a potential solution to alleviate SWI in the aquifer, the recharge rate in the upper layer is most likely the most important parameter for estimating the model prediction while the heterogeneity of hydraulic conductivity is secondary but also important. For such an objective, the uncertainties with the recharge rates should be analyzed and included in the prediction uncertainty analysis using the methodology proposed in chapter 3.

BIBLIOGRAPHY

Abarca, E., Carrera, J., Sánchez-Vila, X., & Dentz, M. (2007). Anisotropic dispersive Henry problem. *Advances in Water Resources*, *30*(4), 913–926. https://doi.org/10.1016/j.advwatres.2006.08.005

Abarca, E., & Prabhakar Clement, T. (2009). A novel approach for characterizing the mixing zone of a saltwater wedge. *Geophysical Research Letters*, *36*(6). https://doi.org/10.1029/2008GL036995

Abd-Elhamid, H. F., & Javadi, A. A. (2011). A density-dependant finite element model for analysis of saltwater intrusion in coastal aquifers. *Journal of Hydrology*, *401*(3–4), 259–271. https://doi.org/10.1016/j.jhydrol.2011.02.028

Abd-Elhamid, H. F., Sherif, M., & Abd-Elaty, I. (2016). Impact of Aquifer Geometry and Boundary Conditions on Saltwater Intrusion in Coastal Aquifers, World Environmental and Water Resources Congress (EWRI)At: West Palm Beach, Florida, USA, May 22-26.

Akbarpour, S., & Niksokhan, M. H. (2018). Investigating effects of climate change, urbanization, and sea level changes on groundwater resources in a coastal aquifer: an integrated assessment. *Environmental Monitoring and Assessment*, *190*(10). https://doi.org/10.1007/s10661-018-6953-3

Alameddine, I., Tarhini, R., & El-Fadel, M. (2018). Household economic burden from seawater intrusion in coastal urban areas. *Water International*, *43*(2), 217–236. https://doi.org/10.1080/02508060.2017.1416441

Alcolea, A., Carrera, J., & Medina, A. (2006). Pilot points method incorporating prior information for solving the groundwater flow inverse problem. *Advances in Water Resources*, *29*(11), 1678–1689. https://doi.org/10.1016/j.advwatres.2005.12.009

Alesandrini, K., & Larson, L. (2002). Teachers Bridge to Constructivism. *The Clearing House: A Journal of Educational Strategies, Issues and Ideas*, *75*(3), 118–121. https://doi.org/10.1080/00098650209599249

Alfarrah, N., Berhane, G., Bakundukize, C., & Walraevens, K. (2017). Degradation of groundwater quality in coastal aquifer of Sabratah area, NW Libya. *Environmental Earth Sciences*, *76*(19). https://doi.org/10.1007/s12665-017-6999-5

Aliewi, A. S., Mackay, R., Jayyousi, A., Nasereddin, K., Mushtaha, A., & Yaqubi, A. (2001). Numerical simulation of the movement of saltwater under skimming and scavenger pumping in the Pleistocene aquifer of Gaza and Jericho Areas, Palestine. *Transport in Porous Media*, *43*(1), 195–212. https://doi.org/10.1023/A:1010698516886

Ammar, K., Khalil, A., McKee, M., & Kaluarachchi, J. (2008). Bayesian deduction for redundancy detection in groundwater quality monitoring networks. *Water Resources Research*, *44*(8). https://doi.org/10.1029/2006WR005616

Anderson, M. P., Woessner, W. W., & Hunt, R. J. (2015). *Applied groundwater modeling: simulation of flow and advective transport*. Academic press, Inc, San Diego, CA, 381 pp.

Andrews, C. B. (2007). *Effective Groundwater Model Calibration: With Analysis of Data, Sensitivities, Predictions, and Uncertainty. Ground Water* (Vol. 46). https://doi.org/10.1111/j.1745-6584.2007.00398.x

Andricevic, R., & Foufoula-Georgiou, E. (1991). A Transfer Function Approach to Sampling Network Design for Groundwater Contamination. *Water Resources Research*, *27*(10), 2759–2769. https://doi.org/10.1029/91WR01391

Angelini, C., Griffin, J. N., Van De Koppel, J., Lamers, L. P. M., Smolders, A. J. P.,

Derksen-Hooijberg, M., … Silliman, B. R. (2016). A keystone mutualism underpins resilience of a coastal ecosystem to drought. *Nature Communications*, *7*. https://doi.org/10.1038/ncomms12473

Asada, M., Ishikawa, A., & Horiuchi, S. (2005). Large-scale cutoff wall model test using ethanol bentonite slurry. Journal of materials in civil engineering, 17(6), 719-724.

Asefa, T., Kemblowski, M. W., Urroz, G., McKee, M., & Khalil, A. (2004). Support vectors-based groundwater head observation networks design. *Water Resources Research*, *40*(11). https://doi.org/10.1029/2004WR003304

Aster, R. C., Borchers, B., & Thurber, C. H. (2013). *Parameter Estimation and Inverse Problems*. *Parameter Estimation and Inverse Problems*. https://doi.org/10.1016/C2009-0-61134-X

Ataie-Ashtiani, B., Volker, R. E., & Lockington, D. A. (1999). Tidal effects on sea water intrusion in unconfined aquifers. *Journal of Hydrology*, *216*(1–2), 17–31. https://doi.org/10.1016/S0022-1694(98)00275-3

Ataie-Ashtiani, B., Werner, A. D., Simmons, C. T., Morgan, L. K., & Lu, C. (2013). Quelle est l'importance de l'impact de l'inondation des terres sur l'intrusion marine causée par l'élévation du niveau de la mer? *Hydrogeology Journal*, *21*(7), 1673–1677. https://doi.org/10.1007/s10040-013-1021-0

Baalousha, H. M. (2016). Development of a groundwater flow model for the highly parameterized Qatar aquifers. *Modeling Earth Systems and Environment*, *2*(2), 67. https://doi.org/10.1007/s40808-016-0124-8

Badaruddin, S., Werner, A. D., & Morgan, L. K. (2015). Water table salinization due to seawater intrusion. *Water Resources Research*, *51*(10), 8397–8408. https://doi.org/10.1002/2015WR017098

Bakalowicz, M. (2005). Karst groundwater: A challenge for new resources. *Hydrogeology Journal*, *13*(1), 148–160. https://doi.org/10.1007/s10040-004-0402-9

Bakker, M., Oude Essink, G. H. P., & Langevin, C. D. (2004). The rotating movement of three immiscible fluids - A benchmark problem. *Journal of Hydrology*, *287*(1–4), 270–278. https://doi.org/10.1016/j.jhydrol.2003.10.007

Bardossy, A., Bogardi, I., & Duckstein, L. (1990). Fuzzy regression in hydrology. *Water Resources Research*, *26*(7), 1497–1508. https://doi.org/10.1029/WR026i007p01497

Barlow, P. M., & Reichard, E. G. (2010). L'intrusion d'eau salée dans les régions côtières d'Amérique du Nord. *Hydrogeology Journal*, *18*(1), 247–260. https://doi.org/10.1007/s10040-009-0514-3

Bear, J. (1972). Dynamics of fluids in porous media. New York: Dover, 764 pp.

Bear, J., Cheng, A. H. D., Sorek, S., Ouazar, D., & Herrera, I. (1999). Seawater intrusion in coastal aquifers: concepts, methods and practices (Vol. 14). Springer Science & Business Media, 625 pp.

Beaujean, J., Nguyen, F., Kemna, A., Antonsson, A., & Engesgaard, P. (2014). Calibration of seawater intrusion models: Inverse parameter estimation using surface electrical resistivity tomography and borehole data. *Water Resources Research*, *50*(8), 6828–6849. https://doi.org/10.1002/2013WR014020

Beck, L., & Bernauer, T. (2011). How will combined changes in water demand and climate affect water availability in the Zambezi river basin? *Global Environmental Change*, *21*(3), 1061–1072. https://doi.org/10.1016/j.gloenvcha.2011.04.001

Beven, K., & Binley, A. (1992). The future of distributed models: Model calibration and uncertainty prediction. *Hydrological Processes*, *6*(3), 279–298.

https://doi.org/10.1002/hyp.3360060305

BOBBA, A. G. (2002). Numerical modelling of salt-water intrusion due to human activities and sea-level change in the Godavari Delta, India. *Hydrological Sciences Journal*, *47*(sup1), S67–S80. https://doi.org/10.1080/02626660209493023

Bredehoeft, J. (2005). The conceptualization model problem - Surprise. *Hydrogeology Journal*, *13*(1), 37–46. https://doi.org/10.1007/s10040-004-0430-5

Bredehoeft, J. D. (2003). From Models to Performance Assessment: The Conceptualization Problem. *Ground Water*. https://doi.org/10.1111/j.1745-6584.2003.tb02395.x

Carneiro, J. F., Boughriba, M., Correia, A., Zarhloule, Y., Rimi, A., & Houadi, B. El. (2010). Evaluation of climate change effects in a coastal aquifer in Morocco using a density-dependent numerical model. *Environmental Earth Sciences*, *61*(2), 241–252. https://doi.org/10.1007/s12665-009-0339-3

Carrera, J., Alcolea, A., Medina, A., Hidalgo, J., & Slooten, L. J. (2005). Inverse problem in hydrogeology. *Hydrogeology Journal*. https://doi.org/10.1007/s10040-004-0404-7

Carrera, J., Hidalgo, J. J., Slooten, L. J., & Vázquez-Suñé, E. (2010). Problèmes conceptuels et de calibration des modèles d'intrusion marines. *Hydrogeology Journal*, *18*(1), 131–145. https://doi.org/10.1007/s10040-009-0524-1

Carretero, S., Rapaglia, J., Bokuniewicz, H., & Kruse, E. (2013). Impact of sea-level rise on saltwater intrusion length into the coastal aquifer, Partido de La Costa, Argentina. *Continental Shelf Research*, *61–62*, 62–70. https://doi.org/10.1016/j.csr.2013.04.029

Cau, P., Lecca, G., Putti, M., & Paniconi, C. (2002). The influence of a confining layer on saltwater intrusion under surface recharge and groundwater extraction conditions. *Developments in Water Science*, *47*(C), 493–500. https://doi.org/10.1016/S0167-5648(02)80100-9

Chadalavada, S., & Datta, B. (2008). Dynamic optimal monitoring network design for transient transport of pollutants in groundwater aquifers. *Water Resources Management*, *22*(6), 651–670. https://doi.org/10.1007/s11269-007-9184-x

Chadalavada, S., Datta, B., & Naidu, R. (2011). Uncertainty based optimal monitoring network design for a chlorinated hydrocarbon contaminated site. *Environmental Monitoring and Assessment*, *173*(1–4), 929–940. https://doi.org/10.1007/s10661-010-1435-2

Chang, S. W., & Clement, T. P. (2012). Experimental and numerical investigation of saltwater intrusion dynamics in flux-controlled groundwater systems. *Water Resources Research*, *48*(9). https://doi.org/10.1029/2012WR012134

Chang, S. W., Clement, T. P., Simpson, M. J., & Lee, K. K. (2011). Does sea-level rise have an impact on saltwater intrusion? *Advances in Water Resources*, *34*(10), 1283–1291. https://doi.org/10.1016/j.advwatres.2011.06.006

Cheng, J. M., & Chen, C. X. (2001). Three-dimensional modeling of density-dependent salt water intrusion in multilayered coastal aquifers in Jahe River Basin, Shandong Province, China. *Ground Water*, *39*(1), 137–143. https://doi.org/10.1111/j.1745-6584.2001.tb00359.x

Chen, B. F., & Hsu, S. M. (2004), Numerical study of tidal effects on seawater intrusion in confined and unconfined aquifers by time independent finite difference method, J. Waterw. Port Coastal Ocean Eng., 130, 191–206.

Cherubini, C., & Pastore, N. (2011). Critical stress scenarios for a coastal aquifer in southeastern Italy. *Natural Hazards and Earth System Science*, *11*(5), 1381–1393. https://doi.org/10.5194/nhess-11-1381-2011

Chesnaux, R. (2015). Closed-form analytical solutions for assessing the consequences of sea-level rise on groundwater resources in sloping coastal aquifers. *Hydrogeology Journal*,

23(7), 1399–1413. https://doi.org/10.1007/s10040-015-1276-8

Chitsazan, N., Pham, H. V., & Tsai, F. T. C. (2015). Bayesian Chance-Constrained Hydraulic Barrier Design under Geological Structure Uncertainty. *Groundwater*, *53*(6), 908–919. https://doi.org/10.1111/gwat.12304

Chitsazan, N., & Tsai, F. T. C. (2015). A hierarchical bayesian model averaging framework for groundwater prediction under uncertainty. *Groundwater*, *53*(2), 305–316. https://doi.org/10.1111/gwat.12207

Christensen, S., & Doherty, J. (2008). Predictive error dependencies when using pilot points and singular value decomposition in groundwater model calibration. *Advances in Water Resources*, *31*(4), 696–722. https://doi.org/10.1016/j.advwatres.2008.01.003

Cieniawski, S. E., Eheart, J. W., & Ranjithan, S. (1995). Using Genetic Algorithms to Solve a Multiobjective Groundwater Monitoring Problem. *Water Resources Research*, *31*(2), 399–409. https://doi.org/10.1029/94WR02039

Cobaner, M., Yurtal, R., Dogan, A., & Motz, L. H. (2012). Three dimensional simulation of seawater intrusion in coastal aquifers: A case study in the Goksu Deltaic Plain. *Journal of Hydrology*, *464–465*, 262–280. https://doi.org/10.1016/j.jhydrol.2012.07.022

Comte, J. C., Cassidy, R., Obando, J., Robins, N., Ibrahim, K., Melchioly, S., … Davies, J. (2016). Challenges in groundwater resource management in coastal aquifers of East Africa: Investigations and lessons learnt in the Comoros Islands, Kenya and Tanzania. *Journal of Hydrology: Regional Studies*, *5*, 179–199. https://doi.org/10.1016/j.ejrh.2015.12.065

Cooper, P. (2007). The Constructed Wetland Association UK database of constructed wetland systems. *Water Science and Technology*, *56*(3), 1–6. https://doi.org/10.2166/wst.2007.490

Cushman, J. H., & Tartakovsky, D. M. (2016). *The handbook of groundwater engineering: Third edition. The Handbook of Groundwater Engineering: Third Edition*. https://doi.org/10.1201/9781315371801

Custodio, E. (2010). Coastal aquifers of Europe: an overview. *Hydrogeology Journal*, *18*(1), 269–280. https://doi.org/10.1007/s10040-009-0496-1

Dagan, G., & Zeitoun, D. G. (1998). Seawater-freshwater interface in a stratified aquifer of random permeability distribution. *Journal of Contaminant Hydrology*, *29*(3), 185–203. https://doi.org/10.1016/S0169-7722(97)00013-2

Dagan, G. (2002). An overview of stochastic modeling of groundwater flow and transport: From theory to applications. *Eos*. https://doi.org/10.1029/2002EO000421

Dahlstrom, D. J. (2015). Calibration and Uncertainty Analysis for Complex Environmental Models. *Groundwater*, *53*(5), 673–674. https://doi.org/10.1111/gwat.12360

Danard, M., Munro, A., & Murty, T. (2003). Storm surge hazard in Canada. *Natural Hazards*, *28*(2–3), 407–431. https://doi.org/10.1023/A:1022990310410

Datta, B., Vennalakanti, H., & Dhar, A. (2009). Modeling and control of saltwater intrusion in a coastal aquifer of Andhra Pradesh, India. *Journal of Hydro-Environment Research*, *3*(3), 148–159. https://doi.org/10.1016/j.jher.2009.09.002

Dausman, A. M., Doherty, J., Langevin, C. D., & Sukop, M. C. (2010). Quantifying data worth toward reducing predictive uncertainty. *Ground Water*, *48*(5), 729–740. https://doi.org/10.1111/j.1745-6584.2010.00679.x

Debernard, J., Sætra, Ø., & Røed, L. P. (2002). Future wind, wave and storm surge climate in the northern North Atlantic. *Climate Research*, *23*(1), 39–49. https://doi.org/10.3354/cr023039

Demirel, Z. (2004). The history and evaluation of saltwater intrusion into a coastal aquifer in Mersin, Turkey. *Journal of Environmental Management*, *70*(3), 275–282. https://doi.org/10.1016/j.jenvman.2003.12.007

Deng, Y., Young, C., Fu, X., Song, J., & Peng, Z. R. (2017). The integrated impacts of human activities and rising sea level on the saltwater intrusion in the east coast of the Yucatan Peninsula, Mexico. *Natural Hazards*, *85*(2), 1063–1088. https://doi.org/10.1007/s11069-016-2621-5

Dhar, A., & Datta, B. (2009). Saltwater Intrusion Management of Coastal Aquifers. I: Linked Simulation-Optimization. *Journal of Hydrologic Engineering*, *14*(12), 1263–1272. https://doi.org/10.1061/(ASCE)HE.1943-5584.0000097

Dogan, A., & Fares, A. (2008). Effects of land-use changes and groundwater pumping on saltwater intrusion in coastal watersheds. In *Coastal Watershed Management* (pp. 219–249). https://doi.org/10.2495/978-1-84564-091-0/08

Doherty, J. E., Hunt, R. J., & Tonkin, M. J. (2010). Approaches to Highly Parameterized Inversion: A Guide to Using PEST for Model-Parameter and Predictive-Uncertainty Analysis. *U.S. Geological Survey*, (Scientific Investigations Report 2010 – 5211), 71. https://doi.org/2010-5211

Dokou, Z., & Karatzas, G. P. (2012). Estimation de l'intrusion d'eau salée dans un systéme karstique côtier à l'aide d'une modélisation dépendant de la densité et comparaison avec l'approche d'interface abrupte. *Hydrological Sciences Journal*, *57*(5), 985–999. https://doi.org/10.1080/02626667.2012.690070

Dokou, Z., & Pinder, G. F. (2009). Optimal search strategy for the definition of a DNAPL source. *Journal of Hydrology*, *376*(3–4), 542–556. https://doi.org/10.1016/j.jhydrol.2009.07.062

Drexler, J. z., & Ewel, K. C. (2001). Effect of the 1997-1998 ENSO-Related Drought on Hydrology and Salinity in a Micronesian Wetland Complex. *Estuaries*, *24*(3), 347. https://doi.org/10.2307/1353237

El-Bihery, M. A. (2009). Groundwater flow modeling of Quaternary aquifer Ras Sudr, Egypt. *Environmental Geology*, *58*(5), 1095–1105. https://doi.org/10.1007/s00254-008-1589-1

El-Fiky, A. A. (2010). Hydrogeochemical characteristics and evolution of groundwater at the Ras Sudr-Abu Zenima area, southwest Sinai, Egypt. *Journal of King Abdulaziz University, Earth Sciences*, *21*(1), 79–109. https://doi.org/10.4197/Ear.21-1.4

Elsayed, S. M., & Oumeraci, H. (2018). Modelling and mitigation of storm-induced saltwater intrusion: Improvement of the resilience of coastal aquifers against marine floods by subsurface drainage. *Environmental Modelling and Software*, *100*, 252–277. https://doi.org/10.1016/j.envsoft.2017.11.030

Elshinnawy, I. A., & Abayazid, H. O. (2011). Vulnerability Assessment of Climate Change Impact on Groundwater Salinity in the Nile Delta Coastal Region—Egypt. In *Coastal Engineering Practice (2011)* (pp. 422–435). https://doi.org/10.1061/41190(422)35

Ergil, M. (2001). Estimation of Saltwater Intrusion through a Salt Balance Equation and its Economic Impact with Suggested Rehabilitation Scenarios: A Case Study. In *First International Conference on Saltwater Intrusion and Coastal Aquifers- Monitoring, Modeling, and Management* (Vol. 150000). Retrieved from http://olemiss.edu/sciencenet/saltnet/swica1/Ergil-paper.pdf

Fatorić, S., & Chelleri, L. (2012). Vulnerability to the effects of climate change and adaptation: The case of the Spanish Ebro Delta. *Ocean and Coastal Management*, *60*, 1–10. https://doi.org/10.1016/j.ocecoaman.2011.12.015

Feener, D. H., Orr, M. R., Wackford, K. M., Longo, J. M., Benson, W. W., & Gilbert, L. E. (2008). *Geographic variation in resource dominance discovery in Brazilian ant communities. Ecology* (Vol. 89). https://doi.org/10.1890/07-0659.1

Felisa, G., Ciriello, V., & Di Federico, V. (2013). Saltwater intrusion in coastal aquifers: A primary case study along the adriatic coast investigated within a probabilistic framework. *Water (Switzerland)*, *5*(4), 1830–1847. https://doi.org/10.3390/w5041830

Ferguson, G., & Gleeson, T. (2012). Vulnerability of coastal aquifers to groundwater use and climate change. *Nature Climate Change*. https://doi.org/10.1038/nclimate1413

Feseker, T. (2007). Numerical studies on saltwater intrusion in a coastal aquifer in northwestern Germany. *Hydrogeology Journal*, *15*(2), 267–279. https://doi.org/10.1007/s10040-006-0151-z

Fetter, C. W. (2001), *Applied Hydrogeology*, 4th ed., Prentice Hall, Upper Saddle River, New Jersey, USA. 598 pp.

Fleury, P., Bakalowicz, M., & de Marsily, G. (2007). Submarine springs and coastal karst aquifers: A review. *Journal of Hydrology*, *339*(1–2), 79–92. https://doi.org/10.1016/j.jhydrol.2007.03.009

Gaaloul, N. (2012). Simulation of Seawater Intrusion in Coastal Aquifers: Forty Five-Years Exploitation in an Eastern Coast Aquifer in NE Tunisia. *The Open Hydrology Journal*, *6*(1), 31–44. https://doi.org/10.2174/1874378101206010031

Gambolati, G., Putti, M., and Paniconi, C. (1999). Three-Dimensional Model of Coupled Density-Dependent Flow and Miscible Salt Transport. In: Bear, J., Cheng, A.HD., Sorek, S., Ouazar, D., Herrera, I. (eds) Seawater Intrusion in Coastal Aquifers — Concepts, Methods and Practices. Theory and Applications of Transport in Porous Media, Springer, Dordrecht, vol 14.

Gemail, K. S., El-Shishtawy, A. M., El-Alfy, M., Ghoneim, M. F., & Abd El-Bary, M. H. (2011). Assessment of aquifer vulnerability to industrial waste water using resistivity measurements. A case study, along El-Gharbyia main drain, Nile Delta, Egypt. *Journal of Applied Geophysics*, *75*(1), 140–150. https://doi.org/10.1016/j.jappgeo.2011.06.026

Georgopoulou, E., Kotronarou, A., Koussis, A., Restrepo, P. J., Gómez-Gotor, A., & Rodriguez Jimenez, J. J. (2001). A methodology to investigate brackish groundwater desalination coupled with aquifer recharge by treated wastewater as an alternative strategy for water supply in Mediterranean areas. *Desalination*, *136*(1–3), 307–315. https://doi.org/10.1016/S0011-9164(01)00193-X

Ghasemizadeh, R., Yu, X., Butscher, C., Hellweger, F., Padilla, I., Alshawabkeh, A., & Cao, B. Y. (2015). Equivalent porous media (EPM) simulation of groundwater hydraulics and contaminant transport in Karst aquifers. *PLoS ONE*, *10*(9). https://doi.org/10.1371/journal.pone.0138954

Giambastiani, B. M. S., Antonellini, M., Oude Essink, G. H. P., & Stuurman, R. J. (2007). Saltwater intrusion in the unconfined coastal aquifer of Ravenna (Italy): A numerical model. *Journal of Hydrology*, *340*(1–2), 91–104. https://doi.org/10.1016/j.jhydrol.2007.04.001

Gossel, W., Sefelnasr, A., & Wycisk, P. (2010). Mod??elisation d'une pal??eo-intrusion d'eau sal??ee dans la partie Nord du Syst??eme Aquif??ere Nubien, Nord-Est de l'Afrique. *Hydrogeology Journal*, *18*(6), 1447–1463. https://doi.org/10.1007/s10040-010-0597-x

Gourley, J. J., & Vieux, B. E. (2006). A method for identifying sources of model uncertainty in rainfall-runoff simulations. *Journal of Hydrology*, *327*(1–2), 68–80. https://doi.org/10.1016/j.jhydrol.2005.11.036

Green, N. R., & MacQuarrie, K. T. B. (2014). Une évaluation de l'importance relative des effets du changement climatique et du prélèvement d'eau souterraine sur l'intrusion d'eau marine dans les aquifères côtiers du Canada atlantique. *Hydrogeology Journal*, 22(3), 609–623. https://doi.org/10.1007/s10040-013-1092-y

Guillaume, J. H. A., Hunt, R. J., Comunian, A., Blakers, R. S., & Fu, B. (2016). Methods for exploring uncertainty in groundwater management predictions. In *Integrated Groundwater Management: Concepts, Approaches and Challenges* (pp. 711–737). https://doi.org/10.1007/978-3-319-23576-9_28

Halihan, T., Mace, R.E., & Sharp, J.M. (2000) Flow in the San Antonio segment of the Edwards aquifer: matrix, fractures, or conduits? Groundwater flow and contaminant transport in carbonate aquifers Wicks and Sasowsky (eds), AA Balkema, Rotterdam, Netherlands: 129–146.

Hartmann, A., Goldscheider, N., Wagener, T., Lange, J., & Weiler, M. (2014). Karst water resources in a changing world: Review of hydrological modeling approaches. *Reviews of Geophysics*. https://doi.org/10.1002/2013RG000443

Hartweg, J., Farmer, A. J., Holman, R. R., & Neil, H. A. (2007). *Meta-analysis of the effects of n-3 polyunsaturated fatty acids on haematological and thrombogenic factors in type 2 diabetes. Diabetologia* (Vol. 50). https://doi.org/10.1007/s00125-006-0486-y

Harvey, C. F., & Gorelick, S. M. (1995). Mapping Hydraulic Conductivity: Sequential Conditioning with Measurements of Solute Arrival Time, Hydraulic Head, and Local Conductivity. *Water Resources Research*, 31(7), 1615–1626. https://doi.org/10.1029/95WR00547

Hemond, H. F., & Fechner, E. J. (2014). *Chemical Fate and Transport in the Environment: Third Edition. Chemical Fate and Transport in the Environment: Third Edition.* https://doi.org/10.1016/C2011-0-09677-1

Hendricks Franssen, H. J., Alcolea, A., Riva, M., Bakr, M., van der Wiel, N., Stauffer, F., & Guadagnini, A. (2009). A comparison of seven methods for the inverse modelling of groundwater flow. Application to the characterisation of well catchments. *Advances in Water Resources*, 32(6), 851–872. https://doi.org/10.1016/j.advwatres.2009.02.011

Herckenrath, D., Langevin, C. D., & Doherty, J. (2011). Predictive uncertainty analysis of a saltwater intrusion model using null-space Monte Carlo. *Water Resources Research*, 47(5). https://doi.org/10.1029/2010WR009342

Herrera, G. S., & Pinder, G. F. (2005). Space-time optimization of groundwater quality sampling networks. *Water Resources Research*, 41(12), 1–15. https://doi.org/10.1029/2004WR003626

Hoeksema, R. J., & Kitanidis, P. K. (1984). An Application of the Geostatistical Approach to the Inverse Problem in Two-Dimensional Groundwater Modeling. *Water Resources Research*, 20(7), 1003–1020. https://doi.org/10.1029/WR020i007p01003

Holzbecher, E. (2005). Free and forced convection in porous media open at the top. *Heat and Mass Transfer/Waerme- Und Stoffuebertragung*, 41(7), 606–614. https://doi.org/10.1007/s00231-004-0601-x

Holzbecher, E. (2001). On the relevance of oscillatory convection regimes in porous media - review and numerical experiments. *Computers and Fluids*, 30(2), 189–209. https://doi.org/10.1016/S0045-7930(00)00008-6

Holzbecher, E. (2005). Groundwater flow pattern in the vicinity of a salt lake. *Hydrobiologia*, 532(1), 233–242. https://doi.org/10.1007/s10750-004-6421-7

Holzbecher, E. O. (1998). *Modeling Density-Driven Flow in Porous Media. Springer Verlag.*

https://doi.org/10.1007/978-3-642-58767-2

Hosseinifard, S. J., & Mirzaei Aminiyan, M. (2015). Hydrochemical Characterization of Groundwater Quality for Drinking and Agricultural Purposes: A Case Study in Rafsanjan Plain, Iran. *Water Quality, Exposure and Health*, *7*(4), 531–544. https://doi.org/10.1007/s12403-015-0169-3

Howard, K. W., & Israfilov, R. G. (2012). *Current problems of hydrogeology in urban areas, urban agglomerates and industrial centres.* Series IV: Earth and Environmental Sciences – Vol. 8, Kluwer Academic Publishers, Dordecht, 500 pp.

Hussain, M. S., Javadi, A. A., Sherif, M. M., & Naseri-Karim-Vand, R. (2016). Control of saltwater intrusion by aquifer storage and recovery. *Proceedings of the Institution of Civil Engineers - Engineering and Computational Mechanics*, *169*(3), 148–155. https://doi.org/10.1680/jencm.15.00021

Huyakorn, P. S., Andersen, P. F., Mercer, J. W., & White, H. O. (1987). Saltwater intrusion in aquifers: Development and testing of a three-dimensional finite element model. *Water Resources Research*, *23*(2), 293–312. https://doi.org/10.1029/WR023i002p00293

Insigne, M. S. L., & Kim, G.-S. (2010). Saltwater Intrusion Modeling in the Aquifer Bounded by Manila Bay and Parañaque River, Philippines. *Environmental Engineering Research*, *15*(2), 117–121. https://doi.org/10.4491/eer.2010.15.2.117

Jeppesen, J., Christensen, S., & Ladekarl, U. L. (2011). Modeling the historical water cycle of the Copenhagen Area 1850-2003. *Journal of Hydrology*, Vol. 404, No. 3-4, 11.07, p. 117-129.

Kaleris, V. (2006). Submarine groundwater discharge: Effects of hydrogeology and of near shore surface water bodies. *Journal of Hydrology*, *325*(1–4), 96–117. https://doi.org/10.1016/j.jhydrol.2005.10.008

Kaleris, V. K., & Ziogas, A. I. (2013). The effect of cutoff walls on saltwater intrusion and groundwater extraction in coastal aquifers. *Journal of Hydrology*, *476*, 370–383. https://doi.org/10.1016/j.jhydrol.2012.11.007

Kanzari, S., Ben Nouna, B., Ben Mariem, S., & Rezig, M. (2018). Hydrus-1D model calibration and validation in various field conditions for simulating water flow and salts transport in a semi-arid region of Tunisia. *Sustainable Environment Research*. https://doi.org/10.1016/j.serj.2018.10.001

Kazakis, N., Pavlou, A., Vargemezis, G., Voudouris, K. S., Soulios, G., Pliakas, F., & Tsokas, G. (2016). Seawater intrusion mapping using electrical resistivity tomography and hydrochemical data. An application in the coastal area of eastern Thermaikos Gulf, Greece. *Science of the Total Environment*, *543*, 373–387. https://doi.org/10.1016/j.scitotenv.2015.11.041

Keating, E. H., Doherty, J., Vrugt, J. A., & Kang, Q. (2010). Optimization and uncertainty assessment of strongly nonlinear groundwater models with high parameter dimensionality. *Water Resources Research*, *46*(10). https://doi.org/10.1029/2009WR008584

Kerrou, J., & Renard, P. (2010). Analyse numérique des effets dimensionnels et des hétérogénéités sur les intrusions d'eau marine en milieu dispersif. *Hydrogeology Journal*, *18*(1), 55–72. https://doi.org/10.1007/s10040-009-0533-0

Kerrou, J., Renard, P., Cornaton, F., & Perrochet, P. (2013). Stochastic forecasts of seawater intrusion towards sustainable groundwater management: application to the Korba aquifer (Tunisia). *Hydrogeology Journal*, *21*(2), 425–440. https://doi.org/10.1007/s10040-012-0911-x

Ketabchi, H., Mahmoodzadeh, D., Ataie-Ashtiani, B., & Simmons, C. T. (2016). Sea-level

rise impacts on seawater intrusion in coastal aquifers: Review and integration. *Journal of Hydrology*, *535*, 235–255. https://doi.org/10.1016/j.jhydrol.2016.01.083

Khadra, W. M., & Stuyfzand, P. J. (2018). Simulation of saltwater intrusion in a poorly karstified coastal aquifer in Lebanon (Eastern Mediterranean). *Hydrogeology Journal*, *26*(6), 1839–1856. https://doi.org/10.1007/s10040-018-1752-z

Kim, S. D., Lee, H. J., & Park, J. S. (2012). Simulation of Seawater Intrusion Range in Coastal Aquifer Using the FEMWATER Model for Disaster Information. *Marine Georesources and Geotechnology*, *30*(3), 210–221. https://doi.org/10.1080/1064119X.2011.602388

Kitanidis, P. K. (1996). On the geostatistical approach to the inverse problem. *Advances in Water Resources*, *19*(6), 333–342. https://doi.org/10.1016/0309-1708(96)00005-X

Klassen, J., & Allen, D. M. (2017). Assessing the risk of saltwater intrusion in coastal aquifers. *Journal of Hydrology*, *551*, 730–745. https://doi.org/10.1016/j.jhydrol.2017.02.044

Kolesnikov, A. (1997). The early Muslim geographers on the ethnic situation in Khurasan. *Iran and the Caucasus*, *1*(1), 17–24. https://doi.org/10.1029/2007WR006678

Kollat, J. B., Reed, P. M., & Kasprzyk, J. R. (2008). A new epsilon-dominance hierarchical Bayesian optimization algorithm for large multiobjective monitoring network design problems. *Advances in Water Resources*, *31*(5), 828–845. https://doi.org/10.1016/j.advwatres.2008.01.017

Kollat, J. B., Reed, P. M., & Maxwell, R. M. (2011). Many-objective groundwater monitoring network design using bias-aware ensemble Kalman filtering, evolutionary optimization, and visual analytics. *Water Resources Research*, *47*(2). https://doi.org/10.1029/2010WR009194

Kollat, J. B., & Reed, P. (2007). A framework for Visually Interactive Decision-making and Design using Evolutionary Multi-objective Optimization (VIDEO). *Environmental Modelling and Software*, *22*(12), 1691–1704. https://doi.org/10.1016/j.envsoft.2007.02.001

Kooi, H., & Groen, J. (2001). Offshore continuation of coastal groundwater systems; predictions using sharp-interface approximations and variable-density flow modelling. *Journal of Hydrology*, *246*(1–4), 19–35. https://doi.org/10.1016/S0022-1694(01)00354-7

Kopsiaftis, G., Mantoglou, A., & Giannoulopoulos, P. (2009). Variable density coastal aquifer models with application to an aquifer on Thira Island. *Desalination*, *237*(1–3), 65–80. https://doi.org/10.1016/j.desal.2007.12.023

Kourakos, G., & Mantoglou, A. (2009). Pumping optimization of coastal aquifers based on evolutionary algorithms and surrogate modular neural network models. *Advances in Water Resources*, *32*(4), 507–521. https://doi.org/10.1016/j.advwatres.2009.01.001

Koussis, A. D., Mazi, K., & Destouni, G. (2012). Analytical single-potential, sharp-interface solutions for regional seawater intrusion in sloping unconfined coastal aquifers, with pumping and recharge. *Journal of Hydrology*, *416–417*, 1–11. https://doi.org/10.1016/j.jhydrol.2011.11.012

Kreydiyyeh, S. I., Usta, J., Knio, K., Markossian, S., & Dagher, S. (2003). *Aniseed oil increases glucose absorption and reduces urine output in the rat*. *Life Sciences* (Vol. 74). https://doi.org/10.1016/j.lfs.2003.07.013

Kuan, W. K., Jin, G., Xin, P., Robinson, C., Gibbes, B., & Li, L. (2012). Tidal influence on seawater intrusion in unconfined coastal aquifers. *Water Resources Research*, *48*(2). https://doi.org/10.1029/2011WR010678

Kumar, C. P. (2001). Simulation of sea water intrusion and tidal influence. *ISH Journal of*

Hydraulic Engineering, 7(1), 1–11. https://doi.org/10.1080/09715010.2001.10514684

Kura, N. U., Ramli, M. F., Ibrahim, S., Sulaiman, W. N. A., Zaudi, M. A., & Aris, A. Z. (2014). A preliminary appraisal of the effect of pumping on seawater intrusion and upconing in a small tropical island using 2D resistivity technique. *Scientific World Journal*, *2014*. https://doi.org/10.1155/2014/796425

Laattoe, T., Werner, A. D., & Simmons, C. T. (2013). Groundwater in the Coastal Zones of Asia-Pacific. In *Groundwater in the Coastal Zones of Asia-Pacific* (Vol. 7). https://doi.org/10.1007/978-94-007-5648-9

Langevin, C. D., Dausman, A. M., & Sukop, M. C. (2010). Solute and heat transport model of the Henry and Hilleke laboratory experiment. *Ground Water*, *48*(5), 757–770. https://doi.org/10.1111/j.1745-6584.2009.00596.x

Langevin, C. D., & Zygnerski, M. (2013). Effect of sea-level rise on salt water intrusion near a coastal well field in Southeastern Florida. *Groundwater*, *51*(5), 781–803. https://doi.org/10.1111/j.1745-6584.2012.01008.x

Laskey, K. B. (2014). Information, physics and the representing mind. *Cosmos and History*. https://doi.org/10.1126/science.1185782

Lathashri, U. A., & Mahesha, A. (2015). Simulation of saltwater intrusion in a coastal aquifer in Karnataka, India. Aquatic Procedia, 4, 700-705.

Lecca, G., & Cau, P. (2004). Stochastic modeling for seawater intrusion risk assessment in exploited coastal aquifers: The Oristano (Sardinia, Italy) case study. *Developments in Water Science*, *55*(PART 2), 1619–1628. https://doi.org/10.1016/S0167-5648(04)80171-0

Lecca, G., & Cau, P. (2009). Using a Monte Carlo approach to evaluate seawater intrusion in the Oristano coastal aquifer: A case study from the AQUAGRID collaborative computing platform. *Physics and Chemistry of the Earth*, *34*(10–12), 654–661. https://doi.org/10.1016/j.pce.2009.03.002

Li, S. G., McLaughlin, D., & Liao, H. S. (2003). A computationally practical method for stochastic groundwater modeling. *Advances in Water Resources*, *26*(11), 1137–1148. https://doi.org/10.1016/j.advwatres.2003.08.003

Lin, J., Snodsmith, J. B., Zheng, C., & Wu, J. (2009). A modeling study of seawater intrusion in Alabama Gulf Coast, USA. *Environmental Geology*, *57*(1), 119–130. https://doi.org/10.1007/s00254-008-1288-y

Liu, G., Lu, Z., & Zhang, D. (2007). Stochastic uncertainty analysis for solute transport in randomly heterogeneous media using a Karhunen-Loève-based moment equation approach. *Water Resources Research*, *43*(7). https://doi.org/10.1029/2006WR005193

Liu, J., Yang, S., & Jiang, C. (2013). Coastal Reservoirs Strategy for Water Resource Development—A Review of Future Trend. *Journal of Water Resource and Protection*, Vol. 5 No. 3A, pp. 336-342. http://dx.doi.org/10.4236/jwarp.2013.53A034.

Llopis-Albert, C., & Pulido-Velazquez, D. (2014). Discussion about the validity of sharp-interface models to deal with seawater intrusion in coastal aquifers. *Hydrological Processes*, *28*(10), 3642–3654. https://doi.org/10.1002/hyp.9908

Loaiciga, H. A. (1989). An optimization approach for groundwater quality monitoring network design. *Water Resources Research*, *25*(8), 1771–1782. https://doi.org/10.1029/WR025i008p01771

Loáiciga, H. A., Pingel, T. J., & Garcia, E. S. (2012). Sea water intrusion by sea-level rise: Scenarios for the 21st century. *Ground Water*, *50*(1), 37–47. https://doi.org/10.1111/j.1745-6584.2011.00800.x

Lu, C., Kitanidis, P. K., & Luo, J. (2009). Effects of kinetic mass transfer and transient flow

conditions on widening mixing zones in coastal aquifers. *Water Resources Research*, *45*(12). https://doi.org/10.1029/2008WR007643

Lu, C., & Werner, A. D. (2013). Timescales of seawater intrusion and retreat. *Advances in Water Resources*, *59*, 39–51. https://doi.org/10.1016/j.advwatres.2013.05.005

Lu, W., Yang, Q., Martín, J. D., & Juncosa, R. (2013). Numerical modelling of seawater intrusion in Shenzhen (China) using a 3D density-dependent model including tidal effects. *Journal of Earth System Science*, *122*(2), 451–465. https://doi.org/10.1007/s12040-013-0273-3

Luoma, S., & Okkonen, J. (2014). Impacts of future climate change and Baltic Sea level rise on groundwater recharge, groundwater levels, and surface leakage in the Hanko aquifer in southern Finland. *Water (Switzerland)*, *6*(12), 3671–3700. https://doi.org/10.3390/w6123671

Mahesha, A. (1995). Parametric Studies on the Advancing Interface in Coastal Aquifers Due to Linear Variation of the Freshwater Level. *Water Resources Research*, *31*(10), 2437–2442. https://doi.org/10.1029/95WR02040

Mahmoodzadeh, D., Ketabchi, H., Ataie-Ashtiani, B., & Simmons, C. T. (2014). Conceptualization of a fresh groundwater lens influenced by climate change: A modeling study of an arid-region island in the Persian Gulf, Iran. *Journal of Hydrology*, *519*(PA), 399–413. https://doi.org/10.1016/j.jhydrol.2014.07.010

Mahmuduzzaman, M., Ahmed, Z. U., Nuruzzaman, A. K. M., & Ahmed, F. R. S. (2014). Causes of Salinity Intrusion in Coastal Belt of Bangladesh. *International Journal of Plant Research*, *4*(4A), 8–13. https://doi.org/10.5923/s.plant.201401.02

Mao, X., Enot, P., Barry, D. A., Li, L., Binley, A., & Jeng, D. S. (2006). Tidal influence on behaviour of a coastal aquifer adjacent to a low-relief estuary. *Journal of Hydrology*, *327*(1–2), 110–127. https://doi.org/10.1016/j.jhydrol.2005.11.030

Mao, X., Prommer, H., Barry, D. A., Langevin, C. D., Panteleit, B., & Li, L. (2006). Three-dimensional model for multi-component reactive transport with variable density groundwater flow. *Environmental Modelling and Software*, *21*(5), 615–628. https://doi.org/10.1016/j.envsoft.2004.11.008

Martínez Fernández, J., & Selma, M. A. E. (2004). The dynamics of water scarcity on irrigated landscapes: Mazarrón and Aguilas in south-eastern Spain. *System Dynamics Review*, *20*(2), 117–137. https://doi.org/10.1002/sdr.290

Martínková, N., Nová, P., Sablina, O. V., Graphodatsky, A. S., & Zima, J. (2004). *Karyotypic relationships of the Tatra vole (Microtus tatricus)*. *Folia Zoologica* (Vol. 53). https://doi.org/10.1007/s13398-014-0173-7.2

Masciopinto, C. (2013). Management of aquifer recharge in Lebanon by removing seawater intrusion from coastal aquifers. *Journal of Environmental Management*, *130*, 306–312. https://doi.org/10.1016/j.jenvman.2013.08.021

Mehdizadeh, S. S., Vafaie, F., & Abolghasemi, H. (2015). Assessment of sharp-interface approach for saltwater intrusion prediction in an unconfined coastal aquifer exposed to pumping. *Environmental Earth Sciences*, *73*(12), 8345–8355. https://doi.org/10.1007/s12665-014-3996-9

Melloul, A., & Collin, M. (2006). Hydrogeological changes in coastal aquifers due to sea level rise. *Ocean and Coastal Management*, *49*(5–6), 281–297. https://doi.org/10.1016/j.ocecoaman.2006.03.009

Method, F. (2004). Numerical Study of Tidal Effects on Seawater Intrusion in Confined and Unconfined Aquifers by Time-Independent. *October*, *130*(4), 191–206.

https://doi.org/10.1061/(ASCE)0733-950X(2004)130:4(191)

Meyer, R., Engesgaard, P., Høyer, A. S., Jørgensen, F., Vignoli, G., & Sonnenborg, T. O. (2018). Regional flow in a complex coastal aquifer system: Combining voxel geological modelling with regularized calibration. *Journal of Hydrology*, *562*, 544–563. https://doi.org/10.1016/j.jhydrol.2018.05.020

Michael, H. A., Scott, K. C., Koneshloo, M., Yu, X., Khan, M. R., & Li, K. (2016). Geologic influence on groundwater salinity drives large seawater circulation through the continental shelf. *Geophysical Research Letters*, *43*(20), 10,782-10,791. https://doi.org/10.1002/2016GL070863

Mohd, H. A., Sarva, M. R., & Aris, A. Z. (2010). A numerical modelling of seawater intrusion into an oceanic island aquifer, Sipadan Island, Malaysia. *Sains Malaysiana*, *39*(4), 525–532. https://doi.org/10.3899/jrheum.111196.Seasonal

Montas, H. J., Mohtar, R. H., Hassan, A. E., & Alkhal, F. A. (2000). Heuristic space-time design of monitoring wells for contaminant plume characterization in stochastic flow fields. *Journal of Contaminant Hydrology*, *43*(3–4), 271–301. https://doi.org/10.1016/S0169-7722(99)00108-4

Moore, C., & Doherty, J. (2005). Role of the calibration process in reducing model predictive error. *Water Resources Research*, *41*(5), 1–14. https://doi.org/10.1029/2004WR003501

Morgan, L. K., Bakker, M., & Werner, A. D. (2015). Occurrence of seawater intrusion overshoot. *Water Resources Research*, *51*(4), 1989–1999. https://doi.org/10.1002/2014WR016329

Morgan, L. K., Stoeckl, L., Werner, A. D., & Post, V. E. A. (2013). An assessment of seawater intrusion overshoot using physical and numerical modeling. *Water Resources Research*, *49*(10), 6522–6526. https://doi.org/10.1002/wrcr.20526

Morgan, L. K., & Werner, A. D. (2015). A national inventory of seawater intrusion vulnerability for Australia. *Journal of Hydrology: Regional Studies*, *4*, 686–698. https://doi.org/10.1016/j.ejrh.2015.10.005

Morton, R. a, Buster, N. a, & Krohn, M. D. (2002). Subsurface Controls on Historical Subsidence Rates and Associated Wetland Loss in Southcentral Louisiana. *Transactions of Gulf Coast Association of Geological Societies*, *52*(2), 767–778. Retrieved from http://coastal.er.usgs.gov/gc-subsidence/gcags-paper/GCAGS02.pdf

Mtoni, Y., Mjemah, I. C., Bakundukize, C., Van Camp, M., Martens, K., & Walraevens, K. (2013). Saltwater intrusion and nitrate pollution in the coastal aquifer of Dar es Salaam, Tanzania. *Environmental Earth Sciences*, *70*(3), 1091–1111. https://doi.org/10.1007/s12665-012-2197-7

Naji, A., Cheng, A. H. D., & Ouazar, D. (1999). BEM solution of stochastic seawater intrusion problems. *Engineering Analysis with Boundary Elements*, *23*(7), 529–537. https://doi.org/10.1016/S0955-7997(99)00012-0

Narayan, K. A., Schleeberger, C., & Bristow, K. L. (2007). Modelling seawater intrusion in the Burdekin Delta Irrigation Area, North Queensland, Australia. *Agricultural Water Management*, *89*(3), 217–228. https://doi.org/10.1016/j.agwat.2007.01.008

Neubauer, S. C., Franklin, R. B., & Berrier, D. J. (2013). Saltwater intrusion into tidal freshwater marshes alters the biogeochemical processing of organic carbon. *Biogeosciences*, *10*(12), 8171–8183. https://doi.org/10.5194/bg-10-8171-2013

Neuman, S. P. (2003). Maximum likelihood Bayesian averaging of uncertain model predictions. *Stochastic Environmental Research and Risk Assessment*, *17*(5), 291–305. https://doi.org/10.1007/s00477-003-0151-7

Nilsson, B., Højberg, A. L., Refsgaard, J. C., & Troldborg, L. (2007). Uncertainty in geological and hydrogeological data. *Hydrology and Earth System Sciences*, *11*(5), 1551–1561. https://doi.org/10.5194/hess-11-1551-2007

Nishikawa, T., Siade, A. J., Reichard, E. G., Ponti, D. J., Canales, A. G., & Johnson, T. A. (2009). Stratigraphic controls on seawater intrusion and implications for groundwater management, Dominguez Gap area of Los Angeles, California, USA. *Hydrogeology Journal*, *17*(7), 1699–1725. https://doi.org/10.1007/s10040-009-0481-8

Nofal, E. R., Amer, M. A., El-Didy, S. M., & Fekry, A. M. (2015). Delineation and modeling of seawater intrusion into the Nile Delta Aquifer: A new perspective. *Water Science*, *29*(2), 156–166. https://doi.org/10.1016/j.wsj.2015.11.003

Nunes, L. M., Cunha, M. C., & Ribeiro, L. (2004). Groundwater monitoring network optimization with redundancy reduction. *Journal Of Water Resources Planning And Management-Asce*, *130*(1), 33–43. https://doi.org/10.1061/(ASCE)0733-9496(2004)130:1(33)

Nunes, L. M., Cunha, M. C., & Ribeiro, L. (2004). Optimal space-time coverage and exploration costs in groundwater monitoring networks. *Environmental Monitoring and Assessment*, *93*(1–3), 103–124. https://doi.org/10.1023/B:EMAS.0000016795.91968.13

Nur, Y., Fazi, S., Wirjoatmodjo, N., & Han, Q. (2001). Towards wise coastal management practice in a tropical megacity - Jakarta. *Ocean and Coastal Management*, *44*(5–6), 335–353. https://doi.org/10.1016/S0964-5691(01)00054-0

Oude Essink, G. H. P. (2001). Salt water intrusion in a three-dimensional groundwater system in the Netherlands: A numerical study. *Transport in Porous Media*, *43*(1), 137–158. https://doi.org/10.1023/A:1010625913251

Oude Essink, G. H. P. (2001). Saltwater intrusion in 3D large-scale aquifers: A Dutch case. *Physics and Chemistry of the Earth, Part B: Hydrology, Oceans and Atmosphere*, *26*(4), 337–344. https://doi.org/10.1016/S1464-1909(01)00016-8

Oude Essink, G. H. P., Van Baaren, E. S., & De Louw, P. G. B. (2010). Effects of climate change on coastal groundwater systems: A modeling study in the Netherlands. *Water Resources Research*, *46*(10). https://doi.org/10.1029/2009WR008719

Ozler, H. M. (2001). Active Saltwater Encroachment (from Lake Van) in the Van Aquifer, East Turkey, First International Conference on Saltwater Intrusion and Coastal Aquifers— Monitoring, Modeling, and Management. Essaouira, Morocco, April 23–25.

Paniconi, C., Khlaifi, I., Lecca, G., Giacomelli, A., & Tarhouni, J. (2001). Modeling and analysis of seawater intrusion in the coastal aquifer of Eastern Cap-Bon, Tunisia. *Transport in Porous Media*, *43*(1), 3–28. https://doi.org/10.1023/A:1010600921912

Park, H. Y., Jang, K., Ju, J. W., & Yeo, I. W. (2012). Hydrogeological characterization of seawater intrusion in tidally-forced coastal fractured bedrock aquifer. *Journal of Hydrology*, *446–447*, 77–89. https://doi.org/10.1016/j.jhydrol.2012.04.033

Paster, A., Dagan, G., & Guttman, J. (2006). The salt-water body in the Northern part of Yarkon-Taninim aquifer: Field data analysis, conceptual model and prediction. *Journal of Hydrology*, *323*(1–4), 154–167. https://doi.org/10.1016/j.jhydrol.2005.08.018

Peña-Haro, S., Pulido-Velazquez, M., & Llopis-Albert, C. (2011). Stochastic hydro-economic modeling for optimal management of agricultural groundwater nitrate pollution under hydraulic conductivity uncertainty. *Environmental Modelling and Software*, *26*(8), 999–1008. https://doi.org/10.1016/j.envsoft.2011.02.010

Pierfelice, K. N., Graeme Lockaby, B., Krauss, K. W., Conner, W. H., Noe, G. B., & Ricker, M. C. (2017). Salinity Influences on Aboveground and Belowground Net Primary

Productivity in Tidal Wetlands. *Journal of Hydrologic Engineering*, *22*(1), D5015002. https://doi.org/10.1061/(ASCE)HE.1943-5584.0001223

Pinault, J. L., Doerfliger, N., Ladouche, B., & Bakalowicz, M. (2004). Characterizing a coastal karst aquifer using an inverse modeling approach: The saline springs of Thau, southern France. *Water Resources Research*, *40*(8). https://doi.org/10.1029/2003WR002553

Pinder, G. F., & Cooper, H. H. (1970). A Numerical Technique for Calculating the Transient Position of the Saltwater Front. *Water Resources Research*, *6*(3), 875–882. https://doi.org/10.1029/WR006i003p00875

Poeter, E., & Anderson, D. (2005). Multimodel ranking and inference in ground water modeling. *Ground Water*, *43*(4), 597–605. https://doi.org/10.1111/j.1745-6584.2005.0061.x

Pool, M., & Carrera, J. (2010). Dynamique des barrières hydrauliques nègatives pour prèvenir Íintrusion ̇deau de mer. *Hydrogeology Journal*, *18*(1), 95–105. https://doi.org/10.1007/s10040-009-0516-1

Post, V. E. A., Bosserelle, A. L., Galvis, S. C., Sinclair, P. J., & Werner, A. D. (2018). On the resilience of small-island freshwater lenses: Evidence of the long-term impacts of groundwater abstraction on Bonriki Island, Kiribati. *Journal of Hydrology*, *564*, 133–148. https://doi.org/10.1016/j.jhydrol.2018.06.015

Pramada, S. K., & Mohan, S. (2015). Stochastic Simulation of Seawater Intrusion into Freshwater Aquifers. *Aquatic Procedia*, *4*, 87–94. https://doi.org/10.1016/j.aqpro.2015.02.013

Prata, T. S., Lima, V. C., Guedes, L. M., Biteli, L. G., Teixeira, S. H., de Moraes, C. G., … Paranhos, A. (2012). Association between corneal biomechanical properties and optic nerve head morphology in newly diagnosed glaucoma patients. *Clinical and Experimental Ophthalmology*, *40*(7), 682–688. https://doi.org/10.1111/j.1442-9071.2012.02790.x

Qahman, K., Larabi, A., Ouazar, D., Naji, A., & Cheng, A. H. D. (2005). Optimal and sustainable extraction of groundwater in coastal aquifers. *Stochastic Environmental Research and Risk Assessment*, *19*(2), 99–110. https://doi.org/10.1007/s00477-004-0218-0

Ragan, G. E., Young, R. A., & Makela, C. J. (2000). New evidence on the economic benefits of controlling salinity in domestic water supplies. *Water Resources Research*, *36*(4), 1087–1095. https://doi.org/10.1029/1999WR900324

Rahman, M. A., Jose, S. C., Nowak, W., & Cirpka, O. A. (2005). Experiments on vertical transverse mixing in a large-scale heterogeneous model aquifer. *Journal of Contaminant Hydrology*, *80*(3–4), 130–148. https://doi.org/10.1016/j.jconhyd.2005.06.010

Rajabi, M. M., & Ataie-Ashtiani, B. (2016). Efficient fuzzy Bayesian inference algorithms for incorporating expert knowledge in parameter estimation. *Journal of Hydrology*, *536*, 255–272. https://doi.org/10.1016/j.jhydrol.2016.02.029

Rajabi, M. M., & Ataie-Ashtiani, B. (2014). Sampling efficiency in Monte Carlo based uncertainty propagation strategies: Application in seawater intrusion simulations. *Advances in Water Resources*, *67*, 46–64. https://doi.org/10.1016/j.advwatres.2014.02.004

Rajabi, M. M., Ataie-Ashtiani, B., & Simmons, C. T. (2015). Polynomial chaos expansions for uncertainty propagation and moment independent sensitivity analysis of seawater intrusion simulations. *Journal of Hydrology*, *520*, 101–122. https://doi.org/10.1016/j.jhydrol.2014.11.020

Ranjan, P., Kazama, S., & Sawamoto, M. (2006). Effects of climate change on coastal fresh groundwater resources. *Global Environmental Change*, *16*(4), 388–399. https://doi.org/10.1016/j.gloenvcha.2006.03.006

Rasmussen, P., Sonnenborg, T. O., Goncear, G., & Hinsby, K. (2013). Assessing impacts of climate change, sea level rise, and drainage canals on saltwater intrusion to coastal aquifer. *Hydrology and Earth System Sciences*, *17*(1), 421–443. https://doi.org/10.5194/hess-17-421-2013

Reed, P., Minsker, B., & Valocchi, A. J. (2000). Cost-effective long-term groundwater monitoring design using a genetic algorithm and global mass interpolation. *Water Resources Research*, *36*(12), 3731–3741. https://doi.org/10.1029/2000WR900232

Reed, P. M., & Minsker, B. S. (2004). Striking the Balance: Long-Term Groundwater Monitoring Design for Conflicting Objectives. *Journal of Resource Planning and Management*, *130*(2), 140–149. https://doi.org/10.1061/(ASCE)0733-9496(2004)130:2(140)

Reed, P., Minsker, B. S., & Goldberg, D. E. (2003). Simplifying multiobjective optimization: An automated design methodology for the nondominated sorted genetic algorithm-II. *Water Resources Research*, *39*(7). https://doi.org/10.1029/2002WR001483

Refsgaard, J. C., van der Sluijs, J. P., Brown, J., & van der Keur, P. (2006). A framework for dealing with uncertainty due to model structure error. *Advances in Water Resources*, *29*(11), 1586–1597. https://doi.org/10.1016/j.advwatres.2005.11.013

Rizzo, D., D. Dougherty, and M. Yu (2000), An adaptive monitoring and operations system (aLTMOsTM) for environmental management, in Proceedings 2000 ASCE Joint Conference on Water Resources Engineering and Water Resources Planning and Management, edited by R. H. Hotchkiss and M. Glade, ASCE, Minneapolis, MN.

Robinson, C., Li, L., & Barry, D. A. (2007). Effect of tidal forcing on a subterranean estuary. *Advances in Water Resources*, *30*(4), 851–865. https://doi.org/10.1016/j.advwatres.2006.07.006

Rojas, R., Feyen, L., & Dassargues, A. (2008). Conceptual model uncertainty in groundwater modeling: Combining generalized likelihood uncertainty estimation and Bayesian model averaging. *Water Resources Research*, *44*(12). https://doi.org/10.1029/2008WR006908

Romanowski, S. A. (2010). Storm Surge Flooding : Risk perception and coping strategies of residents in Tsawwassen , British Columbia by Master of Arts Department of Earth and Atmospheric Sciences. *ProQuest Dissertations and Theses*.

Rouhani, S., & Hall, T. J. (1988). Geostatistical schemes for groundwater sampling. *Journal of Hydrology*, *103*(1–2), 85–102. https://doi.org/10.1016/0022-1694(88)90007-8

Rusnak, I., Weiss, H., & Barkana, I. (2014). Improving the performance of existing missile autopilot using simple adaptive control. *International Journal of Adaptive Control and Signal Processing*, *28*(7–8), 732–749. https://doi.org/10.1002/acs.2457

Safi, A., Rachid, G., El-Fadel, M., Doummar, J., Abou Najm, M., & Alameddine, I. (2018a). Synergy of climate change and local pressures on saltwater intrusion in coastal urban areas: effective adaptation for policy planning. *Water International*, *43*(2), 145–164. https://doi.org/10.1080/02508060.2018.1434957

Safi, A. , Vilhelmsen, T. N., Alameddine, I. , Abou Najm, M. and El Fadel, M. (2018b), Data-Worth Assessment for a Three-Dimensional Optimal Design in Nonlinear Groundwater Systems. Groundwater. doi:10.1111/gwat.12835

Sakr, S. A. (1999). Validity of a sharp-interface model in a confined coastal aquifer. *Hydrogeology Journal*, *7*(2), 155–160. https://doi.org/10.1007/s100400050187

Sanchez-Vila, X., Guadagnini, A., & Carrera, J. (2006). Representative hydraulic conductivities in saturated grqundwater flow. *Reviews of Geophysics*, *44*(3). https://doi.org/10.1029/2005RG000169

Sanford, W. E., & Pope, J. P. (2010). Défis actuels de l'utilisation des modèles pour prédire l'intrusion d'eau de mer: Des leçons de la côte est de la Virginie, USA. *Hydrogeology Journal*, *18*(1), 73–93. https://doi.org/10.1007/s10040-009-0513-4

Santha Sophiya, M., & Syed, T. H. (2013). Assessment of vulnerability to seawater intrusion and potential remediation measures for coastal aquifers: A case study from eastern India. *Environmental Earth Sciences*, *70*(3), 1197–1209. https://doi.org/10.1007/s12665-012-2206-x

Sanz, E., & Voss, C. I. (2006). Inverse modeling for seawater intrusion in coastal aquifers: Insights about parameter sensitivities, variances, correlations and estimation procedures derived from the Henry problem. *Advances in Water Resources*, *29*(3), 439–457. https://doi.org/10.1016/j.advwatres.2005.05.014

Scanlon, B. R., Mace, R. E., Barrett, M. E., & Smith, B. (2003). Can we simulate regional groundwater flow in a karst system using equivalent porous media models? Case study, Barton Springs Edwards aquifer, USA. *Journal of Hydrology*, *276*(1–4), 137–158. https://doi.org/10.1016/S0022-1694(03)00064-7

Sedki, A., & Ouazar, D. (2011). Simulation-Optimization Modeling for Sustainable Groundwater Development: A Moroccan Coastal Aquifer Case Study. *Water Resources Management*, *25*(11), 2855–2875. https://doi.org/10.1007/s11269-011-9843-9

Sefelnasr, A., & Sherif, M. (2014). Impacts of Seawater Rise on Seawater Intrusion in the Nile Delta Aquifer, Egypt. *Groundwater*, *52*(2), 264–276. https://doi.org/10.1111/gwat.12058

Şen, Z. (2015). *Groundwater Hydraulics and Confined Aquifers. Practical and Applied Hydrogeology*. https://doi.org/10.1016/B978-0-12-800075-5.00003-0

Shamir, U., & Dagan, G. (1971). Motion of the Seawater Interface in Coastal Aquifers: A Numerical Solution. *Water Resources Research*, *7*(3), 644–657. https://doi.org/10.1029/WR007i003p00644

Shang, X., Li, Z., & Li, W. (2009). Mining functional associated patterns from biological network data. *Proceedings of the 2009 ACM Symposium on Applied Computing -   9*, 1488. https://doi.org/10.1002/wrcr.20213

Sherif, M. M., & Singh, V. P. (1999). Effect of climate change on sea water intrusion in coastal aquifers. *Hydrological Processes*, *13*(8), 1277–1287. https://doi.org/10.1002/(SICI)1099-1085(19990615)13:8<1277::AID-HYP765>3.0.CO;2-W

Sherif, M., Kacimov, A., Javadi, A., & Ebraheem, A. A. (2012). Modeling Groundwater Flow and Seawater Intrusion in the Coastal Aquifer of Wadi Ham, UAE. *Water Resources Management*, *26*(3), 751–774. https://doi.org/10.1007/s11269-011-9943-6

Shi, L., Cui, L., Park, N., & Huyakorn, P. S. (2011). Applicability of a sharp-interface model for estimating steady-state salinity at pumping wells-validation against sand tank experiments. *Journal of Contaminant Hydrology*, *124*(1–4), 35–42. https://doi.org/10.1016/j.jconhyd.2011.01.005

Shi, L., & Jiao, J. J. (2014). Seawater intrusion and coastal aquifer management in China: a review. *Environmental Earth Sciences*, *72*(8), 2811–2819. https://doi.org/10.1007/s12665-014-3186-9

Shoemaker, W. B. (2004). Important observations and parameters for a salt water intrusion model. *Ground Water*, *42*(6), 829–840. https://doi.org/10.1111/j.1745-6584.2004.t01-2-.x

Sidiropoulos, P., & Mylopoulos, N. (2015). The Value of Hydraulic Conductivity Information for the Optimal Restoration of an Over-exploited Aquifer. *Procedia*

Environmental Sciences, 25, 227–234. https://doi.org/10.1016/j.proenv.2015.04.031

Simmons, C. T. (2005). Variable density groundwater flow: From current challenges to future possibilities. *Hydrogeology Journal*, *13*(1), 116–119. https://doi.org/10.1007/s10040-004-0408-3

Singaraja, C., Chidambaram, S., Anandhan, P., Prasanna, M. V., Thivya, C., & Thilagavathi, R. (2015). A study on the status of saltwater intrusion in the coastal hard rock aquifer of South India. *Environment, Development and Sustainability*, *17*(3), 443–475. https://doi.org/10.1007/s10668-014-9554-5

Singh, A. (2014). Optimization modelling for seawater intrusion management. *Journal of Hydrology*. https://doi.org/10.1016/j.jhydrol.2013.10.042

Soupios, P., Kourgialas, N. N., Dokou, Z., Karatzas, G. P., Panagopoulos, G., Vafidis, A., & Manoutsoglou, E. (2015). Modeling Saltwater Intrusion at an Agricultural Coastal Area Using Geophysical Methods and the FEFLOW Model. In *Engineering Geology for Society and Territory - Volume 3: River Basins, Reservoir Sedimentation and Water Resources* (pp. 249–252). https://doi.org/10.1007/978-3-319-09054-2_51

Spechler, R. M. (2001). The Relation Between Structure and Saltwater Intrusion in the Floridan Aquifer System, Northeastern Florida, U.S. Geological Survey, 224 West Central Parkway, Suite 1006, Altamonte Springs, FL 32714, p. 25-29.

Šperl, J., & Trčková, J. (2008). Permeability and porosity of rocks and their relationship based on laboratory testing. *Acta Geodynamica et Geomaterialia*, *5*(1), 41–47. https://doi.org/10.1029/WR024i008p01225

Steyer, G. D., Perez, B. C., Piazza, S., & Suir, G. (2007). Potential consequences of saltwater intrusion associated with Hurricanes Katrina and Rita: Chapter 6C in Science and the storms-the USGS response to the hurricanes of 2005. *Science and the Storms-the USGS Response to the Hurricanes of 2005: US Geological Survey Circular 1306*, 137–146.

Steyl, G., & Dennis, I. (2009). Review of coastal-area aquifers in Africa. *Hydrogeology Journal*, *18*(1), 217–225. https://doi.org/DOI 10.1007/s10040-009-0545-9

Stigliano, E., Di Sansebastiano, G. Pietro, & Neuhaus, J. M. (2014). Contribution of chitinase A's C-terminal vacuolar sorting determinant to the study of soluble protein compartmentation. *International Journal of Molecular Sciences*, *15*(6), 11030–11039. https://doi.org/10.3390/ijms150611030

Stigter, T. Y., Nunes, J. P., Pisani, B., Fakir, Y., Hugman, R., Li, Y., … El Himer, H. (2014). Comparative assessment of climate change and its impacts on three coastal aquifers in the Mediterranean. *Regional Environmental Change*, *14*(SUPPL.1), 41–56. https://doi.org/10.1007/s10113-012-0377-3

Stocker, T. F., Qin, D., Plattner, G. K., Tignor, M. M. B., Allen, S. K., Boschung, J., … Midgley, P. M. (2013). *Climate change 2013 the physical science basis: Working Group I contribution to the fifth assessment report of the intergovernmental panel on climate change*. *Climate Change 2013 the Physical Science Basis: Working Group I Contribution to the Fifth Assessment Report of the Intergovernmental Panel on Climate Change* (Vol. 9781107057999). https://doi.org/10.1017/CBO9781107415324

Stoltman, J. P., Lidstone, J., & Dechano, L. M. (2007). International perspectives on natural disasters: Occurrence, mitigation, and consequences (Vol. 21). Springer Science & Business Media. Kluwer Academic Publisher. Dordrecht, Netherlands, 480 pp.

Stratis, P. N., Karatzas, G. P., Papadopoulou, E. P., Zakynthinaki, M. S., & Saridakis, Y. G. (2016). Stochastic optimization for an analytical model of saltwater intrusion in coastal aquifers. *PLoS ONE*, *11*(9). https://doi.org/10.1371/journal.pone.0162783

Sulzbacher, H., Wiederhold, H., Siemon, B., Grinat, M., Igel, J., Burschil, T., … Hinsby, K. (2012). Numerical modelling of climate change impacts on freshwater lenses on the North Sea Island of Borkum using hydrological and geophysical methods. *Hydrology and Earth System Sciences*, *16*(10), 3621–3643. https://doi.org/10.5194/hess-16-3621-2012

Sun, D. mei, Niu, S. xiang, & Zang, Y. ge. (2017). Impacts of inland boundary conditions on modeling seawater intrusion in coastal aquifers due to sea-level rise. *Natural Hazards*, *88*(1), 145–163. https://doi.org/10.1007/s11069-017-2860-0

Sunitha, M. S., & Mathew, S. (2013). Fuzzy Graph Theory: A Survey. *Annals of Pure and Applied Mathematics*, *4*(1online), 92–110. Retrieved from www.researchmathsci.org

Sutter, L. A., Chambers, R. M., & Perry, J. E. (2015). Seawater intrusion mediates species transition in low salinity, tidal marsh vegetation. *Aquatic Botany*, *122*, 32–39. https://doi.org/10.1016/j.aquabot.2015.01.002

Szymkiewicz, A., Gumuła-Kawęcka, A., Šimůnek, J., Leterme, B., Beegum, S., Jaworska-Szulc, B., Pruszkowska-Caceres, M., Gorczewska-Langner, W., Angulo-Jaramillo, R., & Jacques, D. (2018). Simulations of freshwater lens recharge and salt/freshwater interfaces using the HYDRUS and SWI2 packages for MODFLOW, Journal of Hydrology and Hydromechanics, 66(2), 246-256. doi: https://doi.org/10.2478/johh-2018-0005

Tavakoli, R., Yoon, H., Delshad, M., ElSheikh, A. H., Wheeler, M. F., & Arnold, B. W. (2013). Comparison of ensemble filtering algorithms and null-space Monte Carlo for parameter estimation and uncertainty quantification using CO2sequestration data. *Water Resources Research*, *49*(12), 8108–8127. https://doi.org/10.1002/2013WR013959

Tiedeman, C. R., Ely, D. M., Hill, M. C., & O'Brien, G. M. (2004). A method for evaluating the importance of system state observations to model predictions, with application to the Death Valley regional groundwater flow system. *Water Resources Research*, *40*(12), 1–14. https://doi.org/10.1029/2004WR003313

Tiedeman, C. R., Hill, M. C., D'Agnese, F. A., & Faunt, C. C. (2003). Methods for using groundwater model predictions to guide hydrogeologic data collection, with application to the Death Valley regional groundwater flow system. *Water Resources Research*, *39*(1). https://doi.org/10.1029/2001WR001255

Tonkin, M. J., & Doherty, J. (2005). A hybrid regularized inversion methodology for highly parameterized environmental models. *Water Resources Research*, *41*(10). https://doi.org/10.1029/2005WR003995

Tribbia, J., & Moser, S. C. (2008). More than information: what coastal managers need to plan for climate change. *Environmental Science and Policy*, *11*(4), 315–328. https://doi.org/10.1016/j.envsci.2008.01.003

Trotta, C., Menegoni, P., Manfredi Frattarelli, F. M., & Iannetta, M. (2015). Assessing desertification vulnerability on a local scale: The Castelporziano study case (central Italy). *Rendiconti Lincei*, *26*, 421–450. https://doi.org/10.1007/s12210-014-0362-5

Tasi, W. & Kou, C. (1998), Numerical analysis of hydrological and geological effects on seawater intrusion, Transactions on Ecology and the Environment, 17, 743-3541.

Tularam, G. a, Singh, R., & Queensland, N. C. (2009). Estuary, river and surrounding groundwater quality deterioration associated with tidal intrusion. *Journal of Applied Science in Environmental Sanitation*, *4*(2), 141–150. Retrieved from file:///D:/KUR/Literatur/Mendeley Copy/Tularam, Singh, Queensland_2009_Estuary, river and surrounding groundwater quality deterioration associated with tidal intrusion.pdf

Uddameri, V., Singaraju, S., & Hernandez, E. A. (2014). Impacts of sea-level rise and urbanization on groundwater availability and sustainability of coastal communities in semi-

arid South Texas. *Environmental Earth Sciences*, *71*(6), 2503–2515. https://doi.org/10.1007/s12665-013-2904-z

Uusitalo, L., Lehikoinen, A., Helle, I., & Myrberg, K. (2015). An overview of methods to evaluate uncertainty of deterministic models in decision support. *Environmental Modelling and Software*. https://doi.org/10.1016/j.envsoft.2014.09.017

Vandenbohede, A., & Lebbe, L. (2003). Combined interpretation of pumping and tracer tests: Theoretical considerations and illustration with a field test. *Journal of Hydrology*, *277*(1–2), 134–149. https://doi.org/10.1016/S0022-1694(03)00090-8

Vandenbohede, A., & Lebbe, L. (2011). Heat transport in a coastal groundwater flow system near De Panne, Belgium. *Hydrogeology Journal*, *19*(6), 1225–1238. https://doi.org/10.1007/s10040-011-0756-8

Vilhelmsen, T. N., & Ferré, T. P. A. (2018). Extending Data Worth Analyses to Select Multiple Observations Targeting Multiple Forecasts. *Groundwater*, *56*(3), 399–412. https://doi.org/10.1111/gwat.12595

Volker, R. E., Zhang, Q., & Lockington, D. A. (2002). Numerical modelling of contaminant transport in coastal aquifers. In *Mathematics and Computers in Simulation* (Vol. 59, pp. 35–44). https://doi.org/10.1016/S0378-4754(01)00391-3

Wagner, B. J. (1995). Sampling Design Methods For Groundwater Modeling Under Uncertainty. *Water Resources Research*, *31*(10), 2581–2591. https://doi.org/10.1029/95WR02107

Wallis, I., Moore, C., Post, V., Wolf, L., Martens, E., & Prommer, H. (2014). Using predictive uncertainty analysis to optimise tracer test design and data acquisition. *Journal of Hydrology*, *515*, 191–204. https://doi.org/10.1016/j.jhydrol.2014.04.061

Walther, M., Delfs, J. O., Grundmann, J., Kolditz, O., & Liedl, R. (2012). Saltwater intrusion modeling: Verification and application to an agricultural coastal arid region in Oman. In *Journal of Computational and Applied Mathematics* (Vol. 236, pp. 4798–4809). https://doi.org/10.1016/j.cam.2012.02.008

Wang, Y., & Jiao, J. J. (2012). Origin of groundwater salinity and hydrogeochemical processes in the confined Quaternary aquifer of the Pearl River Delta, China. *Journal of Hydrology*, *438–439*, 112–124. https://doi.org/10.1016/j.jhydrol.2012.03.008

Watson, T. A., Werner, A. D., & Simmons, C. T. (2010). Transience of seawater intrusion in response to sea level rise. *Water Resources Research*, *46*(12). https://doi.org/10.1029/2010WR009564

Webb, M. D., & Howard, K. W. F. (2011). Modeling the transient response of saline intrusion to rising sea-levels. *Ground Water*, *49*(4), 560–569. https://doi.org/10.1111/j.1745-6584.2010.00758.x

Werner, A. D. (2010). A review of seawater intrusion and its management in Australia. *Hydrogeology Journal*, *18*(1), 281–285. https://doi.org/10.1007/s10040-009-0465-8

Werner, A. D. (2017). On the classification of seawater intrusion. *Journal of Hydrology*, *551*, 619–631. https://doi.org/10.1016/j.jhydrol.2016.12.012

Werner, A. D., Bakker, M., Post, V. E. A., Vandenbohede, A., Lu, C., Ataie-Ashtiani, B., … Barry, D. A. (2013). Seawater intrusion processes, investigation and management: Recent advances and future challenges. *Advances in Water Resources*, *51*, 3–26. https://doi.org/10.1016/j.advwatres.2012.03.004

Werner, A. D., & Gallagher, M. R. (2006). Characterization of sea-water intrusion in the Pioneer Valley, Australia using hydrochemistry and three-dimensional numerical modelling. *Hydrogeology Journal*, *14*(8), 1452–1469. https://doi.org/10.1007/s10040-006-

0059-7

Werner, A. D., & Lockington, D. A. (2006). Tidal impacts on riparian salinities near estuaries. *Journal of Hydrology*, *328*(3–4), 511–522. https://doi.org/10.1016/j.jhydrol.2005.12.011

Werner, A. D., & Simmons, C. T. (2009). Impact of sea-level rise on sea water intrusion in coastal aquifers. *Ground Water*, *47*(2), 197–204. https://doi.org/10.1111/j.1745-6584.2008.00535.x

Werner, A. D., Ward, J. D., Morgan, L. K., Simmons, C. T., Robinson, N. I., & Teubner, M. D. (2012). Vulnerability indicators of sea water intrusion. *Ground Water*, *50*(1), 48–58. https://doi.org/10.1111/j.1745-6584.2011.00817.x

White, E., & Kaplan, D. (2017). Restore or retreat? Saltwater intrusion and water management in coastal wetlands. *Ecosystem Health and Sustainability*, *3*(1), e01258. https://doi.org/10.1002/ehs2.1258

White, J., Langevin, C. D., & Hughes, J. D. (2010). Evaluating the effect of Tikhonov regularization schemes on predictions in a variable density groundwater model. In 21st Salt Water Intrusion Meeting (SWIM21–AZORES 2010) pp. 344-348.

Williams, V. J. (2010). Identifying the Economic Effects of Salt Water Intrusion after Hurricane Katrina. *Journal of Sustainable Development*, *3*(1). https://doi.org/10.5539/jsd.v3n1p29

Wöhling, T., Geiges, A., & Nowak, W. (2016). Optimal Design of Multitype Groundwater Monitoring Networks Using Easily Accessible Tools. *Groundwater*, *54*(6), 861–870. https://doi.org/10.1111/gwat.12430

Woodbury, A. D., & Ulrych, T. J. (2000). A fullBayesian approach to the groundwater inverse problem for steady state flow. *Water Resources Research*, *36*(8), 2081–2093. https://doi.org/10.1029/2000WR900086

Wu, J. C., & Zeng, X. K. (2013). Review of the uncertainty analysis of groundwater numerical simulation. *Chinese Science Bulletin*. https://doi.org/10.1007/s11434-013-5950-8

Wu, J., Meng, F., Wang, X., & Wang, D. (2008). The development and control of the seawater intrusion in the eastern coastal of Laizhou Bay, China. *Environmental Geology*, *54*(8), 1763–1770. https://doi.org/10.1007/s00254-007-0954-9

Wu, W. M., Carley, J., Fienen, M., Mehlhorn, T., Lowe, K., Nyman, J., … Criddle, C. S. (2006). Pilot-scale in situ bioremediation of uranium in a highly contaminated aquifer. 1. Conditioning of a treatment zone. *Environmental Science and Technology*, *40*(12), 3978–3985. https://doi.org/10.1021/es051954y

Wu, Y. (2004). Optimal design of a groundwater monitoring network in Daqing, China. *Environmental Geology*, *45*(4), 527–535. https://doi.org/10.1007/s00254-003-0907-x

Xu, T., Valocchi, A. J., Ye, M., & Liang, F. (2017). Quantifying model structural error: Efficient Bayesian calibration of a regional groundwater flow model using surrogates and a data-driven error model. *Water Resources Research*, *53*(5), 4084–4105. https://doi.org/10.1002/2016WR019831

Xu, Z., & Hu, B. X. (2017). Development of a discrete-continuum VDFST-CFP numerical model for simulating seawater intrusion to a coastal karst aquifer with a conduit system. *Water Resources Research*, *53*(1), 688–711. https://doi.org/10.1002/2016WR018758

Yakirevich, A., Melloul, A., Sorek, S., Shaath, S., & Borisov, V. (1998). Simulation of seawater intrusion into the Khan Yunis area of the Gaza Strip coastal aquifer. *Hydrogeology Journal*, *6*(4), 549–559. https://doi.org/10.1007/s100400050175

Yawen Chang, Bill X. Hu, Zexuan Xu, Xue Li, Juxiu Tong, Lin Chen, Hanxiong Zhang,

Jinjie Miao, Hongwei Liu, Zhen Ma. (2018). Numerical simulation of seawater intrusion to coastal aquifers and brine water/freshwater interaction in south coast of Laizhou Bay, China. Journal of Contaminant Hydrology, 215, 1-10, https://doi.org/10.1016/j.jconhyd.2018.06.002.

Ye, M., Meyer, P. D., & Neuman, S. P. (2008). On model selection criteria in multimodel analysis. *Water Resources Research*, *44*(3). https://doi.org/10.1029/2008WR006803

Ye, M., Neuman, S. P., & Meyer, P. D. (2004). Maximum likelihood Bayesian averaging of spatial variability models in unsaturated fractured tuff. *Water Resources Research*, *40*(5). https://doi.org/10.1029/2003WR002557

Ye, M., Pohlmann, K. F., Chapman, J. B., Pohll, G. M., & Reeves, D. M. (2010). A model-averaging method for assessing groundwater conceptual model uncertainty. *Ground Water*, *48*(5), 716–728. https://doi.org/10.1111/j.1745-6584.2009.00633.x

Yechieli, Y., Shalev, E., Wollman, S., Kiro, Y., & Kafri, U. (2010). Response of the Mediterranean and Dead Sea coastal aquifers to sea level variations. *Water Resources Research*. https://doi.org/10.1029/2009WR008708

Yeh, T. C. J., Jin, M., & Hanna, S. (1996). An iterative stochastic inverse method: Conditional effective transmissivity and hydraulic head fields. *Water Resources Research*, *32*(1), 85–92. https://doi.org/10.1029/95WR02869

Yeh, T. chyi J., Mao, D. qiang, Zha, Y. yuan, Wen, J. chau, Wan, L., Hsu, K. chin, & Lee, C. haw. (2015). Uniqueness, scale, and resolution issues in groundwater model parameter identification. *Water Science and Engineering*, *8*(3), 175–194. https://doi.org/10.1016/j.wse.2015.08.002

Yin, X., Zhang, J., & Wang, X. (2004). *Sequential injection analysis system for the determination of arsenic by hydride generation atomic absorption spectrometry. Fenxi Huaxue* (Vol. 32). https://doi.org/10.1017/CBO9781107415324.004

Yin, X., Zhang, J., & Wang, X. (2004). *Sequential injection analysis system for the determination of arsenic by hydride generation atomic absorption spectrometry. Fenxi Huaxue* (Vol. 32). https://doi.org/10.1017/CBO9781107415324.004

Yuan, R., & Zhu, J. (2015). The Effects of Dredging on Tidal Range and Saltwater Intrusion in the Pearl River Estuary. *Journal of Coastal Research*, *316*, 1357–1362. https://doi.org/10.2112/JCOASTRES-D-14-00224.1

Zeng, X., Wu, J., Wang, D., & Zhu, X. (2016). Assessing the pollution risk of a groundwater source field at western Laizhou Bay under seawater intrusion. *Environmental Research*, *148*, 586–594. https://doi.org/10.1016/j.envres.2015.11.022

Zhang, H., Baray, D. A., & Hocking, G. C. (1999). Analysis of continuous and pulsed pumping of a phreatic aquifer. *Advances in Water Resources*, *22*(6), 623–632. https://doi.org/10.1016/S0309-1708(98)00038-4

Zhang, Q., Volker, R. E., & Lockington, D. A. (2001). Influence of seaward boundary condition on contaminant transport in unconfined coastal aquifers. *Journal of Contaminant Hydrology*, *49*(3–4), 201–215. https://doi.org/10.1016/S0169-7722(00)00194-7

Zhao, Z., Zhao, J., & Fu, C. (2013). Uncertainty analysis of seawater intrusion forecasting. *Water Science and Engineering*, *6*(4), 380–391. https://doi.org/10.3882/J.ISSN.1674-2370.2013.04.002.

APENDIX

A. Modeling saltwater intrusion codes

1.A. General physical and computational features of a groundwater code

Concept	Feature
Physical concepts	Dimension (1D, 2D, 3D)
	Flow model
	(Saturated/Unsaturated; Steady state/Transient flow)
	Transport model
	(Advection-dispersion equation; Adsorption; Chemical reaction; Steady state, Transient transport)
Computational concepts	Source code availability (Public domain / Commercial)
	Language
	Numerical Method
	Media type/ Aquifer type/ Boundary conditions
	Coordinate system
	Solver
	Graphical interface availability

2.A. SEAWAT equations

In SEAWAT, the variable density groundwater flow equation representing flow and solute transport processes is based on Darcy's Law as the linear macroscopic fluid momentum balance equation, and the conservation of mass as expressed in Equation 1.

$$\overline{\quad} \quad \overline{\quad}\,\overline{\quad} \tag{1}$$

Where   is the gradient operator,   is fluid density [ML^{-3}],   is specific density vector [LT^{-1}],   is the density of inflow water from source/sink [ML^{-3}],   is volumetric inflow rate per unit volume of aquifer [T^{-1}],   is porosity,   is specific storage in terms of pressure [$M^{-1}LT^2$] (where   is compressibility of rock formation), and t is time [T].

In the vicinity of a concentration source (e.g. sea), the solute mass is transmitted and distributed by the flow movement. As the transmitted concentration alters the density of the fluid which retards or accelerates the flow movement, both groundwater flow and solute transport equations must be solved jointly. Solute transport is defined as a function of flow movement, molecular diffusion, and mechanical dispersion (Equation 2).

$$\overline{\quad} \quad\quad\quad \overline{\quad} \tag{2}$$

Where D is the hydrodynamic dispersion [L^2T^{-1}],   is the fluid velocity [LT^{-1}],   is the solute concentration [$ML^{-3}T^{-1}$], and   is the decay rate of solute transport. The fluid density is a function of the solute concentration for coupling the variable-density flow and solute-transport simulations using a linear equation to convert concentration to density as expressed in Equation 3:

$$\overline{} \tag{3}$$

where ─ is the slope of density over concentration.

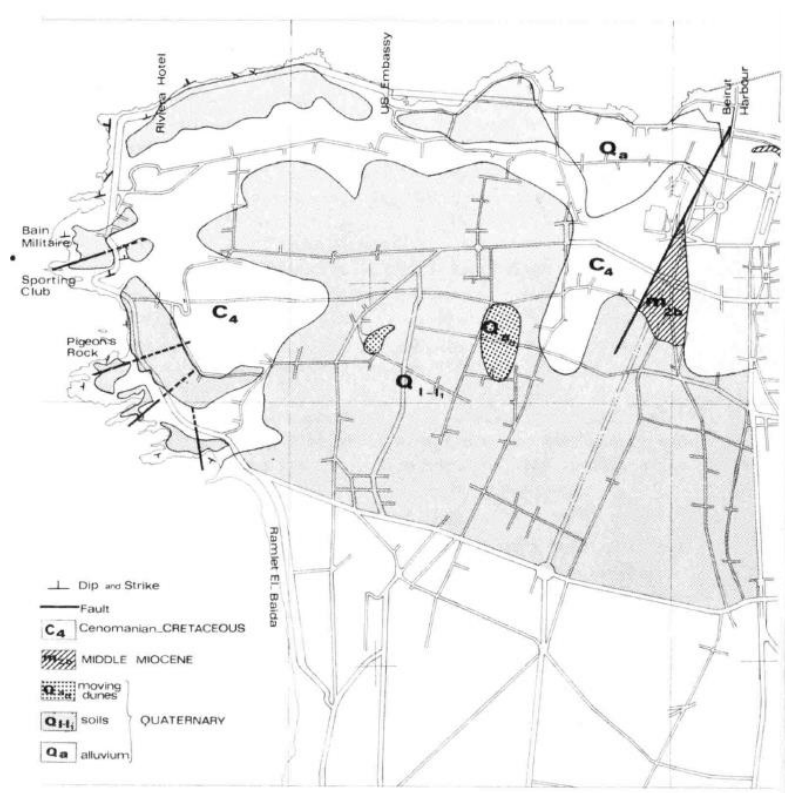*3.A. Horizontal and vertical anisotropy of hydraulic conductivity in the Beirut aquifer*

Figure 3.A.1. Faults orientation in the Beirut City (adopted from Peltikian 1980) - the Beirut river fault in northeast has a N-NE direction and runs parallel to the river with a strike of   . The two faults cutting the northwestern flank of Beirut (Bain Military) have dips of   and   , and strikes of   and   .
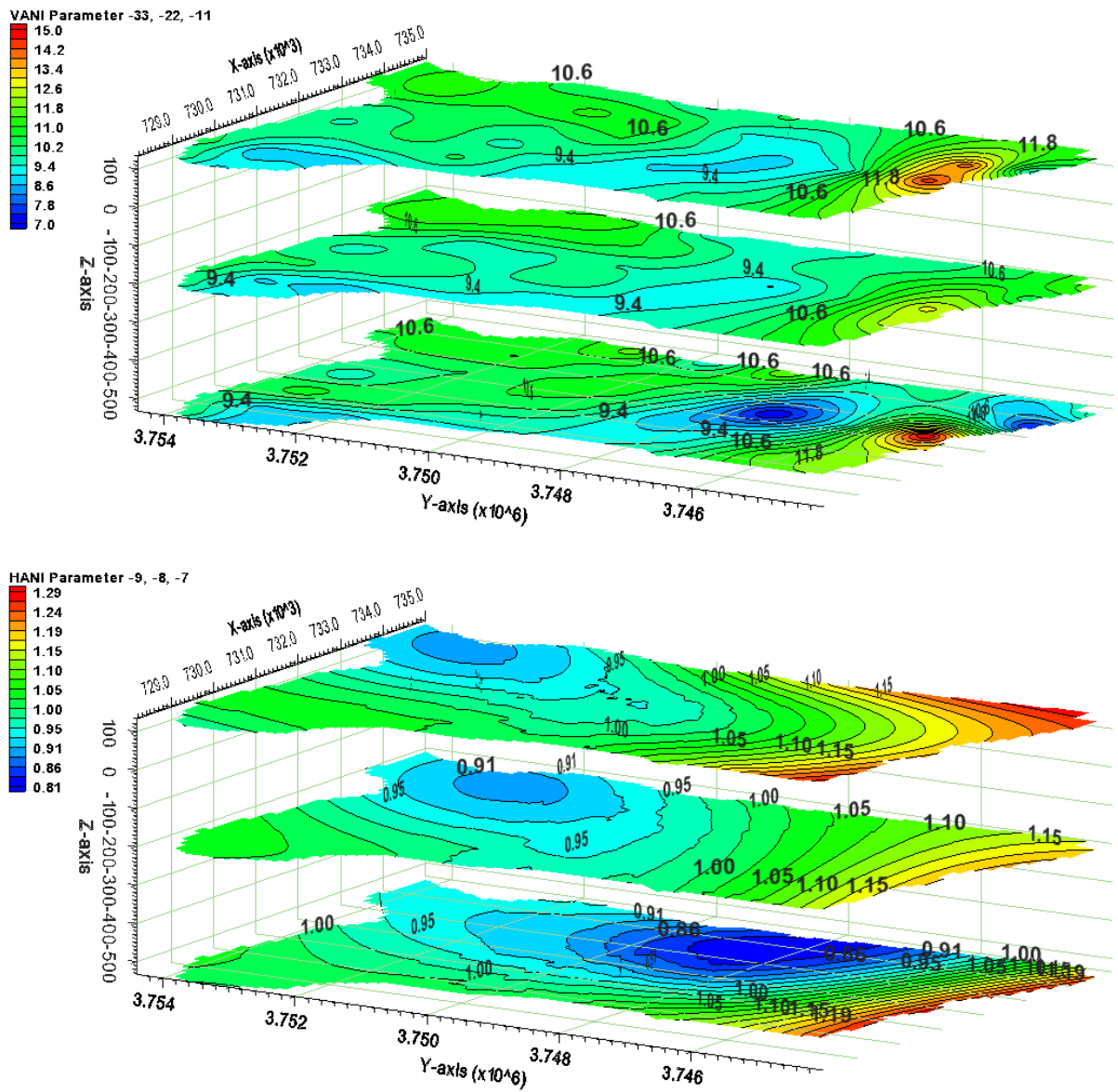
Figure 3.A.2. Calculated horizontal anisotropy (HANI) and vertical anisotropy (VANI) from the dips and strikes of faults in the Beirut aquifer

B. Supply wells in the Beirut aquifer

Available query of the database reports bottom elevation for only 100 (out of 2478) wells in the Beirut City. In the set-up of model, top screens of 2478 supply-wells were adjusted based on the topography while their bottom screens vary spatially as to the available dataset for the 100 wells.

1.B. Spatial distribution and bottom screens of the supply-wells

Area	Wells Bottom Screen (ASL)	NO. of supply-wells	Area (m)
Achrafieh	-30, 0, 20	145	3180230
Ain el-Mraisse	-10	9	997846
Bachoura	-10, 0	18	527005
Bourj El-Brajneh	-40	273	3,20370
Chiyah	-70, -30, 0	413	8806260
Choueifat El-Aamrousiyé	-70	129	300000
FurnEch-Chebbak	0	8	1047900
Hadath	-50	161	5514560
HaretHreik	-70	189	1817570
Hazmieh	-30	6	7000
KfarChima	-80	17	2828690
Laylaké	-40	67	350950
Marfa'	0	1	981595
Mazraa	-70, -50	411	3799740
Mdawar	0	1	2039150
Minet el-Hosn	-10, 0	11	597014
Msaitbé	-10, 0	361	4058070
RasBeyrouth	-10	163	2506680
Rmeil	0	13	1040310
Saifi	0	2	423600
Sinn El-Fil	5	10	160000
Tahouitat-el-Ghadir	-30	36	2537970
Zqaq el-Blat	0	30	466130
Total		**2474**	**47308640**

2. B. Seasonal groundwater abstraction rate in the Beirut aquifer

Scenario 1: Given 1.75% population growth rate & 180l/c/d water consumption rate

Variable	Simulation year		
	1970	2019	2032
Total Water Consumption (MCM/yr)	30.2	101.2	127
Network water supply (MCM/yr)	43	97.7	110.7
Losses (MCM/yr)	20.7	46.9	53.2
Water provided to houses (MCM/yr)	22.4	50.8	57.6
Deficit (MCM/yr)	7.8	50.4	69.5
Wet (MCM/7 months) consumption	13.9	46.6	58.5
Wet supply initial	26.7	58	58
Wet supply after losses	13.9	30.2	30.2
Deficit Wet/ Abstraction	0.1	16.5	28.4
Dry (MCM/5 months) consumption	16.3	54.6	68.5
Dry supply initial	16.4	35.7	35.7
Dry supply after lossed	8.5	18.5	18.6
Deficit dry / Abstraction	7.8	36	49.9
Total deficit	7.8	52.5	78.3

Scenario 2: Given 1.75% population growth rate & 200l/c/d increasing to 300 l/c/d water consumption rate

| Variable	Simulation year		
	1970	2019	2032
Total Water Consumption (MCM/yr)	33.6	130.5	202.4
Network water supply (MCM/yr)	43.1	93.7	93.7
Losses (MCM/yr)	20.7	45.0	45.0
Water provided to houses (MCM/yr)	22.4	48.7	48.7
Deficit (MCM/yr)	11.2	81.7	153.7
Wet (MCM/7 months) consumption	15.5	60.1	93.3
Wet supply initial	26.7	58.0	58.0
Wet supply after losses	13.9	30.2	30.2
Deficit Wet/ Abstraction	1.6	29.9	63.1
Dry (MCM/5 months) consumption	18.1	70.3	109.1
Dry supply initial	16.4	35.7	35.7
Dry supply after lossed	8.5	18.6	18.6
Deficit dry / Abstraction	9.6	51.8	90.6
Total deficit	11.2	81.7	153.7

Scenario 3: Given 2.5% population growth rate & 180l/c/d water consumption rate

| Variable	Simulation year		
	1970	2019	2032
Total Water Consumption (MCM/yr)	33.2	120.3	165.9
Network water supply (MCM/yr)	43.1	93.7	93.7
Losses (MCM/yr)	20.7	45.0	45.0
Water provided to houses (MCM/yr)	22.4	48.7	48.7
Deficit (MCM/yr)	10.8	71.6	117.1
Wet (MCM/7 months) consumption	15.3	55.5	76.4
Wet supply initial	26.7	58.0	58.0
Wet supply after losses	13.9	30.2	30.2
Deficit Wet/ Abstraction	1.4	25.3	46.3
Dry (MCM/5 months) consumption	17.9	64.9	89.4
Dry supply initial	16.4	35.7	35.7
Dry supply after lossed	8.5	18.6	18.6
Deficit dry / Abstraction	9.4	46.3	70.9
Total deficit	10.8	71.6	117.1

Scenario 4: Given 2.5% population growth rate & 200l/c/d increasing to 300 l/c/d water consumption rate

Variable	Simulation year		
	1970	2019	2032
Total Water Consumption (MCM/yr)	33.6	139.4	237.8
Network water supply (MCM/yr)	43.1	93.7	93.7
Losses (MCM/yr)	20.7	45.0	45.0
Water provided to houses (MCM/yr)	22.4	48.7	48.7
Deficit (MCM/yr)	11.2	90.6	189.1
Wet (MCM/7 months) consumption	15.5	64.2	109.6
Wet supply initial	26.7	58.0	58.0
Wet supply after losses	13.9	30.2	30.2
Deficit Wet/ Abstraction	1.6	34.0	79.4
Dry (MCM/5 months) consumption	18.1	75.1	128.2
Dry supply initial	16.4	35.7	35.7
Dry supply after lossed	8.5	18.6	18.6
Deficit dry / Abstraction	9.6	56.6	109.7
Total deficit	11.2	90.6	189.1

227

C. Geologic cross-sections in the Beirut aquifer
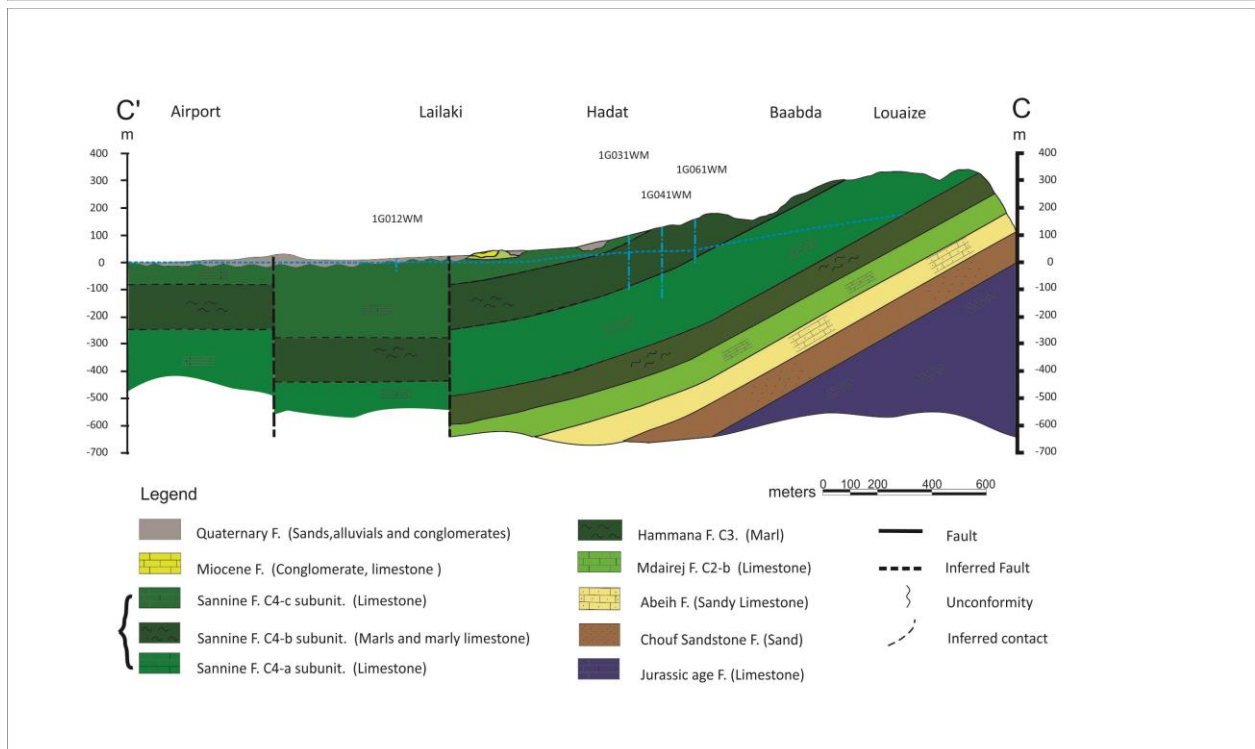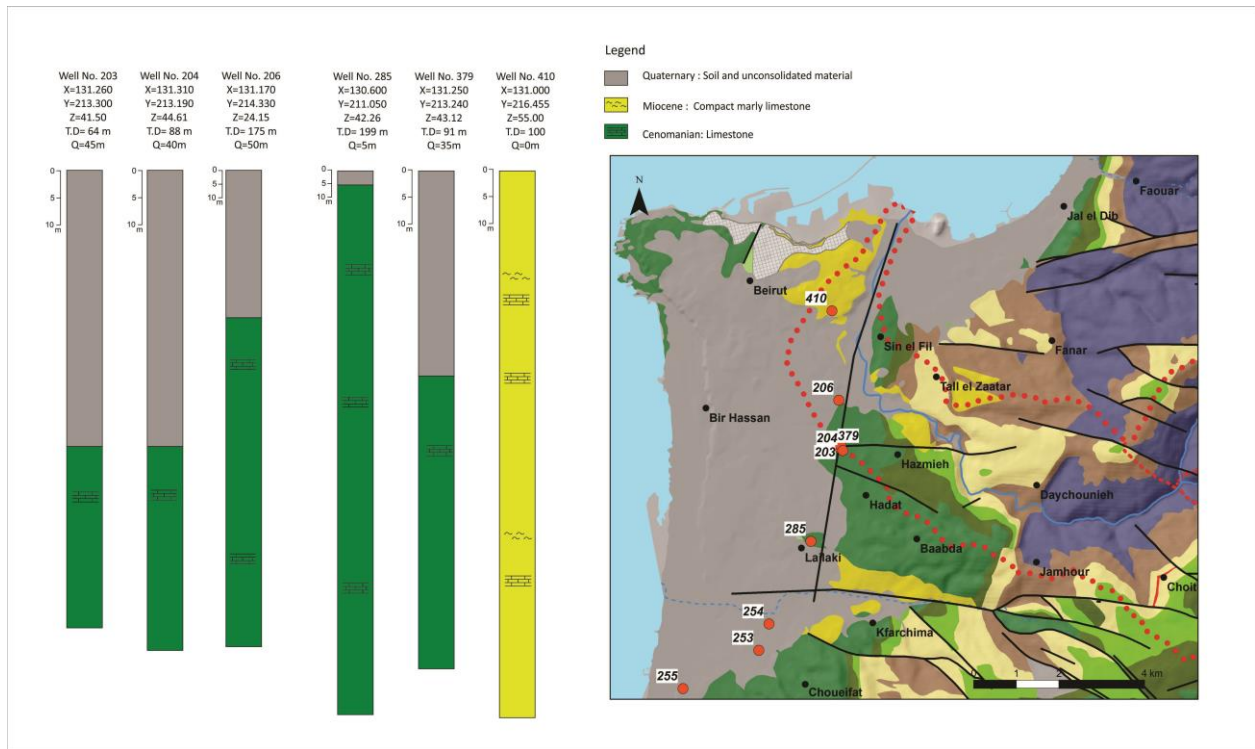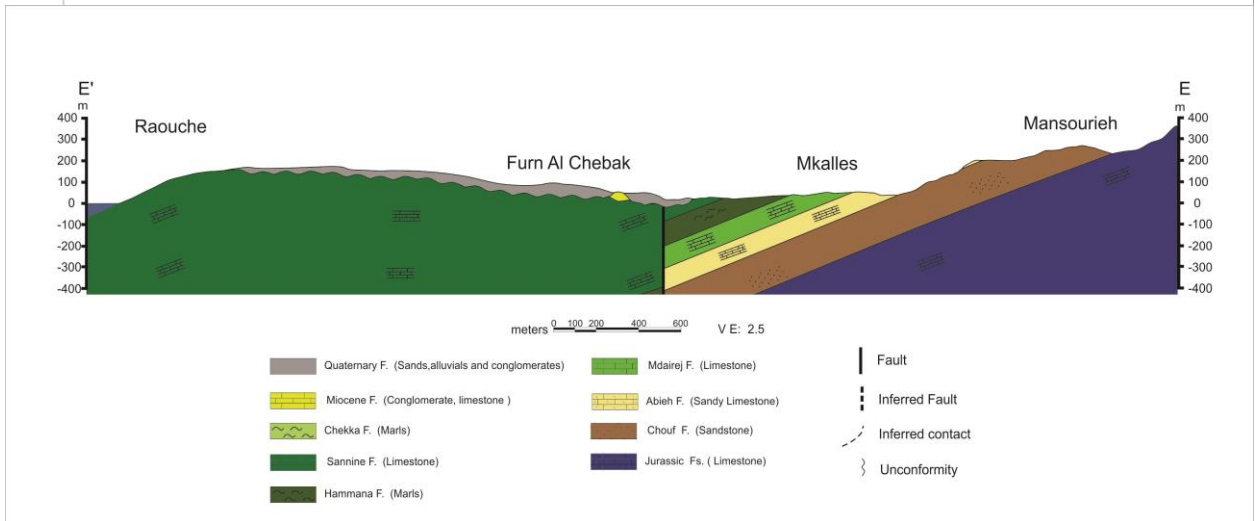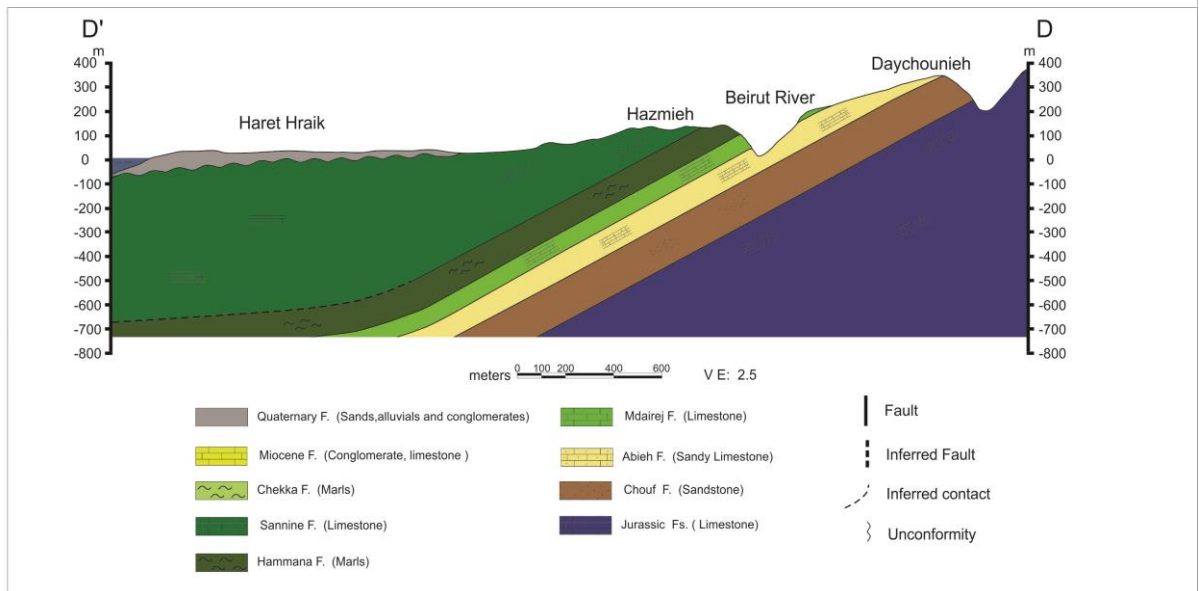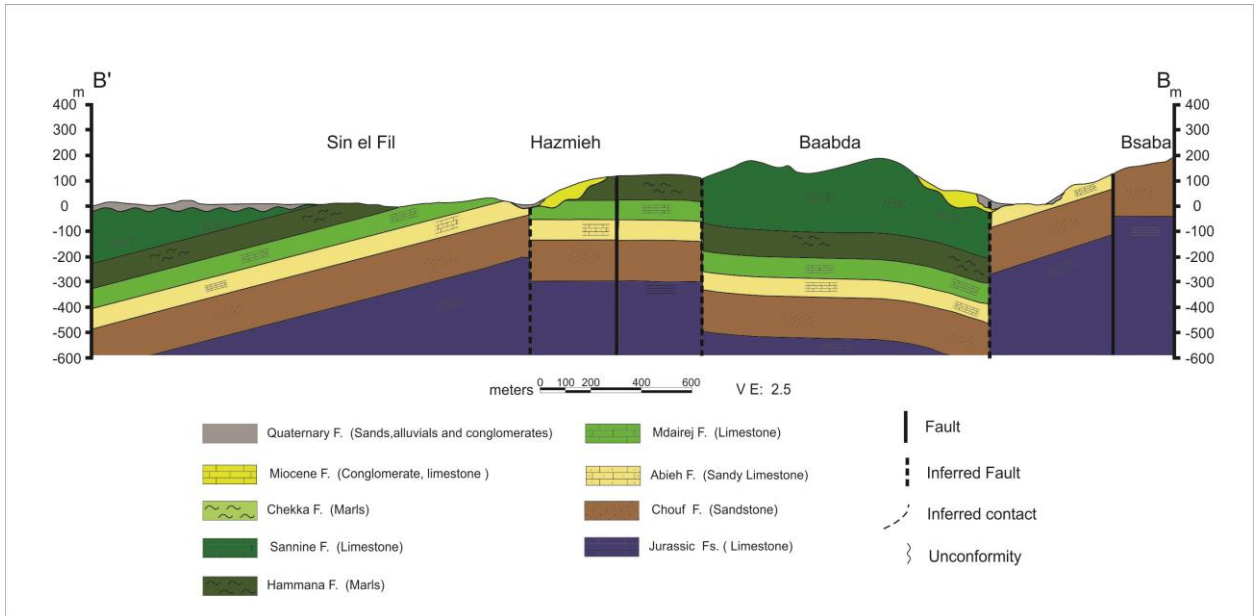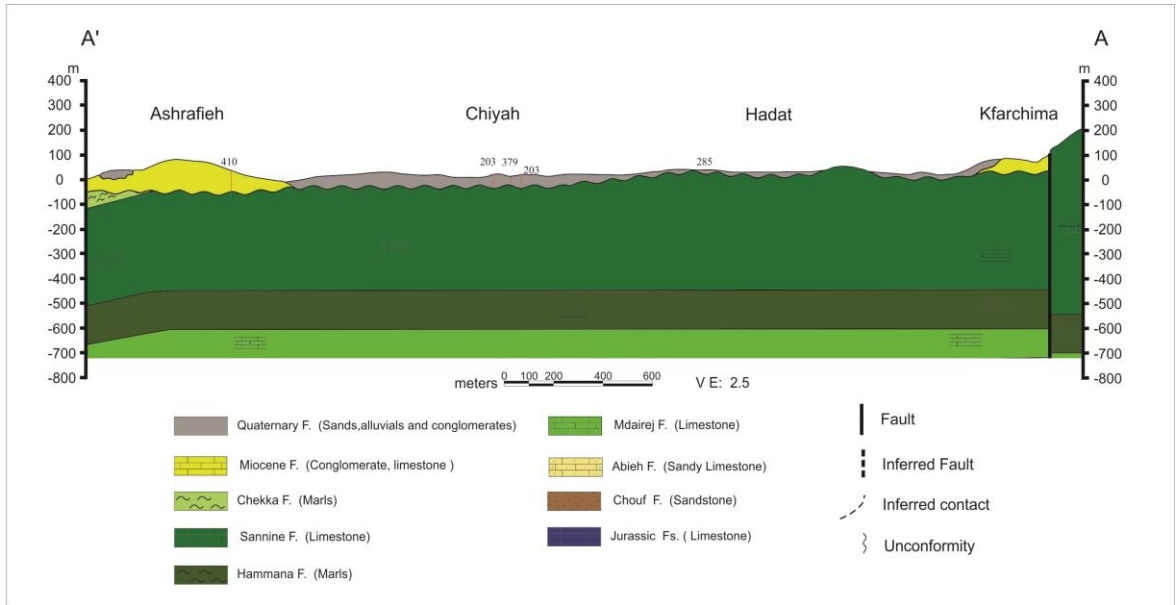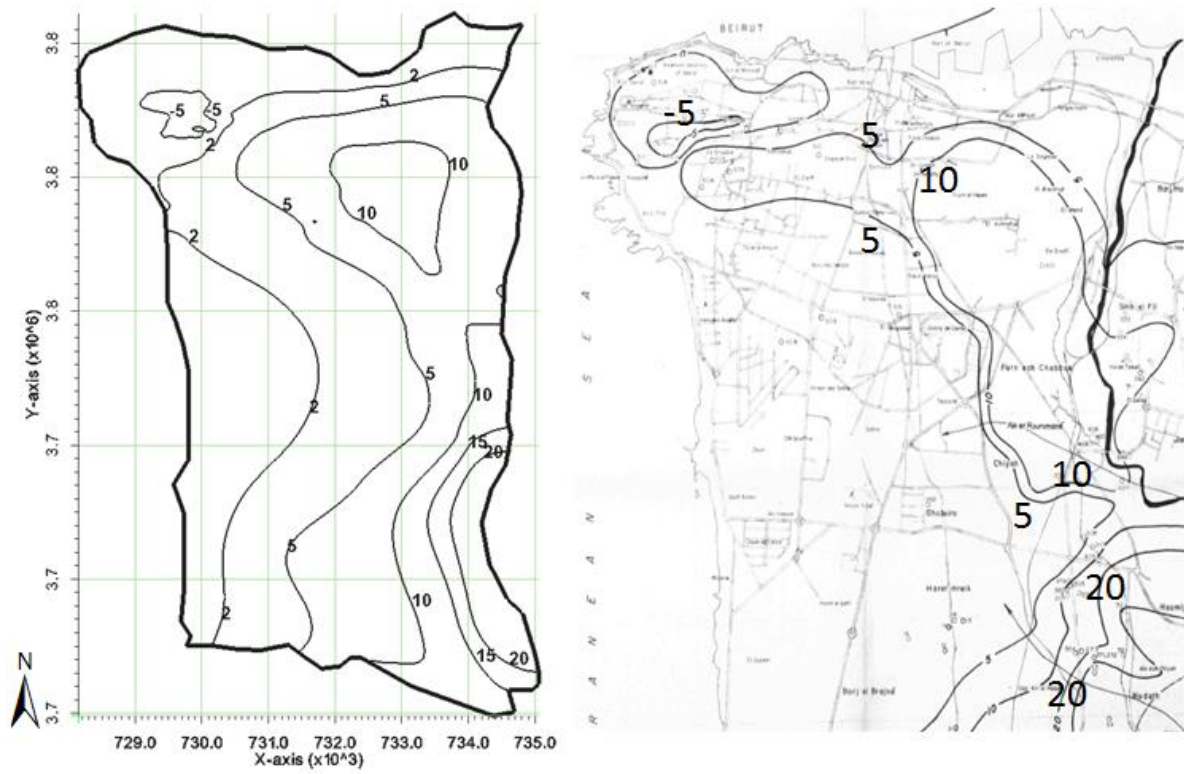
D. Groundwater contour map in the Beirut aquifer

Figure D.1. Groundwater contour map in 1969 (adopted from Ukayli 1971-right map) versus the estimated model results for water level in 1969 (left map)
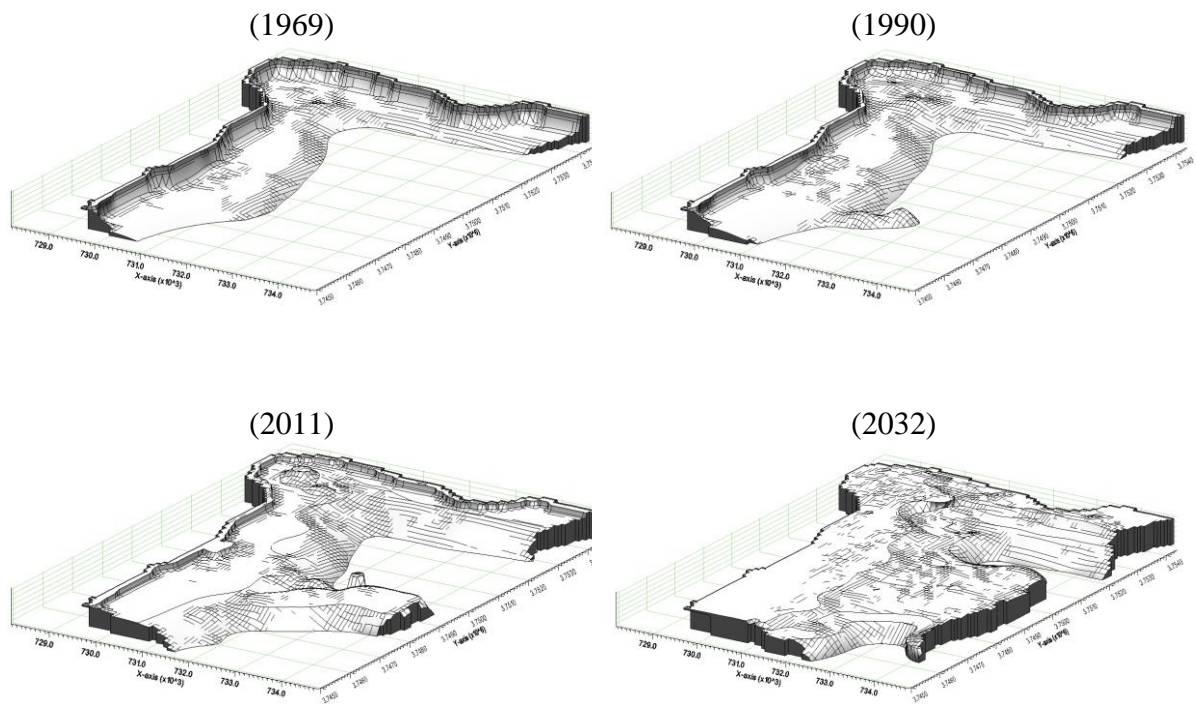
E. Salt/fresh water interface in the Beirut aquifer

(1969)

(1990)

(2011)

(2032)

Figure E.1. Computed 3D displacement of salt/fresh water interface with elevated concentrations (> 7000 mg/)
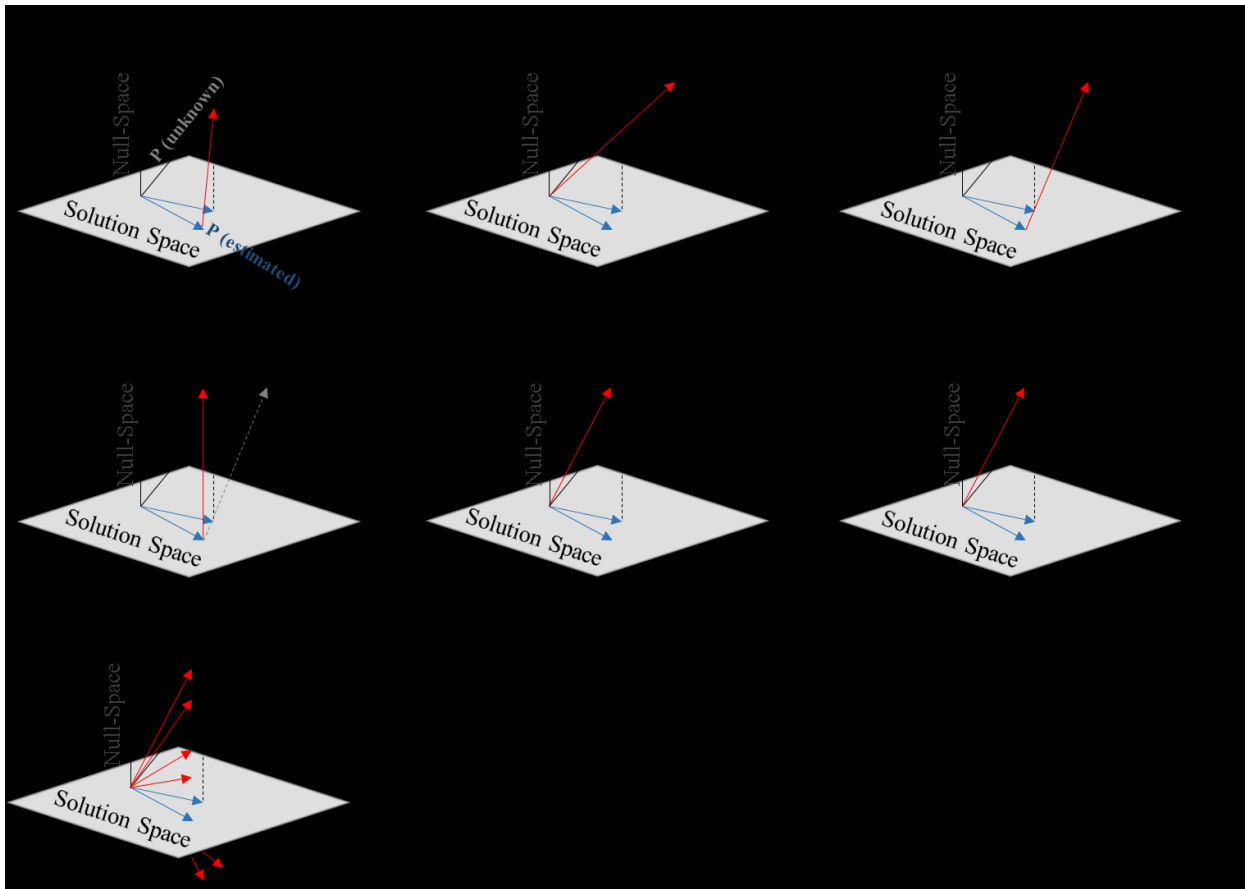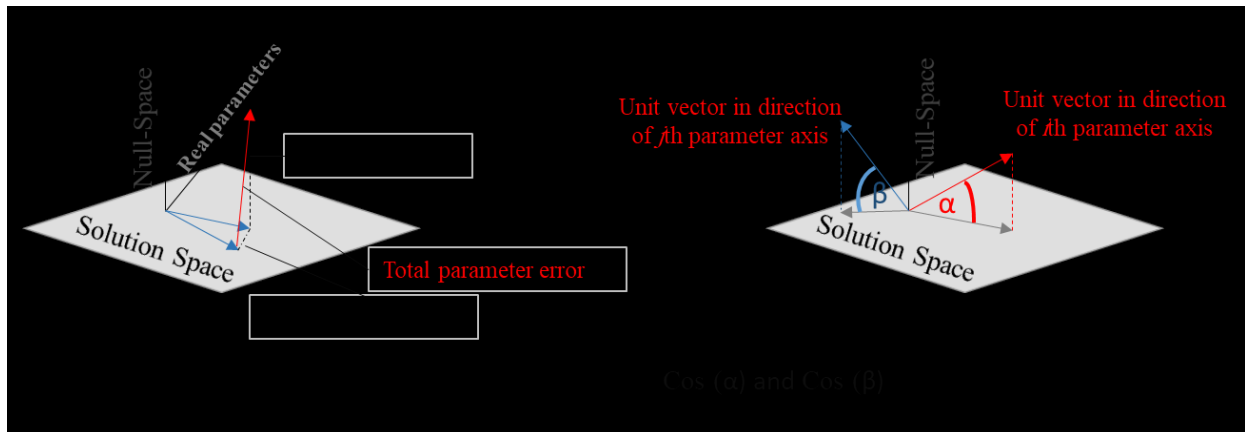from 1969 to 2032

F. Null-space Monte Carlo

Figure F.1. Schematic depiction of steps undertaken in the NSMC methodology (adopted from Doherty et al. 2010)

G. Parameter Identifiability

H. Impact of heterogeneity

Evaluating the impact of heterogeneity on SWI (Figure ii) by assessing the variability in model prediction (Figure i) in response to variability in geologic heterogeneity (Table i)

Table H.1. Geologic scenarios in zone 6 of the Beirut aquifer

Scenario	Expected range for Log Hydraulic conductivity (m/day)	Initial log value at all pilot point (m/day)	Variance-multiplier to the of covariance matrix*	Description of zone 6
1	-1.7 to 2.7	1	10	highly heterogeneous
2	-1.7 to 2.7	1.7	1.02	mildly heterogeneous
3	-1.7 to 2.7	1.7	10	highly heterogeneous

* The diagonal elements are multiplied by the Variance-multiplier
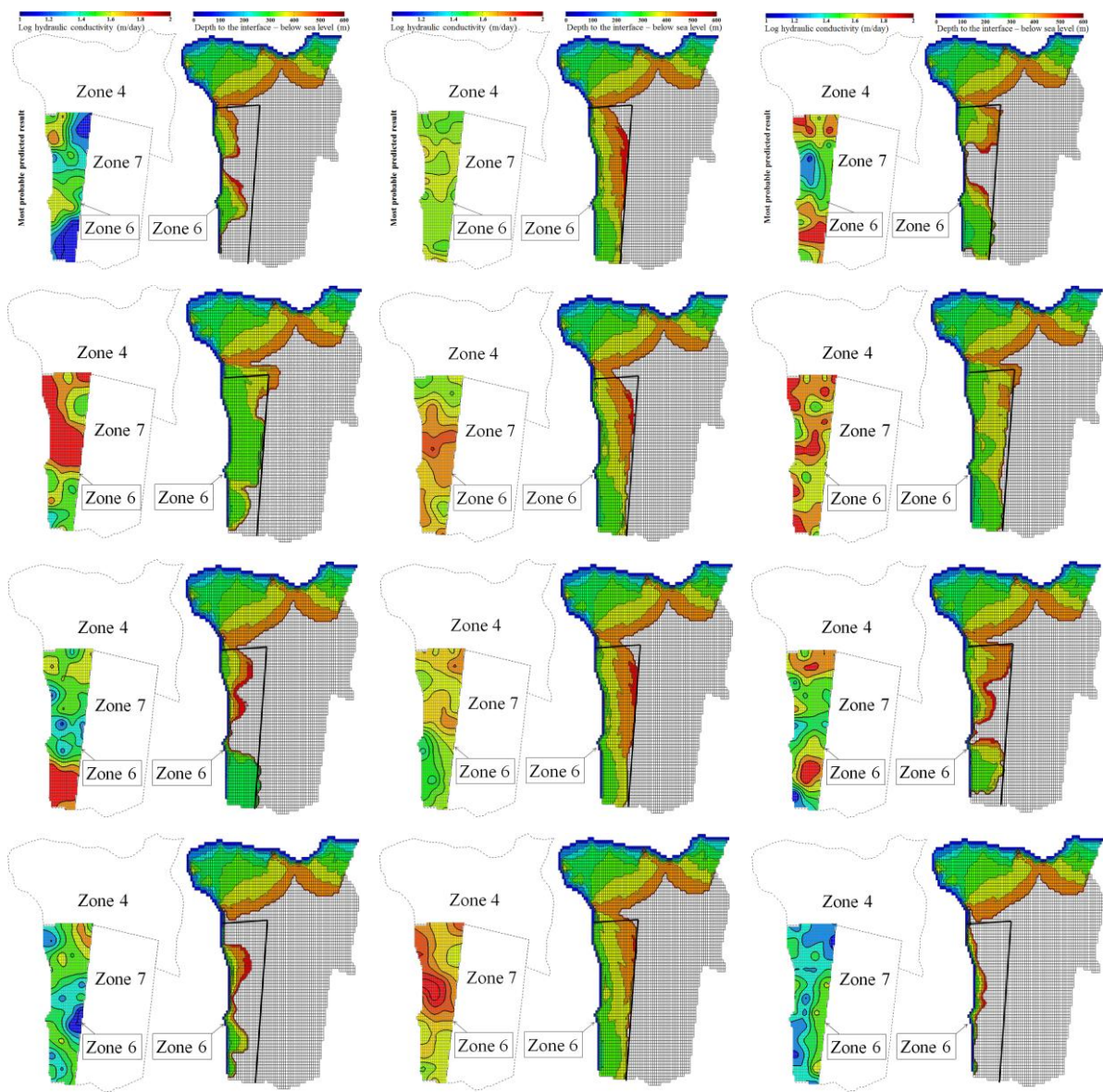
(a) *Scenario 1*   (b) *Scenario 2*   (c) *Scenario 3*

Figure H.1. Some selected stochastic realizations of hydraulic conductivity in the third layer (only zone 6 is represented) using SGS with NSMC versus corresponding depths to the salt/fresh water interface computed for the entire aquifer
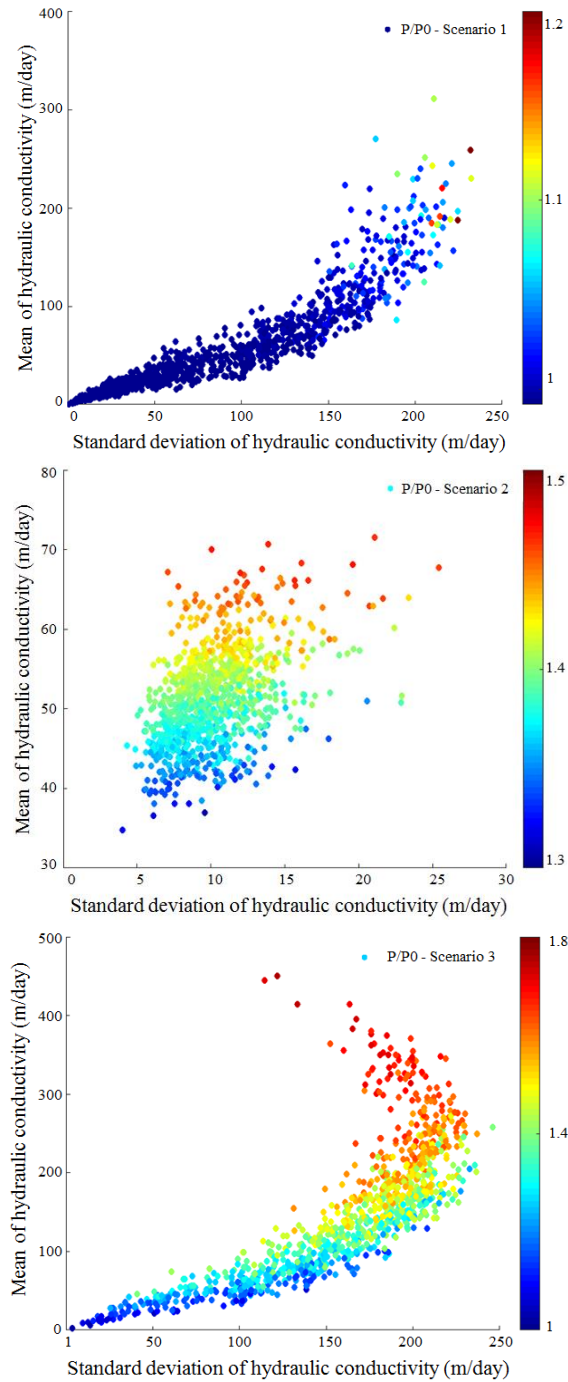
Figure H.2. Ratio of P/P0 (i.e. computed predictions (P) using stochastic models divided by the initial prediction (P$_0$) estimation calculated using the deterministic model) in response to different means and standard deviations of hydraulic conductivity in scenarios

I. LIST OF PUBLICATIONS

Peer Reviewed Papers

1. **Safi, A.,** Vilhelmsen, T. N., Alameddine, I., Abou Najm, M., & El-Fadel, M. (2018). Data-worth assessment for a 3D optimal design in non-linear groundwater systems. *Groundwater*. https://doi.org/10.1111/gwat.12835

2. **Safi, A.,** Rachid, G., El-Fadel, M., Doummar, J., Abou Najm, M., & Alameddine, I. (2018). Synergy of climate change and local pressures on saltwater intrusion in coastal urban areas: Effective adaptation for policy planning. *Water International*, 43: 145–164. https://doi.org/10.1080/02508060.2018.1434957

3. **Safi, A.,** Vilhelmsen, T. N., Alameddine, I., Abou Najm, M., Doummar, J., Christensen, S., & El-Fadel, M. (2018). Stochastic Modelling of saltwater intrusion in heterogeneous coastal aquifers under field-data deficit: Coupling NSMC with SGS and Fuzzy parameter sets. *Water Resources Research*. In review.

4. **Safi, A.,** & M. El-Fadel. (2019). Modelling saltwater intrusion in coastal aquifers: A critical review and framework for uncertainty analysis. *Critical Reviews in Environmental Science and Technology*. In review.

Abstracts in International Conferences

1. **Safi A.,** El-Fadel M., Doummar J., Abou Najm M., and Alameddine I. (2017). Optimal data acquisition strategy for sampling of future hydraulic head: Uncertainty minimization in model predictions, *European Geosciences Union General Assembly*, 23–28 April, Austria.

2. **Safi A.,** El-Fadel M., Doummar J., Abou Najm M., and Alameddine I. (2016). Synergy of climate change and local pressures on saltwater intrusion in heterogeneous coastal aquifers, *American Geophysical Union*, San Francisco, 12-16 December, USA.

3. **Safi A.,** El-Fadel M., Doummar J., Abou Najm M., and Alameddine I. (2016). Modelling saltwater intrusion in highly heterogeneous coastal aquifers, *European Geosciences Union General Assembly*, 17–22 April, Austria.

4. **Safi A.,** El-Fadel M., Doummar J., Abou Najm M., and Alameddine I. (2016). Inverse modelling of saltwater intrusion in heterogeneous coastal aquifers, *The XXI International Conference Computational Methods in Water Resources*, 20–24 June, Toronto, Canada.

5. **Safi A.,** El-Fadel M., Doummar J., Abou Najm M., and Alameddine I. (2015). Modelling heterogeneity impact on saltwater intrusion in coastal aquifers, *42nd IAH Congress*, Rome, Italy.